Cranfield University

RAMON FERNANDO COLMENARES QUINTERO

TECHNO-ECONOMIC AND ENVIRONMENTAL RISK ASSESSMENT OF INNOVATIVE PROPULSION SYSTEMS FOR SHORT-RANGE CIVIL AIRCRAFT

SCHOOL OF ENGINEERING

PhD THESIS

Cranfield University

School of Engineering

Department of Power and Propulsion

PhD Thesis

Academic year 2005-2008

RAMON FERNANDO COLMENARES QUINTERO

Techno-Economic and Environmental Risk Assessment of Innovative Propulsion Systems for Short-Range Civil Aircraft

Supervisors: Dr. Stephen Ogaji and Prof. Riti Singh

Abril 2009

This thesis is submitted in partial fulfillment of the requirements for the degree of Doctor of Philosophy.

Abstract

Aircraft are thought to contribute about 3.5% (IPCC, 1999) to the total radiative forcing (a measure of change in climate) of all the human activities and this figure is forecaste to increase. Future concerns for aviation's role in climate change are mainly due to the envisaged continued growth in this sector. Growth rates for emissions are less than those for traffic growth since fuel efficiency continues to improve over the years. Despite regular improvements in fuel efficiency, emissions will carry on increasing and several solutions need to be found.

The growth of air travel as well and its effect on world economics is hampered by local opposition to aircraft noise. Besides, restrictions on night take-off and landing because of aircraft noise levels leads to a negative impact on the revenues of Europe's airlines and often results in non-European over-night airport refuelling stops.

According to ACARE (Strategic Research Agenda, 2005), the sustainable development of air transport depends on achieving a significant across-the-board reduction in environmental impact, in terms of greenhouse gases, local pollution and noise around airports. Over the past 40 years the introduction of new technology has mitigated the environmental impact of aviation growth, but at the expense of increasing operating costs. Consequently, in order to make aviation more sustainable environmentally and economically, radically innovative turbofans need to be considered and optimised at the aircraft level.

Based on the above, this PhD project addresses the following research questions:

- *The potential of different novel propulsion systems with enhanced propulsive efficiency (using advanced, contra-rotating and geared turbofans) and thermal efficiency (using intercooled and recuperated, and constant volume combustion turbofans) to meet future environmental and economical goals.*

- *The trade-offs to be made between noise, emissions, operating cost, fuel burn and performance using single- and multi-objective optimisation case study.*

In order to achieve this, a multidisciplinary design framework was developed which is made up of: aircraft and engine performance, weight, cost, noise, emissions, environment, and economics and risk models. An appropriate commercially available optimiser is coupled with this framework in order to generate a powerful aero-engine preliminary design tool.

The innovative turbofans were benchmarked against the baseline turbofan at the aircraft level using the A320. The multi-objective trade case study for minimum fuel burn, NO_x emissions, engine direct operating cost (DOC) and noise proves that these engines are feasible to meet future noise and emissions requirements for an acceptable cost of ownership. The key driver to lower engine DOC is a considerable fall in fuel consumption. Nevertheless, acquisition and maintenance cost rise owing to hardware complexity. Consequently, further study of these engines is recommended as their environmental performance potential is considerable.

Acknowledgements

First of all I want to thank the Lord Jesus Christ and GOD, our Father, for the faith, patience, perseverance, prudence and strength given during my life. Without them, I would not become who I am.

For this research project I would like to thank Prof. Riti Singh, Prof. Pericles Pilidis and Dr. Stephen Ogaji. They provided me technical support and helped me to develop my critical thinking and creativity.

VITAL project, Universidad de San Buenaventura Bogota, and Allan and Nesta Ferguson Charitable Trust Award sponsored this PhD financially.

Also, I would like to express my acknowledgements to Arnie McCullers and Karl Geiselhart for the advice on the models NASA provided. Their support was very helpful in understanding and using the models.

This work gave me the opportunity to work with different students of the Thermal Power Master with whom the regular meetings and discussions were invaluable.

Gillian Hargreaves was a wonderful departmental administrator. Her patience and efficiency to solve problems is a great added value in the Department of Power and Propulsion.

My compadre and parcero Jacinto Carrasco-Muñoz Guerra, thanks for the philosophical debates and exchanges of ideas which were very stimulating.

Acknowledgment is given to other colleagues at Cranfield University for sharing time and technical discussions: Josué and Birute.

Thanks for my mother Margarita Quintero Trillos, my aunt Rosa, my uncle Alfonso, my cousins Jairo and Marlene, and my brothers: Juanka, Alex and Mauro and their family for emotional support during the highs-and-lows that appear in this PhD project, and also Sandra (my love) and my children Santi and Raquelita for showing me another perspective of life.

Finally, I am grateful to Maureen and John Chacksfield for their support and appearance in the appropriate moment in my life.

Table of Contents

NOMENCLATURE

ABBREVIATIONS AND ACRONYMS

ACARE	Advisory Council for Aeronautics Research in Europe
AEA	Association of European Airlines
AFT	Adiabatic Flame Temperature or flame temperature (same as T_{pz})
ATF	Advanced TurboFan
ANOP	Aircraft Noise Prediction Program by NASA
ATA	Air Transport Association
BFGS	Broyden-Fletcher-Goldfarb-Shano optimisation algorithm
BPR	By-Pass Ratio
C	Compressor
CAEP	Committee on Aviation Environmental Protection
C_t	Cash flow at time
CC	Combustion Chamber
CCD	Computational Combustion Dynamics
CDA	Continuous Descent Approaches
CER	Cost Estimation Relationships
CFC	ChloroFluoroCarbons
CFD	Computational Fluid Dynamics
CHEMKIN	Program for solving complex chemical kinetics problems
CH_4	Methane
CLEAN	Component Validator for Environmentally-Friendly Aero-Engine

CO	Carbon Monoxide
CO_2	Carbon Dioxide
CPC	Constant Pressure Combustion
CPU	Central Processing Unit
CRTF	Contra-Rotating TurboFan
CT	Carbon Threshold
CU	Cranfield University
CVC	Constant Volume Combustion
C1	Low pressure compressor
C2	High pressure compressor
^oC	Celsius degree
dB	Decibel
DDTF	Direct Drive TurboFan
DFP	Davidon-Fletcher-Powell optimisation algorithm
D_{ff}	Front flange diameter
DHS	Directed Heuristic Search
DLE	Dry Low Emissions
DLN	Dry Low NO_x
DLR	Deutsches Zentrum für Luft- und Raumfahrt
D_{max}	Maximum diameter
D_{nac}	Nacelle diameter
DNL	Day-Night Level
DNS	Direct Numerical Simulation
DOC	Direct Operating Cost

DOE	Design of Experiments
DREAM	valiDation of Radical Engine Architecture systeMs
D_{rf}	Rear flange diameter
$(D_p/F_{oo})_{NOx}$	ICAO parameter for LTO NO_x
E	Exhaust valve
EAS	Equivalent Air Speed
EDOC	Engine Direct Operating Cost
EI	Emission Index
EGT	Exhaust Gas Temperature
ENGGEN	Engine Cycle Analysis Program by NASA Langley Research Centre
EP	Engine Price
EPNL	Effective Perceived Noise Level
EQR	Equivalence Ratio (same as ϕ)
EU	European Union
F	Future value
FAA	Federal Aviation Administration
FAR	Federal Aviation Regulation
FAR	Fuel-Air Ratio
FB	Fuel Burn (Block Fuel)
FLOPS	FLight OPtimization System by NASA Langley Research Centre
FM	Fiacco-McCormick penalty function
FN	Net Thrust
FORM	First Order Reliability Method

FP	Fuel Price
ft	Feet
g	Constraint
GA	Genetic Algorithm
Gas Turb	Gas-turbine simulation model
GCM	Global Circulation Model
GDP	Gross Domestic Product
GTF	Geared TurboFan
GTF-CVC	Geared TurboFan with Constant Volume Combustion
GTP	Global Temperature Potential
GWP	Global Warming Potential
h	Constraint
HERMES	Aircraft performance model by Cranfield University
HP	High Pressure
HPC/HPT	High Pressure Compressor / Turbine
HPRTE	High Pressure Regenerative Turbine Engine
HX	Heat eXchanger
H_2O	Water Vapour
i	Rate of interest
I	Intake valve
IATA	International Air Transport Association
IC	Inter Cooler
ICAO	International Civil Aeronautics Organization
ICHXMDO	MDO for baseline, intercooled, recuperated, and ICR turbofans

ICR	Intercooled and Recuperated aero engine
IOC	Indirect Operating Cost
IPCC	Intergovernmental Panel on Climate Change
IRA	Intercooled Recuperative Aero Engine
i-SIGHT	Engineous Software's optimiser
ITB	Interstage Turbine Burner
J	Objective
JAR	Joint Aviation Requirement
K	Kelvin degree
KENG	Weight correction factor applied to the complete engine
kg	Kilogram
Kgg	Ratio of gas generator weight to the total engine weight
KHP	Weight correction factor applied to high pressure (HP) section
KIGV	Length correction factor for inclusion/exclusion of fan inlet guide vanes
KLBPR	Length correction factor for bypass ratio
KLP	Weight correction factor applied to low pressure system
KLW_c	Length correction factor for airflow size
KLY	Length correction factor for technology level
km	Kilometer
kN	Kilonewton
KOPR	Length correction factor for overall cycle pressure rati
KS	Kreisselmeier-Steinhauser envelope function
kt	Knot
L_{bare}	Bare engine length

LBO	Lean Blow Out
LCC	Life Cycle Cost
LDI	Lean Direct Injection
LES	Large Eddy Simulations
L_{nac}	Nacelle length
LP	Low Pressure
LPC/LPT	Low Pressure Compressor / Turbine
LPP	Lean Premix Pre-vaporise
LTO	Landing and Take-Off
m	Meter
MCS	Monte Carlo Simulation
MDO	MultiDisciplinary Optimisation
ms	Meter second
m/s	Meter per second
MOST	Mixed Integer Optimisation algorithm
MTU	Motoren- und Turbinen-Union
MW	Megawatt
MVFO	Mean Value First Order method
$\dot{m}$	Mass flow
n	Number of years
NASA	National Aeronautics and Space Administration
NEAV	Net Equivalent Annual Value
NEWAC	NEW Aero-engine core Concepts
NFV	Net Future Value

NGV	Nozzle Guide Vane
NO	Nitric Oxide
Non-dim	Non-dimensional
NO_x	Nitrogen Oxides
NO_2	Nitrogen Dioxide
N_2O	Nitrous Oxide
NPC	Net Present Cost
NPSS	Numerical Propulsion System Simulation by NASA
NPV	Net Present Value
NTT	Noise Threshold for Tax
OD	Off-Design
OEM	Original Equipment Manufacturer
OH	Hydroxyl Radicals
OPR	Overall Pressure Ratio
O_2	Oxygen
O_3	Ozone
P	Present value
PCN	Rotating component speed
PDE	Pulse Detonation Engine
PERM	Partially Evaporating Rapid Mixing
PF	Penalty Function
PMDF	Preliminary Multidisciplinary Design Framework
PT	Power Turbine
PS	Power Setting

Pythia	Diagnostics and Gas Path Analysis by Cranfield University
QC	Quota Count
QEM	Quality Engineering Methods
QNEP	Quick Navy Engine Performance computer program by NASA
r	Discount rate
RBO	Reliability-Based Optimisation
REC	RECuperated
R&D	Research and Development
RDT&E	Research, Development, Test and Evaluation
RF	Radiative Forcing
RQL	Rich-burn, Quick-quench, Lean-burn
SAC	Simple Annular Combustor
SAE	Society of Automotive Engineers
SFC	Specific Fuel Consumption
SilenceR	European Union noise-reduction program
SLS	Sea Level Static
SMD	Sauter Mean Diameter
SNO_x	NO_x severity index
Soprano	Noise module by ANOTEC
SO_x	Oxides of Sulphur
SPL	Sound Pressure Level
SQP	Sequential Quadratic Programming algorithm
t	Time
T	Turbine/ Temperature

TBO	Time Between Overhaul
TBRR	Time Between Repairs/Removals
TERA	Techno-Economical Risk Assessment
TET/TIT	Turbine Entry / Inlet Temperature
TM	TradeMark
T-O	Take-Off
TOA	Time Of Arrival
ToC	Top of Climb
TURBOMATCH	Gas-turbine simulation model by Cranfield University
T1	High pressure turbine
T2	Low pressure turbine
UDF	UnDucted Fan
UHBPR	Ultra-High ByPass Ratio
UHCs	Unburned Hydro-Carbons
U.S.	United States
USA	United States of America
USTUTT	Stuttgart University
V	Volume
VHBR	Very High Bypass Ratio
VITAL	enVIronmenTALly friendly aero-engine (EU project)
$\frac{V_{id.18}}{V_{id.8}}$	Ideal jet velocity ratio
WATE-1	Weight Analysis of Turbine Engines
WeiDim	Propulsion system weight and dimension module
WF	Fuel flow

W_C	Carbon atomic weight
W_{eng}	Engine weight
W_H	Hydrogen atomic weight
W_{nac}	Nacelle weight
W_O	Oxygen atomic weight/ Specified total fan face airflow
W/m^2	Watt per square meter
μm	Micrometer

GREEK SYMBOLS

Δ	Relative values with respect to those obtained in the baseline configuration
εic	Intercooler effectiveness
εrec	Recuperator effectiveness
η_{th}	Thermal efficiency
λ	Evaporation constant
τ	Time
ϕ	Equivalence ratio (Same as EQR)
Ω	Design space

SUBSCRIPTS

A	Air
c	Combustion
C	Carbon
cr	Cruise

eff	Effective
ev	Evaporation
H	Hydrogen
O	Oxygen
pz	Combustor primary zone
ref	Reference value
res	Residence
sls	Sea level static
st	Stoichiometric
t	time
3	Entry of the combustor
4	Entry of the turbine

List of Tables and Figures

CHAPTER 1

INTRODUCTION:

AVIATION IMPACT ON THE GLOBAL ENVIRONMENT

The global air traffic is expected to grow at a rate of 5% annually over the next 15 years. This growth will greatly impact aviation environmental concerns. As a result, the aviation industry will face a vast challenge to fulfill this growing need while guaranteeing economic, safe and environmentally-friendly air travel.

Both Europe and the USA have made large investments through collaborative projects and programmes to decrease negative environmental effects produced by aviation. The Advisory Council for Aeronautics Research in Europe (ACARE) has set two ambitious goals for 2020, cutting in half both the perceived aircraft noise (a reduction of 10 dB) and CO_2 emissions (Strategic Research Agenda, 2005). According to ACARE, the sustainable development of air transport depends on achieving a significant across-the-board reduction in environmental impact, in terms of greenhouse gases, local pollution and noise around airports.

Over the past 40 years the introduction of new technology has mitigated the environmental impact of aviation growth, but at the expense of increasing operating costs. Consequently, in order to make aviation more sustainable (i.e. more significant decrease in pollution and noise at a reasonable cost), radically innovative turbofans need to be considered and optimised at the aircraft level.

1.1 Aviation and Environment

The gases and particles emitted by the engines contribute to local air quality degradation around airports and to the greenhouse effect worldwide. Also, the noise environment around airports is a main source of concern within Europe, with many local communities subjected to high levels of aircraft noise. Consequently, restrictions on night take-off and landing due to aircraft noise levels leads to a negative impact on the revenues of Europe's airlines and often results in non-European over-night airport refuelling stops.

1.1.1 Emissions

Over the last 40 years the fuel efficiency of civil aero-engines (which is a direct measure of carbon dioxide emissions) has steadily improved. This has been achieved by increased overall pressure ratio, higher temperature cycles, better materials and cooling, more efficient turbo-machinery and high bypass ratio architecture, which have benefited both thermal and propulsive efficiencies. At the same time engine generated noise and emissions of both carbon monoxide (CO) and unburnt hydrocarbon (UHC) have been dramatically reduced. Only nitrogen oxides (NO_x) emissions have remained relatively steady, since the rising compressor delivery temperature associated with increasing overall pressure ratio favours NO_x production. During this period, it has been possible to optimise the engine for minimum mission fuel burn and still meet the requirements for noise and other emissions. However the introduction of noise operating restrictions leads to noise optimised solutions which tend to compromise fuel efficiency, at least for the largest aircraft, and NO_x reduction targets will impinge on the introduction of further increases in pressure ratio. Hence the targets for CO_2, noise and NO_x are becoming highly interactive, and for conventional engine architectures, improvements are becoming more and more challenging (Strategic Research Agenda, 2005).

Whilst the performance of the conventional engine cycle and architecture will continue to improve throughout the period to 2020, when noise and NO_x targets are taken into account it is asserted that the target specific fuel consumption (SFC) improvement will not be achieved by some margin and therefore unconventional solutions will have to be evaluated. This will introduce different, higher risk, technology requirements (Strategic Research Agenda, 2005 and Sixth Framework Programme, 2005).

Thrust based SFC is dependent on flight velocity and two engine related efficiencies, propulsive efficiency and thermal efficiency, which are discussed in the next sections. However it should not be forgotten that reducing cruise speed will also reduce CO_2 emissions, albeit at the expense of journey time (Strategic Research Agenda, 2005 and Sixth Framework Programme, 2005).

1.1.2 Noise

There are two main contributors to engine noise: the fan, mainly by its tip speed (so-called fan noise), and the nozzle, mainly by jet velocity (so-called jet noise).

An increase in BPR (i.e. propulsive efficiency) reduces jet noise but increases the aero-engine frontal area leading to a higher fan noise, a greater weight and a higher pod drag (Guénon, 2003). For conventional turbofan configurations the future gain in propulsive efficiency and noise reduction will be limited (see Figure 1.1).

When increasing the BPR beyond 10 the engine will suffer from an increasing mismatch of fan and low pressure system. The increase of BPR drives the fan towards lower pressure ratios and lower rotor speeds which has to be counteracted

by increasing the stage count for the booster and low pressure turbine (LPT) to retain acceptable efficiencies for these components. But the increasing high rotor torques associated with reduced speeds call for bigger LP-shaft diameters which are increasingly difficult to accommodate underneath the core engine discs. This would imply the use of high hub-to-tip ratios but it would compromise the efficiencies in the core since the blade heights reduce and consequently increase the detrimental impact from tip clearances. Therefore, in order to obtain further increases in BPR in favour of fuel burn and noise emissions new innovative concepts must be introduced (Krammer, 2003 and Boggia and Rüd, 2004 and 2005).

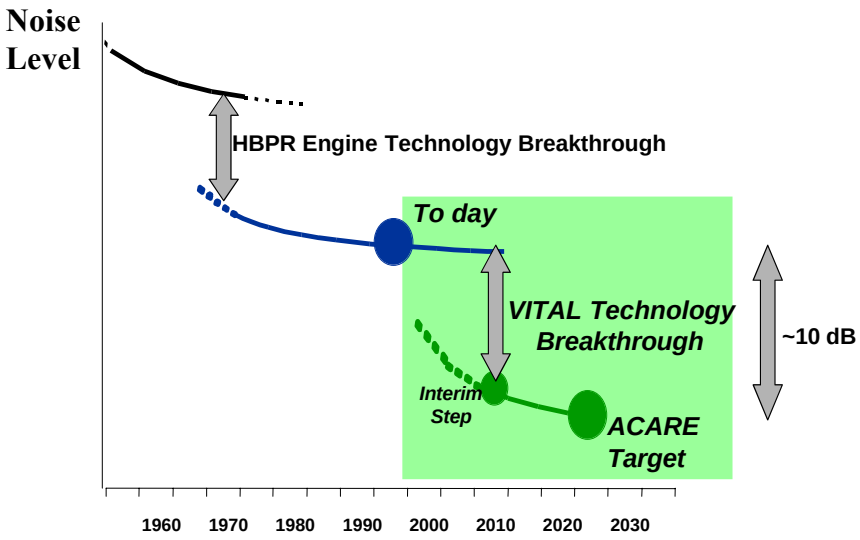

Figure 1.1: Trends in aircraft noise reduction (Sixth Framework Programme, 2005)

1.1.3 Thermal Efficiency

Thermal efficiency for aero engines is a measure of the quality of the thermodynamic cycle, indicating how much energy contained in the fuel is used to increase the kinetic energy of the gases (Pilidis and Palmer, 2005 and Walsh, and Fletcher, 2004). A thermal efficiency increase can be obtained by a change in the engine cycle itself (characterised by overall pressure ratio and turbine entry temperature) or by more advanced component technology (cooling and sealing

methods, component efficiencies, pressure losses in ducts) or a different overall thermodynamic cycle; an example for the latter case is the introduction of unconventional components, such as intercoolers and recuperators as will be discussed later.

1.1.4 Propulsive Efficiency

The propulsive efficiency in aero engines is a measure of the effectiveness with which the available core power (i.e. the sum of the thrust power and the unused kinetic energy of the jet) is being used for propelling the aircraft (Pilidis and Palmer, 2005). Propulsive efficiency is improved by reducing the specific thrust (thrust per unit airflow which is a measure of jet velocity); this is typically achieved by increasing the bypass ratio and reducing the fan pressure ratio. Departure noise also benefits from reduced specific thrust (relative to current levels), but weight and nacelle drag both increase at constant technology and today's engines with bypass ratios of around 8 or 9 are already at or beyond the CO_2 emissions optimum in conventional installations.

1.1.5 Overall Efficiency

The overall efficiency is defined as the product of the thermal and propulsive efficiencies. An increase in overall efficiency causes a reduction in specific fuel consumption. As known by definition, the overall efficiency can be improved by rising thermal efficiency and/or propulsive efficiency.

When modifying the cycle of the jet engine special attention has to be paid to these efficiencies: an improvement in thermal efficiency sometimes leads to a reduction in propulsive efficiency and therefore an increase in jet noise (Pilidis and Palmer, 2005).

1.2 Multidisciplinary Optimisation and its Application to the Preliminary Design of a Propulsion System

The aero-engine preliminary design processes were based, mainly, on delivering aero-engines which meet performance requirements at minimum fuel consumption or maintenance costs. Environmental performance has been taken into account at post-design phase where adjustments have to be made to satisfy the noise and emissions requirements of specific airlines and/or airports. This approach does not assure that the final aero-engine is the optimal design. One example to illustrate this scenario is the Trent 900 installed in the A380: in this case both engine and airframe had to be modified, at the request of airlines, to meet night time noise restrictions at Heathrow airport in London. This involves using a larger fan than required for minimum SFC and having to redesign the aero-engine, nacelle, pylon and wing. These modifications led to a decrease of 1-2 dB in noise at the expense of 1-2% in fuel burn (Pacull, 2002), considered a very expensive trade-off. This sort of situation is likely to become more frequent in the future, as regulations become increasingly stringent.

The methodology developed in this PhD project considers all the disciplines such as: engine and aircraft performance, weight, economics, noise, emission and optimization, at the same time during the conceptual and preliminary design phase of the engine. This approach is vital to avoid situations as explained above.

1.3 Project Objectives and Scope

The overall objective of this work is to address the following research questions:

- The potential of different novel propulsion systems to meet environmental and economical goals.

- The trade-offs to be made between noise, emissions, operating cost, fuel burn and performance using a single- and multi-objective optimisation case study.

The selection of each case study characterised by different optimisation scenarios (e.g. environmental and economical requirements) is motivated by the above-mentioned research questions.

In order to achieve this objective, a multidisciplinary design framework was developed which is made up of: aircraft and engine performance, weight, cost, noise, emissions, environment and economics and risk models. An appropriate commercially available optimiser is coupled with this framework in order to generate a powerful aero-engine preliminary design tool. Additionally, this approach can be used to form recommendations for the aeronautical industry with regard to future product strategies and the basis of advice given to legislative bodies on what is achievable in terms of noise, fuel burn (CO_2) and NO_x reductions whilst still retaining the economic benefits to society.

This study is focused on aero-engines for short-range aircraft. Several alternative aero-engines' configurations are considered in this research: geared, contra-rotating, intercooled, recuperated, intercooled and recuperated, and constant-volume combustion among others, for minimal environmental and economical impact. This will be achieved in a first step by analysing their potential and in a second step in optimising these engines.

1.4 Contribution to Knowledge

There are three main contributions to knowledge:

- The development of a tool that consists of the integration of multidisciplinary modules that affect the future power plant's requirements and constraints – environment and economics – which will then be interfaced with an automated optimiser to design the power plants for particular environmental and economic requirements. Also, risk and global warming are modelled, which are not considered in the traditional multidisciplinary optimisation (MDO) tools available in the literature. The modules of this framework will be simplified as appropriate since all the exiting modules tend to be complex (refer to chapter 3).

- The assessment of radical power plants at system level and using single- and multi-objective optimisation, and trade-off analysis in terms of their potential to meet environmental and economical goals. The engines being proposed will be assessed for different scenarios (case studies) using the afore-mentioned tool. It is worth mentioning that the assessment of these turbofans at engine level is available in the public domain. Therefore, this research project will reduce the already existing gap in the knowledge of the innovative turbofans proposed (refer to chapter 4 and 5).

- In order to achieve the above, critical information about different aspects in aviation (i.e. emissions, noise, economics, environment, optimisation, novel engine cycles and so on) was gathered from several sources: published and unpublished becoming a fundamental starting point for further research in this field (refer to chapter 1 and 2).

1.5 Organisation of the Thesis

In chapter 2, the literature survey is presented. This chapter provides a brief insight into emissions, noise, and several novel engine concepts proposed and developed so far. The multidisciplinary design tool and its models are explained in chapter 3. The case studies are presented in chapter 4 and in chapter 5 conclusions and future work are given.

CHAPTER 2

LITERATURE REVIEW:

ENVIRONMENT, ECONOMICS, NOVEL CYCLES AND OPTIMISATION

2.1 Aviation Emissions

2.1.1 Introduction

As shown in figure 2.1, the most dominant emissions in the whole flight are CO_2 and H_2O species which represent approximately 99.6% of the aircraft emissions while NO_x, CO, UHC, soot, smoke and SO_x comprise the remainder.

The emissions' concentration levels per kg of fuel burned depend on several factors (Lefebvre, 1999) associated with the combustor operating conditions such as: mass flow, fuel-air mixture, pressure, temperature, combustion residence time, the concentration logs of the reactants and products whose simulations are very complex, and finally the combustor geometry which influences the combustion concentration and time. In summary, the emission concentrations are directly proportional to engine operating conditions for a certain fuel and combustor. The only exception applies for carbon dioxide (CO_2) and water vapour (H_2O) whose emissions' levels are set, for a specified fuel, along the whole mission.

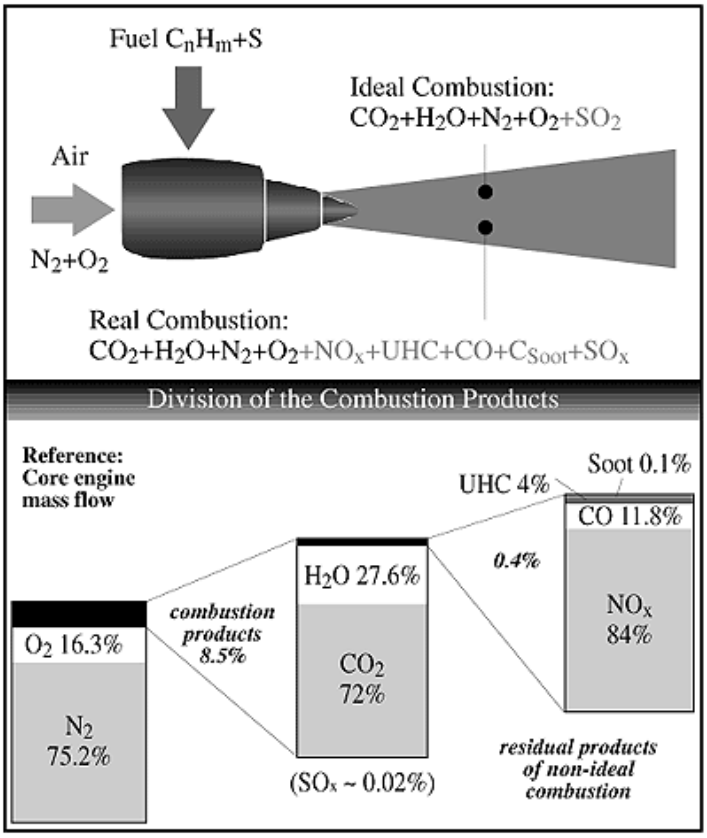

Figure 2.1: Engine emission species and their percentages (IPCC, 1999)

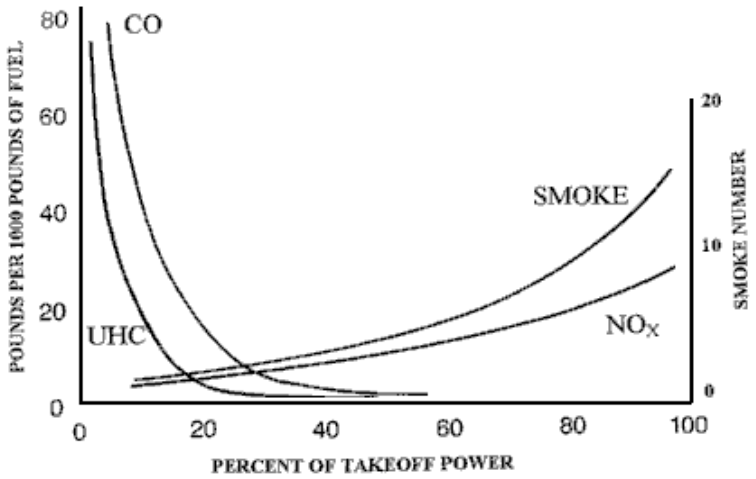

Figure 2.2: Levels of emission as a function of the engine power setting (Lefebvre, 1999)

At low power settings, the leading emissions are carbon monoxide (CO) and unburned hydrocarbons (UHCs) while at the same time oxides of nitrogen (NO_x) and smoke are in their low levels as seen in figure 2.2. At high power settings they behave oppositely.

2.1.2 Emissions-related Combustion Parameters

2.1.2.1 Equivalence Ratio

The equivalence ratio (EQR) represents the relationship between the actual fuel-air ratio (FAR) and stoichiometric FAR. A mixture of fuel and air is called 'lean' when EQR is below 1 (i.e. less fuel, more air), and 'rich' when EQR is above 1 (i.e. more fuel, less air). In the combustion chamber primary zone standard values of EQR range from 0.45 to 0.9 depending on the power setting used; low values correspond to part power while high ones to full power level. Another parameter to be considered is the lean blow-out (LBO) limit whose values are between 0.35 and 0.5 depending on the bulk velocity and the fuel (Nair et al., 2004).

2.1.2.2 Adiabatic Flame Temperature

The maximum gas temperature for a given fuel in the adiabatically combustion process without work is known as the adiabatic flame temperature (AFT) (Spakovszky et al., 2006). The maximum value of AFT (refer to figure 2.3) takes place at stoichiometry and in the local hot spots located close to fuel droplets; this temperature (and consequently TET) is regulated by the amount of air. The total primary-zone EQR sets up AFT ($T_{af\text{-}eqr}$), and hence the mean primary zone temperature (T_{pz}).

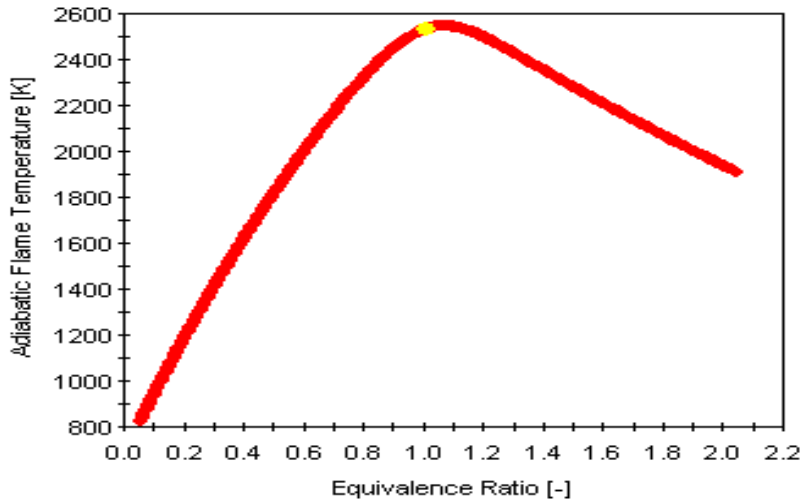

Figure 2.3: AFT as a function of EQR for the kerosene (Depcik, 2008)

Lower values of AFT are due to the heat transfer (owing to radiation losses), the incomplete combustion, and the dissociation of the molecules (over temperatures of 1900 K). During the dissociation process the linear relationship between the internal energy, enthalpy and temperature is not applicable as the first two parameters rise more quickly than the last one.

As can be seen in figure 2.4, the CO emissions are high at primary-zone temperatures less than 1670 K and at about 1900 K the emissions start to increase owing to CO_2 dissociation into the molecules of CO and O; additionally, the NO_x emissions are at their highest values. From the previous observation it can be concluded that: the primary-zone temperature has a huge impact on the emissions formation and their control, therefore it is not only the material and cooling issues which restrict the use of higher TET's (i.e. better thermal efficiency and hence less specific fuel consumption), but also the formation of NO_x and CO species linked to the regulations.

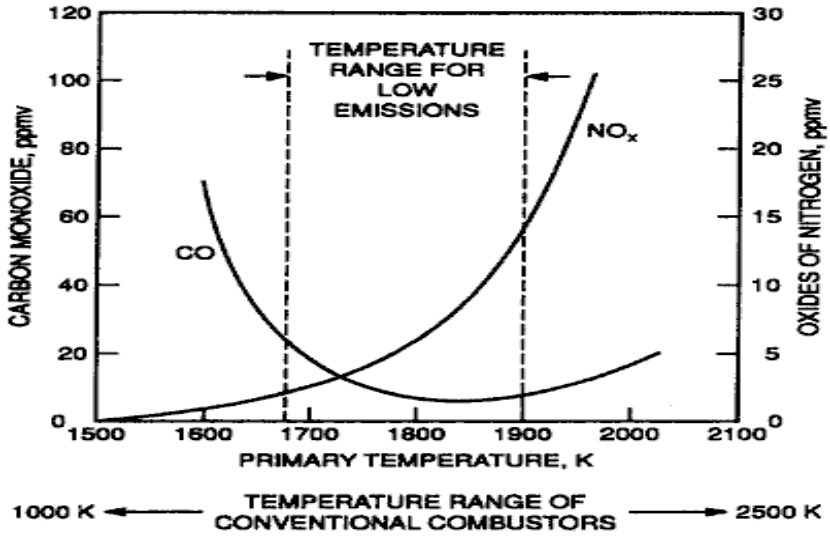

Figure 2.4: Emission levels versus combustor primary-zone temperatures (Lefebvre, 1995)

2.1.3 Engine Emissions

2.1.3.1 Carbon Dioxide and Water Vapour

The CO_2 and H_2O emissions are the result of the complete combustion of the hydrocarbon-fuel in the aero engine. These two species are considered to be the main contributors to global warming, thus to the climate change. The former can remain in the atmosphere between 100 and 150 years or even more (IPCC, 1999). An increase in their concentration alters the atmosphere's radiative balance causing the atmosphere to warm (i.e. global warming). The latter makes the formation of contrails and cirrus clouds possible, which lead to the warming effect. Their formation only depends on the type of fuel being used during the combustion process regardless of combustor geometry and operating conditions. One of the techniques to reduce these emission species is through burning less fuel.

2.1.3.2 Oxides of Nitrogen

The oxides of nitrogen are divided into two types: nitric oxide (NO) and nitrogen dioxide (NO_2). Both are referred to as NO_x as NO is transformed into NO_2 due to the oxidation process occurring in the atmosphere. The following methods are used to produce NO_x emissions: Thermal NO, prompt NO, fuel NO and nitrous oxide mechanisms.

Thermal NO is generated in the combustor high temperature zones where the oxidation process of ambient nitrogen is taking place. The thermal NO rates are considerable at temperatures exceeding 1850K after which the correlation between its production and temperature becomes exponential. On the contrary, for the temperatures below 1800K and residence times of 5ms, a linear correlation between these both parameters and formation of NO applies. In the case of lean premixed combustors (i.e. ϕ<0.4), the NO production rate does not depend on the time. At lower temperatures and equivalence ratios values thermal NO is 5% of the total NO_x produced, while 60% can be found at higher temperatures and equivalence ratios.

Prompt NO is produced in the flame zone as a result of the contact between CH molecules and nitrogen, and its oxidations soon after, as shown in the following chemical notation:

$$\begin{aligned} &N_2 + CH \rightarrow HCN + N \\ &HCN + 2O_2 \rightarrow NO + CO_2 + OH \\ &N + O_2 \rightarrow NO + O \end{aligned} \qquad \textbf{(2.1)}$$

The prompt NO correlation based upon pressure is still under development. The conclusions drawn from the recent studies are that prompt NO represents 65% and 30% of overall NO_x at lower and higher values of temperatures and equivalence ratios, respectively.

Fuel NO is owing to the nitrogen contained in the fuel whose quantity can be between 0.06% and 1.8% for light and heavy distillates, correspondingly. The formation rate of these NO emissions is directly proportional to flame temperature and can be relevant to the overall NO emitted.

Nitrous oxide NO is formed from the interaction of the nitrous oxide (N_2O) (i.e. the ambient nitrogen oxidation) and O, H or CO as follows:

$$\begin{aligned} &N_2 + O \rightarrow N_2O \\ &N_2O + O \rightarrow 2NO \\ &N_2O + H \rightarrow NO + NH \\ &N_2O + CO \rightarrow NO + NCO \end{aligned} \qquad \textbf{(2.2)}$$

At lower temperatures and equivalence ratios nitrous oxide NO is between 30% and 40% while at higher temperatures and equivalence ratios is as low as 10%.

The NO_x emissions depend on the primary zone temperature exponentially (see figure 2.4). At 1900K approximately, NO_x formation is predominant due to thermal NO mechanism. Furthermore, fuel atomisation is another key driver in NO_x release because of the temperature effect. The fuel droplet size plays an important role in these species formation mainly at lower average equivalence ratios. Also, the residence time in the primary zone, which is in turn a function of the combustion volume and the chemical reaction rate, has a nearly linear correlation with thermal NO mechanism (refer to figure 2.5) leading to a log correlation of the total NO_x emissions.

There is proportionality between the NO_x emitted and the inlet pressure to the power n (i.e. P^n), where the exponent n varies from 0.5 to 1.4. This exponent increases for high values of primary zone temperatures related to high equivalence ratios (Lefebvre, 1999).

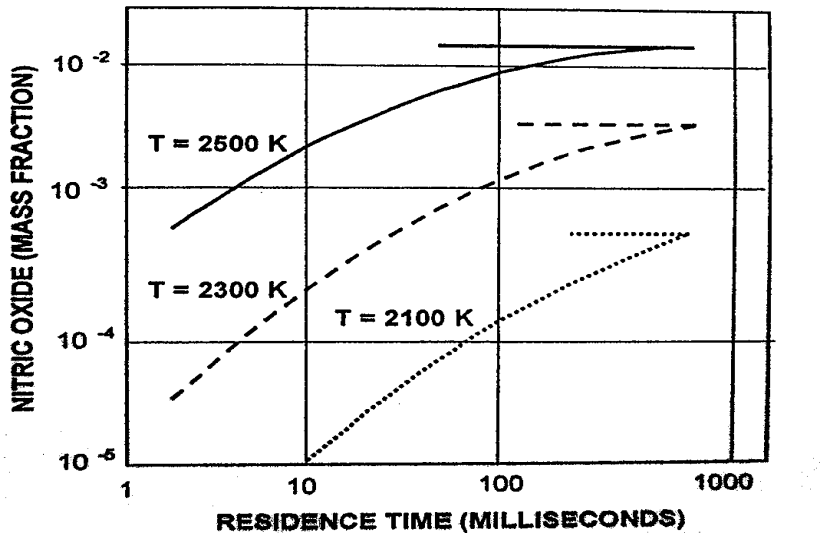

Figure 2.5: Effect of residence time on NO at several temperatures (Singh, 2007)

The mitigation strategies of NO_x formation based upon the previous discussions are, the use of lower combustor inlet pressures, smaller residence times (i.e. smaller primary-zone volume), lean mixtures, smaller primary zone temperatures and 'hot spots'. This can be achieved by means of better atomisers (reduction of hot spots), introducing additional air (lean mixtures) into the primary zone, and smaller combustion chambers. Another way to reduce the NO_x emissions is through water injection into the combustor so that the flame temperature is decreased; this would lead mostly to an aircraft weight penalty due to the additional component weight, therefore this method is not utilised in aero engines.

2.1.3.3 Carbon Monoxide

Carbon monoxide (CO) is formed in the combustor primary zone due to a lack of enough oxygen to complete the combustion such as the combustion process of a fuel-rich mixture at low temperature. Also, inappropriate combustion rates, short

residence time, inadequate fuel-air distribution and combustion products' quenching in cooling air lead to CO emissions. According to Lefebvre (1999), their formation rate is affected by the pressure and temperature at the inlet of the combustor, primary-zone equivalence ratio, ambient air temperature and the mean fuel-drop size. Low CO formation levels are found for high equivalence ratios where the oxidation rates are also high.

During the combustion of the stoichiometric mixtures, the carbon dioxides dissociation takes place which in turn produces further CO emissions. On the other hand, the pressures and temperatures inside the engine depend to some extent on the ambient conditions which affect the CO formation: Low ambient temperatures bring a high level of CO. Finally, at low power settings there is not enough room available in the combustion chamber (a bigger space of the primary zone is needed for atomization) for a complete combustion leading to an increment in CO.

2.1.3.4 Unburned Hydrocarbons

Emissions of UHC are generated due to incomplete combustion in regions of low temperature and/or short residence in the combustion chamber. These are circumstances that in most cases occur at low power conditions. The UHC emissions are reduced by redistribution of the air flow to bring the primary zone equivalence ratio closer to the optimum value (about 0.8), and by an increase in the primary zone volume and/or residence time (Lefebvre, 1999). Moreover, these are lowered by a reduction in liner wall-cooling air and by improved fuel atomisation.

Emissions of UHC are toxic and produce a hazard around the airports owing to their smell and potential to cause smog. The methods to mitigate UHC and CO are the same.

2.1.3.5 Smoke and Particulate Matter

The smoke formation is driven by pressure, fuel type and atomisation (Lefebvre, 1999). A rise in pressure leads to an extension of flammability limit and an increase in the chemical reaction rates as well as a reduction in the spray cone angle. Consequently, larger fuel droplets and a higher local equivalence ratio are created leading to additional fuel concentration in the flame high-temperature regions causing the smoke. Both physical and chemical properties influence the soot formation by means of fuel diffusion and atomisation and its molecular composition. Inappropriate atomisation gives rise to larger fuel droplets which are burned in a diffusion manner resulting in higher smoke levels.

Particulate matter is a common notation for various particles with differing chemical compositions which come in many different sizes and shapes and which can originate from a variety of different sources. With respect to particles from aviation, these can be divided into two different types: volatile particles and soot (Rogers et al., 2002). This sort of emission has come to be viewed by health experts and environmental regulators as one of the most serious pollution problems. Some harmful effects caused by particulate matter are: respiratory problems (such as asthma), reduction in visibility and contrail formation, among others.

2.1.3.6 Emission Mitigation Methods

Basically, there are two approaches to mitigate the emissions generated by the engine. By selecting an engine cycle with the lowest value of fuel consumed and combustor design improvements will result in a lower emission index.

Higher values of overall pressure ratios (OPRs) lead to a complete combustion, which in turn diminishes the fuel consumption (i.e. CO_2 emissions). But, for a conventional turbofan this approach produces higher NO_x emissions owing to an increase in the adiabatic flame temperature (i.e. nitrogen dissociation gets higher resulting in a growth of NO_x emission index). Consequently, trade-offs between NO_x and CO_2 need to take place. Higher BPR turbofans give rise to higher OPRs (more power must be taken out from the low pressure system to drive bulky fans) and in turn higher combustion temperatures resulting in more NO_x formation.

On the other hand, this increased NO_x production can be somewhat compensated for by using a new combustor design such as advanced double-annular, lean direct injection, lean premixed prevaporised, partially evaporating rapid mixing, and rich-quench-lean combustors. During this research only conventional combustors were used, but if data about those advanced combustors were made available then these could be included in the design frameworks to aid further understanding.

2.2 Aircraft Noise

Growth in air traffic has led the communities neighboring airports to push hard for strict restrictions on the aircraft noise. These are more stringent certification limits, penalties for airlines which do not meet the local noise legislation, and also to charge airlines and passengers with noise fees.

The operations during the night also are being restricted more and more. At Heathrow airport in London, for instance, only the quieter aircraft are allowed to take off and land during the night. In addition to that, the Department for Transport

developed a noise system called "Quota Count" (QC) (Anon., 1999), which is a cumulative points strategy based on the certification noise of the aircraft.

Bearing in mind the paramount importance of the noise issue, aircraft manufacturers like Airbus and Boeing use the QC system as key design guidance in their development of long haul aircraft such as the new A380. For this sector of the market the London QC limit sets the de facto world-wide noise standard as it is more stringent than the Chapter 4 standard agreed by the ICAO.

2.2.1. Noise Regulation

Before giving an overview of the current regulation, the noise metrics should be explained for a better understanding of the whole picture.

The noise in the aircraft is caused mostly by the pressure disturbances produced as a result of the flowing air discontinuities occurring on the airframe (e.g. high-lift devices and landing gear) and engines, which affects the communities living in the vicinity of airports.

Due to the non-linear response of the human ear and its sensitivity to a wide range of frequencies and pressure levels changes, a logarithmic unit (so-called decibel – dB) was introduced to measure noise intensity. This unit is defined as follows:

$$dB = 10\log_{10}\frac{SPL}{SPL_{ref}} \quad \textbf{(2.3)}$$

Where: SPL is actual sound pressure level and SPL_{ref} is a reference value, usually the threshold of hearing.

From the certification point of view, an aircraft for civil transport must meet FAA Part36 regulations, which are based on ICAO Annex 16 guidelines (Anon., 1999). Main measurement points during the certification phase are: flyover, sideline and approach (figure 2.6). The noise is recorded continuously at these points. The Effective Perceived Noise Level (EPNL), which represents the total level of the three points, must not exceed a certain limit based on the aircraft maximum take-off weight and the number of engines.

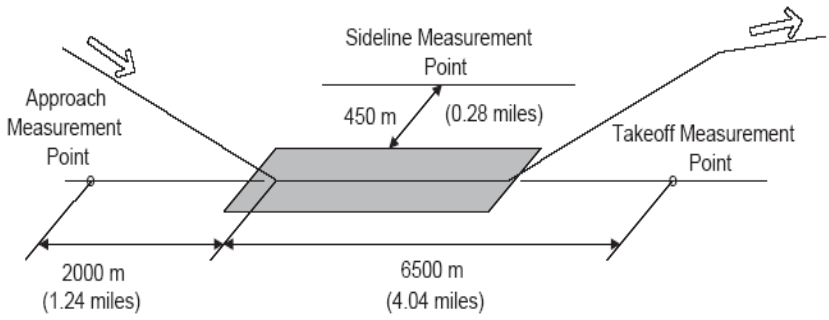

Figure 2.6: ICAO noise measurement points (Antoine and Kroo, 2002)

Usually, the community noise is reported in Day-Night Levels (DNLs), which considers the total sound energy (AdB) of the whole airport operation in a period of 24 hours. This figure is suitable for quantifying the total noise exposure of the airport operations, which considers fleet mix, runway usage and operational procedures.

The Effective Perceived Noise Levels are the noise metric in this research as its motivation is at the system level. This parameter is independent of airport, fleet mix and operational factors.

2.2.2. Noise Sources

Airframe-generated noise is a factor in the overall noise footprint of an aircraft; however the main contributor of the total noise is the engine. As part of this research the following noise sources are considered: fan and compressors, combustors, turbines, exhaust jets, and airframe. These noise sources follow different laws and generation mechanisms but all are affected by the airflow velocity at different levels, for instance, when keeping the same level of velocities, the variation of the jet noise has a stronger influence than that of the compressor or turbine noise (Rolls-Royce, 1986).

2.2.2.1 Fan and Compressor Noise

The noise caused by fans and compressors includes both tonal and broadband components.

Broadband noise is mainly generated by the motion of the fan tip through the boundary layer generated inside the inlet duct as explained in figure 2.7. Another contributor to the total noise is the turbulence that appears in the wakes of the fan blades. This issue is becoming important as there is a trend towards higher by-pass ratios (higher fan diameters).

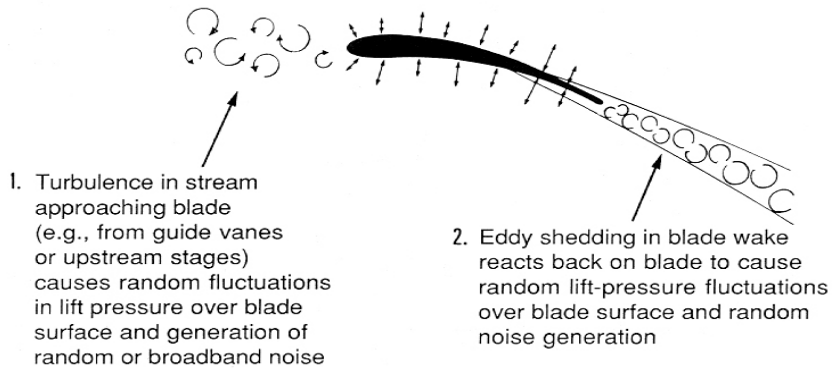

Figure 2.7: Fan broadband noise (Smith, 1989)

Tonal noise may be generated simply by the interaction between airflow disturbances and blade stages. This is particularly the case with fans where the flow relative to the blades at fan tip region is supersonic and then the propagation of shock waves occurs.

The other main source of tonal noise is the interaction between the lift fluctuations and the wakes produced from the guide vanes and rotating blades. Acoustic power is inversely proportional to the rotor-stator spacing, for this reason compressor stages are located in an optimum distance leading the wake interaction to become the most important phenomenon.

Furthermore, the interaction between the turbulence produced in the atmosphere and the rotating blades gives a component of noise.

2.2.2.2 Combustor Noise

The noise created in the combustor is considerable but is not the main component source of the overall engine noise spectrum, due in part to the fact that it is “buried” in the core of the engine. However, it contributes to the broadband noise because of the highly turbulent aerodynamic processes taking place inside the combustor.

2.2.2.3 Turbine Noise

The same principles applied for noise generation in fans and compressors can be used in the case of the turbines.

The turbine noise results from the interaction between the pressure fields and turbulent wakes from stationary and rotating blades giving tonal (single frequency) and broadband (a wide range of frequency) noise. Due to the higher spacing

between the turbine stages in the modern turbofans, the tonal noise is less important.

The turbine noise is radiated from the core nozzle because the Nozzle Guide Vane (NGV) is choked.

2.2.2.4 Jet Noise

The noise caused by the exhaust jet is associated with the turbulent mixing process between the exhaust gases and the atmosphere and is influenced by the sharing action produced by the relative speed between the exhaust jet and atmosphere.

Lighthill's theory shows that the above-mentioned action caused broadband noise that depends on the 8^{th} power of the jet velocity. At take-off conditions, the exhaust jet velocity of the turbojet or very low by-pass ratio turbofan is in a range of 500 to 600 m/s, thus giving huge levels of noise. In the case of high by-pass ratio turbofans, the total noise level reduces due to the lower values of jet velocities that can be as much as 50% less than in turbojets. Illustrating the high-power dependence between noise and jet velocities, for the same thrust level the reduction of 50% in velocity it leads to a 21 dB reduction in noise.

2.2.2.5 Airframe Noise

With the introduction of higher values of BPR in today's turbofans, the role of airframe-generated noise is expected to increase especially during approach and landing when the aircraft is in high-lift and high-drag configuration.

Broadband noise is generated by the clean airframe and tonal noise may be perceived as a result of the wing trailing-edge vortex shedding. Low-frequency tones have been detected due to the cavities and gaps in the airframe. To illustrate the impact of the cavities the following example is given. The Boeing 777 wing anti-icing exhaust vents were redesigned to get rid of a discrete tone that was higher than that produced by either the landing gear or lifting surfaces sources (McGregor and Wat, 2004).

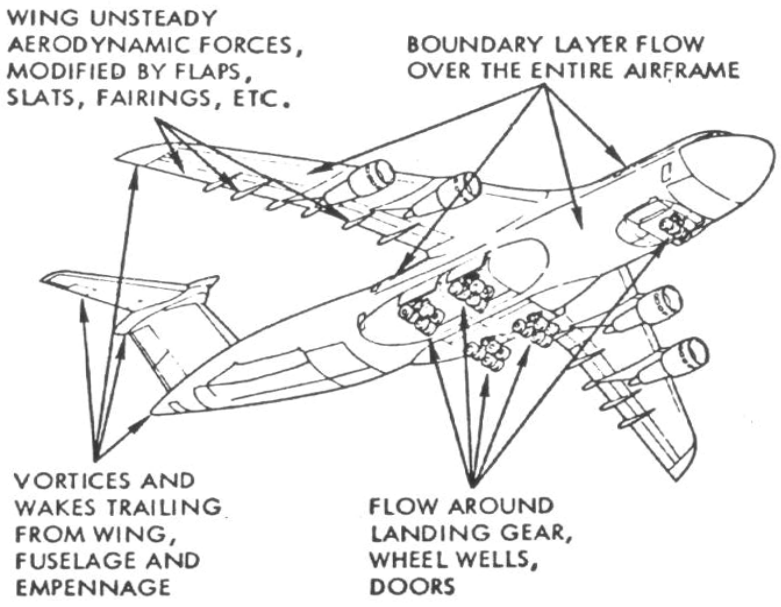

Figure 2.8: Airframe-generated noise sources (Antoine, 2004)

In figure 2.8 the airframe-generated noise sources are shown: the wings, tail landing gear, flaps and slats. The main contributors of the total airframe noise are the boundary layer shear and vortices shedding from the landing gear, high-lift devices (i.e. flats and slats) and other flow separation mechanisms (Antoine, 2004).

According to the theory, the total acoustic power is directly proportional to the 5^{th} or 6^{th} power of the aircraft speed. Experimental studies show that the power dependence may be lower.

2.2.3. Noise Mitigation Methods

The noise reduction at the source is approached in two ways by the aircraft and engine manufacturers: designing for minimum noise and using acoustically absorbent devices. Investing in these technologies will have effect only in the long-term.

For the short-term, the most effective method of reducing aircraft noise has been through the operational procedures: thrust back at take-off and Continuous Descent Approaches (CDA).

2.2.3.1 Engine Design Method

The noise generated by airflow disturbance - leading to turbulence - can be decreased by using minimal rotational and airflow velocities and optimum spacing between the rotating and stationary blades (less wake intensity) (Rolls-Royce, 1986). Besides, the ratio of the number of blades can be an important factor to hold noise inside the engine.

Increasing the BPR of the turbofan can bring a considerable reduction of noise due to the lower jet velocities (see figure 2.9).

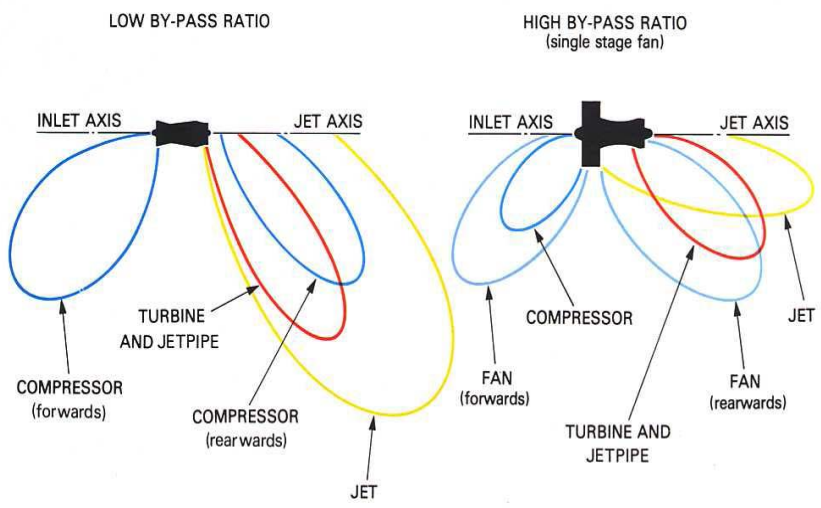

Figure 2.9: Comparative noise sources of low and high by-pass engines (Rolls-Royce, 1986)

As can be seen from figure 4.5, an increase of BPR from 6 to 14 gives a reduction of almost 50% in cumulative noise. These results were given by TERA - the tool developed as part of this research (refer to chapter 4).

2.2.3.2 Acoustically Absorbent Method

The absorbent methods applied in aero engines usually involve a porous skin held by a honeycomb backing (Rolls-Royce, 1986) so that the necessary space between the facesheet and the solid engine duct is provided. The skin acoustic properties and the depth of the liner are appropriately chosen depending on the noise characteristics. There are two main disadvantages regarding the liners, these are an increase in total engine weight and skin friction leading to an increase in fuel burn. Nevertheless, they are very strong noise suppression techniques.

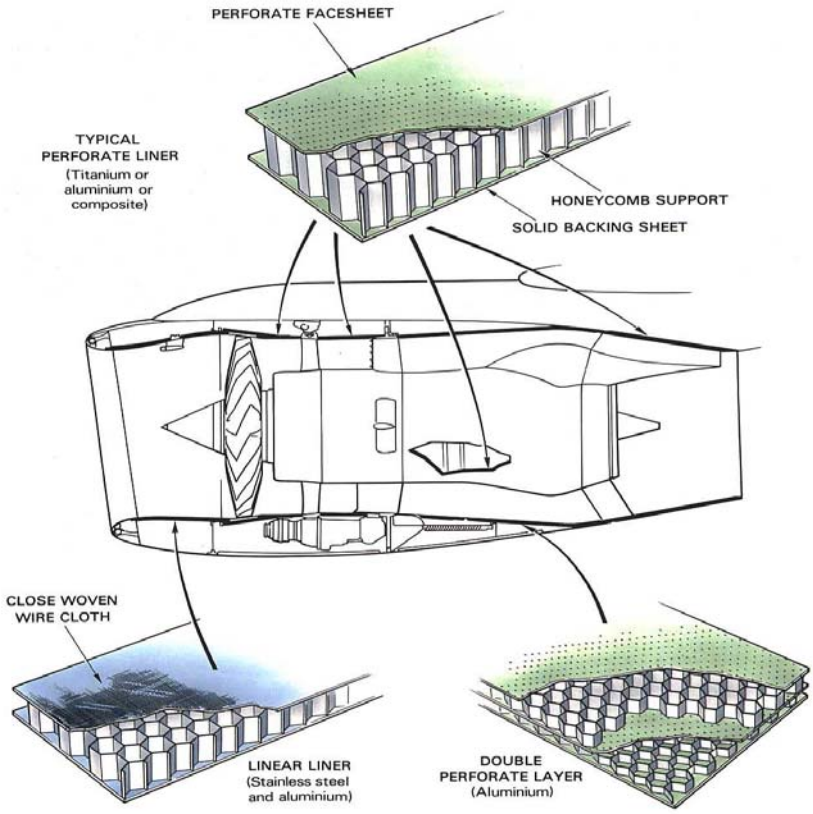

Figure 2.10: Noise absorbing methods in aero engines (Rolls-Royce, 1986)

2.2.3.3 Operational Method

During take-off, the approach used to minimise the noise exposure of the communities living near the airports is the thrust cutback method (figure 2.11). This method has been applied since the beginning of the turbojets era. Nowadays, the thrust cutback is still in used regardless of a very-high by-pass ratio found in the modern turbofans whose noise is much lower in comparison to the early turbojets.

The thrust cutback basically transfers the noise generated during take-off to another area. This is because the power required to reach cruise altitude is fixed causing the total noise produced throughout the climb to be fixed as well. It is worthwhile to mention, also, the aircraft climb angle is reduced leading to increase the location exposed to noise. Therefore, this method is suitable for airports located near to low population communities (e.g. airports near the sea) where the noise is considerably reduced, and the aircraft can continue its full climb promptly once the ocean is reached. According to the FAA and ICAO regulation, the pilots are allowed to carry out thrust cutback in an altitude range of 800 ft (240m) and 3000 ft (900 m).

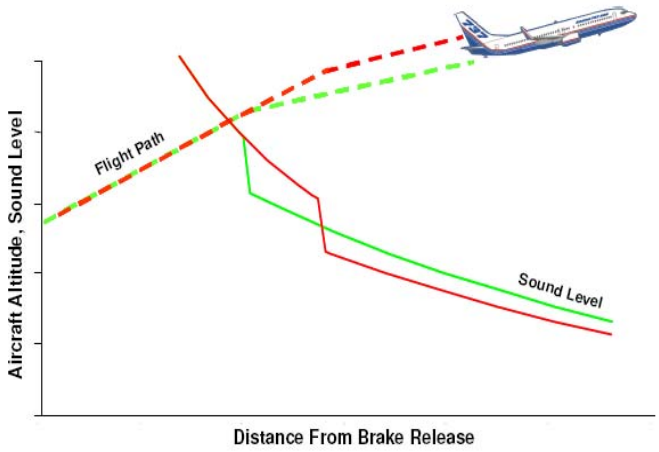

Figure 2.11: Thrust cutback on take-off: noise is displaced from the airport neighbouring communities (McGregor and Wat, 2004)

The conventional aircraft approach begins from the bottom level of the holding stack (an altitude of 6000 or 7000 ft) to descend to an altitude of 3000 ft (Anon., 2006). Then, the aircraft flies for several miles before intersecting the final 3 degree glide path to the runway. During this period of level flight, the pilot needs

to apply additional engine power to maintain constant speed. On the contrary, in the Continuous Descent Approach (CDA) procedure the aircraft remains in the holding stack for longer, descending continuously and avoiding any level flights prior to attaining the 3 degree glide path. A continuous descent requires significantly less engine thrust than prolonged level flight in the conventional approach. The benefits of CDA include significant reduction in noise, fuel burn and emissions, and shorter flights.

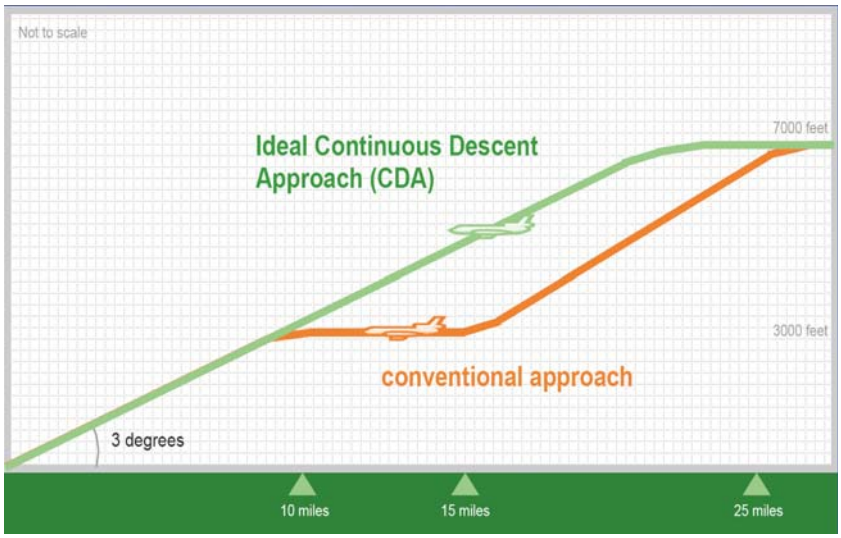

Figure 2.12: Comparison between a CDA and a conventional approach (Anon., 2006)

2.3 Aero-Engine Environmental Impact

2.3.1. Introduction

The majority of the subsonic civil aircraft cruise in the zone of upper troposphere and lower stratosphere where the emissions from the engine play an important role on the climate change. The effects are fostering the ozone formation along with a decrease in methane and also the cloud formation in the upper

troposphere leading to improving the greenhouse effect; and the ozone destruction in the lower stratosphere.

Based on the report issued by IPCC (1999), the aviation contribution to global warming is roughly 3.5% of the total human activities radiative forcing (measured in W/m^2), which is the overall net average of heating radiative imbalance of the earth's atmosphere due to anthropogenic and natural sources. According to Whellens et al (2002), this amount of radiative forcing is expected to increase by between 5% and 15% in 2050 due to the growth in aviation.

Another concern is the local air quality around the airports, which worsens along with the increase of the contamination from emissions generated by aircraft. This leads to human health problems.

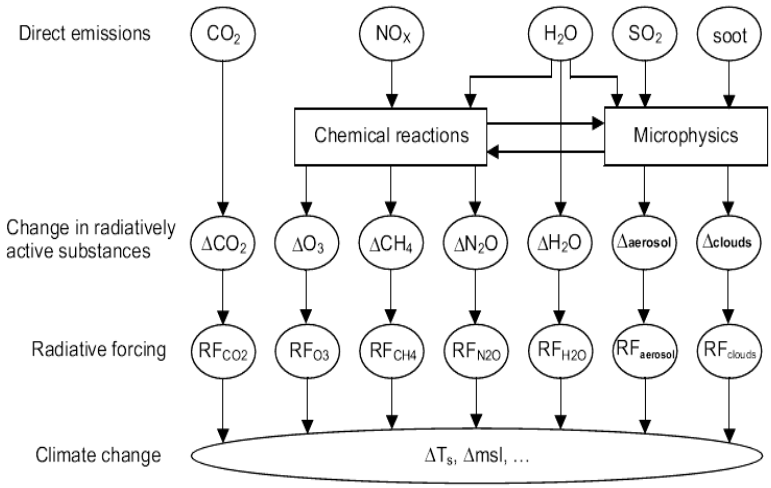

Figure 2.13: Aviation emission contribution to climate change (IPCC, 1999)

As stated in Whellens (2002) it is believed that the aviation emissions that contribute to global warming are those which have a straight radiative forcing influence, emissions which effect the radiative emissions concentration, and emissions which activate the formation of aerosol particles or other particles which give rise to disturbances in normal cloud formation (i.e. contrails). The figure above shows different means by which the aviation emissions have influence on the concentration of the active chemical substances leading to the radiative forcing impact, which in turn produce an increase in the Earth's surface temperature as well as a rise in mean sea level.

The current fuel has both carbon and hydrogen that, after their combustion, generate primary combustion products: carbon dioxide (CO_2) and water vapour (H_2O), and secondary ones such as: carbon monoxide (CO), unburned hydrocarbons (UHC), oxides of nitrogen (NO_x), oxides of sulphur (SO_x) (if the fuel contains sulphur) and particulate matter (Rogers et al., 2002). CO_2, H_2O, NO_x and SO_x matter are of paramount importance with regard to global concerns, as are CO, UHC, NO_x and particulate to local air quality.

CO_2 and H_2O emissions are directly proportional to the fuel burn, hence any changes in their formation magnitude depend on the fuel consumed or the fuel composition variation. The former can be reduced by improving engine overall efficiency or minimising the power plant weight, and the latter by means of using alternative fuels such as hydrogen or bio-fuels. Additionally, an improvement of aircraft aerodynamic efficiency gives a decrease in fuel burn. The emission index of these emissions is based on the kind of fuel being burned as well as on the combustion efficiency whose value is roughly 0.99 in the entire flight mission.

Carbon dioxide is a long-lived gas whose life time in the atmosphere is between 100 and 150 years or more (Rogers et al., 2002). A growth in its concentration changes the atmosphere radiative balance leading to a warming of the

atmosphere called global warming. The current CO_2 contribution of aviation is thought to be 2% of the total human activities source. This value is expected to rise due to the predicted growth in aviation throughout the next 100 years. The quantity and impact of these emissions are unchanged notwithstanding the flight altitude.

Water vapour can affect the environment radiatively in two ways: directly or indirectly, that is through the formation of contrails (see figure 2.14) which may produce a warming effect. Furthermore, it influences the oxides of nitrogen during its reduction process of methane.

Figure 2.14: The contrails of a four-engined aircraft (Wikipedia, 2007)

According to the studies carried out, the contrails contain long-wave or infrared radiations coming from the Earth's surface at a higher rate in comparison to those from the Sun causing warming effect. Nevertheless, there is a level uncertainty regarding this effect owing to the season of year, humidity, the flight day, and so on. For instance, concentrations of contrails are more likely during night flights and in winter seasons. These contrails can turn into cirrus cloud which may

warm or cool the Earth (refer to figure below). For further details of contrails and cirrus cloud, please refer to Noppel et al (2007, 2008 and 2009) and Schumann et al (2000).

The research performed by IPCC (1999) concluded that the direct water vapour effect on the climate in the troposphere is very small but still considerable. Also, the secondary effects are being investigated.

Figure 2.15: A sky filled with cirrus clouds (Wikipedia, 2007)

NO_x emissions result from atmospheric nitrogen oxidation in the flame zone at high temperature. The formation process is endothermic at temperatures above 1800K. These emissions are divided in two species: oxides of nitrogen (NO) and dioxides of nitrogen (NO_2) derived from NO oxidation. For better understanding of NO_x formation, a detailed chemical kinetics is required. Its highest level can be achieved at full power setting, i.e. take-off condition.

The following key NO_x formation mechanisms occur in the aero-engines:

- Thermal NO mechanism implies atmospheric nitrogen oxidation in the flame zone of high temperatures, therefore it relies on flame temperature and residence time within the burner.

The highest values of NO emission are located on the stoichiometric lean area where the high temperature and high oxygen concentration meet.

There are several relationships are found from the public domain for NO_x emission index (EI) calculation: An equation given by Singh et al (2007) is based on the temperature at the entry of the combustor, which in turn affects the flame temperature; Roffe and Venkataramani (1978) arrived at the correlation for NO_x EI as a function of adiabatic flame temperature and residence time using mixtures of propane-air; also, Anderson (1975) investigated the influence of the residence time on NO_x formation within pre-mixed and pre-vaporised combustors provided with gaseous propane fuel concluding that NO_x emissions are directly proportional to the residence time in the combustion chamber.

- Prompt NO takes place for flames of low temperature and are fuel rich. Its formation mechanism is not well known, thus prompt NO emissions are not accurately estimated.
- Fuel NO is produced during the combustion process where nitrogen is contained in the fuel. Where the total fuel nitrogen is very small then this mechanism can be deemed irrelevant.

During the combustion at full power settings, the main NO_x formed is NO. The NO_2 formation process is complicated and may involve numerous mechanisms which are determined by the engine power setting. The transition from NO to NO_2 occurs in the atmosphere where low temperatures and the substantial amount of air

are available. Also, this transition happens at idle conditions achieving sometimes a transfer rate of 50%.

The NO_x emissions have two major consequences depending at which altitude they are discharged:

- At ground level, the NO_x production experiences the highest level when the engine runs at full power resulting in an increment in ozone concentration by means of a photochemical reaction, which may produce respiratory disease, eyesight damage, headaches and allergies (Lefebvre, 1998).
- At altitudes lower than 15 km, the NO_x emissions have an indirect effect on the atmospheric ozone and methane, that is, these species trigger an increase of ozone adding to the global warming as well as atmospheric OH formation which reduces the lifespan of CH_4 according to Tintani (2001) thus lowering the global warming impact. In addition, these emissions contribute to acid rain that may injure trees directly or indirectly through the soil.
- At altitudes higher than 15 km, NO_x emissions result in ozone depletion thus rising Earth's ultraviolet radiation leading probably to skin cancer and eye problems (Singh, 2007).

In summary, the ozone lifespan is a function of altitude and latitude increasing with altitude. There are more ozone sources in the troposphere than in the stratosphere where most civil aircraft transport flies. Methane (CH_4), as a greenhouse gas, tends to warm the atmosphere due to its Earth-infrared radiation absorption and its release back to the atmosphere. However, the NO_x emissions decrease the methane concentration in the atmosphere by the reaction of NO_2 which encourage the production of ambient hydroxyl radicals (-OH) reacting with CH_4 to arrive at the methyl radical leading to a process called global cooling. The reduction of CH_4 changes with the altitude where the emissions occur, it improves with altitude.

Other emissions like unburned hydrocarbon (UHC) and carbon monoxide (CO) are very toxic and hazardous around airports. The CO decreases the faculty of the blood to absorb oxygen and at high levels it can lead to asphyxiation and even death (Lefebvre, 1998).

2.3.2. Greenhouse Effect

The Earth's climate system is made up of the following main constituents: the atmosphere, the hydrosphere, the cryosphere, the lithosphere and the biosphere. These constituents are coupled together through fluxes of mass, heat and momentum. The interactions between them are poorly understood or even unknown. For a deeper explanation about the climatic system the reader is directed to ICAO's environmental report (2007).

In order to maintain certain stability in the climatic system, the inward solar radiation and the outgoing radiation have to be in equilibrium (figure 2.16): Approximately 31% of the inward solar radiation is given back to the atmosphere, clouds and Earth's surface and the remaining 69% is partially retained by the atmosphere and used to warm the Earth's surface (i.e. roughly 168 W/m^2) leading to heat release (i.e. water vapour, infrared radiation and so on) (IPCC, 2001).

The greenhouse gases absorb some of the above-mentioned radiation and then discharge them in all directions; this is what heats up the Earth' surface causing the mean temperature to be increased, this process is described as the greenhouse effect. These gases are carbon dioxide (CO_2), nitrous oxide (N_2O), methane (CH_4), ozone (O_3) and water vapour (H_2O).

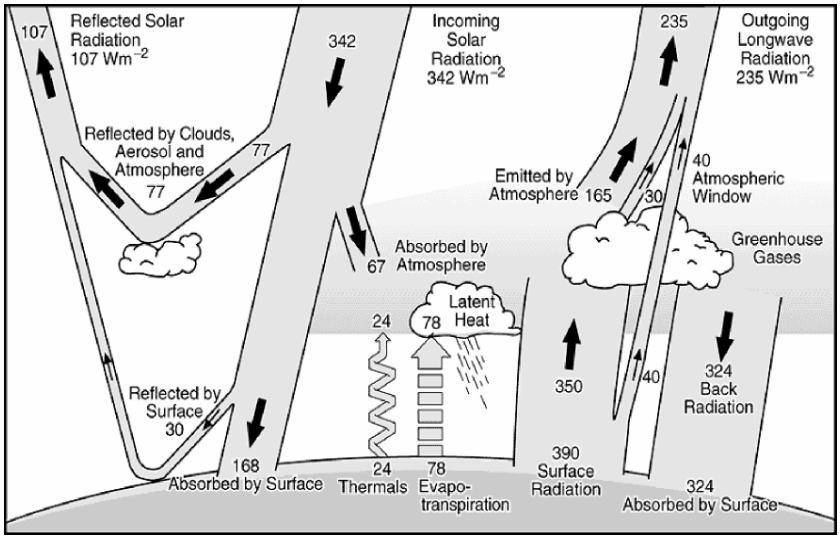

Figure 2.16: Annual global mean energy balance (IPCC, 2001)

Most of these gases are produced by the anthropogenic activities mainly from the fossil fuels' combustion. Furthermore, these are other greenhouse gases produced by human activities, these gases are namely: chlorofluorocarbons (CFCs) and chloride and bromide compounds. Their impact is stronger than that of the CO_2 emissions and their contribution to the depletion of the ozone layer make it necessary to treat these emission species seriously.

Due to the high level of uncertainties resulting from the extreme non-linearity of the processes implied and the fact that many climate system's constituents possess diverse reaction times to a climate change, it is very difficult to detect which greenhouse specie is responsible for a particular climate change. Also, there is a difficulty in detecting whether the climate change is caused owing to a natural phenomenon (i.e. solar variation and volcanic activities) or to human emissions (i.e. greenhouse gases and aerosols).

In IPCC (2001) several model simulations were run and compared to observed data (figure 2.17). As shown in this figure, the warming in the first half of the 20th century probably was due to natural sources, however in the second half an unexpected change in the results led the scientist community to conclude that it was due to anthropogenic effects.

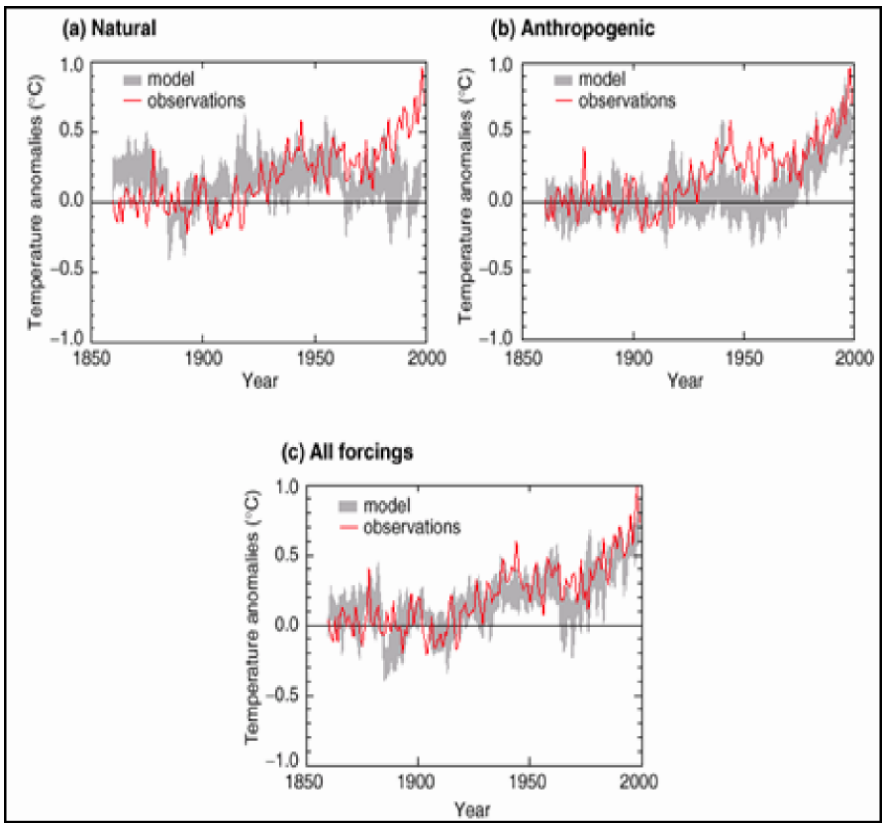

Figure 2.17: Annual global mean surface temperature variations (IPCC, 2001)

2.3.3. Climate Change

The depth of the troposphere varies from one hemisphere to another having a range of 7 to 10 km for the northern hemisphere, where the majority of the civil transport flights take place, while for the mid-latitudinal zone (i.e. equatorial belt) it is between 15 and17 km. The troposphere is based mostly on water vapour and a small amount of ozone, whereas the stratosphere is essentially made up of ozone.

The expression ‘climate change’ means changes (such as wind patterns, mean precipitation and mean temperature) in the mean weather in a specific zone due to modifications in the human activities, sunlight intensity and Earth’s dynamic processes. The world leaders are more concerned about human activities because they can be controlled by the mankind. From the total anthropogenic emissions only about 2% is assigned to aviation but this percentage is expected to increase in the near future due to grow in air traffic. As determined by some studies, the global mean temperature in the atmosphere is believed to increase from 1^{o} to 5 ^{o}C throughout this century.

Some effects of the global warming are described as follows (Tintani, 2008):

- Coastal land loss: The coastal lands are disappearing due to the increase in sea levels which is exacerbated by melting icebergs located in the polar seas as the mean temperature rises. This could lead to the population displacement since alluvia make the ground uninhabitable as has occurred in Europe and the States recently; also, this can cause the disruption to the farming areas (crops) leading to a food crisis, and the pollution of bodies of water causing water shortages.

- Severe weather conditions: Global warming is supposed to cause natural disasters i.e. cyclones, hurricanes, alluvia and droughts; since the sixties the amount of natural disasters has increased three times.
- Spread of contagious diseases: Warmer and wetter weather facilitates the contagious diseases, such as malaria and yellow fever to be spread to new regions.
- Economical effect: Countries whose economies are based mainly on the tourism sector could undergo a drastic decrease in their gross domestic product (GDP) due to the reduced flow of tourists caused by the natural disasters which are in turn proof of global warming.

2.3.4. Contribution of the Aviation to Climate Change

The Intergovernmental Panel on Climate Change (IPCC) made public for the first time the aviation emissions' effect on the atmosphere through a report called 'Aviation and the Global Atmosphere'(IPCC, 1999 and Whellens et al, 2002) in which the following findings were obtained:

- In 1990 aviation discharged over 600 million tonnes of CO_2 to our atmosphere.
- Aviation contributes nearly 3.5% of the global warming coming from the entire human activities.
- Aviation pollutants are expected to increase and may be responsible for up to 15% of global warming over the next 50 years.

Figures 2.18, 2.19, and 2.20 depict the aviation contribution regarding global warming as given by the IPCC in 1999 and its update later on.

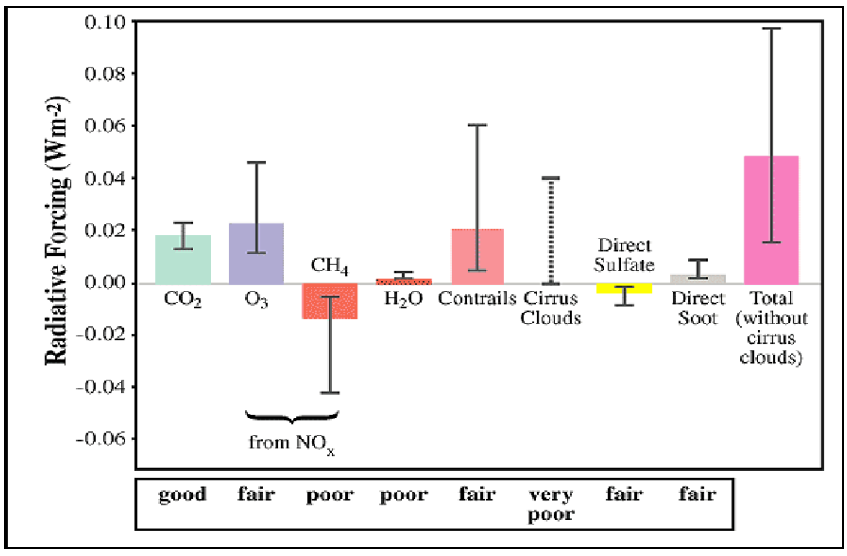

Figure 2.18: Worldwide mean radiative forcing from subsonic aviation pollutans in 1992 (IPCC, 1999)

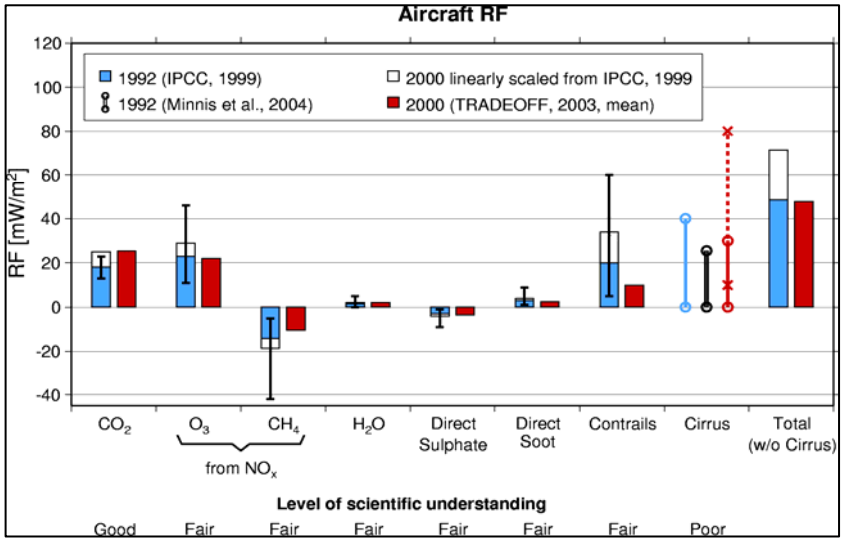

Figure 2.19: Updated radiative forcing for 2000 (Sausen et al, 2005)

Water vapour (H_2O) and nitrogen oxides (NO_x) generated from the combustion process of aero engines are relevant greenhouse gases. H_2O facilitates the emergence of contrails which consecutively lead to the formation of cirrus clouds. Both contrails and cirrus clouds warm the surface of the Earth increasing the aviation global warming impact. NO_x emissions become an important issue where the number of commercial supersonic flights rise as these emission species could cause destruction to the ozone layer by its depletion at high altitudes where these flights would usually take place. In general, the H_2O and NO_x emissions comprise almost two-thirds of the impact of aviation on the atmosphere, therefore any approach to minimise aviation emission must take into account other gases besides CO_2 .

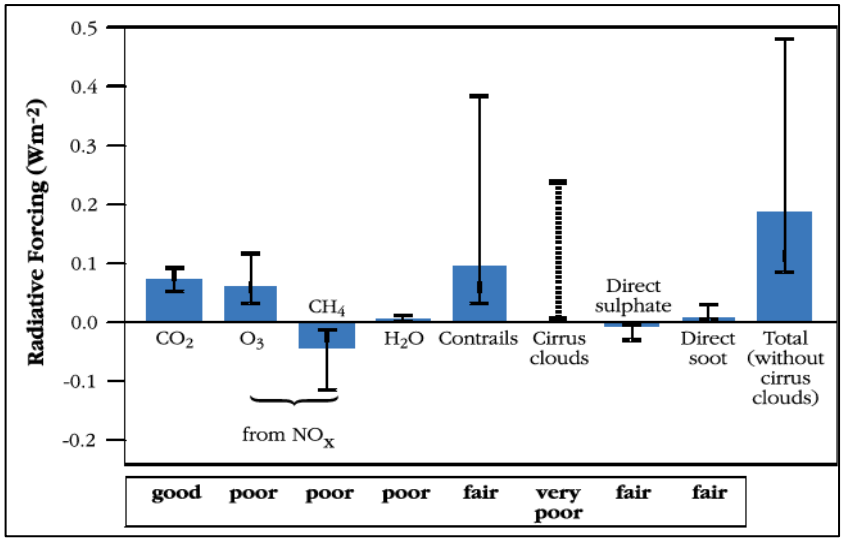

Figure 2.20: Radiative forcing from subsonic aviation pollutants in 2050 (IPCC, 1999)

2.3.5. Metrics for the Climate Change Impact

Two main approaches exist in the scientific community to measure the climate change impact of the greenhouse gases on the atmosphere, they are as radiative forcing (RF) and global warming potential (GWP). There is a lot of discussion regarding which approach to be used. Additionally, another method is proposed with similar way of assessment as that of GWP called global temperature potential (GTP). Both GWP and GTP are based on the RF.

For more accurate predictions, the researchers sometimes utilise atmospheric models which consider the description of how the atmosphere works. This description relies on the following factors: knowledge of the processes, the time scale of interest and the availability of computer resources. The majority of these models use meteorological fields obtained from either global circulation models (GCMs) or analysis based on observations (Marais et al, 2008).

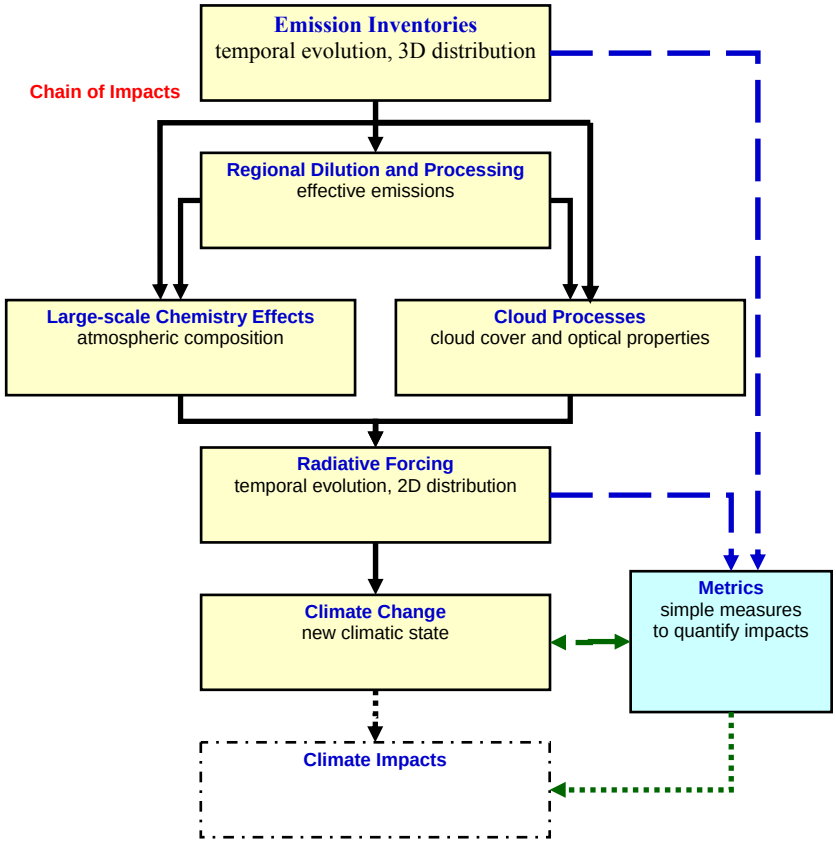

Figure 2.21: Flow diagram for emissions and their climate change impact analysis (Tintani, 2008)

The first step in the figure above is to generate emissions inventories followed by an analysis of their regional and global dilution processes at large-scale chemistry and cloud level. Then the RF, owing to these emissions and processes, is quantified allowing for the climate change impact to be assessed by means of a climate model based on the atmosphere radiative balance.

For a more detailed explanation about the radiative forcing modelling, please refer to Tintani (2008) whose thesis was developed as part of this PhD project.

2.4 New Aero-Engine Concepts

2.4.1. Recuperated Aero-Engine

This is a type of cycle which is widely used in ground gas turbine plants to increase the thermal efficiency thus reducing the SFC. It is not yet used in aero engines mainly because of the difficulties related to the size and weight of the recuperator. Nevertheless, its introduction can have positive results in terms of fuel consumption and emissions levels. Additionally, the jet velocity reduces causing a reduction in specific thrust and an increase in propulsive efficiency (Walsh and Fletcher, 2004).

Figure 2.22 shows a schematic diagram of a turbofan engine with recuperator. The air delivered by the high pressure compressor (HPC) is heated before entering the combustor by the hot gases which expanded in LPT by means of the recuperator. In this way it requires less fuel to raise the gas temperature at the fixed turbine entry temperature (TET).

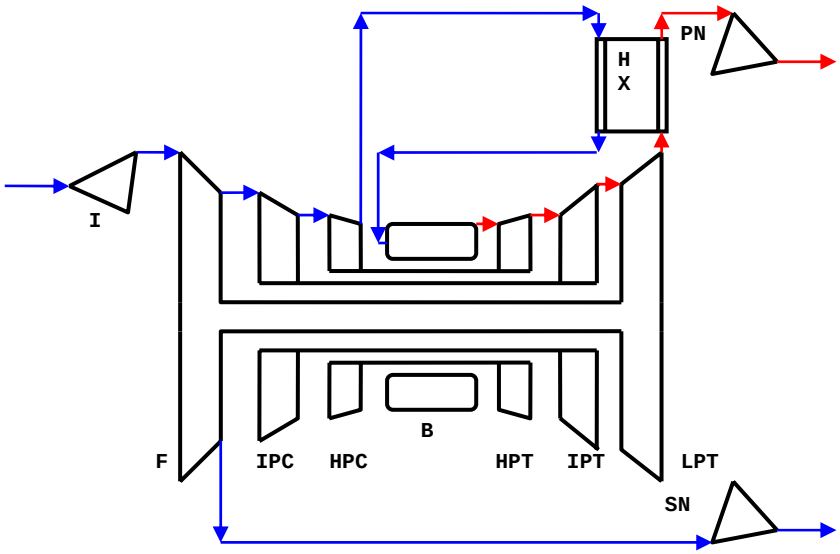

Figure 2.22: Scheme of a turbofan with recuperator

The behaviour of a turbofan with a recuperator in design and off-design conditions have been analysed for effectiveness of different recuperators (Andriani and Ghezzi, 2000 and 2005; Pasini, S. et al, 2000). The results were compared with that of a modern high by-pass ratio turbofan giving interesting results in terms of SFC and overall efficiency as reported in figure 2.23.

Apart from that, different locations of the recuperator such as: before entering the hot nozzle both during and after the expansion in it, were assessed; the first configuration seems to ensure good results, at least according to numerical simulations (Pasini et al, 2000).

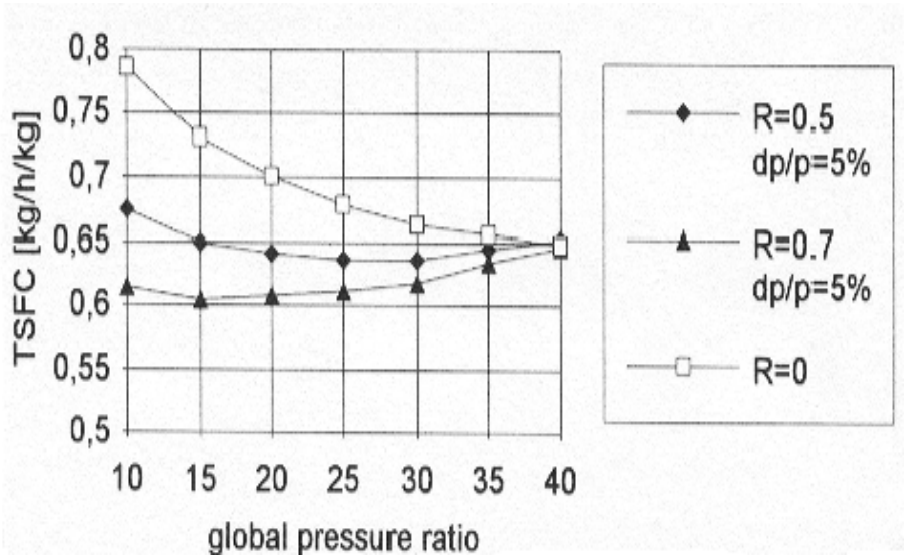

Figure 2.23: SFC for a conventional turbofan and two regenerated turbofan engines (Altitude=1000 m and flight Mach number = 0.8) (Andriani and Ghezzi, 2005).

2.4.2. Intercooled Aero-Engine

In this cycle the introduction of an intercooler gives an improvement of specific output (power or thrust) but at the expense of a reduction in thermal efficiency, hence an increase in SFC (Walsh and Fletcher, 2004).

It involves dividing the compression process into two or more stages, cooling down the air temperature between the outlet of one stage to the inlet of the following (see figure 2.24). With fixed overall pressure ratio (OPR), the work necessary to increase the air pressure is less with respect to the simple cycle. In the case of aero engines, since the compressor absorbs less power, it becomes available in the hot nozzle to be converted in thrust. But in order to offset the heat removed from the compressors more heat input (fuel flow) must be required (Walsh and Fletcher, 2004).

An improvement of thermal efficiency of this cycle can be achieved by means of an increase of OPR – overall pressure ratio (Andriani and Ghezzi, 2005). Usually this parameter is restricted by the following: for a given TET, there is an optimum pressure ratio in terms of the highest efficiency; the materials used for compressors, their tolerance to high temperatures; and finally the need to cool the turbine. A higher compressor exit temperature will require a large air bleed and this will result in a negative impact on the cycle. Because of that the recuperator is introduced in order to avoid the loss in thermal efficiency at low OPRs, as discussed in the next section.

This practice is not new and many power systems adopt it to increase the output power; it is not yet implemented in aero engines. However, NEWAC project is considering Intercooled High OPR concept (NEWAC, 2006). It can be conceived in two ways, as follows:

- For a given cycle pressure ratio and combustor technology, the NO_x will be lower due to lower combustor entry temperature.
- For a given NO_x level and material technology, the cycle pressure ratio can be increased leading to CO_2 reduction.

In order for this concept to be viable the following technology is required:

- Compact and efficient intercooler.
- Aggressive duct technology for minimised weight and pressure loss.
- Compressors with improved transient behaviour when integrated with an intercooler.
- Improved high pressure compressor to realise a high OPR and compensate for pressure loss and weight penalty of intercooler.

2.4.3. Intercooled and Recuperated Aero-Engine

This results from the combinations of intercooled and recuperated cycles. The thermal efficiency loss due to intercooling is compensated by recuperation (Walsh and Fletcher, 2004).

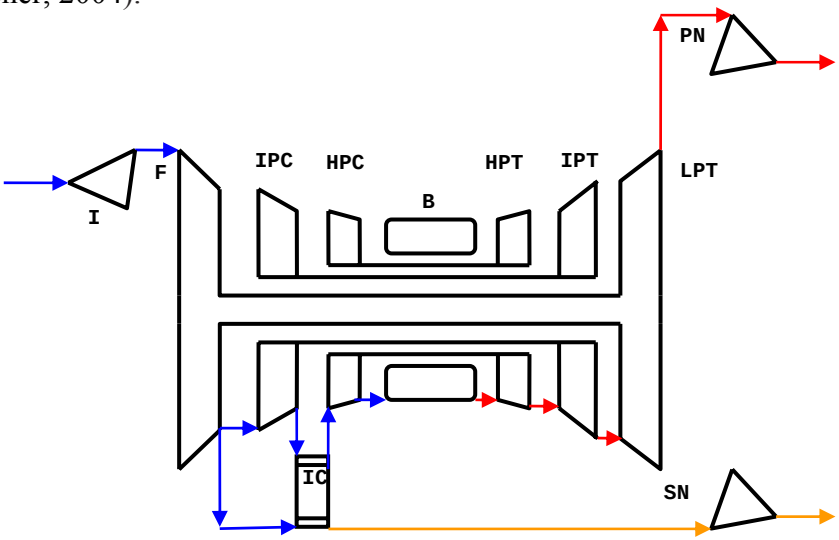

Figure 2.24: Scheme of a turbofan with intercooler between LPC and HPC

The recuperator transfers heat from the exhaust gases to the high pressure discharge air at the combustor inlet. This temperature rise of the air does not need to be generated by fuel injection and thus contributes to the reduction of fuel consumption and emissions of the engine (Wilfert et al, 2005; da Cunha Alves et al, 2001).

By using the intercooler between compressors and exploiting the energy in the exhaust gases, the thermal efficiency is noticeably improved in comparison to simple, intercooled, and recuperated cycles.

The intercooler allows reduced air temperature at the entry of HPC leading to less power being demanded of it. On the other hand, this permits a larger temperature difference between the delivered air and the exhaust gases, leading to an efficient temperature increase upstream, ahead of the combustor.

In practice, the intercooled and recuperated cycle has been used to improve gas turbine performance, mainly at part-load operation. This sort of cycle has given good results in naval propulsion applications.

For aviation propulsion, this concept has been introduced recently, being dubbed IRA: Intercooled Recuperative Aero Engine (Mühling and Vollmuth 2002). As shown in figure 2.25, the engine configuration is based on an advanced high by-pass ratio 3-shaft concept. This configuration features a geared fan, an intermediate axial-radial compressor, an intercooler and a high pressure radial compressor. The compressed air passes through the recuperator before entering the combustor. The inlet guide vane nozzle area of the LPT is varied for every operating point, in order to keep the TET as constant as possible (Krammer et al, 2003). A more detailed description can be found in Wilfert and Massé (2001).

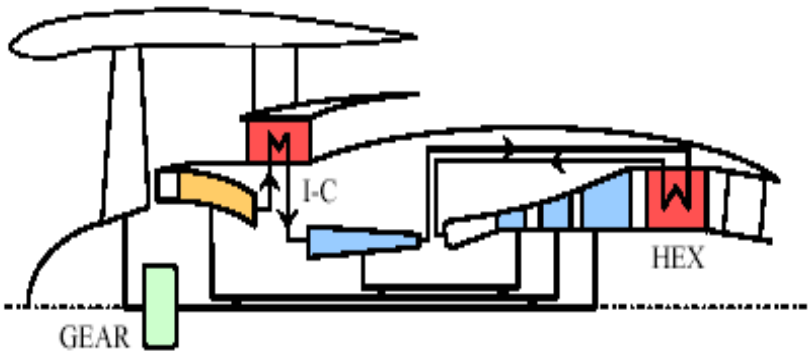

Figure 2.25: IRA concept (Boggia and Rüd, 2004)

The EU-funded CLEAN (Component Validator for Environmentally-Friendly Aero-Engine) (5th Framework Program) demonstrator was led by MTU Aero Engines and Snecma Moteurs and has been aimed at the validation of the components of this above configuration. This campaign was successfully completed in December 2005 after a test period of two and a half months (Wilferet et al, 2005).

The GTF and IRA studies on an optimised aircraft architecture proved that the targets set by the programme can be accomplished (see figure 2.26). CLEAN was only the first step specifically for IRA. Future validations will be carried out (Wilferet et al, 2005).

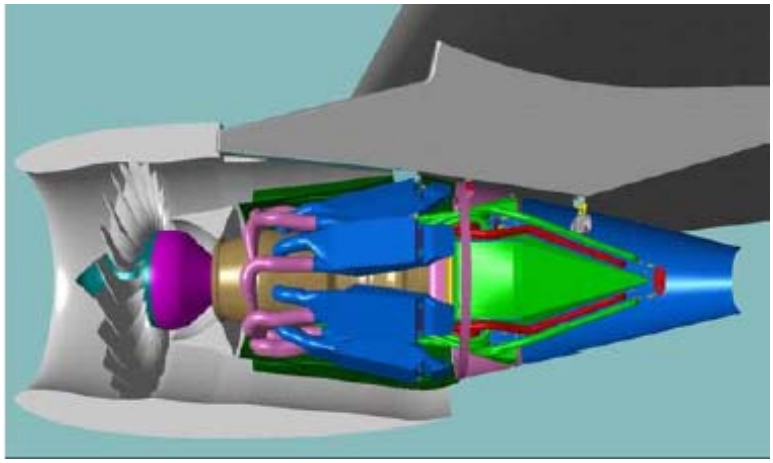

Figure 2.26: On-wing installation of IRA (Boggia and Rüd, 2004)

Boggia and Rüd (2004) have simulated the thermal (core) efficiency for different but consistent cycles (consistent technology level and same simulation tool). As seen from figure 2.27, IRA cycles offer higher efficiencies in comparison to other cycles with lower OPR values. Thus NO_x formation will be reduced as well as the engine core weight.

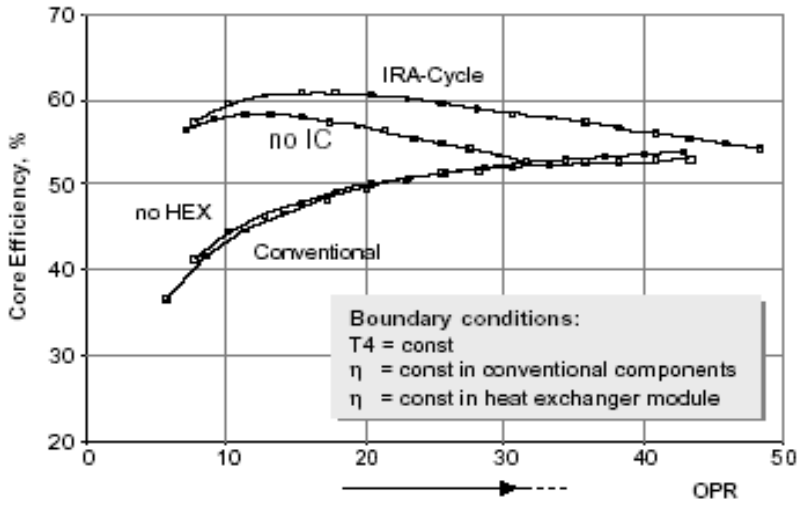

Figure 2.27: Thermal efficiencies of conventional, intercooled, recuperated and IRA concepts (Boggia and Rüd, 2004)

A feasibility study for intercooled and/or recuperated turbine engines (IRA-engine) for medium to long range commercial transport applications has been performed from aircraft fuel consumption and operating cost point of view (Lundbladh and Sjunnesson, 2003). The results show that a recuperated engine will not yield a lower operating cost or fuel burn. An engine with a mid-compressor intercooler may give significant reduction of fuel burn and a slight reduction in costs, if the new technology is accepted. The intercooled and recuperated cycle, while being superior in its ideal form, can only compete at a fuel price several times higher than current prices.

Thermal and stress characteristics of the recuperator invented by MTU have been analysed in order to produce a reliable life prediction of it, that is: creep and low cycle fatigue prediction (Schönenborn et al, 2004). This combined analysis shows the high life potential of the recuperator which is important for economic operation of a recuperative aero-engine.

Also, NEWAC is considering this configuration along with the following technological requirements (NEWAC, 2006):

- Optimised recuperator arrangement in the exhaust of an aero engine including flow field investigation and model testing.
- Innovative duct design to minimise the weight of the system and pressure losses due to friction.
- Innovative miniaturisation of profile tube recuperator configurations including component tests.
- Innovative integration of accessories for low weight and size.

2.4.4. Interstage Turbine Reheat Aero-Engine

This cycle also known as Interstage Turbine Burner (ITB) is relatively new in modern jet engine propulsion. The expanding gases from HPT are reheated before the next expansion process in LPT, as shown in figure 2.28. The fuel is burnt at a higher pressure than a conventional afterburner, leading to a better thermal efficiency. The major advantages associated with the use of this sort of cycle are better thrust and potential reduction in NO_x emission. As can be seen from figure 2.28 the TET remains unchanged. As the gas flow undergoes secondary combustion, higher specific thrust is achieved. This results in a smaller and a lighter engine and hence, lowers cost and increases payload (Liew et al, 2003 and 2004; da Cunha Alves et al, 2001).

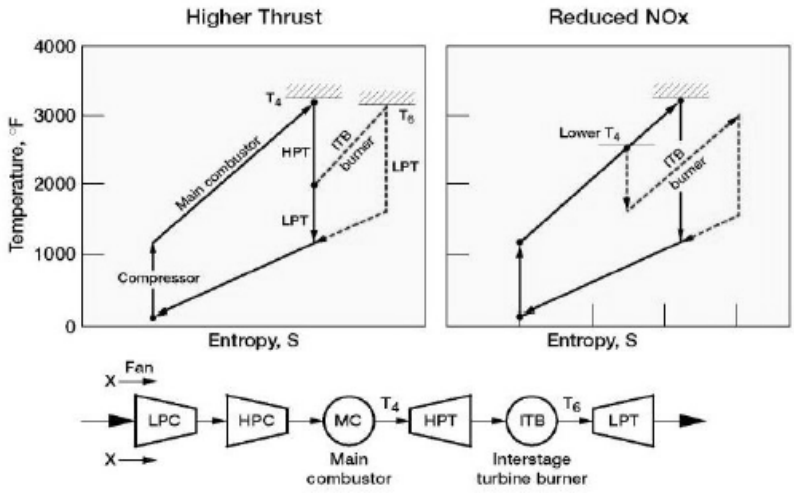

Figure 2.28: Thermodynamic cycles of a turbofan with ITB (Liew et al, 2003)

Recent studies of on-design and off-design conditions on this sort of cycle for a high-bypass turbofan with an ITB can be found in the literature (Liu and Sirignano, 1999 and 2001; Liew et al, 2003; Chiu, 2004; Liew, et al, 2004). These studies showed that the ITB engine gains more benefit when operating at higher

flight Mach numbers. It provides a design basis for high-performance engines applicable to lightweight and/or high-speed aircraft.

As discussed in Liew et al (2003) there are many issues that needed to be resolved before implementing the aforementioned cycle in aero engines: high velocities with possible swirl in transition ducts in terms of the flame stability and the ITB performance; redesign of the LPT cooling system; and integration and complexity of a second combustor, including all associated cooling and control requirements.

2.4.5. Wave Rotor Aero-Engine Topped

There are several unsteady flow devices such as: shock tubes, shock tunnels, pulse combustors, pulse detonation engines (PDE) and wave rotors where the energy transfer is by means of pressure waves (Akbari et al, 2006a).

In the particular case of a wave rotor device the energy transfer can be made straightaway among different fluids without using mechanical components such as compressors and turbines, through generating compression and expansion waves in special channels. Therefore, use of wave rotors in a turbofan leads to overall engine weight reduction due to the removal of a compressor, for instance: HPC.

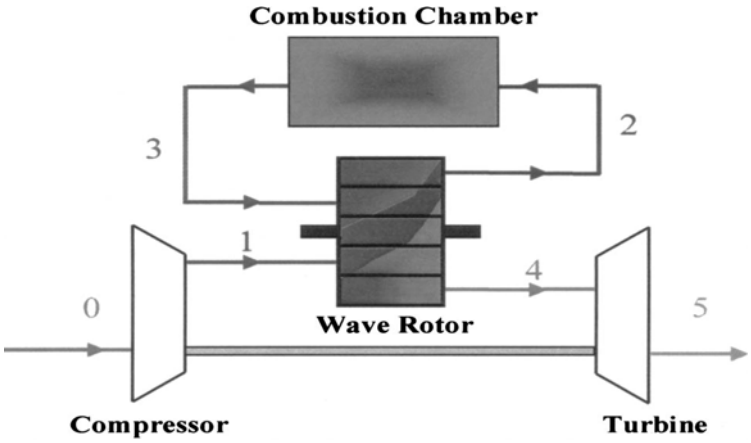

Figure 2.29: Concept of a gas turbine topped by a through-flow wave rotor (Akbari et al, 2006a)

Some advantages of wave rotors are to produce large pressure changes in short time or distance, to withstand transient peak fluid pressures and temperatures, and to be self-cooled. This pressure gain produces an increase in specific thrust and a reduction in SFC. On the other hand, the disadvantages found in this arrangement are sealing, thermal expansion, and turbine cooling system issues, among others.

In the public domain, two main wave rotor configurations have been found: through-flow wave rotor, which is more suitable for gas turbine application, and reverse-flow wave rotor for low-temperature application. In the former, both air and gas inlet ports are placed on one side of the rotor while the outlet ports on the other side of the rotor (figure 2.29); in the latter, the air inlet and exit are located at the same end of the rotor while the gas inlet and exit are at the other end, refer to figure 2.30.

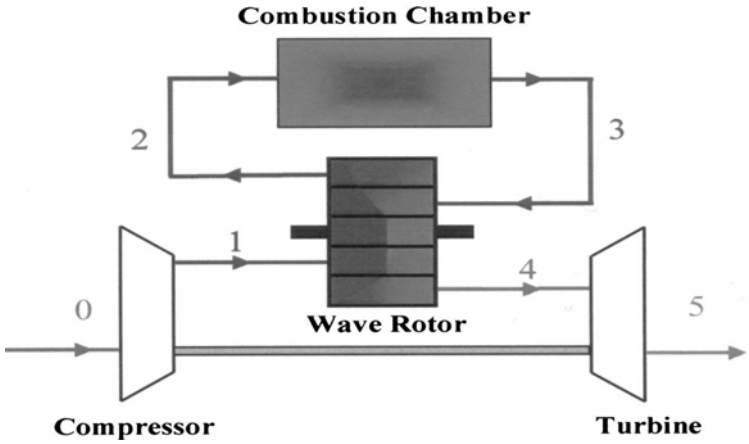

Figure 2.30: Concept of a gas turbine topped by a reverse-flow wave rotor (Akbari et al, 2006a)

As can be seen from figure 2.29, the compressed air goes into the wave rotor (station 1) where the air pressure is risen more by means of the combustion gases leaving the burner at station 3 before entering the combustion chamber (station 2). The hot gases are expanded within the wave rotor channels and directed to the turbine for work extraction to drive the compressor (Akbari and Müller, 2003).

Akbari and Müller (2003) concluded that incorporating a wave rotor into a turbofan with the same OPR and TET as for the baseline configuration leads to a great performance enhancement. However, the higher values of pressure and temperature inside the burner would lead to modifications in its structure, fuel injection and cooling system.

2.4.6. Constant-Volume Combustion Aero-Engine

Basically, the constant volume combustion gas turbine is a gas turbine engine that combines some features of the conventional gas turbine and piston engines. In fact, instead of constant pressure combustion chambers utilised in gas turbine

engines, the combustion process takes place in a closed volume (constant volume), similar to that of piston engines. Therefore the pressure rise of working fluid is obtained in two phases: first by means of the compressor and second as a consequence of the closed volume combustion. In this way, once the maximum cycle pressure is fixed, the power needed to drive the compressor is less than that of a conventional gas turbine engine. As a result, the output power available and the efficiency are greater (Andriani and Ghezzi, 2005).

In order to understand the working principle of the engine, refer to figure 2.31. Air, at station 1, enters the compressor (C) which increases its temperature and pressure to the condition defined at station 2. Then it gets in the combustion chamber (CC) passing through intake valve (I), while fuel is introduced by a nozzle. Once the chamber is completely filled, intake valve (I) is closed, and then the mixture is started by an igniter thereby commencing the combustion process. Since it takes place in a closed volume both temperature and pressure increases, reaching their maximum value. When the combustion process is finished, exhaust valve (E) opens, allowing gas to pass through turbine (T), to drive the compressor, and power turbine (PT) that provides the output power. When the combustion chamber has been evacuated, valve E is closed, valve I opens and the cycle starts again. Besides the engine scheme, the thermal cycle is reported in the temperature-entropy Cartesian coordinates. For simplicity, the thermodynamic process is considered ideal (Andriani and Ghezzi, 2005).

This concept was considered at the beginning of gas turbine development when the main components of the engine (the compressor and the turbine) were not able to achieve satisfactory levels of thermal efficiencies. Many trials to build an engine with such principles were made, but most of them were unsuccessful. A major success was the Holzwarth turbine which was built in different models. At that time the main limits found were: the high gas temperature level that the

combustion chamber and turbine blades had to withstand, and control of the valves. For this reason the project was cancelled.

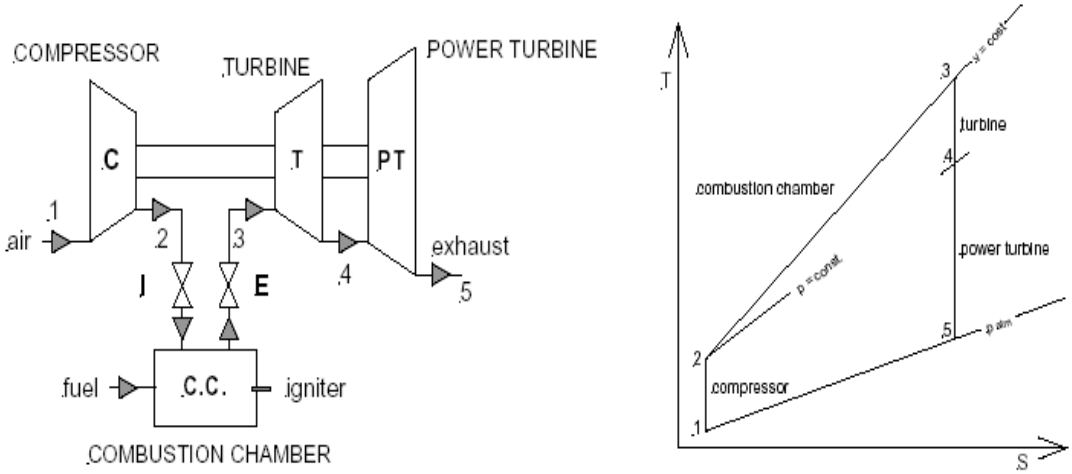

Figure 2.31: Engine scheme and thermal cycle of constant volume combustion gas turbine (Andriani and Ghezzi, 2005)

A study of this thermodynamic cycle has been performed (Andriani et al, 2005). It was found that for a pressure ratio of 3 the thermal efficiency, depending on the maximum temperature, is about 40% (see figure 2.32).

Nowadays, with the possibility of electronic control of the valves and of the combustion process, and the development of new materials and cooling technologies, this cycle could now be more applicable.

The most popular CVC (Humphrey) cycle proposal that can be found in the public domain is the internal combustion wave rotor (Smith et al., 2002 and Won and Waters, 2003). In this engine arrangement the conventional combustor is substituted with the CVC one. The conclusions drawn from these studies are that the engine size and weight reduces leading to less fuel burn for a given mission. As a result, the total CO_2 and NO_x emissions would be decreased. The drawbacks of

this configuration are the complexity of the CVC hardware and its weight, as well as the turbine weight penalty owing to high pressures and temperatures involved in the combustion process. Therefore, new materials and cooling technologies have to be sought out.

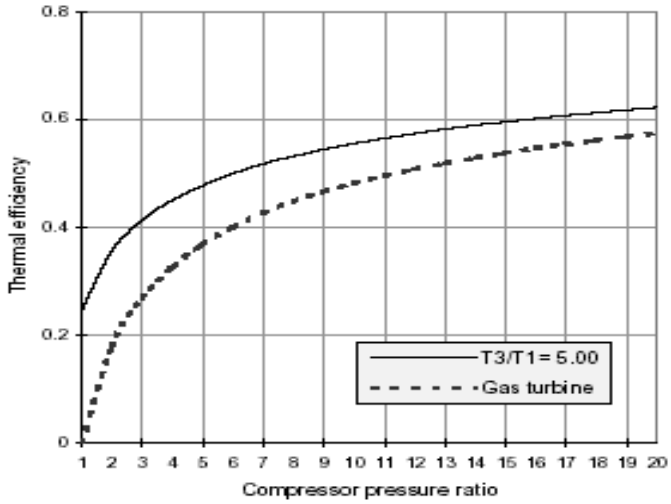

Figure 2.32: Thermal efficiency as function of pressure ratio and T3/T1 (Andriani and Ghezzi, 2005)

2.4.7. Semi-Closed Brayton Aero-Engine

At the beginning of gas turbine development, semi-closed cycles were proposed by R. Anxionaz (1945, 1948) as alternatives to the gas turbine engines of the early days. The potential advantages of this sort of cycle were then low fuel consumption over the power range, its size and weight, and therefore reduced air flow requirements. Nevertheless, the more complex arrangements and high sulphur fuels at that time hindered their development as a result of the risk of corrosion due to the recirculating flow in the compression section (Lear and Laganelli, 2001).

In the past there were two known development programs: the works of the Sulzer Brothers and the U.S. Navy Project ‘Wolverine’. Between 1945 and 1949 the

Sulzer Brothers operated two power plants: 5 MW and 20 MW of power. These gas turbine engines had problems relating to the formation of deposits and corrosion in the combustor due to the burning of crude oil. Project Wolverine was a classified submarine propulsion application intended to provide an alternative solution in the event that nuclear propulsion proved unfeasible. However, initial testing on the semi-closed cycle propulsion system reflected the predicted attributes of semi-closed cycle engines (Lear and Laganelli, 2001).

A number of additional arrangements have been proposed by Gasparovic in 1967 and 1968 for semi-closed cycles that may be used in power generation or propulsion applications (Laganelli et al, to be published). NASA funded a study (Lear and Laganelli, 2001) to highlight the benefits of this novel cycle with emphasis on power diversity, capability, SFC and emissions over a wide range of power. Two papers were generated from this study (Laganelli et al). In the first paper, a small single shaft and two-spooled semi-closed HPRTE (High Pressure Regenerative Turbine Engine) was compared to a conventional intercooled and recuperated (ICR) open cycle gas turbine engine. In the second paper, two-spooled semi-closed cycle HPRTE were simulated and the results in respect of SFC were compared to two open-cycle recuperated gas turbine engines. The NASA sponsored work clearly demonstrates the attributes of HPRTE semi-closed cycles and in particular, it meets the challenges of suppressing greenhouse gas into the atmosphere hence mitigating the potential of global warming.

It is likely that some developments for aircraft application have been performed, but no documentation was found during the literature survey.

The improvements of gas turbine technology: component efficiencies, cooling methods, component materials, improved fuels, for example, and the results obtained so far give the possibility of re-examination of semi-closed cycles for a wide range of applications including the air transport industry.

2.4.7.1 Exhaust Gas Recirculation Principle

The fundamental principle of this approach is the reduction of flame temperature by recirculating cooled combustion products back into the primary zone of the combustion chamber, as shown in figure 2.33. Recirculated gases reduce the oxygen concentration of the air in the inlet and thus leave less oxygen to react with nitrogen. In addition to this, the presence of high heat capacity inert gases, such as H_2O and CO_2, in the inlet air allows the flame temperature to reduce (Muley and Lear, 2003).

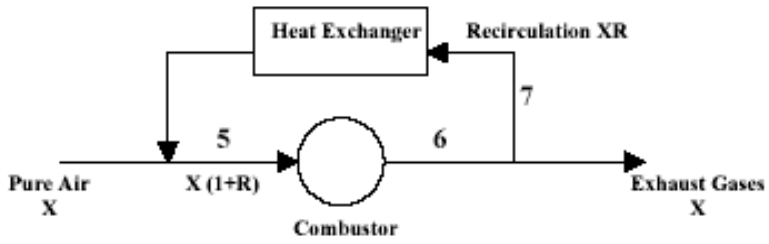

Figure 2.33: Schematic diagram of exhaust gas recirculation (Muley and Lear, 2003)

Exhaust gas recirculation has some advantages over the NO_x control techniques in that there is little or no combustor development and no expensive hot section treatment is needed; there is no requirement for water or steam injection and these have demineralisation costs associated with them reducing combustion efficiency and thus increasing emissions of CO and unburnt hydrocarbons (UHC).

2.4.7.2 Semi-Closed Cycle Description

A schematic diagram of the NASA HPRTE for a shaft power configuration is shown in figure 2.34. Air enters the low pressure compressor (C1) at station 1 and exits at station 2. Afterwards, the compressed air is mixed with recirculated exhaust

gases at station 2.1. The cooling process is by means of an optional spray cooler and an intercooler. The exit is station 3 where the air/exhaust mixture enters the high pressure compressor (C2).

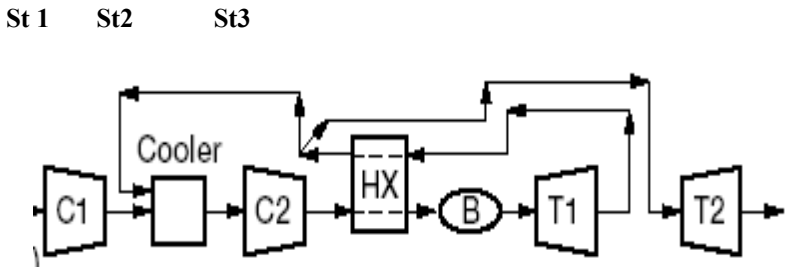

Figure 2.34: Schematic diagram of HPRTE cycle (Meitner et al, 2000)

The path from station 3 to station 9 is that of a conventional recuperated gas turbine engine, except that the inlet and exit pressures (p3 and p9) are increased (though nearly equal). At station 9 the flow is split in two parts, one being routed to the mixing junction downstream of station 2, and the remainder passing through the low pressure turbine (T2). Conceptually, the low pressure turbomachinery, C1 and T2, can be coupled to the same shaft as C2 and T1, can form a separate power-producing spool, or may be implemented by a turbocharger, with a wastegate valve controlling the T2 turbine bypass flow.

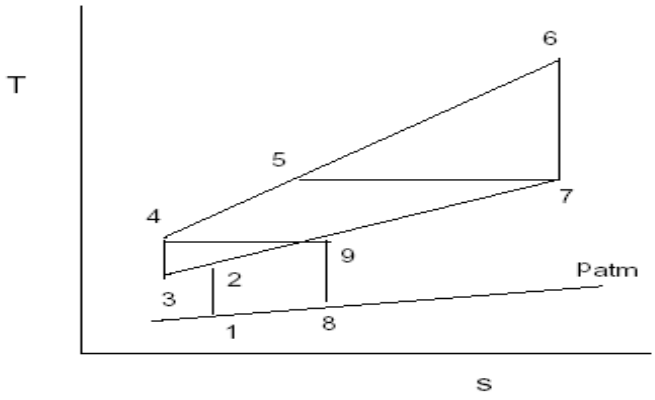

Figure 2.35: Temperature-entropy diagram of HPRTE cycle (Laganelli et al, to be published)

A detailed discussion of the benefits of the HPRTE cycle can be found in the NASA contractor final report (Lear and Laganelli, 2001). The major HPRTE benefits are briefly described below:

- **Reduced air flow and lower burner temperature:** The HPRTE requires far less inlet air flow passing through C1 for the same power output as a conventional ICR engine. In a conventional ICR open cycle engine, the air makes only one pass through the engine. This places a premium on high operating temperatures to reduce the large air flow requirement and to minimise the size of the engine. Minimum air flow occurs when burning at the stoichiometric temperature, which is not achievable due to material and cooling limitations. In contrast, an HPRTE operates at conventional (far below stoichiometric) temperatures, and recirculates a portion of the exhaust gases which still contains unburned oxygen. Therefore, only enough inlet air has to be supplied to sustain combustion. In essence, an HPRTE can burn a mixture of fresh air and unburned exhaust products (having a far lower oxygen concentration than pure air) stoichiometrically, but at conventional operating temperatures. The amount of recirculated exhaust flow can be more than 2.5 times as large as the inlet air flow, depending on the chosen burner temperature. The specific power (power produced per unit inlet air flow) can thus be more than 3 times greater than for a conventional ICR engine operating at the same TET.

- **Compactness:** The HPRTE operates at its optimum at high OPRs. Since recuperation takes place in the high pressure loop (with elevated pressures on both sides of the heat exchanger), the size of the recuperator is reduced by an order of magnitude comparable to open cycle ICR engines. Additionally, the LPC and LPT components can be much smaller because of significantly lower air flow requirements. It is estimated that, for a given

power output, an HPRTE will be approximately half the size and weight of the conventional ICR engine.

- **Flat SFC curve:** The HPRTE retains its low SFC characteristic down to far lower power levels (below approximately 20% of power) than open cycle engines.

- **Low emissions:** At higher levels of exhaust gas recirculation, NO_x and CO levels are significantly reduced.

- **Reduced ducting, signature and filtration:** The HPRTE low air flow characteristics reduce the engine inlet and exhaust stack sizes, the total exhaust signature, as well as inlet filtration hardware requirements. These features can have a significant impact, especially on naval engines and ground combat vehicles.

2.4.8. Direct Drive Aero-Engine

The direct drive turbofan (DDTF) concept, shown in figure 2.36, has been developed by Rolls-Royce. It maintains the current fan layout. The innovation here is in reducing the number of blades (with each blade having to support a higher aerodynamic load), and increasing their size and thus the overall fan diameter. These new fans will provide a very high bypass ratio (from 10 to 12:1), at lower rotational speeds. Tests are also aimed to check out new and lighter materials (Baudier and Piquet, 2004).

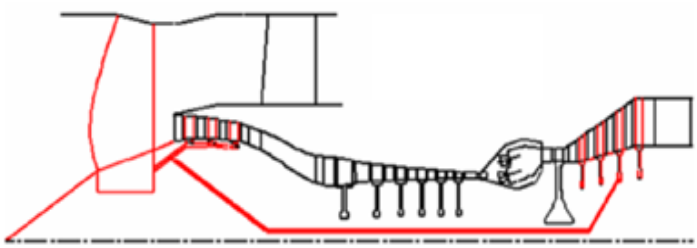

Figure 2.36: Direct drive turbofan (Sixth framework programme, 2005)

2.4.9. Geared Aero-Engine

The development of this concept is coordinated by MTU Aero Engines. As its name implies, the geared turbofan (GTF) introduces a reduction gearbox (see figure 2.37) between the fan and the remaining components in the low pressure system (booster, shaft and turbine). This will require innovative solutions for both the compressor and low pressure turbine. A setup of this type will offer an ultra-high bypass ratio (UHBPR), in the neighbourhood of 12:1 to 15:1. The fan itself will be similar to that in the DDTF, meaning no specific tests will be required for the GTF version (Baudier and Piquet, 2004; Sixth Framework Programme, 2005).

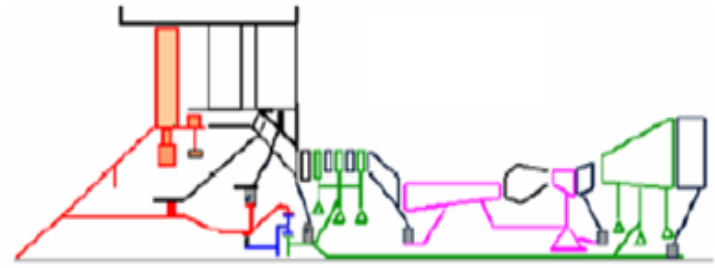

Figure 2.37: Geared turbofan (Sixth framework programme, 2005)

The reduction gearbox allows both fan and low pressure system to run at their optimum speeds. The fan can be set to the low speed required to achieve maximum efficiency and minimum fan noise. On the other hand, the LP shaft speed can be higher thus allowing a considerable reduction of LPC and LPT stages. Consequently, low pressure systems and engine cores can be designed to be more compact with benefits for cost and weight. A further advantage is the LPT noise being shifted into higher (inaudible) frequencies (see figure 2.38). A significant engine noise reduction is the outcome, especially during approach and landing. Lastly, due to higher speed of the LP shaft, its diameter can be kept small with advantages for the weight and disc of the HPT (Boggia and Rüd, 2004).

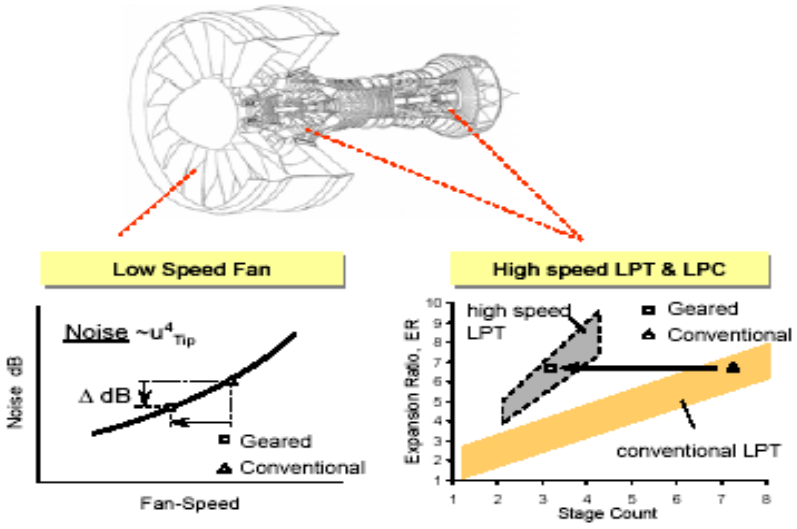

Figure 2.38: Geared turbofan concept (Boggia and Rüd, 2004)

2.4.10. Contra-Rotating Aero-Engine

This concept has been developed by Snecma Moteurs (see figure 2.39). In this layout, which is particularly innovative, there are two independent shafts rotating in opposite directions. At the other end of the low-pressure section they are joined to a low pressure turbine with several stages of counter-rotating blades as shown in figure below (Baudier and Piquet, 2004).

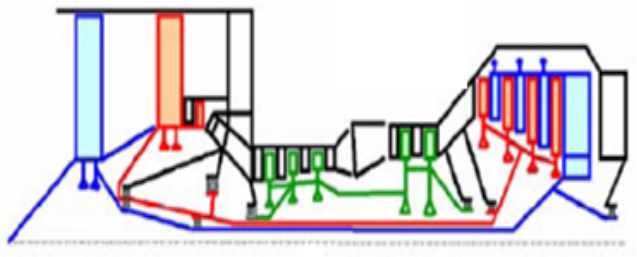

Figure 2.39: Contra-rotating turbofan concept (Sixth framework programme, 2005)

For a given aerodynamic load, this configuration will reduce the fan rotating speed by 30% or even more. Marius Goutines, aeronautical R & T program manager at Snecma Moteurs explained, "The advantage of this technology is that it offers the same performance as a conventional fan, but with lower tip speed. In other words: this is potentially a very advantageous solution to reduce fan noise" (Baudier and Piquet, 2004).

2.4.11. Open Rotor Aero-Engine

The unducted fan UDF (or open rotor) is a concept which has been tested extensively during the 1980s by General Electric, NASA, Boeing and McDonnell Douglas.

It comprises two contra-rotating unducted fan stages. In combination with contra-rotating power turbines a gearbox is redundant. Contra-rotation of fan rotors enables the second rotor to recover the exit swirl from the first rotor. Therefore, increased stage loading is justified. The UDF comprises two modules: a low-speed propulsor (with power turbines and contra-rotating fan) and a high-speed gas generator are aerodynamically coupled via a mixer.

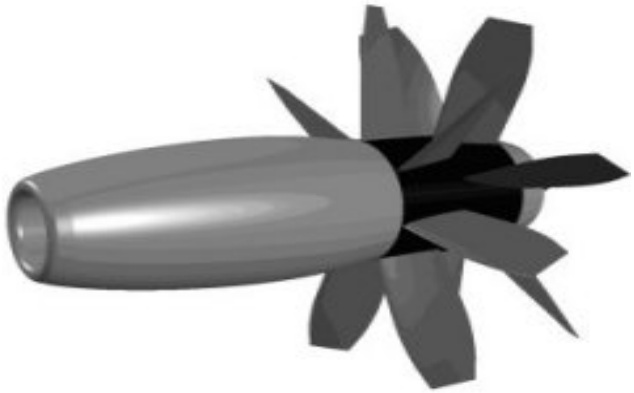

Figure 2.40: Open rotor turbofan (University of Cambridge, 2007)

Variable pitch fan blades are mounted for optimum performance and reverse thrust capability. UDF combines the high subsonic speed of a turbofan with the propulsive efficiency of a turboprop for very low SFC. For aerodynamic as well as acoustic performance rotor spacing, fan blade tip speed and tip vortex management are key design drivers.

DREAM (Rolls-Royce, 2007) is a new EU R&D programme under the seventh framework. This project comprises the assessment of open rotor cycles.

Advantages of the open rotor:

- Exceptionally low SFC (Nichols, 1988).
- Very high BPR and therefore, high propulsive efficiency.
- Potential of a lighter and more compact engine with lower in-flight drag, since the fan casing and bypass duct are absent.

Disadvantages of the open rotor:

- Noise reduction is accomplished with a complex fan design due to the absence of the nacelle.

- Fuselage skin acoustic treatment is required to keep cabin noise at an acceptable level.
- Sonic fatigue is a major design issue for aircraft-engine integration.
- The general public perceives an open rotor as a safety hazard.

2.5 Engineering Economics

2.5.1. Economical Assessment of the Project

There are several ways to appraise the viability of the project in terms of its return to choose the best option, which are called time-value-of-money methods. These methods are broadly used in the gas turbine sector where the huge investments are needed and are based on compound-interest approach leading to the following overall formula (Ostwald and McLaren, 2004 and Brink, 2008):

$$F = P \cdot (1+i)^n \qquad \textbf{(2.4)}$$

Where: F is the future value, i is rate of interest, n is the number of years and P is the present value.

Currently, there are four time-value-of-money methods available: net present value (NPV), net future value (NFV), net equivalent annual value (NEAV), and finally return on investment (ROI). The NPV approach uses both the first investment and the present value of potential returns for project evaluation; this is based on a chosen interest rate. The NFV considers the initial sum invested and the initial-asset value's investment as well as returns' reinvestment adopting a specific interest rate. The NAEV takes into account the costs per annum and returns associated with an investment; this method considers opportunities for future investments of assets and profits based on a pre-determined interest rate. Finally, ROI is used to compare the performance of several investments; this metric is

obtained dividing the investment profit (i.e. return) by the investment cost as shown below:

$$ROI = \left(\frac{investment\_profit - investment\_cost}{investment\_cost} \right) \quad \textbf{(2.5)}$$

This metric is very common due to its flexibility and simplicity: if an investment has a negative value of the ROI, then this investment should be rejected.

The NPV evaluates different projects directly: an interest rate is employed to the cash flow of each period to calculate the net present value leading to the following formula:

$$NPV = \sum_{i=1}^{i=n} \frac{C_t}{(1+r)^t} \quad \textbf{(2.6)}$$

Where: C_t is cash flow at time t, NPV is net present value, r is the discount rate and t is the time.

Negative values of NPV indicate that the projects being evaluated would give losses to a company while the projects with positive NPV values would bring profits. A zero value represents the break-even point of the projects.

2.5.2. Cost Assessment in Aviation

There have been different approaches to cost calculation developed for aviation. The current methods of direct operating cost appraisal come from the procedure set up by Air Transport Association (ATA) in 1967; so-called 'Standard Method of Estimating Comparative Direct Operating Costs of Turbine Powered Transport Airplanes'. Later, Boeing and then NASA took over the method for more

improvements. In the 1970's NASA put together all information about operating costs existing from the aviation industry for a thorough understanding of aviation operating costs (van Bodegraven, 1990). A DOC's method for short- and long-haul aircraft was given by the Association of European Airlines (AEA) in1989 based on cost estimation relationships; this approach includes a typical mission plus reserves for hold, diversion and FAA requirements, but it does not take into account the noise and emissions fees. Another method for DOC calculation of an aircraft with a certain payload-range performance was derived by Hertel and Albers (1993), which utilise a 'rubber aircraft' whose configuration adjusts as the engine parameters varies. On the other hand, there is an approach where the cost and airframe structural area are correlated (Giesing and Wakayama, 1997). In addition, Jenkinson (1999) shows a simple way for estimating the DOC, and was used in the economical model of the first methodology described in chapter 3. Finally, there are several methods to compute the life cycle cost for the whole aircraft as demonstrated in Roskam (1990) and Raymer (1999).

2.6 Engine Design Optimisation

2.6.1. Introduction

During the engine design phases several figures of merit have to be minimised or maximised like, for example, the operating cost or the thrust. For that reason, the multidisciplinary optimisation has been used in engine design at all stages successfully.

At the conceptual and preliminary design phase, optimising the future propulsion system for environmental and economical performance involves a holistic methodology which assesses the multidisciplinary features of the turbofans, and can consider variables and constraints from all pertinent disciplines concurrently. Furthermore, when some objectives are conflicting there is a need for

trade-off analysis by means of a multi-objective optimisation approach that is required in the methodology employed.

2.6.2. Single- and Multi-Objective Optimisation

A single objective optimisation problem can be expressed using the following mathematical notation (Sweeney, 2003):

$$\text{Minimise } J(x) \quad \textbf{(2.7)}$$
$$\text{Where } J : x \in \Omega \subset R^n \rightarrow R$$
$$\text{Subject to } g(x) \leq 0, h(x) = 0$$

Ω represents the design space while $J(\Omega)$ is the objective space. The g and h are constraints which must be accomplished.

The notation for multi-objective optimisation is as follows:

$$\text{Minimise } J(x) \quad \textbf{(2.8)}$$
$$\text{Where } \forall J : x \in \Omega \subset R^n \rightarrow R$$
$$\text{Subject to } g(x) \leq 0, h(x) = 0$$

Two sorts of problems for the multi-objective optimisation exist: cooperative and competing. The best solution in the case of cooperative objectives ends up in a single point (similar to single-objective optimisation). However, when several objectives are competing, an improvement in one objective leads to a detriment in another; hence, a trade-off analysis must occur.

In single-objective space, the solution ordering takes place which means that the solution with a minimum or maximum objective is selected (Deb, 2001). On the other hand, in multi-objective problems the solution comparison is carried out based upon whether one solution is dominant with regard to another. In other words, one solution can perform better than another in some objectives or vice versa. These solutions are non-dominated and their set is called Pareto front, which is related to the optimal trade-offs among different objectives. In chapter 4, several Pareto fronts are shown for some conflicting objectives.

2.6.3. Optimisation Technique Selection

In order to choose an appropriate optimisation technique for a given problem, the following questions must be addressed:

- What is the topology of the objective space?
- How many variables does the problem have?
- Is the problem single- or multi-objective case?

The objective topology is a very important criterion in selecting the optimisation technique. Gradient-based techniques are more appropriate to smooth objective functions while genetic algorithms have been applied successfully in noisy objectives. Gradient-based methods are more likely to converge to local minima in the case of noisy objectives.

The number of variables, also, can be a paramount importance: Simplex techniques do well with reasonably low variable numbers (less than 8), other techniques are more robust and consistent for high numbers of variables as is the case of genetic algorithms (GAs). The GAs tend to be expensive in terms of CPU time, however they can converge to the global optimum.

Lastly, gradient-based and sequential methods are more suitable for single-objective optimisation while for multi-objective design space the weighted functions and genetic algorithms are applied.

CHAPTER 3

METHODOLOGY:

MULTIDISCIPLINARY OPTIMISATION DESIGN FRAMEWORK AND MODULES

3.1 Overview

One of the definitions of the multidisciplinary optimisation (MDO) available in the public domain can be as follows: "A methodology for the design of systems in which strong interaction between disciplines motivates designers to simultaneously manipulate variables in several disciplines" (Sobieszczanski-Sobieski and Haftka, 1996).

The disciplines are described by governing equations from different design areas: performance, economics, emissions, noise, weight, etc.; these disciplines are of low fidelity and complexity producing shorter computational time. Their coupling results in a multidisciplinary analysis tool.

The integration of an optimiser to this analysis tool would generate a MDO design framework allowing the automation of the conceptual and preliminary design processes. The available optimisers contain a variety of optimisation techniques which are selected (either manually or automatically) depending upon the problem characteristics to be tackled.

The advantages of MDO systems are time and cost reduction as well as better design solutions. Also, it can be used to assess the connection between the optimal designs, and economic and environmental factors; this would provide a key guidance for the OEM's future product strategies and aeronautical authority regulations.

The following section deals with MDO approaches developed to assess and optimise the advanced and radical turbofans. These have been found in the literature domain suitable for addressing the research questions mentioned in chapter 1 at different environmental and economic scenarios.

3.1.1 MDO for Baseline, Advanced, Contra-Rotating, Geared Turbofans (TERA)

This tool is made up of eight simulation modules to calculate many aspects of engine design and performance as well as its environmental and economical impact (figure 3.1). Aircraft performance, environment, engine performance and economics with risk analysis capability are assessed using in-house software; and weights and dimensions, production cost, gaseous emissions and noise are provided by other partners (Chalmers University, Cranfield University (CU), Stuttgart University (USTUTT) and Supaero) as shown in figure 3.1. The engine performance and noise were modified to fit into their required role in TERA. The other modules are being wholly developed during this PhD project. These modules are then coupled with a commercially available optimiser, i-SIGHT from Engineous Software (Engineous Software, 2007). All of these modules are being evaluated individually and integrated.

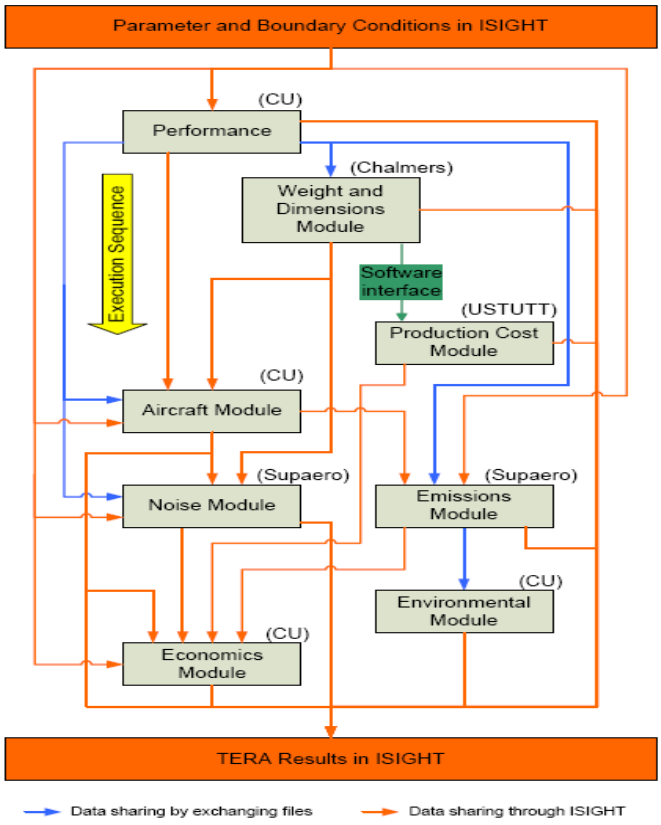

Figure 3.1: TERA architecture and calculation sequence including data flow chart (Bretschneider et al, 2007)

All modules are delivered as standalone executables. This approach was chosen to maximise the exchangeability of the single modules for future updates and the later integration of TERA into the partners' individual in-house simulation environments.

The subsequent sections describe some module characteristics which are necessary to fully understand the TERA architecture; also, the optimisation techniques available in i-SIGHT are explained.

3.1.2 MDO for Baseline, Intercooled, Recuperated, and Intercooled and Recuperated (ICR) Turbofans (ICHXMDO)

This MDO design framework which consists of several simulation models to calculate many aspects of engine design and performance as well as its economical concerns is used for evaluating the intercooled, recuperated and ICR turbofans (refer to figure 3.2). Aircraft performance is assessed using in-house software called HERMES. Whilst these are economic and risk aspects with the in-house model (Pascovici et al, 2007), it is worthwhile pointing out that these two models were developed during this PhD project. Engine performance, NO_x emission and design optimisation were carried out with Gas Turb 10 which is a gas-turbine simulation program available commercially (Kurzke, 2004). This software offers a wide variety of predefined engine configurations, thus allowing an immediate commencement of the calculation; also, cycle optimisation capability is incorporated.

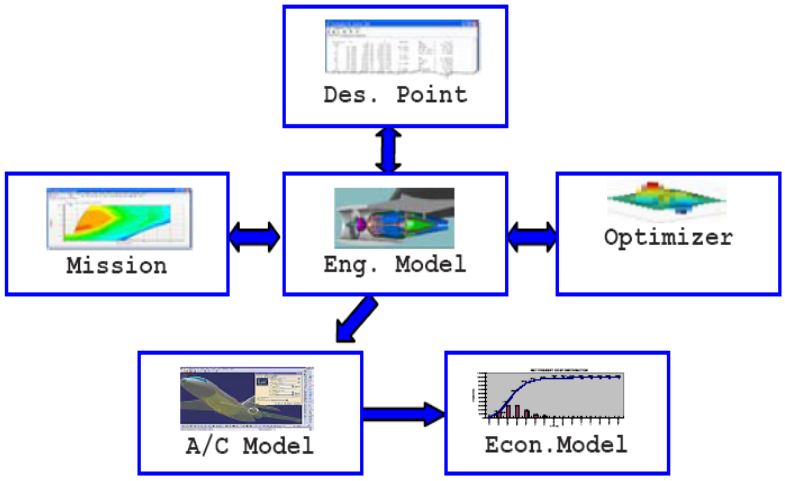

Figure 3.2: Structure of the MDO design method

3.1.3 MDO for Baseline, Geared and Constant-Volume Combustion (CVC) Turbofans (PMDF)

The Flight Optimization System (FLOPS) is an MDO system of computer modules for the assessment and optimisation of advanced aircraft developed by the NASA Langley Research Center (Geiselhart, 1994 and FLOPS, 1995). It consists of nine principal modules: weights, aerodynamics, engine cycle analysis, propulsion data scaling and interpolation, mission performance, take-off and landing, noise footprint, cost analysis, and program control. Single- and multi-objective optimisation techniques of major engine design variables for a range of typical cycle types and also customised ones are included.

A modified version of FLOPS was used for a feasibility study of CVC turbofans for short-range civil aircraft (see figure 3.3). During this research, new engine weight and dimension estimation, risk analysis based on Monte Carlo simulation, emissions and environmental modules were developed and implemented. In addition to that, the life cycle cost estimation was improved using new correlations and scaling factors as well as noise and emission charges. This new system allows environmental issues such as global warming, airport noise and emissions to be addressed early in the design process. The rapid execution of parametric study and optimisation using both engine cycle and aircraft design variables and evaluation of the impact on figures of merit such as: fuel burn, radiative forcing, noise, direct operating cost, etc, should give insight and provide road map for more detailed studies.

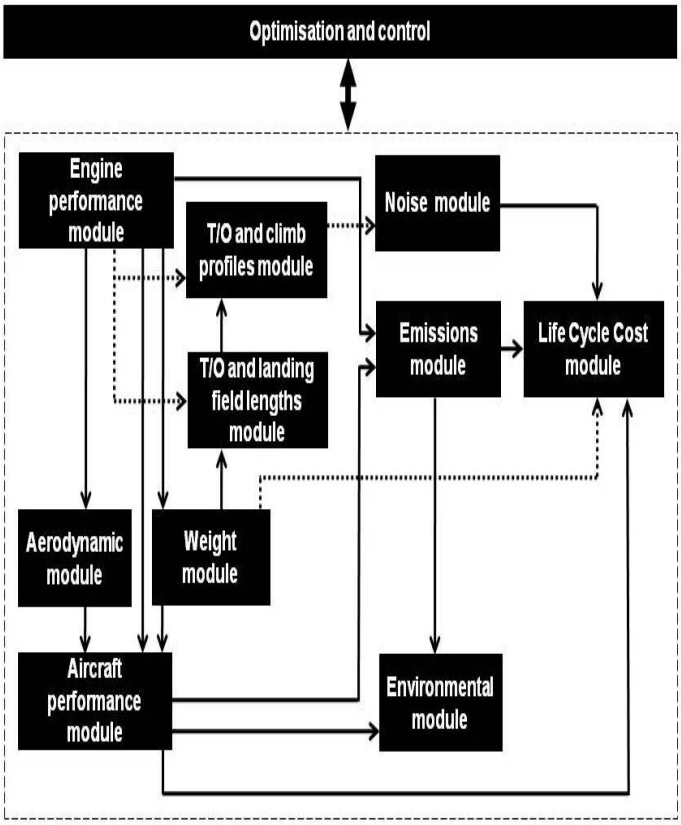

Figure 3.3: Structure of the CVC MDO design tool (Brinks, 2008)

3.2 Aero-Engine Performance Module

Several engine performance simulation codes are available in the public domain. Among them we can find TURBOMATCH (Palmer, 1999), which is being developed by Cranfield University, Gas Turb 10 which is available commercially (Kurzke, 2004), and Enggen (NASA Engine Cycle Analysis Program). Some of them define the cycle using 'blocks' in the logical order of the engine components. Due to their ease of implementation, accuracy and availability, these models were explored in this research.

3.2.1 TERA Engine Performance Module

The TURBOMATCH (Palmer, 1999) was used to assess the engine performance of the following turbofans: baseline, advanced, contra-rotating, and geared turbofans.This is an engine performance simulation tool having been developed at Cranfield University for more than three decades.

This program uses the component matching approach in which the compatibilities of the flow and work among the components must be achieved. In addition, it can be used for simulating arbitrary gas turbines (steady state, transient), diagnostics and Gas Path Analysis (Pythia) and linking with 1-D and 3-D component models (CFD).

Each component is calculated through modules (pre-programmed routines), known as 'bricks', and connected to each other to create an engine cycle. Thermodynamic calculations are therefore executed on the data flowing throughout all the bricks using inputs set by the user (brick data) or/and coming from other bricks (engine vector results) as shown in figure 3.4. This results, lastly, in the output of engine thrust or power, specific fuel consumption, and so on, in addition to details of individual component performance and of the gas properties at different stations within the engine.

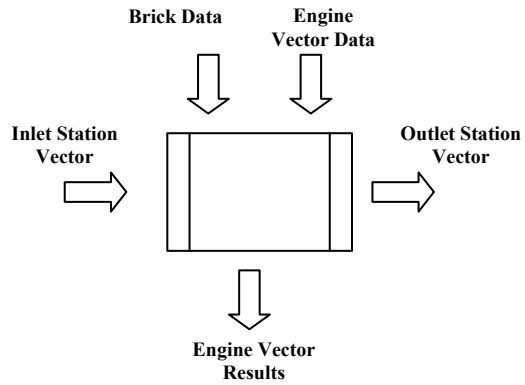

Figure 3.4: TURBOMATCH brick

Before performing the off-design (OD) calculations, the design point has to be run in order to determine the scaling factor for the maps. Then, the OD can be computed using one of the following parameters: turbine entry temperature (TET), or fuel flow, or rotating component speed (PCN). There are five compressor and six turbine maps available in TURBOMATCH. There is also a capability to implement extra maps as required.

This model generates the inputs required by weight, emissions, noise, and aircraft modules in TERA.

3.2.2 ICHXMDO Engine Performance Module

GasTurb 10 is the engine performance software utilised in the MDO for baseline, intercooled, recuperated, and ICR turbofans' case studies. This software calculates design, off-design and transient performance of the most common types of gas turbine for both aircraft and power generation such as: mixed and unmixed turbofans with or without boosters, turbojets, intercooled and recuperated turbofans. These configurations can be chosen from the overview screen within the group of radio buttons (figure 3.5). The detailed configuration, for instance the type of thrust nozzle, will be defined in the design point definition screen. Owing to a good description of gas properties which is required for any accurate cycle calculation, the working fluid is assumed to behave like a half-ideal gas.

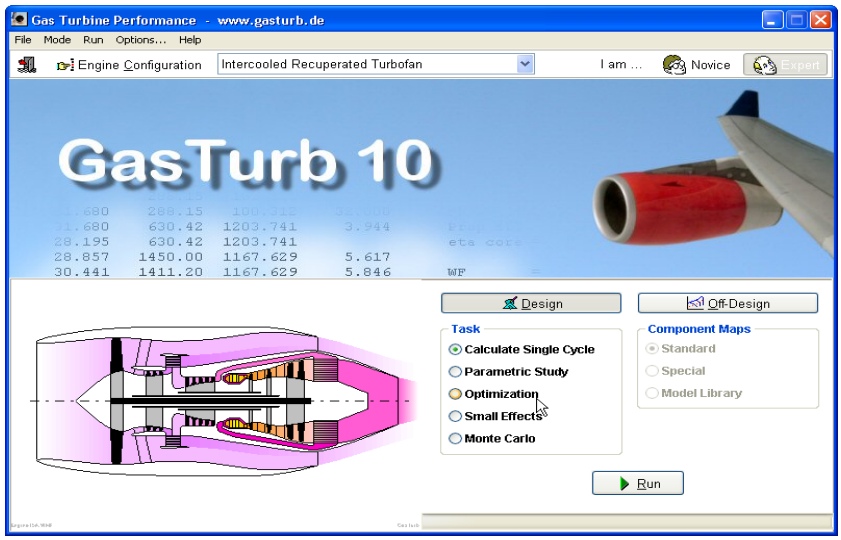

Figure 3.5: GasTurb™ Opening Screen (Kurzke, 2004)

The design point calculation in GasTurb 10 allows the sizing of the engine to be based on the following: Thermodynamic tables and diagrams; parametric study results in color graphics; user-defined graphs to display any combination of calculated parameters; optimisation of the cycle; analysis of small changes to the cycle input parameters.

During an off-design run this software is capable of simulating the following characteristics: single points for given operating conditions, or a series of points from full power to idle; variable geometry and effect of engine deterioration; effects of inlet flow distortion on compression system stability; transient performance, and so on. These simulations require the use of component maps which are embedded in the program.

Once the desired design point is obtained the user can define a series of points as a flight mission. In addition, all the operating points in the component maps can be plotted at the same time.

3.2.3 PMDF Engine Performance Module

The engine performance model was developed by Karl Geiselhart (1994) which is a modified version of QNEP tool (Geiselhart et al, 1991). This model is capable of predicting the performance of a variety of cycles. Based on one dimensional steady-state thermodynamic cycle approach, the design and off-design performance can be computed.

Table 3.1: Table of Component Types

Component Type
Inlet
Duct, Burner, or Afterburner
Compressor or Fan
Turbine
Heat Exchanger
Flow Splitter
Flow Mixer
Nozzle
Load
Shaft
Control

The engine cycle definition follows a logical sequence of the components listed in table 3.1. The station numbering, as shown in figure 3.6, is used to determine the flow path for the component. Compressors, turbines, and loads are coupled together by means of shaft components. Also, there are 15 design parameters for every component: mass flow, component efficiencies, horsepower extraction, rotational speeds, pressure drops, and so on. The data used depends on the component (Geiselhart et al, 1991). The design point calculation determines the

size of the components and the conservation of mass and energy. In order to maintain this conservation during off-design calculations, the control components are required. The purpose of these control components is to connect independent variables (i.e. component input quantities which are allowed to vary) with the dependent variables (i.e. mass flow and energy imbalances) or errors. During a cycle calculation an engine deck containing data for fuel flow and thrust at different Mach number-altitude combinations is created internally.

In order to limit certain engine parameters such as: compressor corrected flow, compressor surge margin, compressor pressure ratio, compressor discharge temperature and/or pressure, and shaft horsepower for turboprops, a control system is incorporated. This control system maintains the limit values of the first three parameters so that the compressor and turbine can work on the maps; the other three are there mainly to avoid surpassing the allowable values of the component stresses and temperatures (material limits).

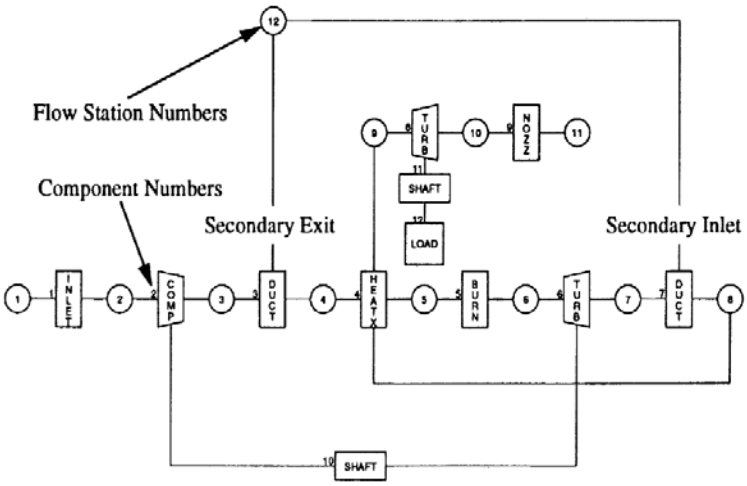

Figure 3.6: Cycle schematic for a regenerative turboshaft (Geiselhart, 1994)

Typical isentropic efficiencies and total pressure losses for components and internal ducts are assumed. Furthermore, the installation effects (total pressure recovery, customer and cooling bleed, power off-take) are included.

3.3 Aircraft Performance Module

3.3.1 TERA Aircraft Performance Module

A model, called HERMES, developed at Cranfield University is being used to assess the performance of the aircraft with the following turbofans' configurations: Advanced baseline, contra-rotating, geared, intercooled, recuperated, and intercooled and recuperated. This model is made up of five different modules whose main subroutines were developed to execute specific tasks: Arithmetic (data input and output), InputFiles (data input to the aircraft model), CalcFiles (ambient variation with altitude and drag calculation), Performance (fuel burn, flight time and flight distance for each flight segment calculations based on aerodynamic and engine performance information) and Main module (overall operation/sequencing of other modules and data gathering). The modules were developed as standalone software and coupled together by means of the Main module. This approach allows for easier software maintenance when needed.

The aircraft model was customised from existing knowledge Cranfield University (Panagiotis, 2004) and is also currently used in various industrial projects and for postgraduate research work. The new capability of the original model includes the following:

- Calculation of aircraft performance data (i.e. lift and drag coefficients), take-off distances and so on, from available information on the geometry and mass of the aircraft.

- Calculation of fuel usage, elapsed time and distance for a given mission.
- Modelling of different aircraft and engine arrangements.
- Estimation of aircraft range for a given maximum take-off weight, payload and fuel load. Conversely, when the range is set then the model computes the aircraft fuel load.

The aircraft performance model is constrained to the main mission profile, that is: no diversion is taken into account. However, reserve fuel provision is specified by the user as the remaining percentage of on-board fuel after landing. Also, contingency fuel can be accounted for using the reserve fuel allowance specification. The accuracy penalties caused by this approach can be alleviated through the optimisation of the fuel load, airframe geometry and weight.

Owing to the civil transport airworthiness regulations, the mission profiles and fuel planning specification provided in this model accomplish the requirements defined by FAR 121 and JAR OPS 1 as well as the ICAO recommendations.

The mission profile used in this aircraft model is shown in figure 3.7. This profile was split into the following segments (Jenkinson et al, 1999):

- Start up and taxi-out
- Take-off and initial climb to 1500ft
- Climb from 1500ft to cruise altitude
- Cruise at selected speed and altitude including any stepped climb required
- Descent to 1500ft
- Approach and landing
- Taxi–in

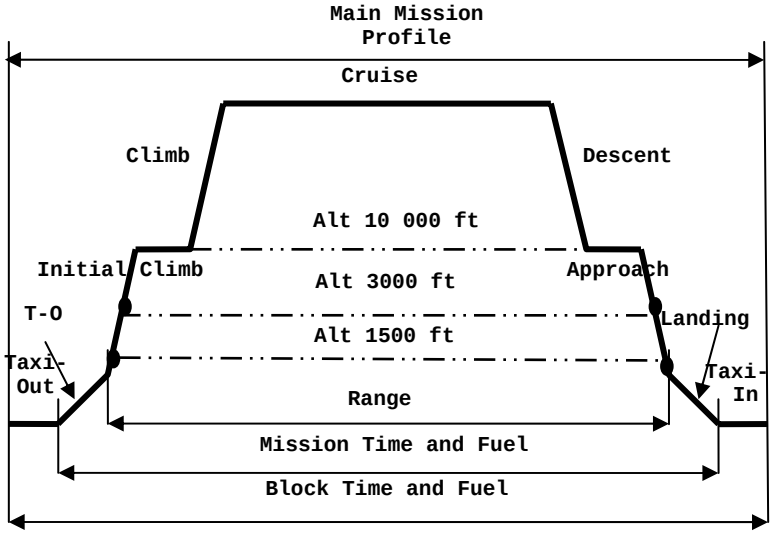

Figure 3.7: Typical mission profile

The climb schedule adapted from 1500ft to initial cruise altitude is:

- From 1500 ft to 10000 ft, restrict speed to 250 kt equivalent air speed (EAS)
- At 10000ft, accelerate to 320 kt EAS
- Thereafter, maintain constant speed up to the height at which the cruise Mach number is achieved and then maintained constant up to the initial cruise altitude.

A typical run in this model is as follows: Data is obtained from different input files and outputs from an engine performance model, if this option is needed. These data determine the aircraft geometry and weight, mission profile as well as the thrust and SFC available throughout the flight mission. Furthermore, the aircraft weight at take-off and at other mission phases is obtained. A weight check is performed to make sure that input data are in harmony with the expected trend, otherwise the aircraft weights are fine-tuned. The atmospheric parameters such as pressures, temperatures, densities, viscosities and speed of sound are calculated, the

wetted areas, form factors and other geometric indices are obtained and then the profile and induced drag on the airframe and engine is calculated.

To facilitate the aircraft performance calculation for different engine layouts, two approaches are provided in the model namely:

- Input the fuel load and determine flight range and time.
- Input the flight range and determine the best cycle to use.

Whatever the above-mentioned approach being considered, using the aerodynamic efficiency as the primary factor of the cruise altitude, concerns about fuel burn, range, mission time and so on, would be established. Therefore, these and other parameters are considered as outcomes of the aircraft model. Lastly, the performance module is called from which the fuel burn, flight range and time is derived.

3.3.2 PMDF Aircraft Performance Module

For the CVC turbofans' MDO, another aircraft performance model was utilised. This model was provided by the NASA Langley Research Center through FLOPS (Geiselhart, 1994 and FLOPS, 1995).

The mission analyses can be obtained for a given take-off gross weight or for a given range. The mission profile can be characterised using as many as 40 segments by means of the following segment indicator names (Geiselhart, 1994 and FLOPS, 1995):

- START: Starting Mach number and altitude.
- CLIMB: Climb schedule number.
- CRUISE: Cruise schedule number and total distance to end.

- REFUEL: Fuel added and time required.
- RELEASE: Weight released.
- ACCEL: Engine power setting and ending Mach number.
- TURN: Turn arc and engine power setting or turn acceleration.
- HOLD: Cruise schedule number and time.
- DESCENT: Descent schedule.
- END: Ending Mach number and altitude.

There are six different cruise schedules available in this model: for maximum specific range (instantaneous distance flown per unit of fuel consumed) or minimum fuel flow with Mach number and/or altitude changing, for maximum altitude at a constant Mach number, for a constant altitude and lift coefficient, or for maximum Mach number at a constant or best altitude.

Regarding the climb profile, four climb schedules are permitted. These profiles may be set or the optimum Mach number and/or altitude are calculated for some combinations of minimum fuel and time to distance.

During a mission analysis run, tables are created of Mach number, altitude, fuel flow, and other mission data against weight for all the cruise schedules. These schedules embrace the range from aircraft empty weight to gross weight at take-off and are updated as required. The cruise segment named ‘free segment’ (figure 3.8), typically the highest altitude, does not have a range related with it. All mission analyses start at START and continue to the ‘free segment’ and then to END and continue to the ‘free segment’ again. This segment is therefore flown as far as possible with the available fuel.

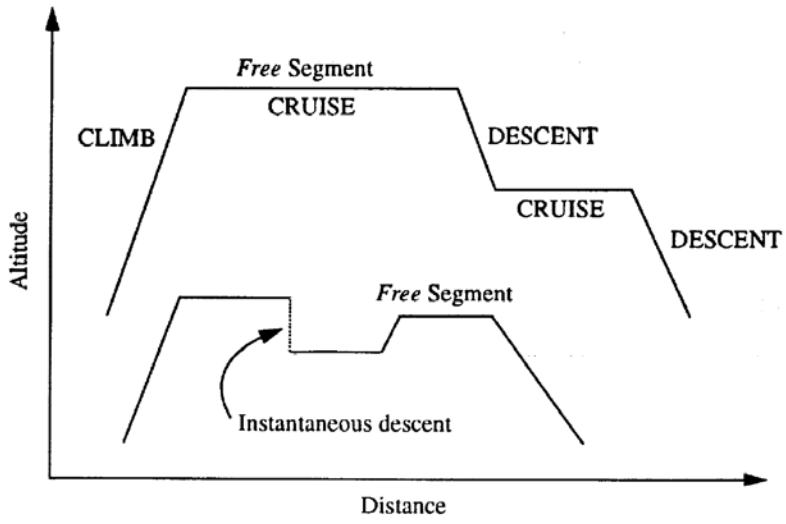

Figure 3.8: Mission profile (Geiselhart, 1994)

Descent may be flown at the optimum lift-drag ratio. In addition, acceleration, turn, refueling, payload release, and hold segments may be specified in any reasonable order.

Reserve calculations can include flight to an alternate airport and a specified hold segment. For supersonic aircraft, sonic boom overpressures are calculated along the flight path using the methodology given by Carlson (1978).

For any mission analyses, the propulsion system performance data, weights data, and aerodynamic data are required.

The takeoff and landing field length calculation is based on all FAR Part 25 regulations (Geiselhart, 1994) together with second segment climb gradient and missed approach climb gradient (figure 3.9). On the other hand, the balanced take-off field length calculation contains one engine-out take-off, all engines operating aborted take-off, and one engine-out aborted takeoff (see figure 3.9). The outcomes of these simulations are inputs for further calculations, such as: detailed take-off and climb profiles and aircraft noise in various points.

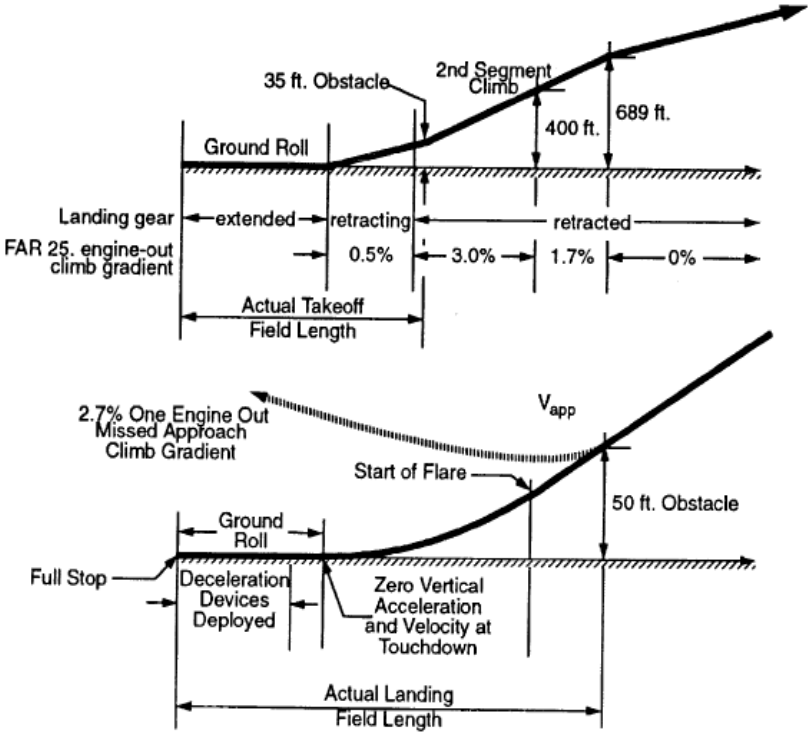

Figure 3.9: Take-off and landing profiles: The climb gradients shown are for aircraft with four engines (Geiselhart, 1994).

From the point of view of aerodynamics, the drag polars are derived from a modified method based on empirical drag estimation technique (Feagin and Morrison, 1979). Additionally the skin friction drag is estimated using the approach of Sommer and Short (1955).

There is another option for the previous method: the user can input the drag polars and then these are scaled by sizing the wing area and engine nacelle.

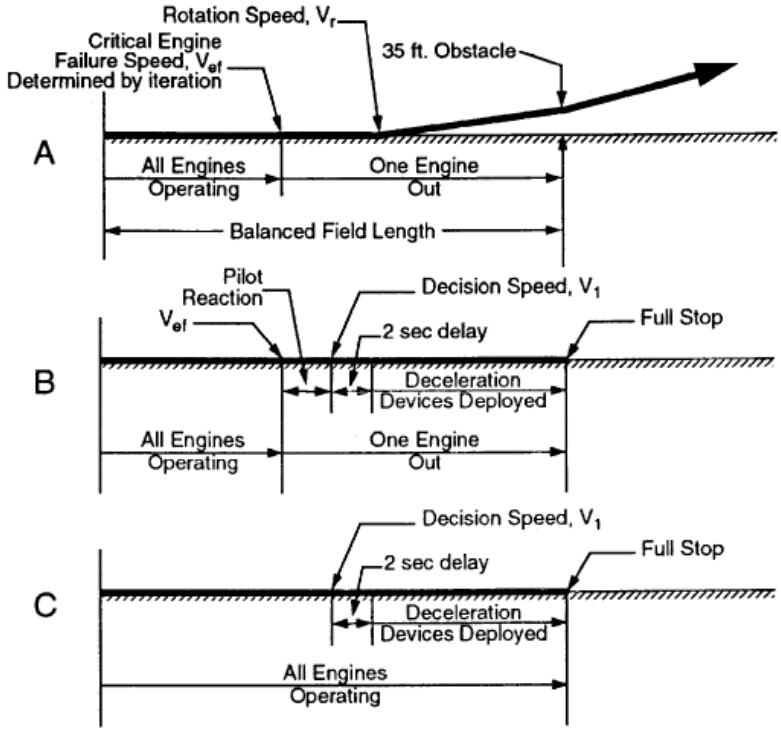

Figure 3.10: Takeoff balanced field length (Geiselhart, 1994)

An aircraft for short-range application, such as A320, was chosen as baseline and its performance and geometric data available from the public domain was used to validate the model. Additionally, the cruise altitude is assumed constant due to the short-range application of the aircraft, and its value is 10 668 m.

Finally, the aircraft performance data: flight times, fuel burn and range for the mission profile as shown in figure 3.7, were computed.

3.4 Emissions Module

The gaseous emission modeling is based on the calculation of a parameter called emission index (EI) whose units are gram of gas per kilogram of fuel consumed [g/kg].

The EI is a function of two factors: the combustor characteristics and the performance parameters. The former includes the mode of combustion (i.e. at constant pressure - CPC or constant volume - CVC), combustor volume and geometry, residence time, combustion efficiency, pressure losses and air fraction in the primary zone; and the latter comprises the pressure and temperature at the entry of the burner, fuel and air mass flow. These parameters together with the fuel combustion chemistry manipulate the emission levels in reality.

There are four approaches to simulate the emission produced in the combustion chamber (Allaire, 2006): empirical, semi-empirical, physics-based or chemical reactor and high-fidelity models.

The empirical models are straightforward and use less CPU-time in comparison to the other modules mentioned above. There are two ways, available in the public domain, to apply these models:

- Models based only on engine thermodynamic parameters, for instance: pressure and temperature at the entry of the combustor and sometimes TET. Also, some constants and exponents obtained from experimental data of a certain combustor geometry and configuration are utilized in these models.
- Models which rely on the resulting fuel flow in the LTO ICAO certification points (i.e. take-off, climb-out, approach and idle) provided in the ICAO engine emissions databank (ICAO, 2008). There are two well-

known methods in this category: ‘Boeing method 2’ and ‘DLR fuel flow method’ (Schulte et al., 1997).

These models are more suitable for calculation of NO_x emissions for conventional combustors with available certification data due to their simplicity. However, they are useless for an innovative combustor whose experimental data may not be accessible. In addition, it is challenging to capture the interaction between NO_x and CO during the combustion process.

The semi-empirical models depend on relationships based on empirical coefficients and exponents as well as on more thermodynamic parameters such as: combustor entry pressures and temperatures, pressure losses inside the combustor, equivalence ratio and flame temperatures in the primary flow, residence time and combustion volume, evaporated fuel volume and characteristic kinetic times.

Owing to the nature of this approach, these models can predict EIs for NO_x, CO and UHCs in a more flexible way but still the consistency of the interaction among these emissions is in doubt (Allaire, 2006). These models are very sensitive to the flame temperature and combustor entry pressure leading to an exponential increase in emission formation levels. Furthermore, the constants and exponents are appropriate to a particular variety of combustors resulting in probably overestimation of NO_x levels for low-NO_x combustors due to the combustion chemistry not being taken into account.

The following correlations, available in the literature, are semi-empirical: Lefebvre’s correlations (NO_x and CO) and Rizk and Mongia’s correlations (NO_x, CO and UHCs).

Physics-based or chemical reactor models are approximated using the ideal reactor’s physics and chemistry methodology based on the performance parameters

giving an acceptable accuracy and computational time to estimate the EIs for NO_x and CO emissions. In this approach, the combustion chemical kinetics in various combustor zones is computed. The input data are as follows: pressure and temperature at the entry of the combustor, air and fuel mass flow, the combustor zones, and so on (Allaire, 2006).

High-fidelity models (known as CCD - computational combustion dynamics) are very expensive computationally due to the detailed simulation of the chemistry and flow required within the combustion chamber. There are some turbulent combustion solvers that can be applied in these models to compute the emissions (Trouvé et al., 2003): large eddy simulations (LES) and direct numerical simulation (DNS). These models are highly recommended to be used in the detailed design stage when the more accurate geometry and performance of the combustor is available.

Empirical emission models are implemented in NASA Enggen and NPSS (Numerical Propulsion System Simulation), and GasTurb™ due to their simplicity and fairly precise calculations in the case of conventional combustors.

Nonetheless, these models are not suitable for more radical combustor designs such as for CVC turbofans. For the conceptual and preliminary design phase of CVCs, the physics-based models are very useful as long as enough data were to be accessible. For detailed design phase, however, CCD models should be applied.

3.4.1 TERA Emission Module

The emission module embedded in the MDO described in section 3.1.1 is based on Rizk and Mongia's correlations. This module was developed by Supaero. A considerable amount of data from different turbofans was used to obtain the modified Rizk and Mongia's correlations for NO_x, CO and UHC emission indexes.

Once the UHC and CO rates are calculated, the combustion efficiency can be computed.

For certifications such as ICAO, targets will be to evaluate the pollutant emission indexes for the main engine pollutants like NO_x, CO and UHC. Then, the total pollutant production during landing and take-off (LTO) cycle (i.e. take-off, climb-out, approach and landing) is estimated (Anon., 1993).

The original Rizk and Mongia's correlations for NO_x, CO and UHC emission index (EI) are as follows:

$$EI_{NOx} = \frac{15E14P_3^{-0.05}.\left(t_{res} - 0.5t_{ev}\right)^{0.5}.e^{\left(-71{,}100/T_{st}\right)}}{\left(\Delta P_3 / P_3\right)^{0.5}} \qquad \textbf{(3.1)}$$

$$EI_{CO} = \frac{18E7.e^{\left(7800/T_{pz}\right)}}{P_3^{\,2}(t_{res} - 0.4t_{ev}).\left(\Delta P_3 / P_3\right)^{0.5}} \qquad \textbf{(3.2)}$$

$$EI_{UHC} = \frac{76E9.e^{\left(9756/T_{pz}\right)}}{P_3^{\,2.3}(t_{res} - 0.35t_{ev})^{0.1}.\left(\Delta P_3 / P_3\right)^{0.6}} \qquad \textbf{(3.3)}$$

where T_{st} is the stoichiometric temperature ; T_{pz} is the combustor primary zone temperature; P_3 is the total pressure at entry of the combustor; t_{res} and t_{ev} are the residence time and evaporation time in the combustor primary zone, respectively; and ΔP_3 is the combustor pressure loss.

The assumptions based on conventional technologies were made so that the EIs can be estimated. These assumptions are as follows:

- The pressure loss inside the combustor, 5%.
- The combustor primary zone volume is assumed to be 40% of the total volume.
- The fuel residence time is obtained from the combustor volume and the air mass flow coming in the primary zone.
- The fuel evaporating time is estimated using the following relationship: $\tau_{ev} = \frac{SMD^2}{\lambda_{eff}}$, where λ_{eff} is the effective evaporation constant and SMD is the Sauter Mean Diameter, which is dependant on P_3 and ranging from 10μm to 50μm. In addition, the air blast atomisers are considered.
- The reaction and primary zone temperatures are obtained using T_3 and the FAR of the mixture in primary zone. Also, the kerosene database available in CHEMKIN - a program for solving complex chemical kinetics problems - was utilised.

3.4.2 PMDF Emission Module

The semi-empirical approach is selected to compute the emission levels generated by conventional and CVC combustors (Coutinho, 2008). The choice is mainly based on the lack of data for the CVC combustors in the literature. This module was implemented in the MDO described in section 3.1.3. It is worthwhile to mention that this research work was carried out as part of this PhD project.

CVC combustion process implies considerable variations in parameters such as: combustion volume, residence time, adiabatic flame temperature (AFT) and

pressure at entry of combustor, hence all of these factors have to be taken into consideration during the development of the module.

Coutinho (2008) concluded from his study that 'the AFT would need to be accurately estimated to within ± 2.5% accuracy (an increase in AFT of 2.5% resulted in the increase of NO_x EI by up to 50% in a take-off temperature scenario), and that the coefficients and exponent constants would have to be modified'.

For this research, the Lefebvre NO_x correlation was considered and modified. This is due to the use of air mass flow parameter in this approach rather than the pressure loss inside the combustor, which appears in the Rizk and Mongia correlation and possibly would cause calculation difficulties in the CVC case (pressure gain combustor).

AFT relies on equivalence ratio, fuel enthalpy, equivalence ratio, pressure and temperature at the entry of the combustor and mode of combustion and combustion efficiency (Coutinho, 2008). The value of AFT for CVC process is higher than that of CPC because the former is carried out without work and in the latter some work has to be done in order to change the volume.

The NO_x formation is exponentially dependent on AFT, thus its calculation must be as precise as possible in order to obtain acceptable results. There are certain chemical equilibrium programs available for AFT accurate calculations, but access to the source code of these programs is not permissible. Thus, a subroutine was written and implemented in the emission module by Coutinho (2008) leading to reasonable results. This program is based on JANAF enthalpy and internal energy approach (Goodger, 1977 and Moss, 2007), which interpolates and extrapolates the total amount of the enthalpies and internal energies of the reactants and products at 1500K and 2500K. In addition, the dissociation effect was estimated to result in a reduction of 25% in temperature above 2000K. The verification procedure of the

developed subroutine was based on the AFT estimation software provided by Depcik (2008) giving an accuracy of 1% for temperatures less than 2000K and 4% for temperatures over 2000K (Coutinho, 2008).

The coefficients and exponent constants were calibrated using the data given by TERA for the simulation of the baseline engine ICAO LTO cycle. The resulting emission indexes were then re-calibrated against the ICAO LTO cycle data (ICAO, 2008). The NO_x EI as a function of AFT for cruise and LTO cycle is shown in figure 3.11 for three approaches: original Lefebvre's, modified Lefebvre's and ICAO data.

The relationship for NO_x EI (modified Lefebvre's correlation) derived by Coutinho (2008) is as follows:

$$EI_{NOx} = \frac{0.004E-3.P_3^{1.25}.V_c.e^{\left(0.0025.T_{pz}\right)}}{\dot{m}_A T_{pz}} \qquad \textbf{(3.4)}$$

where P_3 is the total pressure at entry of the combustor; V_c is the combustion volume; T_{pz} is the combustor primary zone temperature (equivalent to the AFT); and $\dot{m}_A$ is the combustor air mass flow.

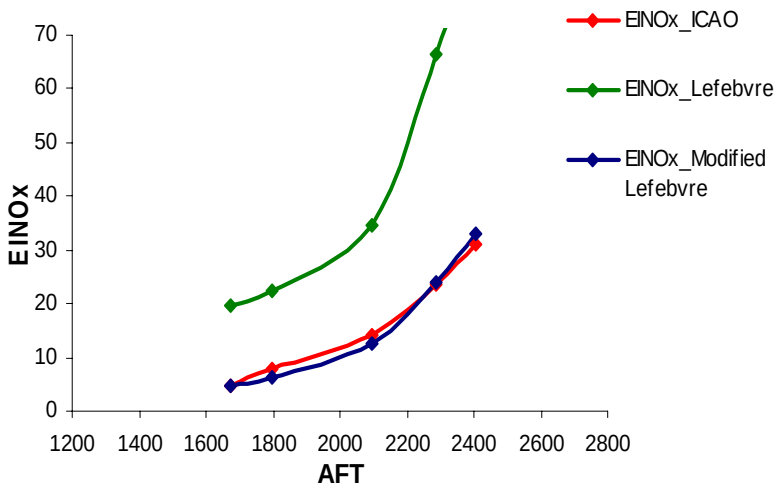

Figure 3.11: NO_x EI as a function of AFT for cruise and LTO cycle (Coutinho, 2008)

The emission indexes for CO_2 (carbon dioxide) and H_2O (water vapour) are based on the type of fuel being burned (particles of carbon and hydrogen contained in the fuel). The mission emissions, then, are directly proportional to the fuel burn for a certain fuel. The CO_2 and H_2O EIs are obtained by means of the atomic weights of each element of the reaction and are formulated as follows (IPCC, 1999):

$$EI_{CO_2} = \frac{x(W_C + 2.W_O)}{xW_C + yW_H} \qquad \textbf{(3.5)}$$

$$EI_{H_2O} = \frac{y/2(2.W_H + W_O)}{xW_C + yW_H} \qquad \textbf{(3.6)}$$

where W_C, W_O and W_H represent the carbon, oxygen and hydrogen atomic weights. In the case of Jet-A, the following values are used: $EI_{CO_2} = 3160\left[\frac{g}{kg}\right]$ and $EI_{H_2O} = 1230\left[\frac{g}{kg}\right]$.

3.5 Noise Module

The noise generation in a turbofan is a complex process as described in chapter 2. As a result, this makes its calculation a challenging task.

There are different approaches to compute the total turbofan noise whose sources are mainly the turbo-machinery (i.e.: fan, compressor, combustor and turbine) and exhaust jet. Usually, the following input data are needed: engine geometry, acoustic properties and rotational speeds.

From the point of view of regulations, there are three main flight points to be verified: approach, sideline and flyover. The positions of measurements are given in the annex 16 ICAO noise certifications. The maximum allowable levels of noise determined by regulations are units of effective perceived noise levels (EPNLs) and depend on the aircraft take-off maximum weight and number of engines. Therefore, the EPNLs for approach, sideline and flyover are used as a figure of merit in this research.

3.5.1 TERA Noise Module

The noise module, so-called Soprano (ANOTEC Consulting S.L., 2007), implemented in the MDO described in section 3.1.1, is based on methods and correlations available publicly. This module is developed in a research program 'SilenceR'.

This software predicts the overall aircraft noise levels based on the aircraft and engine performance modules data. It comprises modeling approaches for different noise sources. The noise sources levels are calculated from the thermodynamic parameters for a certain operating condition and flight path. After that, the noise propagation and the atmospheric absorption corrections are applied.

The methods used in Soprano are described as follows:

- Fan and compressor source noise calculation is based on Heidmann (1979) approach.
- Atmospheric absorption values are a function of temperature and humidity and are computed according to SAE (1975).
- Airframe noise is estimated using the approach given by Fink (1977).
- Core noise is developed using SAE (1994).
- Single jet noise is derived from SAE (1994).
- Turbine noise calculation follows the methodology given by Kazin and Matta (1976).
- Calculation of ground reflection effects are provided by Chien and Soroka (1982).
- Prediction of lateral noise attenuation is based on SAE (1981).
- Prediction of subsonic coaxial jet mixing noise is developed using SAE (1994).
- Prediction of single stream shock associated noise is obtained from SAE (1994).

3.5.2 PMDF Noise Module

The aircraft noise module in MDO of section 3.1.3 is derived from the FOOTPR source code (Clark, 1981) and is a semi-empirical program which includes available noise calculation approaches. This module uses take-off and climb profile calculated in the aircraft performance module in order to generate noise footprint contour data or noise levels in several locations indicated by the user or ICAO certification points (i.e. flyover and sideline).

The noise sources consist of fan inlet and exhaust, jet, combustor, turbine, flap (for powered lift) and airframe. Correction factors for the noise sources propagation

to the observers are applied for the effects of atmospheric attenuation, ground attenuation and reflections and aircraft shielding.

The different noise sources are estimated using subroutines developed at the NASA Lewis Research Center for ANOP (Aircraft Noise Prediction Program): Heidmann (1979) for fan noise, Stone (1974) for coaxial jet noise, Huff et al (1974) for low frequency core engine noise, Krejsa et al (1976) for turbine noise, and Dorsch et al (1975) for externally blown flap noise. The airframe noise is based on the Fink's approach (1977).

In figure 3.12, a flow diagram of the FOOTPR program is presented. The process starts by computing the required geometric parameters between the aircraft source and the observer as a function of time using the main program FOOTPR (Clark, 1981). Observer locations are entered in the input file as a grid. Then, the subroutine NOIS is called for noise calculation at time intervals throughout aircraft path. Finally, propagation corrections for atmospheric attenuation, extra ground attenuation, shielding, and ground reflection are applied to the total noise as requested by the user, and then EPNL calculations are obtained.

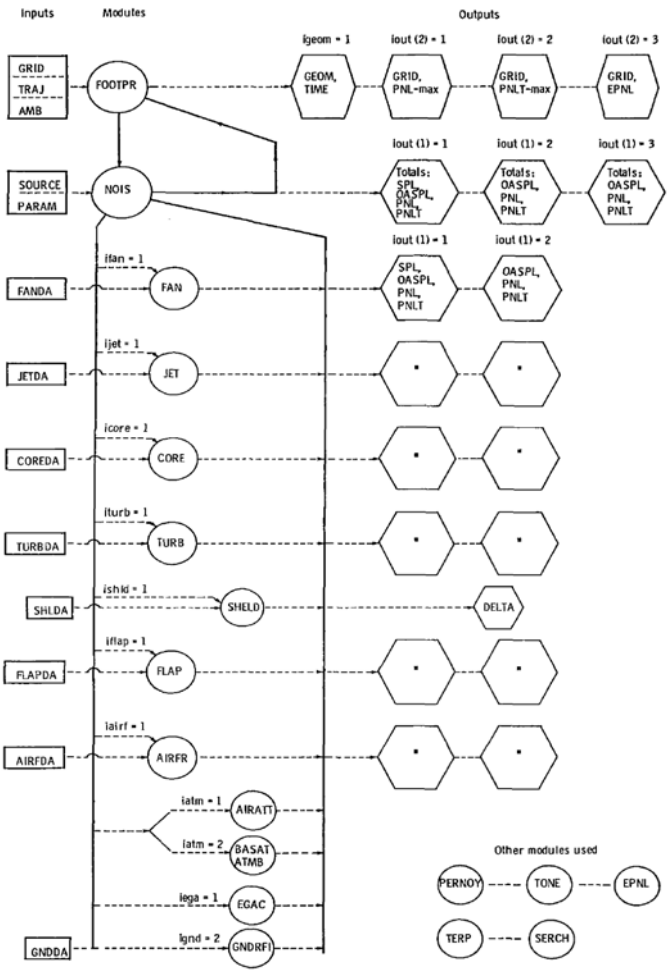

Figure 3.12: FOOTPR Flow diagram (Clark, 1981)

3.6 Weight Module

Propulsion system (engine and nacelle) weight prediction is a vital and challenging task in the preliminary design phase where tradeoffs are involved among engine weight, dimensions, performance, and noise characteristics.

There are three approaches available in the public domain to estimate the engine weight: low-accuracy, component-by-component and cycle parameters-based methods. A brief description of each method is given as follows:

- Low-accuracy method (Svoboda, 2000): The engine weight is associated to one of its main parameters, typically take off thrust; it usually relies on historical data; and the engine weight data points are fitted with a linear correlation.

- Component-by-component method (Pera et al, 1977): Engine weight is obtained from the addition of each component weight calculations which are based on a set of correlations calibrated using historical data. The NASA simulation code WATE-1 (Weight Analysis of Turbine Engines) is based on this approach.

- Cycle parameters-based method: It was developed by Gerend and Roundhill in 1970. Semi-empirical correlations to estimate preliminary weights and dimensions for the entire propulsion system was developed based on data for over 350 engines spanning the 1940-1980 time period. This approach uses the main cycle parameters (i.e. airflow, bypass ratio, pressure ratio and turbine temperature), design flight Mach number, and technology level (entry into service year) to standardise the weights and dimensions. In addition, the engine weight is split into the fan and the gas generator section. The fan section weight is made up of the fan itself, the fan casing, the power turbines and the fan shaft, and its bearings (see figure 3.13). All the remaining weight is assigned to the gas generator section.

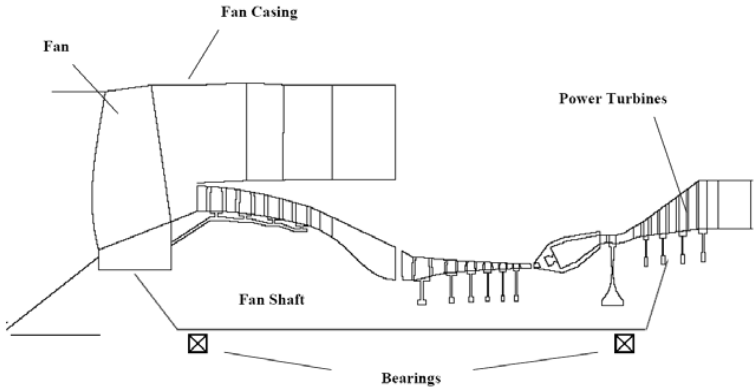

Figure 3.13: Bare engine schematic

3.6.1 TERA Weight Module

The weight model used in the first MDO is based on the work by Onat and Klees (1979) and was developed by Chalmers University of Technology. This model establishes the weight of key components in the engine, for instance: compressors, burners, turbines and frames (component-by-component method). Every module in the model handles a set of required data such as: stress level, material properties, geometry stage loading, hub-to-tip ratio, maximum temperature, and shaft over-speed in order to calculate the above-mentioned component weight. As a minimum, this model will estimate engine weight by the use of performance data only.

The production cost module calculates the engine production cost based on detailed design information given by the weight module (e.g. weights, dimensions, materials, and so on) as well as on the raw material assessment and a value added during the manufacturing and production process. The same manufacturing conditions for all evaluated engines are assumed. This module, whose owner is

Stuttgart University, is linked to the weight module by means of a software interface.

3.6.2 PMDF Weight Module

This weight module uses statistical and empirical equations to predict the weight of each component in a group weight statement (Onat and Klees, 1979).

A more analytical wing weight estimation capability is incorporated for use with more complex wing platforms. Centers of gravity and moments of inertia can also be calculated for multiple fuel conditions.

The estimated weight of the propulsion system is based on the cycle data generated in the engine performance model and preliminary component design. The approach used was to keep the specific input to a minimum, while still achieving a high level of accuracy. This is explained in the next section.

3.6.3 Modified Propulsion System Weight and Dimension Model (WeiDim)

The cycle parameters-based method was chosen for assessing the weight of the novel turbofans such as ICR and CVC turbofans, as there is a good compromise between accuracy, robustness and ease of implementation (no material database and no geometry data are needed). The original correlations were updated by the author for modern and radical turbofans' applications. This module was developed as part of this PhD research project.

The subsequent section offers an overview of the original method and a description of the modifications carried out in order to increase its accuracy. For the nacelle weight calculation, a simple approach given by Jenkinson et al (1999) was used.

3.6.3.1 Original Gerend-Roundhill Approach for Engine Weight Estimation

The engine weight is estimated using the following equation:

$$W_{eng} = \left[\frac{W_{bare-eng}}{W_o}\right][W_o][KENG][Kgg(KHP) + (1 - Kgg)(KLP)] \quad \textbf{(3.7)}$$

Where: $\left[\frac{W_{bare-eng}}{W_o}\right]$ is a constant derived from the normalisation of real engine weight data $(W_{bare-eng})$, and W_o is the specified total fan face airflow.

In the equation above $KENG$ is correction factor applied to the complete engine and is defined as follows:

$$KENG = (KBPR)(KY)(KLIFE)(KM)(KDUCT) \quad \textbf{(3.8)}$$

Where: $KBPR$ is a function of bypass ratio (BPR) and is based on the fact that the engine specific weight (weight per unit mass flow) decreases with increasing bypass ratio; KY is a function of the entry-into-service (EIS) year and considers the advances in technology throughout the years; $KLIFE$ is a factor which reflects the engine weight as a function of design life: engines with shorter design life (such as lift engines) are more likely to weigh less than longer life ones. KM depends on the kind of flight regime for which the engine is designed (subsonic or supersonic); and $KDUCT$ is the correction factor which considers the fact that engines with long ducts weigh more than short duct ones.

In equation (3.9), KHP represents the correction factor applied to high pressure (HP) section and is defined as:

$$KHP = (KT4)(KOPR)(KWc) \quad \textbf{(3.9)}$$

Where: $KT4$ factor contains the entry-into-service year and the turbine entry temperature T4, that is: the turbine cooling and material technology level. $KOPR$ represents the overall pressure ratio and the corrected core mass flow impact on the engine weight. KWc is the scaling factor which relates gas generator corrected mass flow with the gas generator weight.

The factor KLP in equation (3.10) is defined as:

$$KLP = KWo \quad \textbf{(3.10)}$$

Where: KWo associates the overall corrected mass flow with the low pressure system weight.

Finally, the factor Kgg in equation (3.7) represents the ratio of gas generator weight to the total engine weight, and is determined by BPR.

As the scaling factors of the original approach use data for existing engines between 1940 and 1980, these factors have to be recalibrated for engines which have entered service since 1980. The calibration methodology applied in this research is explained below.

3.6.3.2 Modified Gerend-Roundhill Approach for Engine Weight Estimation

Due to the explanation given above, the following scaling factors were recalibrated:

- The $KBPR$, $KOPR$ and Kgg factors (refer to figures 3.14-3.16) were extrapolated to higher values of BPR and OPR, since these cycle parameters are limited to 10 and 35, respectively, in the original method.

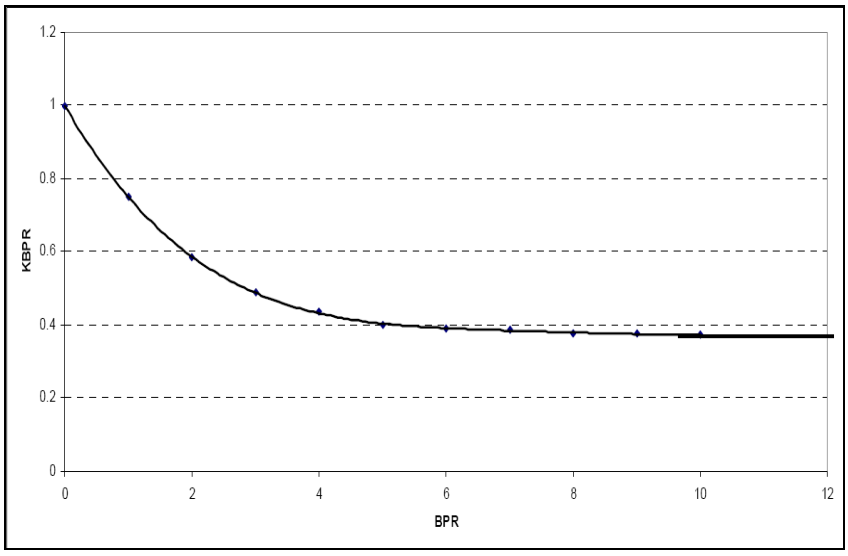

Figure 3.14: Calibration of the $KBPR$ factor to the BPR

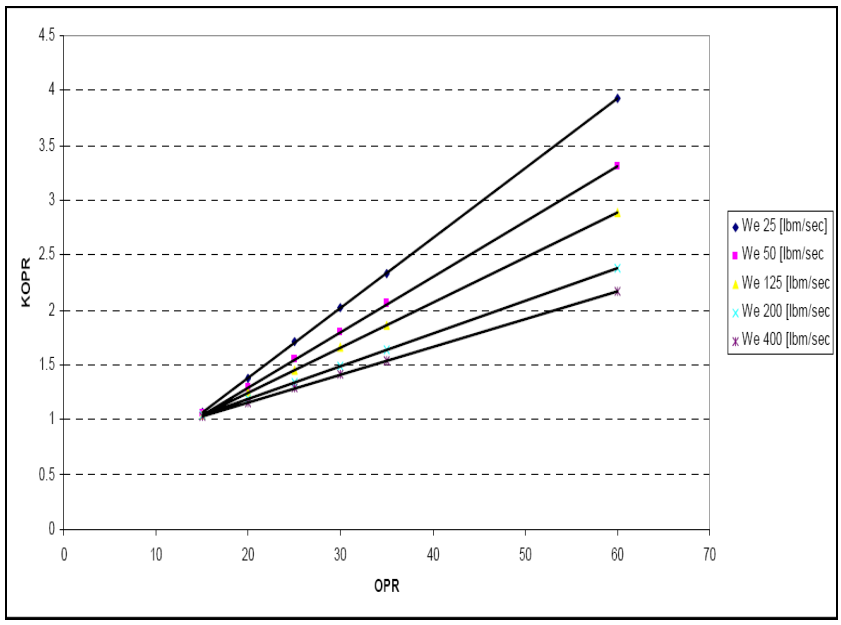

Figure 3.15: Calibration of the $KOPR$ factor to the OPR

- The $KT4$ factor was assumed to be 1.0 due to its smaller value in comparison to the other factors and the high uncertainty in extrapolating the attainable turbine entry temperatures.
- The KY factor was modified and calibrated against recent engines. This was done by using the extended weight estimation program on a pool of nine engines entering into service between 1971 and 2007, and also from different manufacturers, such as: Rolls-Royce (RB211-524B, Trent553, Trent768, Trent875 and Trent977), GE Aircraft Engines (CF6-6D, CF6-80C2B8F, GE90-85B) and Pratt & Whitney (PW4098). The KY factor was achieved by changing its value until each engine's real weight was matched. Then, the KY factor of each engine was plotted against the EIS year. As a result, the solid line was obtained representing the best fit for the weight of recent engines from several OEMs.

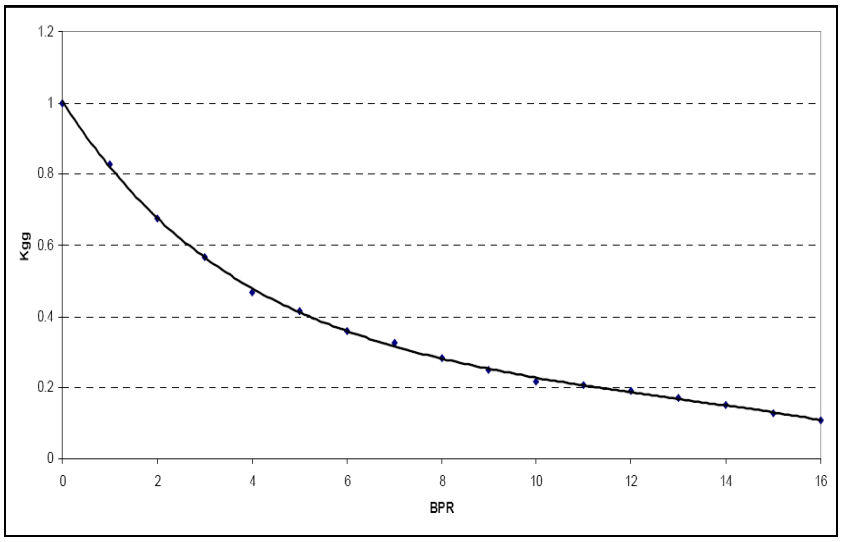

Figure 3.16: Calibration of the *Kgg* factor to the *BPR*

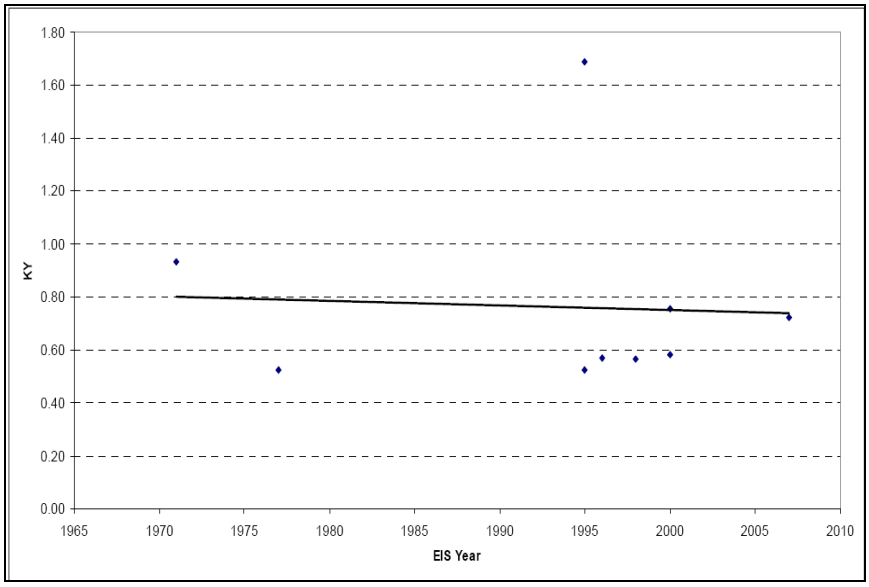

Figure 3.17: Calibration of the *KY* factor to the EIS year against a pool of recent turbofans

After validation of the new weight prediction tool with a pool of nine recent engines, discrepancies of up to 18% must be expected.

3.6.3.3 Nacelle Weight Prediction Approach

In order to calculate the nacelle weight, the approach provided by Jenkinson et al (1999) was used. This method uses the data of existing aircraft nacelle weights, which are plotted against the total installed static sea level thrust. As a result, two correlations - approximated to the linear function - were drawn:

$$Wnac = 6.8 \times Fn[kg] \text{ (for } FN < 600[kN] \quad \textbf{(3.11)}$$

$$Wnac = 2760 + (2.2 \times Fn)[kg] \text{ (for } FN > 600[kN]) \quad \textbf{(3.12)}$$

Where: FN is the total installed take-off static sea level thrust [kN].

If a short length bypass duct is used the nacelle weight value obtained using the above-mentioned approach should be reduced to some extent and increased for large length ducting. An extra reduction of 10% can be obtained if thrust reversers are not included, and, conversely is increased by 10% if additional noise suppression material is required.

3.6.3.4 Modified Gerend-Roundhill Approach for Engine Dimension Estimation

The prediction of critical engine dimensions, i.e. bare engine length and diameters, was based on cycle parameters according to the Gerend and Roundhill approach (1970) with certain calibrating factors.

The bare engine length L_{bare} (see figure 3.18) is estimated using the following equation:

$$L_{bare} = L_{ref}\left(KLWc\right)\left(KLBPR\right)\left(KLY\right)\left(KLOPR\right)\left(KIGV\right) \quad \textbf{(3.13)}$$

Where: $L_{ref} = 85.0"$; $KLWc$ is the correction factor for airflow size; $KLBPR$ is the correction factor for bypass ratio; KLY is the correction factor for technology level; $KOPR$ is the correction factor for overall cycle pressure ratio; and $KIGV$ is the correction factor for inclusion/exclusion of fan inlet guide vanes (IGV's).

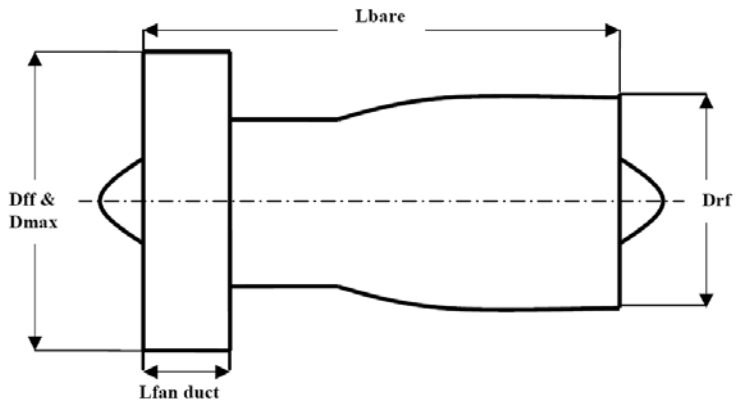

Figure 3.18: Bare engine dimension schematic

The calibration procedure was done in the same way as for the weight model: The $KLWc$, $KLBPR$ and $KOPR$ factor values were obtained by extrapolating the graphs from the original approach (refer to figures 3.19-3.21); $KIGV$ was assumed to be 1.04 if $BPR \rangle 2.5$; and the KLY factor was achieved by changing its value until the real length was matched for recent engine configurations (see figure 3.22).

The diameters (see figure 3.18) calculated are as follows:

The front flange diameter: $D_{ff} = D_{fan-tip} + 3.0["]$ **(3.14)**

Where: $D_{fan-tip} = f(M_{fan-face}, {}^{hub}/_{tip}, Wo)$

The rear flange diameter: $D_{rf} = (A)\sqrt{Wo} + 3.0["]$ **(3.15)**

Where: $A = f(BPR)$

The maximum diameter: $D_{\max} = D_{ff}$ **(3.16)**

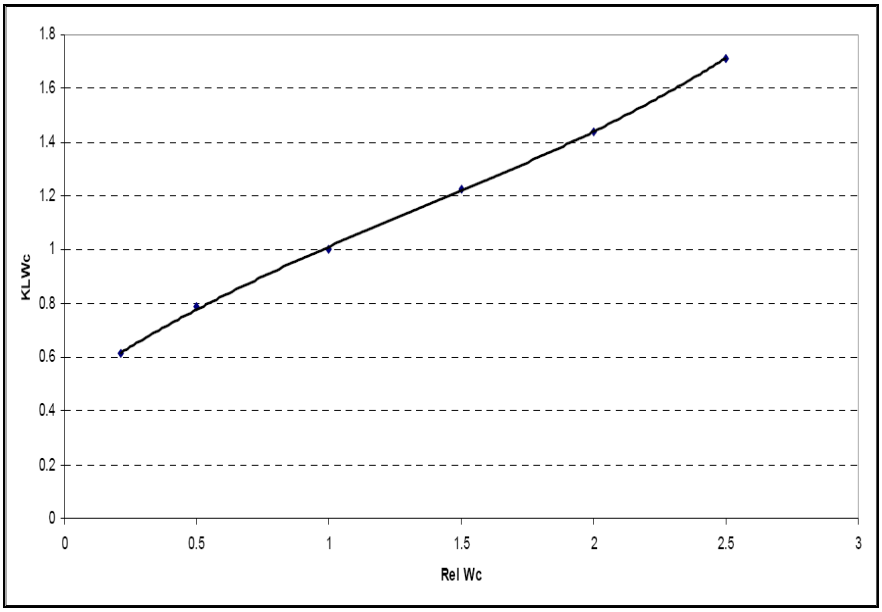

Figure 3.19: Calibration of the $KLWc$ factor to the $\mathrm{Re}lWc$

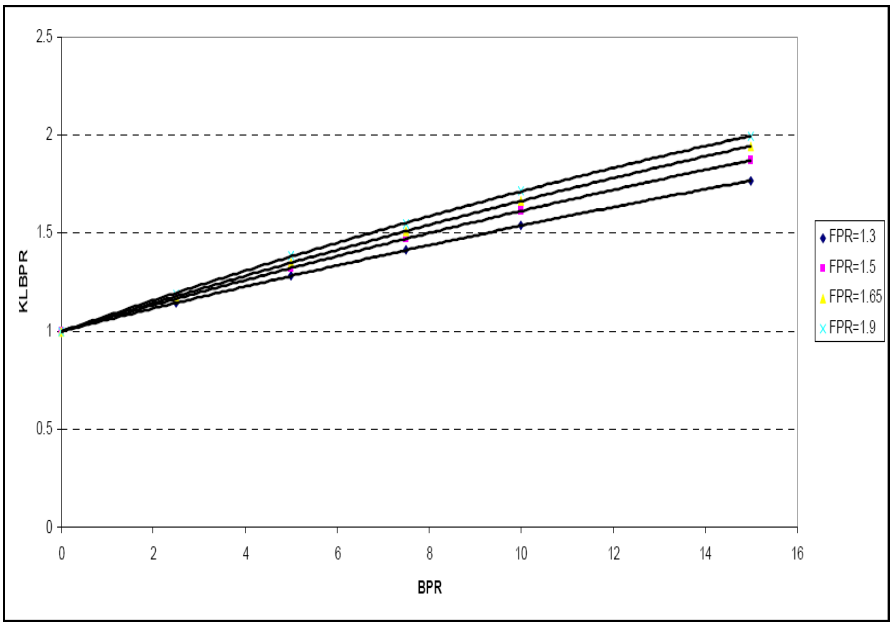

Figure 3.20: Calibration of the $KLBPR$ factor to the BPR

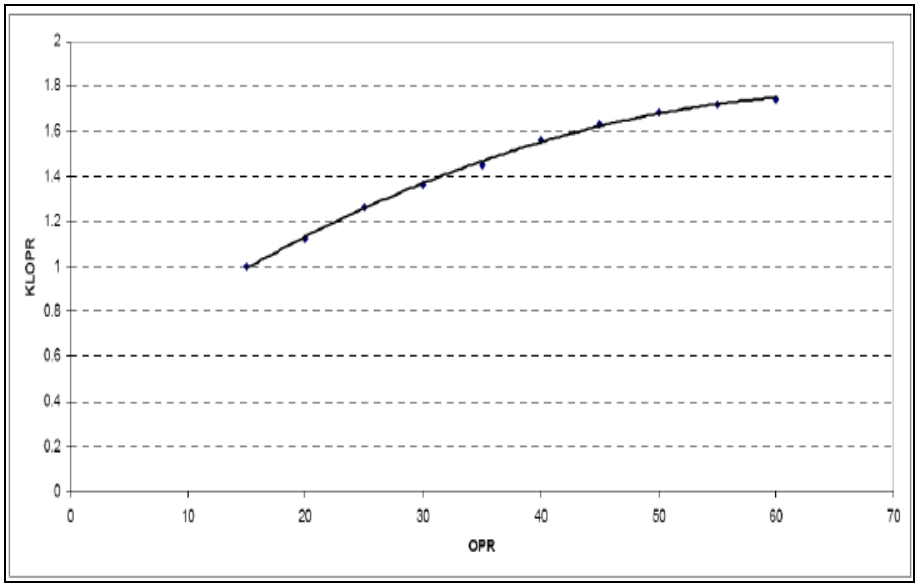

Figure 3.21: Calibration of the *KLOPR* factor to the *OPR*

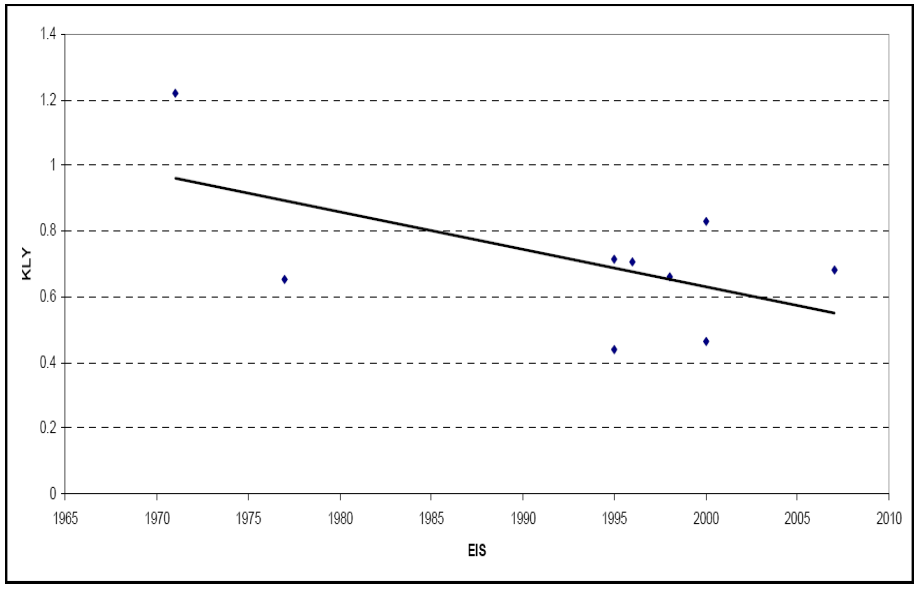

Figure 3.22: Calibration of the *KLY* factor to the EIS year against a pool of recent turbofans

3.6.3.5 Nacelle Dimension Prediction Approach

The nacelle dimensions are calculated making some assumptions based on the bare engine dimensions, as follows:

$$\text{Length: } L_{nac} = 1.5 \times D_{nac} \qquad \textbf{(3.17)}$$

$$\text{Diameter: } D_{nac} = D_{\max} \qquad \textbf{(3.18)}$$

This weight and dimension model (WeiDim) developed as part of this research is currently used in different research projects.

3.7 Economic Module

3.7.1 TERA Economic Module

The economic module (figure 3.23), connected to the MDO for baseline, advanced, contra-rotating, geared turbofans' feasibility studies, consists of two subroutines and one function for lifing, economic and risk calculations (Pascovici et al, 2007). This module was developed as part of this PhD project in collaboration with Daniele Pascovici.

The lifing subroutine calculates the life of the high pressure turbine disk and blades based on the creep and fatigue analysis throughout the whole engine operational cycle. The output of this program is the time between overhaul (TBO), which is the amount of hours that the engine can be in service before its first overhaul.

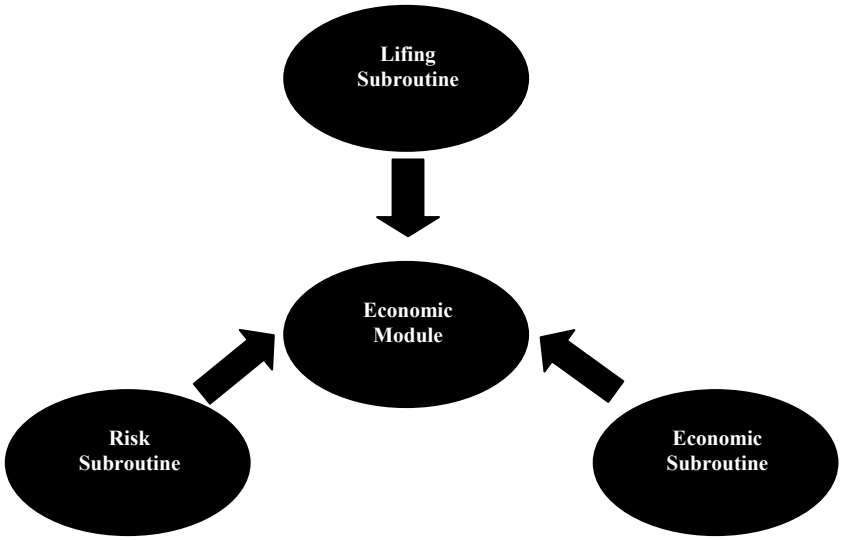

Figure 3.23: Architecture of the Economic module (Pascovici et al, 2007)

Once the time between overhaul, the cost of labour and the cost of the engine (required for the spare parts costs calculation) have been computed, the economic subroutine runs a cost analysis.

The economic subroutine calculates two figures: the engine maintenance cost using the time between overhaul, the cost of labour and the cost of the engine (required for the spare parts costs calculation) once computed; and the airframe maintenance cost based on the operational empty weight and the maximum take off weight. These two parameters define the aircraft cost and the labour cost.

The direct operating costs (DOC) include all the costs related with flying and direct maintenance of an aircraft (Jenkinson, 1999) and consist basically of engine and airframe DOC. The former is derived from maintenance cost, emission and noise taxes, fuel cost, insurance cost and the interest being due on the total investment; and the latter comprise cabin and flight crew cost, landing cost,

navigational and ground handling fees. The total DOC is required to assess the net present cost (NPC) based on a timeframe of 30 years.

The risk subroutine is based on the Monte Carlo approach and considers the uncertainty level of some variables, which have a great impact on the NPC. These variables are as follows: fuel cost, interest percentage on total investment, inflation, downtime, maintenance labour cost per man hour, and emission and noise taxes. This program is run for 10 000 iterations and then a cumulative frequency curve is generated so that the most probable scenarios can be understood.

3.7.2 PMDF Economic Module

The cost estimation module used in the MDO for baseline, geared and CVC turbofans is based on the work carried out by Johnson (1981). This model handles data coming from other modules in the design framework (i.e. weight, engine and aircraft performance, configuration and weights, etc) so that the airframe research, development, test and evaluation (RDT&E) cost, airframe production cost, engine RDT&E and production costs, direct operating cost, and indirect operating cost can be computed, followed by the life cycle cost of the aircraft. Furthermore, it estimates the return on investment (ROI), which is a financial criterion for aircraft design judgments, as well as the engine time between repairs/removals (TBRR).

An improvement to this model was made by Brinks (2008) as part of this PhD project. Implementation of a number of subroutines to calculate the net present value (NPV), engine direct operating cost (DOC), noise and emissions charges, and a risk function based on Monte Carlo Simulation (MCS) to assess the uncertainty level of certain variables will provide a more robust cost estimation package; this risk analysis tool was developed during this research.

This new cost module consists of ten subroutines and one function as shown in figure 3.24, which is connected to the whole MDO using an interface. All cost-specific input data contained in Namelist $COSTIN in the input file are read and transferred to the control subroutine. This subroutine controls the cost module and also calls the other subroutines for different cost calculations. These calculations are adjusted for inflation. There are three subroutines for RDT&E and production costs of the aircraft: two for the airframe and one for the engine. Direct and indirect operating costs are computed by DOC and IOC subroutines, respectively. Finally, noise and emissions charges are obtained from their own subroutines which are called from DOC subroutine as seen in figure below.

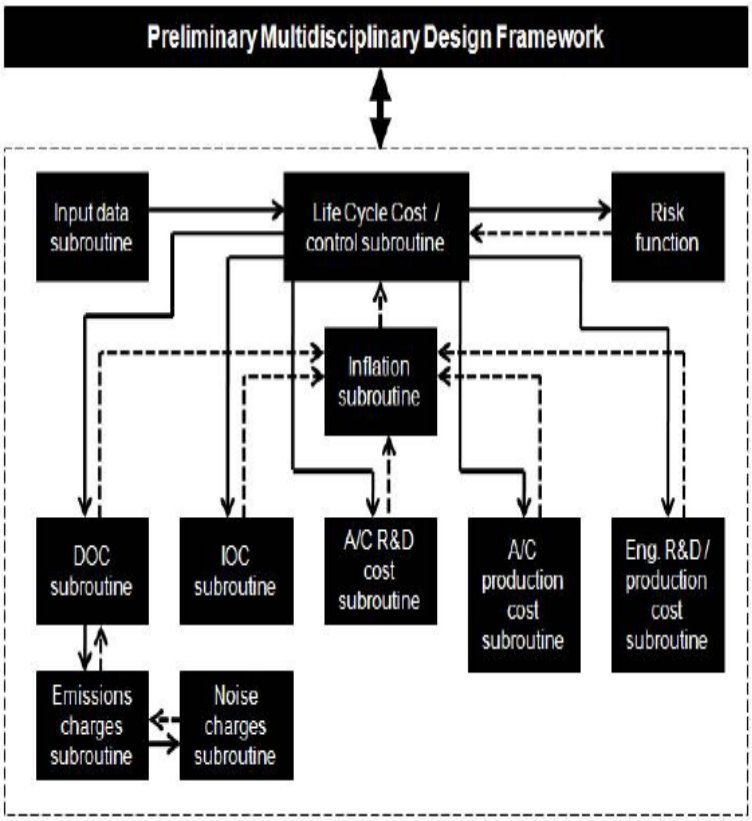

Figure 3.24: Architecture of the LCC module (Brinks, 2008)

This cost analysis module applies statistical and empirical equations that were obtained by means of the cost estimation relationships' (CER) method (Johnson, 1981). The NASA databases of RDT&E, production, operation, and maintenance costs as well as aircraft and engine performance were used to derive such correlations.

The approach used to compute the airframe production cost is given by Beltramo et al (1977). The cost of each component, not including the bare engines, is determined using weights data from the weight module. To facilitate the execution and future maintenance of this subroutine, the components were grouped as follows:

- Structure: wing, tails, fuselage, landing gear and nacelles
- Propulsion: thrust reverser and miscellaneous and fuel systems
- Systems and equipment: surface controls, auxiliary power unit, instruments, hydraulics, electrical, avionics, furnishings and equipment, air conditioning, anti-icing, and pneumatics
- Final assembly and delivery

Airframe RDT&E correlations - derived from the work carried out by Eide (1980) - comprise engineering development cost, development cost for tooling, manufacturing, and materials, development support, and flight test operations.

The engine RDT&E and production costs subroutine was developed using the research conducted by Nelson and Timson (1974), which relates technological development to acquisition cost. The costs are calculated using thrust, Mach number, and dynamic pressure technology factors and the expected time-of-arrival (TOA) for that technology level using cost indices.

The TOA measures technological advances and consists of the time between the start of the jet engine period and the start date of FAA certification testing in calendar quarters. The TOA equation is derived from a database with SFC, FN, weight, TET and OPR.

Calculations of direct operating costs are based on an American Airlines model (1978).

The airframe maintenance costs are due to materials, direct labor and direct labor burden (i.e. airframe inspection, air conditioning, avionics, electrical power, equipment and furnishings, fire protection, flight controls, fuel, structures, nacelles, wings, etc). The engine maintenance costs are calculated including materials, direct labor, and direct labor burden. On the other hand, the remaining direct operating cost items include depreciation, insurance, aircraft servicing, flight crew, and fuel cost. Finally, the total direct operating costs are then calculated per departure, per block hour, per available seat per trip, per available seat mile, and for the life cycle of the aircraft.

This subroutine for indirect operating costs' calculation is based on a Lockheed-Georgia model (Stoessel, 1970). These costs are grouped as follows:

- Ground property and equipment and aircraft handling.
- Cabin crew expenses.
- Passenger service (food and beverage).
- Passenger service support, commissions, adverts, etc.
- Aircraft control.
- Passenger handling, reservations, sales,etc.
- Baggage handling.
- Cargo handling.
- Freight sales, ads, and publicity.

- General and administrative.

An inflation correction factor based on the US consumer price index is applied to all cost calculations.

To use the previously described module in this study, the following engine-associated cost subroutines were changed (Brinks, 2008): RDCOST (which reads data required for cost calculation), CALCST (it computes aircraft LCC for subsonic civil transport), ENCOST (engine RDT&E and production costs' calculations), AADOC (DOC estimation) and finally DOLLRS (inflation correction estimation).

Additional variables were incorporated in RDCOST by means of the alteration of the namelist $COSTIN placed in the input file. For further detail, please refer to Brinks (2008)

The subroutine CALCST was widely changed to incorporate other calculations not considered in the original module. These new capabilities are as follows: net present value (NPV), emissions and noise charges, and DOC. Additionally, MCS-based risk function was implemented to consider the uncertainty level of random variables for cost calculations.

A profit margin of 7% was applied to the engine cost price given by ENCOST (Brinks, 2008). This percentage was based on the net profit margin (TTM) per annum of different original equipment manufacturers (OEMs) such as: MTU Aero Engines, Honeywell and Rolls-Royce plc.

Furthermore, the empirical relationships (i.e. TOA and CERs) were revised based on the non-linear and linear regression analysis approaches using existing data (Brinks, 2008). A pool of 15 turbofans was exploited to obtain the following correlation:

$$TOA15 = -134.515 + 18.299 \cdot LN(TET) - 21.229 \cdot LN(THRMAX) + 12.695 \cdot LN(WENG) + 4.697 \cdot LN(TOTPRS) - 216.718 \cdot LN(SFC) \quad \textbf{(3.19)}$$

Where: TET is turbine entry temperature, $THRMAX$ is sea level static thrust at take-off, $WENG$ is weight of the bare engine, $TOTPRS$ is a pressure expression, and SFC is specific fuel consumption.

The derived TOA equation is very suitable for conventional turbofans according to Brinks (2008); but for novel turbofan configurations it ends at undependable values. As a result, a straightforward correlation based on cruise net thrust and SFC was employed for the calculation of novel-turbofan cost price. A relationship provided by Jenkinson (1999) was adapted leading to the following mathematical expression (Brinks, 2008):

$$EP = 0.6 + 0.945 \cdot \frac{F_{N_{cr}}^{0.88}}{SFC_{cr}^{2.58}} \quad \textbf{(3.20)}$$

Where: EP is the engine price, $F_{N_{cr}}$ is the cruise net thrust in N, and SFC_{cr} is the cruise specific fuel consumption in $\frac{mg}{Ns}$.

In order to fit the research, development and production cost of a current aircraft, a fudge factor of 2.2 was implemented in AFCOST and AFRAD.

Frankfurt Main International Airport's approach was used to establish the gaseous emissions and noise charges (Brinks, 2008). The decision for selecting this scheme was based on the detailed documentation available in the public domain (Fraport AG, 2008). Two subroutines were created and incorporated in the cost module: EMCHR and RDNOI. The EMCHR estimates the emissions charges for

NO_x ,UHC and CO during landing and take-off cycle while RDNOI calculates the noise charges for ICAO points (i.e. RDNOI).

The consumer price indices used in the subroutine DOLLRS were modified with 2007 values given by the US Department of Labour (2008). An inflation rate of 2.85% is assumed from 2008 on (Brinks, 2008).

Lastly, three cost technology parameters were introduced into the cost module as follows (Brinks, 2008): FENRD for engine R&D cost, FMENG for engine production cost, and FOPROP for engine maintenance cost. Figure 3.25 illustrates the variation of these factors with time. FENRD and FMENG are applicable for TOA method whilst FOPROP for both TOA and the Jenkinson's methods.

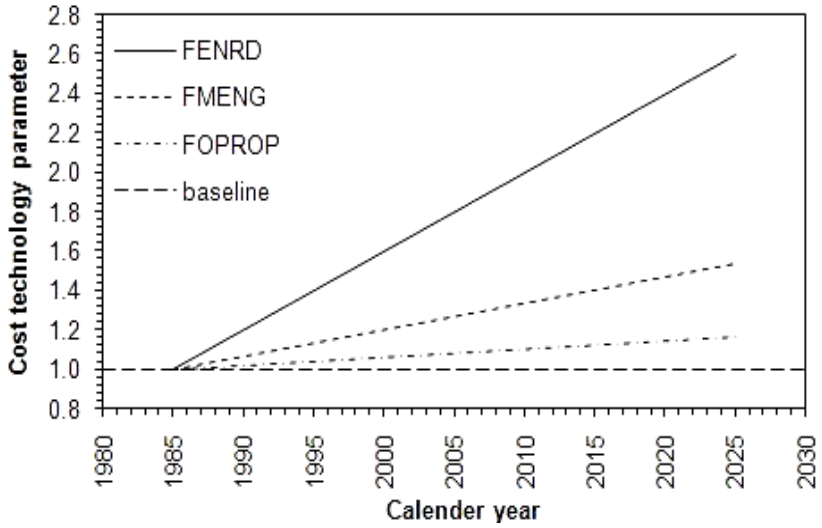

Figure 3.25: Cost technology parameters (Brinks, 2008)

3.8 Environmental Module

The availability of an environmental module would be very useful during the conceptual and preliminary design phase of an aero-engine so that its climate change impact can be assessed, but this part can be very complicated depending on

the sort of emissions being treated, for instance: the NO_x contribution to the climate change relies on the location and time of year, and the global impact is computed using difficult general circulation models (GCM); the converse happens to other greenhouse gases (i.e. CO_2, N_2O and CH_4) (Ponater et al, 2001 and Whellens, 2003).

For the purpose of this research less complicated and accurate methods were applied to evaluate the climate change effect of a particular aero-engine configuration: radiative forcing (MDO for baseline, geared and CVC turbofans) and global warming potential (MDO for baseline, intercooled, recuperated, and ICR turbofans); these models are described as follows.

3.8.1 Radiative Forcing

The computation of the radiactive forcing (RF) of a specific emission is based on the amount emitted and flight segment (Tintani, 2008). The CO_2 emissions impact is measured using the correlations derived from G.Y. Shi (1992), which utilises the following mixing ratio (concentration change):

$$Conc_{ppmv} = \frac{Emission\_rate \bullet \mathrm{Re}sidence\_time \bullet MW_{air}}{Atmosphericmass \bullet MW_{CO_2}} \qquad \textbf{(3.21)}$$

A reference CO_2 mixing ratio of 378 ppmv was used based on IPCC working group 1 assumptions (Climate Change 2007; The Physical Science Basis).

This model requires two inputs: the amount in kilograms of CO_2 generated by the emission model and the flight segment time coming from the mission model, in order to estimate the RF.

The following relationship given by G. Y. Shi for RF is used:

$$RF = 4.841In(\frac{C}{C_o}) + 0.0906(\sqrt{C} - \sqrt{C_o}) \quad \textbf{(3.22)}$$

Where C_o is the CO_2 initial concentration change and C is the final one.

For NO_x emissions, the RF has to be considered for two cases: the ozone formation and the methane depletion. For the validation process, the data available in the literature were employed: Kohler et al (2008) gives findings of the RF for both ozone and methane produced by aviation per annum at several flight conditions. The environmental model utilises an average RF at a specific segment and then multiplies it by the amount of emission released in order to obtain the total radiative forcing. For water vapour RF calculation, the approach provided in Svensson et al (2004) was implemented. For more detail about the model, please refer to Tintani (2008).

3.8.2 Global Warming Potential

The global warming potential (GWP) is based on the approach proposed by Klug et al (1996) which uses an index to assess the RF effect caused by human activity emission during a specific timeframe (i.e. 100 years). The emission impact of a different pollutant species, that is: NO_x and H_2O, is compared to that produced by the same mass of CO_2. This model does not include contrails, cirrus clouds and the NO_x impact on methane.

The GWP index in the case of NO_x emissions is calculated as a function of altitude taking into consideration the life spans of ozone formation rate, and NO_x

and O_3 molecules. The estimations are carried out assuming summer season conditions during which the climate change impact is maximised.

The GWP index is described as follows:

$$GWP = SFC \bullet \sum_{i=1}^{N_{spec}} \left(\frac{EI_i}{1000} \bullet GWP_i \right) \quad \textbf{(3.23)}$$

Where GWP is global warming potential index of a particular turbofan configuration $\left[N^{-1}.s^{-1}\right]$, N_{spec} species involved in the calculation, EI_i represents emission index, GWP_i is the global warming potential coefficient, and SFC denotes specific fuel consumption.

3.9 Risk Module

3.9.1 Monte Carlo Simulation

Simulation refers to an analytical method meant to imitate a real-life system (Blank, and Tarquin, 1999). Without the aid of simulation, one would use a deterministic modelling methodology that would not capture the element of risk; that is, it would produce a single outcome, generally the most likely or average scenario. Robust risk analysis seeks to analyse the effects of varying inputs on outputs of the modelled system, which requires the use of numeric simulation methods.

Numerical simulation methods known as Monte Carlo methods can be best described as statistical simulation methods. Statistical simulation is defined here in

quite general terms to be any method that utilises sequences of random numbers to perform the simulation. Monte Carlo is now used routinely in many financial applications and is quite adaptable for analyses which involve the modelling of uncertainty through descriptive variables. A basic assumption underlying the use of Monte Carlo simulations is that the behaviour of a system can be described by functions and variables, and once these are known, the Monte Carlo simulation can proceed by random sampling from the set of descriptive variables.

Assuming that the evolution of the physical system can be described by specific probability density functions and variables, the Monte Carlo simulation can proceed by sampling from this set of variables, which necessitates a fast and effective way to generate random numbers uniformly distributed. The outcomes of these random or stochastic samplings are compiled to produce and describe the result. However, the essential characteristic of Monte Carlo is the use of random sampling techniques to arrive at a solution to a physical problem. The output of the simulation is a cumulative distribution of values of the output parameter (NPV- Net Present Value), i.e. not just a single line.

3.9.2 Distribution Type

Whilst there are multiple types of distributions that describe data and events, normal distributions are observed in natural phenomena where values are most likely to be clustered around the mean with marginal extreme values occurring equally to the right and left of the mean (Hays, 1981; Lapin, 1990). The use of normal distributions to describe a variable such as NPV reflects the reality that these estimates can move equally in either direction of their respective mean values. Normal (Gaussian) distribution is shown in figure 3.26.

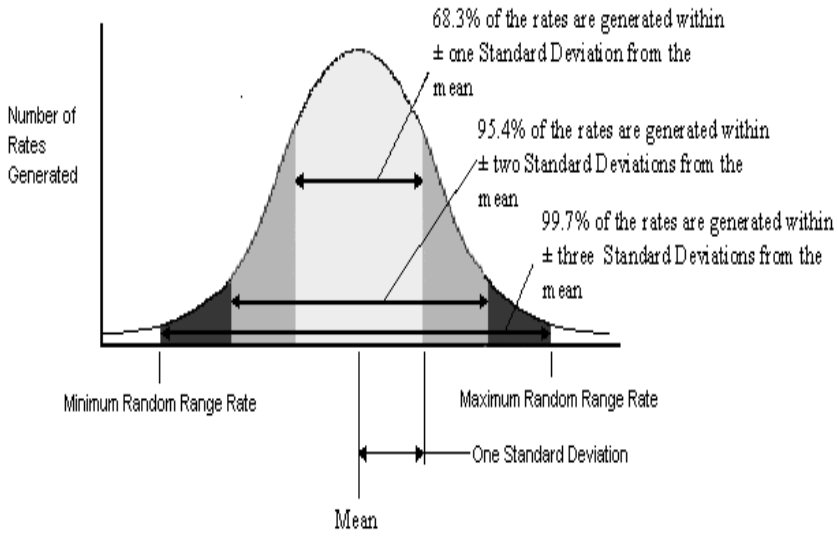

Figure 3.26: Gaussian distribution of random rates (J&L Software, 2005)

3.10 Optimisation Module

The optimiser selected in the MDO described in section 3.1.1 is iSIGHT (figure 3.27), which is a tool for integration of simulation codes, automation of manual design practice, and optimisation based on the interdigitation strategy (i.e. using different combinations of optimisation algorithms for a specific design problem) (Powell, 1990). It significantly diminishes the preliminary design time together with improvements of the product quality and reliability. This optimiser, developed by Engineous Software (2007), is commercially available.

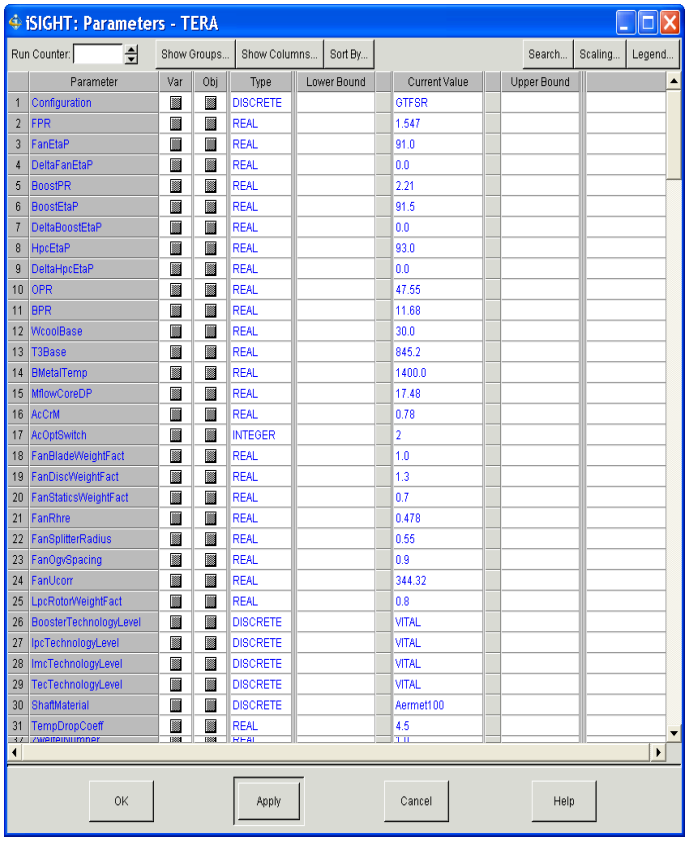

Figure 3.27: iSIGHT problem definition

As shown in figure 3.28, there are three optimisation techniques implemented in iSIGHT: Numeric: gradient-based algorithms (e.g. method of feasible directions); exploratory: global-search algorithms (e.g. genetic algorithms); and heuristic: knowledge-based algorithms (e.g. expert systems). These techniques can be used in several combinations, for instance; start with a genetic algorithm for a design space global search in order to find attractive regions, and then apply a gradient-based algorithm to detect the best solutions.

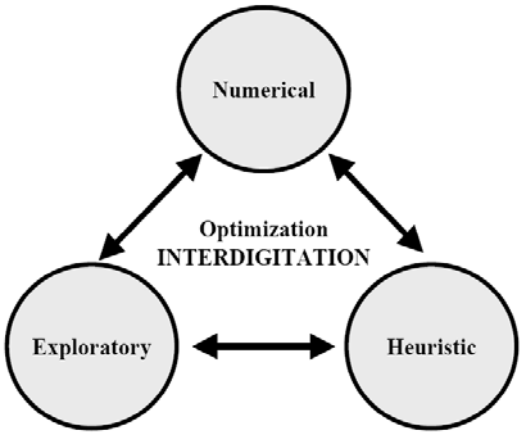

Figure 3.28: Optimisation techniques interdigitation (Koch et al, 2002)

In addition to the above-mentioned optimisation techniques, the design of experiments (DOE) techniques, approximation methods, and quality engineering methods are incorporated in iSIGHT for better design space exploration. A brief description of these techniques is given below.

There are 13 optimisation algorithms divided into three categories as noted at the beginning of this section: numerical, exploratory and heuristic (refer to table 3.2).

As can be seen from the below table, the most common techniques are numerical with nine algorithms available in iSIGHT. There are two direct methods handling constraints directly throughout the search; two penalty methods (i.e. Exterior Penalty and Hooke-Jeeves), which apply a penalty function with the objective to change a constrained problem to an unconstrained problem.

Table 3.2: iSIGHT optimisation techniques (Koch et al, 2002)

TYPE		TECHNIQUE
Numerical	1	Method of Feasible Directions – CONMIN*
	2	Modified Method of Feasible Directions (MMFD)* – ADS
	3	Sequential Linear Programming (SLP)* - ADS
	4	Exterior Penalty* - ADS
	5	Sequential Quadratic Programming (SQP) – DONLP*
	6	Sequential Quadratic Programming (SQP) – NLPQL*
	7	Mixed Integer Optimization – MOST, Tseng (1996)
	8	Hooke-Jeeves Direct Search Method*
	9	Successive Approximation Method (LPSOLVE)*
Exploratory	1	Genetic Algorithm*
	2	Genetic Algorithm with Bulk Evaluation
	3	Simulated Annealing*
Heuristic	1	Directed Heuristic Search (DHS – U.S. Patent No. 6,086,617)

* For reference, see: http://www-unix.mcs.anl.gov/otc/Guide/faq/nonlinear-programming-faq.html#Q4

The NLPQL, which is a sequential quadratic programming (SQP) algorithm, and the mixed integer optimisation algorithm (MOST) have been recently implemented. These techniques have been demonstrated to be very efficient and robust in solving design problems with different characteristics. Most of these techniques are available in the public domain: SQP (Han, 1976), Han (1977), Powell (1978a) and Powell (1978b).

The genetic algorithms and simulated annealing belong to the exploratory algorithms (table 3.2). During the simple genetic algorithm run, the initial design point population is modified by means of so-called genetic operations: selection, crossover and mutation. Then, the new design populations are chosen based on a 'survival of the fittest' approach. The genetic algorithm using bulk evaluation assesses all the group of points at the same time instead of one at a time which

reduces CPU-time. Finally, the simulated annealing algorithm used in iSIGHT is an adaptive simulated annealing algorithm.

Directed Heuristic Search (DHS) is an Engineous Software know-how optimisation algorithm which controls the input parameters provided by the user. It is the user's responsibility to define the path of each input parameter in such a way that is in harmony with its magnitude order and with its impact on the expected outcomes (Koch et al, 2002).

Having all of above-mentioned optimisation algorithms, iSIGHT is capable of dealing with different optimisation problems, for instance: problems with continuous, discrete, integer, and mixed variables, also with linear and non-linear constraints, and finally multidisciplinary and decomposed problems (known as hierarchical optimisation). Furthermore, there is a customisation capability for the users to implement their own optimisation algorithms. An optimisation advisor for the novice users is also provided in iSIGHT. This advisor shows a list of recommendations based on 11 characteristics of the design space (Koch et al, 2002).

The DOE are a collection of statistical techniques providing a systematic and efficient way to sample a design space. They are very useful when tackling a new problem for which the user knows very little about its design space, giving vital information (design space reduction). Also, they study the effects of multiple input variables on one or more output parameters: assessment of design variable impact and of key design variable interactions (Montgomery, 1996).

Additionally, they are often used before setting up a formal optimisation problem in order to identify key drivers among potential design variables, appropriate design variable ranges and achievable objective function values, supporting traditional optimisation procedures. Lastly, the DOE data can be used in

the formation of response surfaces for approximation-based optimisation (Myers and Montgomery, 1995; Kodiyalam et al, 1998).

There are many DOE techniques available in the literature. A full description of these techniques and their engineering design application is given by Simpson et al (1997). In table 3.3 the DOEs incorporated in iSIGHT are briefly described.

Table 3.3: DOE techniques provided in iSIGHT (Koch et al, 2002)

EXPERIMENT	DESCRIPTION
Orthogonal Arrays	Taguchi designs; Fractional factorial designs, with fractional subset carefully selected to maintain orthogonality of factors and certain interactions
Central Composite	5-level design: 2-level full-factorial augmented with a center point and two additional star points for each factor, located on the factor axes
Latin Hypercube	Number of levels for each factor equal to number of points, with random combinations
Full-Factorial	Specify any number of levels for each factor and study all combinations of all factors at all levels.
Parameter Study	Factors studied independently (One factor at a time approach – all other factors held fixed while one varied)
Data File	User defined DOE matrix, specified as file from which to read in data points to analyze.

Taguchi's orthogonal arrays (Taguchi and Konishi, 1987) are developed to obtain the information of the design space which is based on a small amount of data points. The central composite designs are mainly to provide a match for second-order response surfaces (Myers and Montgomery, 1995). Latin hypercube designs, however, are appropriate for design points which are spread all over the design space; they divide the design space uniformly into a specific number of levels for each factor (variable), and then combine the levels randomly. The full-factorial designs evaluate the objectives at every combination of values after specifying levels for each factor. On the other hand, the parameter study changes one factor at a time leaving all others at base level. Lastly, the data file allows the integration of DOE techniques that are not part of iSIGHT.

The approximations - curve-fitting techniques - are used for obtaining correlations between input and output variables based on data collected experimentally. The derived correlations are useful to generate surrogate behavior models. These models can be used to substitute the in-depth analysis leading to the design analysis calculations which is less expensive. In addition to that, the approximation models can reduce the computational noise (i.e. sudden output variations due to the gradual changes in the input variables), which has a negative impact on optimisation by generating different local optima. The approximation techniques available in iSIGHT are classified into the following types: polynomial response surfaces, Taylor's series models, and variable complexity models (see table 3.4).

Table 3.4: iSIGHT approximation techniques (Koch et al, 2002)

TYPE	TECHNIQUE
Response Surface	Linear Polynomial
	Quadratic Polynomial
	Intermediate Polynomial (partial quadratic)
Taylor's Series	Linear Reciprocal Hybrid
	TwoPoint1 TwoPoint2
Variable Complexity	Multiplicative Correction Factor
	Additive Correction Factor

The response surfaces are the most popular of the approximation techniques in use, in particular the low order polynomial models (Myers and Montgomery, 1995). The amount of data points required to create a response surface model is directly proportional to the amount of terms in the model; if there are not enough data points for a complete quadratic polynomial model with the interactions of the two factors, then an intermediate model will be generated by putting the quadratic and interaction terms in the linear polynomial model until any degrees of freedom disappear.

The Taylor's series models apply a truncated Taylor's series in which only the first order terms are involved. The constants term of this first order polynomial is determined by means of a function value at the baseline design, and the coefficients are gradients of this function derived from the finite difference methods. The Taylor's series models included in iSIGHT are shown in table 3.4.

Variable complexity approximation generations are based on two approaches with different degrees of fidelity: more accurate with higher computational time (e.g. a Navier-Stokes CFD flow solver), and less accurate with lower CPU time (e.g. an Euler CFD code) (Giunta et al, 1995). There are two types of models: multiplicative and additive correction factor, when used with the output given by the lower fidelity program, these models calculate the output which would be given by the higher fidelity program. These correction factors are set using data points produced in both programs.

There are different uncertainties involved during the design process, for instance in material properties, operating conditions, simulation model accuracy, manufacturing precision, and so on. In the majority of optimisation methods, however, this uncertainty level is not taken into account. As a consequence, 'high risk' designs are created due to the general tendency of the optimisation algorithms to move designs to the constraint border. Through the use of safety factors any uncertainty can be offset, but usually this leads to over-sized designs. In order to tackle this problem, the quality engineering methods (QEM) were implemented in iSIGHT (Engineous Software, 2004). These methods apply statistical modelling and probabilistic analysis in the optimisation process to seek designs feasible in terms of an objective function and uncertainty level.

The QEMs available in iSIGHT are the following: Monte Carlo simulation techniques, reliability-based design analysis, reliability-based optimization, and

Taguchi's robust design (Engineous Software, 2004). A brief description of these approaches is given below.

Monte Carlo simulation (MCS) techniques are statistical simulation methods for a set of designs with the stochastic characteristics (uncertainty) of the random variables, which are based on describing the statistical character (e.g. mean, range, standard deviation, variance, distribution type, and so on) of the desired outputs (Engineous Software, 2004). There are two MCS models incorporated in iSIGHT: Simple random sampling and descriptive sampling (focused on variance decrease) (Saliby, 1990; Ziha, 1995; Hurtodao and Barbat, 1997).

Reliability-based design analysis methods estimate the probability of failure, or conversely the probability of success (reliability) of a design (Melchers, 1987; Madsen et al, 1986).The probability of failure represents the output distribution area out of a given constraint (on the infeasible side); and the probability of success is determined, therefore, by the output distribution area within a given constraint (on the feasible side). There are three methods available in iSIGHT namely: First order reliability method (FORM) (Hasofer and Lind, 1974; Rackwitz and Fiessler, 1978); mean value first order method (MVFO) (Cornell, 1969); and Monte Carlo simulation (MCS).

Reliability-based optimisation (RBO) is used to find designs with the optimum output satisfying the imposed constraints (i.e. on the minimum required reliability or the maximum acceptable probability of failure). The iSIGHT's RBO algorithm is developed using the approach given by Chen et al (1997).

There are two important concepts in robust design frameworks to be considered: noise factors and control factors. The former is related to the values of the design variables which are random and also to the statistical characteristics (i.e. distribution type) which can be uncertain; the latter are the variables which are

under control during the design process. The aim of the robust design is to seek a design (defined by the control factors) for which the impact of the noise factors on the outputs (responses) would be as minimal as possible (Chen et al, 1996). The robust design method available in iSIGHT is Taguchi's robust design which is a DOE-based method and is used to analyse the responses' sensitivity and therefore the optimised designs' robustness (Byrne and Taguchi, 1987).

The aforementioned design space exploration tools are able to assess particular features of a given problem. There is a capability in iSIGHT to connect these design exploration approaches (interdigitation of design exploration tools), which can be customized in different arrangements to formulate a variety of design exploration scenarios so that the optimal solutions are identified in a more effective manner. This interdigitation strategy is depicted in figure 3.29.

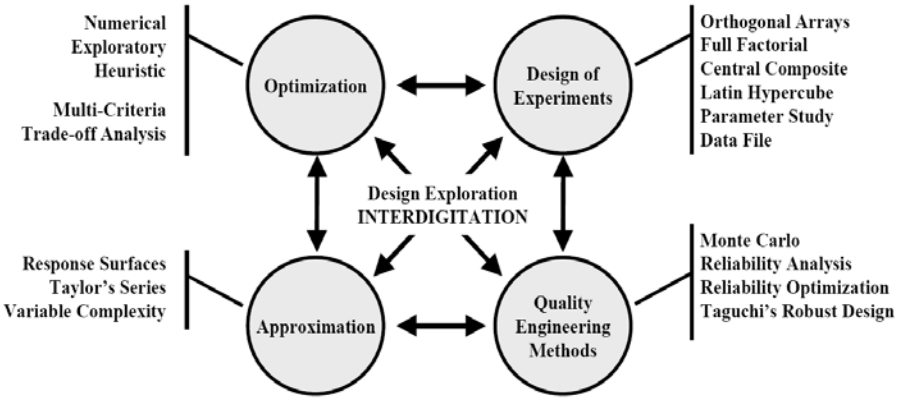

Figure 3.29: Interdigitation of design exploration tools (Koch et al, 2002)

The optimisation tool embedded in the MDO of section 3.1.3 is capable of analysing different effects of the design variables on the figures of merit of interest

(DOE), and also optimising a design with respect to these design variables by means of non-linear optmisation methods.

Some of design variables for the aircraft configuration are: wing sweep, wing area, wing aspect ratio, gross weight, thrust, and so on; for performance: cruise Mach number and altitude; and for engine cycle: bypass ratio, fan pressure ratio, overall pressure ratio, and turbine entry temperature. On the other hand, the figures of merit incorporated in the optimiser are namely: fuel burn, cost, noise, NO_x emission, noise, SFC, range, etc.

The optmisation algorithms are categorised as follows:

- Utility function formulation with a penalty function (PF) approach: Davidon-Fletcher-Powell (DFP), Broyden-Fletcher-Goldfarb-Shano (BFGS), conjugate gradient (Polak-Ribiere), steepest descent, and univariate search algorithm. These methods are used with a Fiacco-McCormick (FM) penalty function (PF) (Geiselhart, 1994).
- Envelope function formulation (KSOPT): Kreisselmeier-Steinhauser function (KS) (Wrenn, 1989).

The optmisation procedure for the first above-mentioned group is as follows: Firstly, the design is optimised by minimising the utility function given in equation (3.24); this function is contained in a quadratic extension PF (i.e. The Fiacco-McCormick PF) (Fiacco and McCormick, 1964) as shown in equation (3.25). Finally, this PF is penalised by $r_p \sum_{j=1}^{m} G_j(X)$ based on the constraint violation level; where r_p is a penalty multiplier and is calculated depending on the problem to be tackled; this multiplier is reduced during the optimisation process in order to reach a minimum constraint value; and the $G_j(X)$ function is provided in equation (3.26).

$$F^*(X)=\sum_{k=1}^{K} w_k F_k(X) \quad \textbf{(3.24)}$$

Where w_k a weighting is factor and F_k is an objective function.

$$\tilde{F}(X,r_p)=F^*(X)-r_p\sum_{j=1}^{m} G_j(X) \quad \textbf{(3.25)}$$

$$G_j(X)=\begin{Bmatrix}\dfrac{1}{g_j(X)} \\ \dfrac{2\varepsilon-g_j(X)}{\varepsilon^2}\end{Bmatrix}\begin{matrix} for: g_j(X)\geq\varepsilon \\ for: g_j(X)<\varepsilon\end{matrix} \quad \textbf{(3.26)}$$

Where ε is a transition parameter set by the user.

KSOPT transfers a constrained into an unconstrained optimisation problem (Wrenn, 1989) and is used for multi-objective optimisation case studies (Sobieski-Sobieszczanski, 1988). Running this algorithm, the design can be initialised from a feasible or infeasible area.

The n-dimensional objectives and constraints are changed in a single surface by the technique derived from a continually differentiable function (Kreisselmeier and Steinhauser, 1975) as shown below:

$$KS(X)=\frac{1}{\rho}\log_e\sum_{k=1}^{K} e^{f_k(X)} \quad \textbf{(3.27)}$$

Where $KS(X)$ is a function surface estimated at X ; $f_k(X)$ is a series of objective and constraint functions; and ρ is a control parameter of $KS(X)$ whose values are between 5 and 200.

The optimiser provided in Gas Turb 10 was used for the cycle optimisation. Seven design variables and seven constraints can be chosen for the optimisation process while any cycle output parameter can be set up as an objective function (figure of merit) for either maximisation or minimisation of its value depending on the problem definition (refer to figure 3.30). Also, the capability of running optimisation with iteration (maximum variables number: 20) is available. Besides, the one off-design operating condition can be considered during the optimisation calculation in parallel with the cycle design point. The data derived from this off-design point calculation is used either as constraint or as figure of merit (Kurzke, 2004).

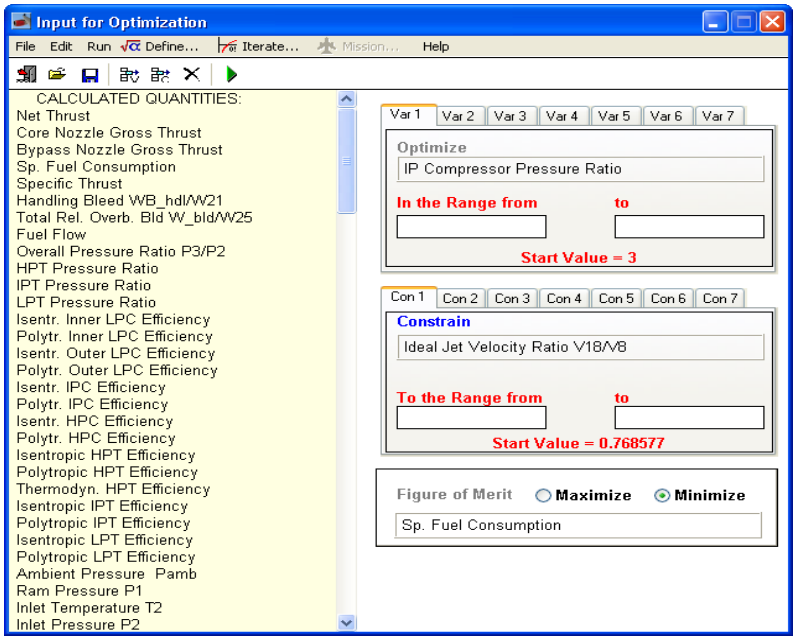

Figure 3.30: Gas Turb Optimiser problem definition (Kurzke, 2004)

The optimisation techniques available in Gas Turb 10 are adaptive random search and gradient search, which are numerical methods.

The adaptive random search is implemented using the approach given by Münzberg (1972). This method uses the random numbers, found close to the prior best result, as the optimisation variables. This algorithm is defined as follows:

$$V_i = V_i^* + \frac{R_i}{k_R}\left(2\Theta - 1\right)^{k_v} \qquad \textbf{(3.28)}$$

Where: V_i is the new value of optimisation variable; V_i^* is the value of V_i giving the best figure of merit; R_i is the search region for V_i; k_R is the range reduction coefficient (positive integer); Θ is a random number ranging from 0 to 1; and k_v is the distribution coefficient (positive odd integer).

The procedure of a run of the adaptive random search is as follows: Firstly, the k_R and k_v are set to 10 and 1, respectively. Next, this algorithm samples several random engine cycles (40 multiplied by the variables' quantity). Once all cycles have been computed, the k_R is doubled and k_v is stepped up by 2; as a result, the search region reduces. The process is repeated again and again up to all cycles until k_R equals 80. The cycles, which violate the imposed constraints, are not taken into account.

The adaptive random search can be run with automatic restarts under the option 'endless random search'. Each time an optimum cycle is achieved, the program starts a new search; these searches can arrive at local or global optima. This approach is suitable for the optmisation problems in which there are different variables as well as constraints.

The gradient search method is based on the work done by Jacob (1982). This approach operates, assuming no constraints, as follows (refer to figure 3.31). It runs from the place labelled 'Start 1' searching for the steepest gradient path called

'Direction 1' and stops when the highest peak is achieved; then it rotates the path orthogonally (by 90 degrees) searching for the highest peak (Direction 2). In order to obtain the next path (Direction 3), this algorithm applies the information given by the first two paths linking 'Start 1' to the highest peak (the best value); it now runs along 'Direction 3' until the highest peak is found. This process is repeated until the variation of the desired objective function happens to be minimal. In the figure 3.31, the optimum solution is located somewhere on the path called 'Direction 4'.

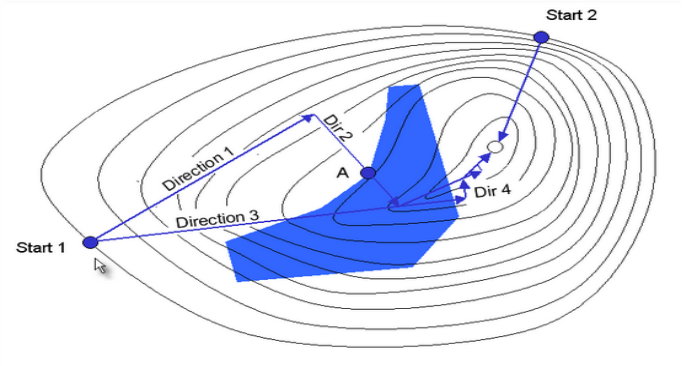

Figure 3.31: Gas Turb Optimiser design space searching (Kurzke, 2004)

Now, let's consider a number of constraints in the problem formulation. The region in the blue colour is prohibited (see figure above); therefore if the afore-mentioned method is used starting from 'Start 1' the quest for the best point will arrive at point A (local optimum); on the other hand, if the run begins from the point called 'Start 2' the global optimum is achieved even faster.

The following recommendations should be taken into consideration for the optimisation process in Gas Turb 10:

- The designer should run the optimiser from different starting points in order to avoid a local optimum.

- The designer should be careful about the variable range chosen: a large range may lead to infeasible designs whereas a small range may not include the optimum and feasible ones.
- Run the optimisation using both techniques to find the global optimum.

CHAPTER 4

RESULTS AND DISCUSSION:

ANALYSIS, OPTIMISATION AND TRADE-OFF CASE STUDIES

4.1 Baseline, Advanced, Contra-Rotating and Geared Turbofans

4.1.1 Introduction

During the relatively short history of commercial aviation air traffic has undergone growth of about 5% p.a., this means doubling every 15 years. The growth tendency will greatly influence environmental issues. Civil aviation authorities and organisations are demanding improvements on noise and emissions regulations for air traffic vehicles. Consequently, this will give rise to higher noise and emissions tax fees paid by airlines and passengers, concern over aviation industry expansion and of economic growth as a whole. Over the past 40 years the introduction of new technology has mitigated the environmental impact of aviation growth, but at the expense of increasing operating costs as shown in figure 4.1. The challenge is therefore to establish the designs offering the optimal trade-off between life cycle cost and environmental performance. Additionally, the improvements to be made by evolving existing technologies are close to the expected maximum, hence more innovative propulsion systems have to be considered.

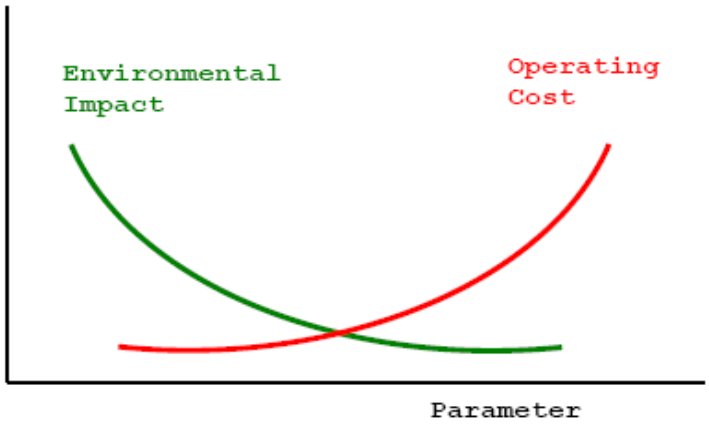

Figure 4.1: Design challenge: the trade-off between cost and environmental impact

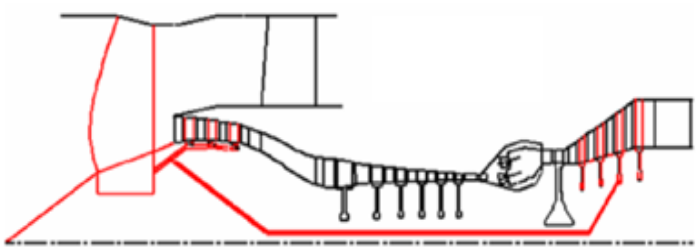

Figure 4.2: Scheme of a turbofan with very -high bypass ratio (Sixth framework programme, 2005)

Both Europe and the USA have defined environmental targets for the aviation industry. For example, the Advisory Council for Aeronautics Research in Europe (ACARE) (Strategic Research Agenda, 2005) has set two ambitious goals for 2020, cutting in half both the perceived aircraft noise (a reduction of 10 dB) and CO_2 emissions. According to ACARE, the sustainable development of air transport depends on achieving a significant across-the-board reduction in environmental impact, in terms of greenhouse gases, local pollution and noise around airports. Cranfield University is working to address the feasibility studies of different

potential novel cycles for both short- and long-range missions (Colmenares et al., 2007a-c, 2008a-c and 2009a-b; Pascovici et al., 2007a-b and 2008; Kyprianidis et al., 2008)

In the public domain there is a little research of potential novel cycles at aircraft level, on the other hand more studies were done at engine performance level (Andriani and Ghezzi, 1996 and 2005; Boggia and Rüd , 2005; Lundbladh and Sjunnesson, 2003). Therefore, a multidisciplinary optimisation tool was developed in order to understand better the interaction of several figures of merit which have to be taken into account during the conceptual and preliminary design phase of these innovative turbofans.

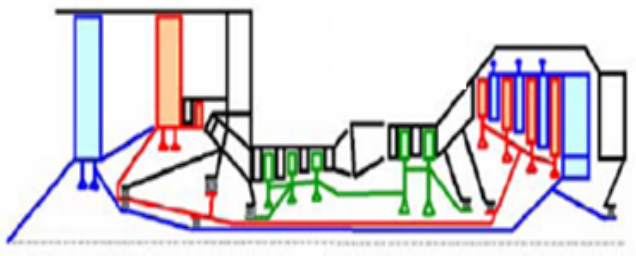

Figure 4.3: Scheme of a turbofan with contra-rotating fans (Sixth framework programme, 2005)

The focus of this study is to determine the feasibility of optmised baseline, advanced, contra-rotating and geared aero engines (see figures 4.2 - 4.4) in terms of economics and environment with regards to a baseline turbofan engine as CFM56. These turbofans, known as very-high bypass ratio engines, are conceived to improve the propulsion efficiency in order to reduce the fuel consumption and noise based on BPR and FPR.

The multidisciplinary design framework used in this research is made up of several simulation models to calculate many aspects of engine design and

performance as well as its economical concerns (refer to chapter 3). These models are coupled together with an optimiser available commercially allowing for their rapid execution and robustness.

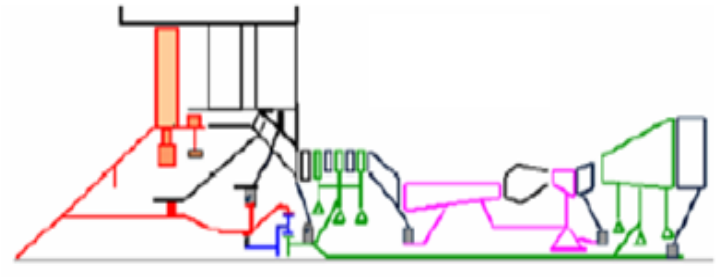

Figure 4.4: Scheme of a geared turbofan (Sixth framework programme, 2005)

4.1.2 Methodology

Using the multidisciplinary optmisation framework described in section 3.1.1, a design-of -experiment technique (i.e. full-factorial) was applied for above-proposed turbofans varying two design parameters (FPR and BPR) simultaneously. The range of these variables was wide enough so as to identify their proper initial and range values for later optimisation either single- or multi-objective.

The design point of the engines was established at top of climb (ToC). The results of several objectives such as: Block fuel, NO_x emissions for landing and take-off (LTO) cycle, cumulative noise margin, direct operating cost (DOC) and global warming potential (GWP), were obtained in the optimiser environment which also acts as a data management system. The simulation codes of engine and aircraft performance, emissions, noise and economics are described in chapter 3 as well as the optimiser.

4.1.3 Results

4.1.3.1 Validation

The baseline configuration was validated against open literature. The validation results are shown in the table below. The SFC at cruise condition is underestimated obtaining a discrepancy of more than 2%. However, the net thrust at the same condition was overpredicted by almost 3%. The worst case scenario was the engine maintenance cost which gives a deviation of approximately 5% from the public data. The validation of the innovative propulsion system was carried out using confidential data leading to a discrepancy of less than +/- 10% (see the appendix A) at engine performance preparation. In summary, the methodology is confirmed with a very good accuracy.

Table 4.1: Validation results for baseline engine

	Simulation	**Public Data**	**Deviation [%]**
SFC_{cr} [g/kN*s]	16.74	17.11	-2.16
FN_{cr} [kN]	21.90	21.32	2.72
Engine weight [kg]	2384	2381	0.13
Engine length [m]	2.55	2.51	1.59
Flyover noise	87.2	88	-0.91
Sideline noise	94.7	94.4	0.32
Approach noise	96	96.3	-0.31
LTO $(D_p/F_{oo})_{NOx}$ [g/kN]	56	57.1	-1.93
Engine maintenance cost [€/hr]	149.3	157.0	-4.90

4.1.3.2 Analysis

In the table below the results of selected innovative propulsion systems are shown in terms of relevant figures of merit.

Table 4.2: Design point data for selected cycles

Configuration	BL	ATF	CRTF	GTF
FN_{TOC} [kN]	30	30	30	30
BPR [-]	4.63	11.00	9.74	11.68
FPR [-]	1.55	1.52	1.57	1.55
OPR [-]	35.50	40.00	37.94	47.55
TET [K]	1660	1850	1920	1955
Mass Flow [kg/s]	149.7	239.1	213.0	224.5
Gear Ratio [-]	N/A	N/A	N/A	3.0
SFC_{Cr} [g/kN*s]	16.74	15.53	14.90	14.19
ΔBlock Fuel [%]	0.0	-13.4	-21.8	-26.9
ΔBlock GWP [%]	0.0	-5.93	-16.53	-19.21
ΔNoise Margin [%]	0.0	153.77	167.92	129.25
ΔEDOC [%]	0.0	9.99	3.54	3.58
$\Delta NO_{x,\,LTO}$ [%]	0.0	18.11	-31.01	-18.75

The ATF has the current fan layout. The innovation of this configuration is as follows: VHBR (BPR = 11.0 @ ToC) increasing the fan diameter; the high aerodynamic loading which translates into low blade numbers; low tip-speed fan; and new lightweight materials. The booster rotates at the same speed as the fan, thus a reduction in rotating speed gives rise to a reduction in booster pressure ratio. Therefore, the booster requires further stages to keep a satisfactory pressure ratio for the LPC system. On the other hand, the slower fan may also produce a lower fan

pressure ratio which the booster may have to offset. This results in heavier and longer engines, thus justifying the need for compact and lightweight boosters.

This turbofan configuration leads to a potential reduction of 13.4% in block fuel (CO_2 emissions) in comparison to that of the baseline turbofan. The global warming impact driven by CO_2 emissions has been diminished by almost 6%. In addition, the noise cumulative margin has a potential increase of 153.77% owing to jet velocity reduction and lower fan tip speed. On the other hand, the ATF direct operating cost went up by almost 10% mostly due to higher TET (leading to reduced time between overhaul) and OPR values (more components to be maintained), hence the cooling and material technology need to be improved to enable this engine concept. High OPR values produce a relative increase of NO_x at LTO cycle by 18%, it is worthwhile to note that the AFT has a similar layout as that of the baseline turbofan. To mitigate this drawback, new combustor technology must be considered (refer to section 1.2.3.6).

The second proposed turbofan concept is the CRTF whose LP system is made up of two separate groups rotating in opposite directions. This layout provides the best noise improvement through significantly lower fan tip speed of the two fan rows. In addition, it offers fuel burn and CO_2 emissions' benefits (21.8%) due to a moderate increase in BPR (see table 4.2) which leads to weight and drag advantages. Besides, the lightweight technology can be also applied to the fan system to maintain its weight as low as possible. On the other hand, the global warming impact is even less than in the ATF design option which represents a reduction of 16.53% relative to the baseline engine. The DOC is still higher (3.54%) but less than the ATF thus becoming a very attractive alternative to the airline customers.

As shown in the table 4.2, for a given aerodynamic load the CRTF configuration may give rise to an increase in the cumulative noise margin by

167.92% with regards to the base line one, this is basically due to the fan noise reduction caused by lower fan tip speed. Moreover, the LTO NO_x is reduced by 31% owing mainly to less SFC.

The challenges in the CRTF are associated with the dynamic problems which might emerge from having the contra-rotating fan overhanging. Therefore, a very compact booster is required to control dynamic instability in order to make this turbofan concept possible. Also, this advanced booster ought to have a higher pressure ratio value to offset the inner fan pressure ratio.

The GTF comprises a reduction gearbox linking the fan and remaining LP-system components (i.e. booster, shaft and turbine). The innovative concept gives an UHBPR of approximately 12 at top of climb, as presented in table 4.2.

The reduction gearbox allows both fan and low pressure system to run at their optimum speeds. The fan can be set to the lowest speed required to achieve maximum efficiency and minimum fan noise. However, as explained previously a lower fan speed causes a reduction in fan pressure ratio, so it is vital that the geared booster attains highly loaded conditions to counteract this. This will decrease the LP turbine size and the LP shaft due to their higher speed but increase the complexity of a gearbox. Therefore, gearbox technology has to be improved in order to make the GTF engine more attractive.

According to the simulations, the cruising SFC of the GTF engine is the lowest among assessed turbofans. This potential along with the advantages of having a gearbox in terms of LP-system dimension and weight, despite the additional weight of gearbox, brings a drop in fuel burn by roughly 27% and one of the lowest operating costs (3.58%) between the novel propulsion systems considered in this study. Furthermore, the global warming potential is decreased by 19.21% (the lowest value in the pool of engines).

Finally, the cumulative noise margin is increased by approximately 129.25% (the second highest value in the assessed innovative engines) while the NO_x for landing and take-off cycle goes down by almost 18.75% (the second lowest values).

4.1.3.3 Parametric Study

The design framework developed as part of this research and described in section 3.1.1 can be used also to assess the effect of different engine variables such as: BPR, OPR, and TET on the aircraft as a whole.

The non-dimensional parameters shown in the graphs below represent the relationship between the innovative turbofan and the baseline turbofan.

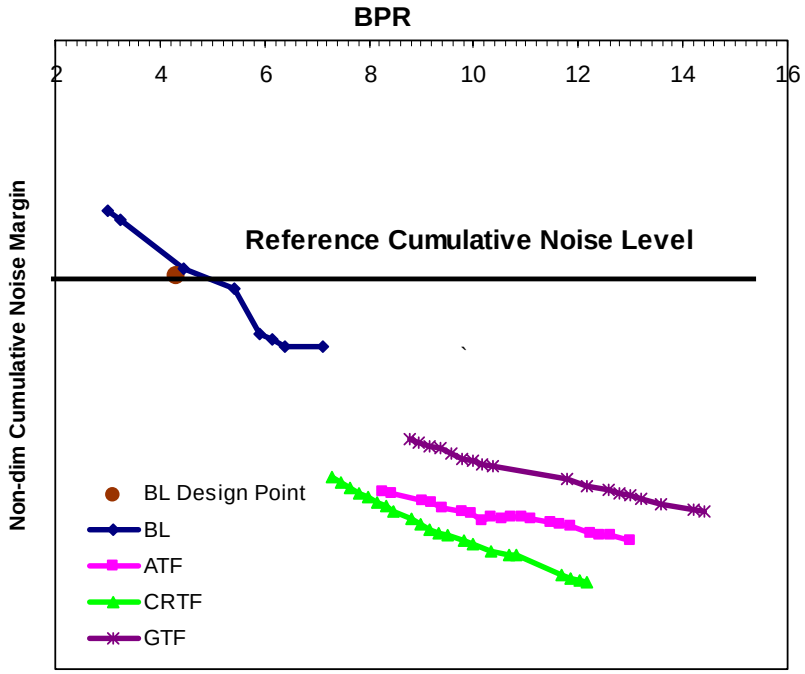

Figure 4.5: Non-dimensional cumulative noise margin vs. BPR

From the point of view of noise, the major contributor at the system level is the engine which generates most of the sideline and flyover noise considered for the engine certification. Hence, the turbofan engine design is vital to the aircraft noise performance. Improvements in materials and the introduction of high BPR propulsion systems have given rise to the reduction of noise, fuel burn and emissions. As can be seen in figure 4.5 increasing BPRs of the baseline configuration (BL) from 4 to 7 result in a cumulative noise margin improvement owing to the reduction of jet velocities. However, the noise reduction limit is reached at a certain BPR. As can be observed in figure 4.5, the three innovative propulsion systems have the potential to achieve the noise goals set by the aeronautical industry.

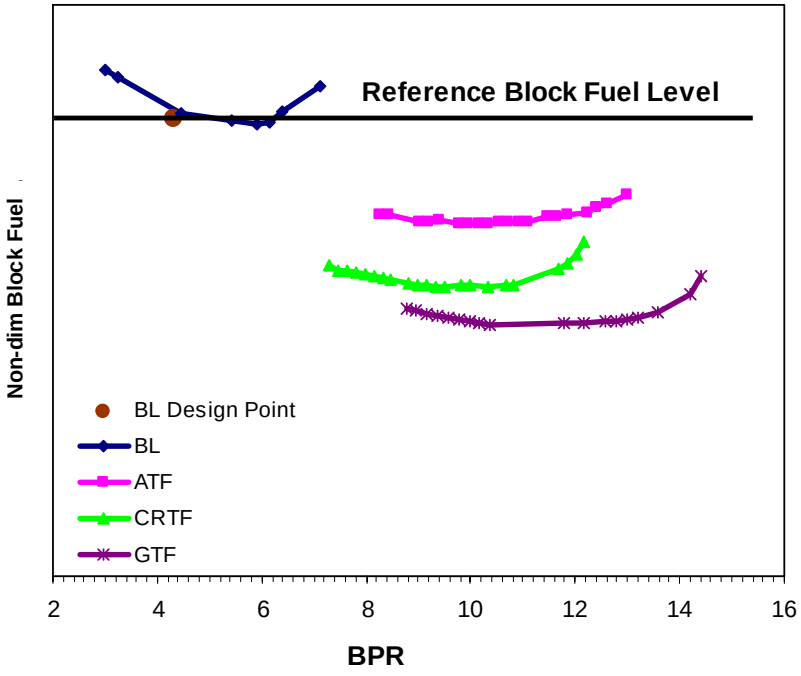

Figure 4.6: Non-dimensional block fuel vs. BPR

Figure 4.6 illustrates the BPR's impact on the block fuel, in the case of the baseline the fuel burn improves when BPR increases from the design point value

(4.63) to about 7, but it rises again when the BPR goes beyond 7. This fuel consumption which increases for very high bypass-ratio (VHBR) turbofans is produced firstly by the considerable parasite drag related to their large fans, and secondly by the weight penalty caused due to the same technology level used (materials, aerodynamics, etc). However, for a specified thrust requirement at cruise conditions, these turbofans will usually need more SLS thrust in order to meet cruising thrust (VHBR turbofans generate less thrust at altitude). In conclusion, the advantage of using VHBR turbofans for noise reduction is offset by the requirement to increase the SLS thrust. On the other hand, the two engines which have a great potential to reduce the consumed fuel are the CRTF and GTF. To allow the ATF more block fuel reduction at a given BPR, weight technology has to be implemented (refer to appendix B).

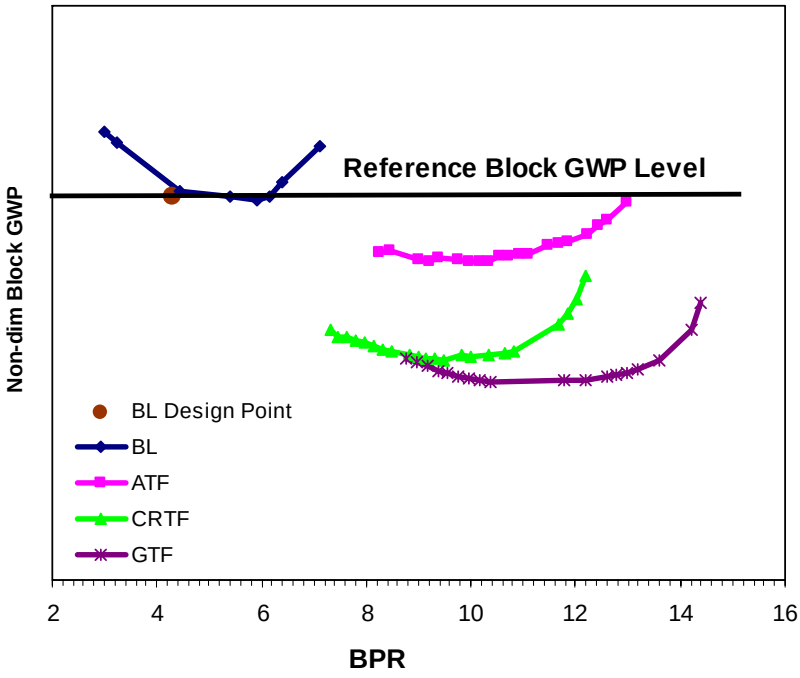

Figure 4.7: Non-dimensional block GWP vs. BPR

At the engine level, the fan pressure ratio (FPR) needs to be optimised with regard to fuel consumption for every BPR. This is why this variable in a combination with BPR was chosen for both the design of experiments and the optimisation process.

From the point of view of environmental impact, the innovative turbofans seem to be very promising. The GTF, according to simulation, arrives at the lowest GWP near a BPR of 12.

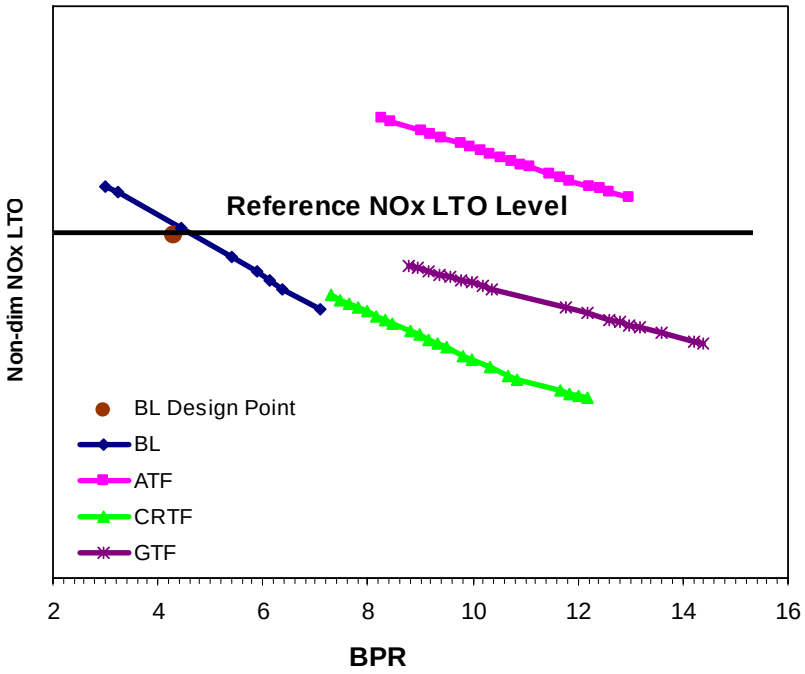

Figure 4.8: Non-dimensional LTO NO_x vs. BPR

From figure 4.8, as BPR goes up the LTO NO_x reduces due to the less SFC regardless of higher values of the emission index generated inside the conventional combustor. In order to obtain more reductions of LTO NO_x, different combustor

technology has to be implemented. Lean pre-mixed and rich-quench-lean combustors can all be introduced in the design framework if data were made available, but this is out of the scope of this research thesis.

In summary, all of these turbofans lead to a reduction in fuel burn, global warming, and noise. NO_x formation during the LTO cycle for ATF increases while the CRTF and GTF go down. On the other hand, the introduction of these new propulsion systems based on the increase of propulsion efficiency leads to an increase in DOC (its highest value is found in the ATF).

4.1.3.4 Single-Objective Optimisation

In this study, the optimisation process is carried out to achieve the best optimal designs reducing block fuel, global warming potential, engine direct operating cost and LTO-NO_x emissions as well as increasing the cumulative noise margin. This approach is called single-objective optimisation whose aim is to assess the impact of the remaining figures of merit while optimising one at a time. Figures 4.9 to 4.14 show the outcome of the optimisation simulations. Also, the reader is referred to appendix C.

As can be observed from the graphs below, the cycle that gives the minimum fuel burn is the GTF engine (27.47% compared to the baseline engine). This gives rise to a reduction in GWP by almost 21% due to less emissions into the atmosphere. The cumulative noise is 108.49% but less than initial design (129.25%) due to a reduction in BPR and an increase in FPR. This smaller diameter fan produces a reduction in engine DOC (less maintenance cost and less emission charges) by -1.11%. Furthermore, the LTO NO_x emissions are decreased by about 22%. This design appears to be a promising solution for the environmental and economical concerns in the aviation industry.

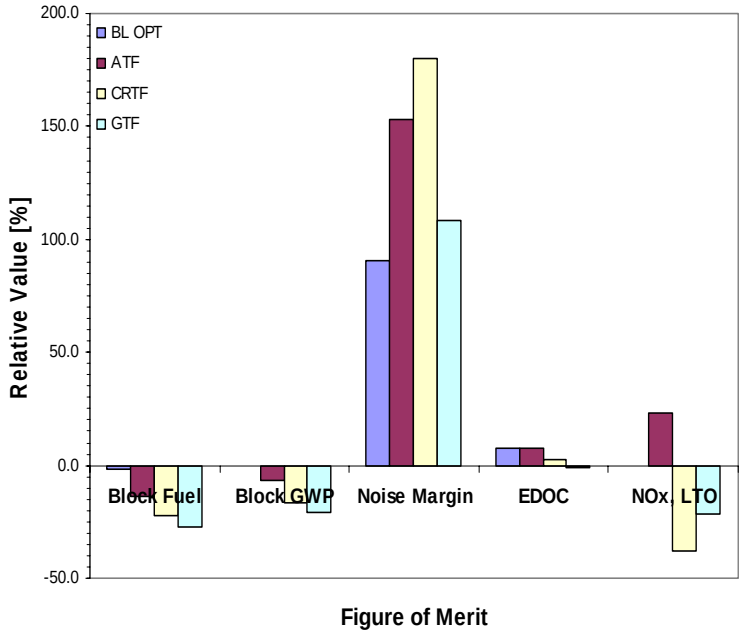

Figure 4.9: Single-objective optimisation for minimum fuel burn

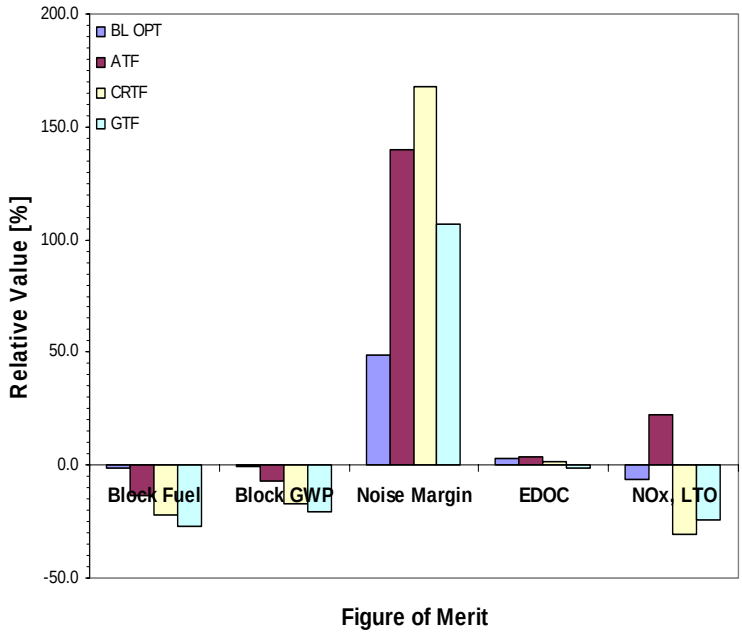

Figure 4.10: Single-objective optimisation for minimum GWP

The CRTF leads to a relative drop of 22.17% in fuel burn and of 16.60% in GWP. This engine cycle has the highest noise margin (180.19%) owing to the fan layout and its lower speed. However, the elevated DOC per annum would be an issue. In the case of the minimal-fuel-burn ATF affects both DOC (7.48%) and LTO NO_x (7.48%) negatively. The high NO_x emissions can be tackled by means of using new combustor technologies. The optimised baseline turbofan gives fuel burn reduced by 1.89% leading to a small impact on other figures of merit. A conclusion can be drawn for baseline turbofan: the technology level has reached the limit.

Optimisation results for minimum GWP are similar to those of minimum fuel burn, but LTO NO_x value for the optimum baseline is reduced with respect to the baseline engine. The DOC of the GWP-optimised GTF is less than block-fuel-optimised GTF as a result of a smaller fan diameter (reduced BPR) leading to a decrease in maintenance cost.

The optimisation for maximum cumulative noise for all engines is presented in figure 4.11 and appendix C. In the case of the baseline turbofan, a higher noise margin (124.53%) is obtained at the expense of a considerable increase of DOC (15%). This is mainly because the noise-optimum BPR does not correspond to the block-fuel-optimum BPR (the propulsion system weight and drag is raised causing a fuel consumption penalty). Moreover, the GWP increases as it basically depends upon the CO_2 emissions generated which in turn is linked to the fuel burn. On the other hand, LTO NO_x goes down owing to lower SFC value obtained.

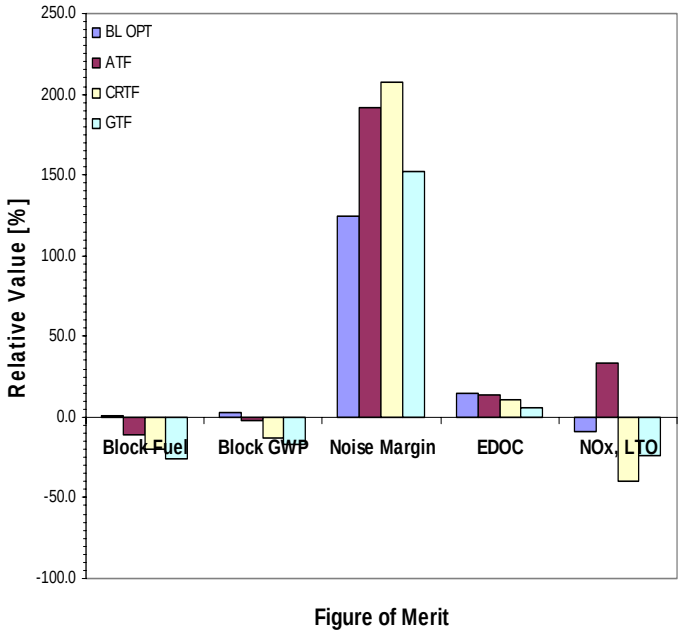

Figure 4.11: Single-objective optimisation for maximum cumulative noise

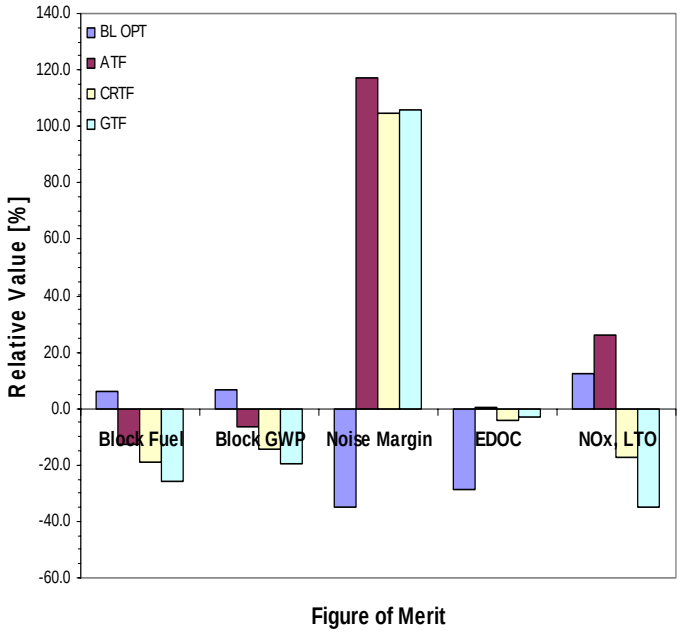

Figure 4.12: Single-objective optimisation for minimum engine DOC

The AFT noise margin goes up by 191.51% to the detriment of DOC (+13.60% driven by maintenance cost) and LTO NO_x (+33.18%). However, a reduction in both block fuel (11.42%) and GWP (1.88%) is expected. The CRTF and GTF have similar trends: An improvement in fuel burn by 19.78% and 25.36%, in GWP by 13.05% and 16.81%, in noise margin by 207.55% and 151.89% and in 39.57% and 23.94%, respectively; and a detriment in DOC (10.73% for CRTF and 5.64% for GTF) because of the high maintenance costs involved in LP system.

In figure 4.12 the outputs of the DOC-optimised turbofans are given. The optimal baseline design, which produces a 28.57% relative reduction in DOC, has a negative impact on the remaining figures of merits becoming the worst design case. The optimum DOC in the ATF engine is reduced as expected but its relative value keeps close to the baseline turbofan (0.40%). This is due to the implications of using higher values of BPR leading to more maintenance costs of the LP system even with the introduction of the technology breakthrough. The effect on the block fuel and the GWP is positive providing a reduction of 12.69% and 6.39%, correspondingly. The former is part of DOC which explains the same trend, and the latter is linked to the former through CO_2 emissions delivered. Finally, the CRTF and GTF show similar behaviour providing a decrease in: Fuel burn (19.11% for the CRTF and 25.79% for the GTF); GWP (14.14% and 19.31%); DOC (4.03% and 2.93%); LTO NO_x (17.51% and 35.03%). The cumulative noise margin is maximised by 104.72% for the CRTF and 105.66% for the GTF.

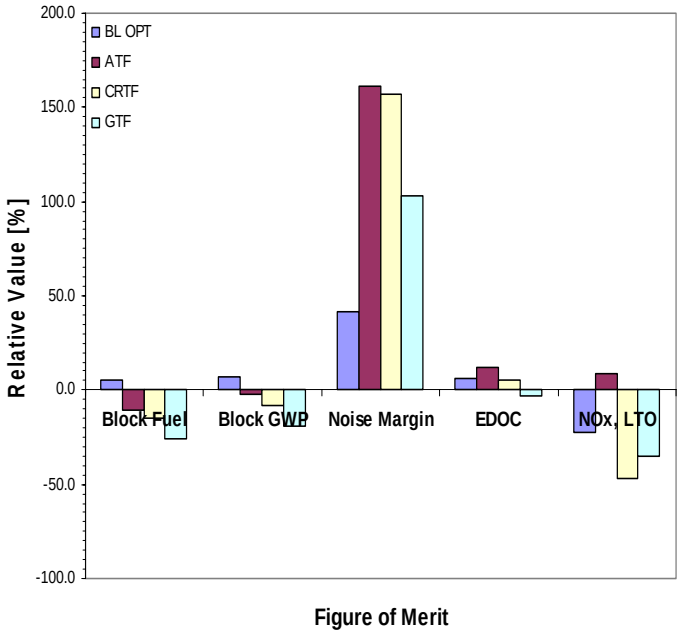

Figure 4.13: Single-objective optimisation for minimum LTO NO_x emissions

The results for the minimum LTO NO_x emissions are shown in figure 4.13. The optimised baseline turbofan produces a reduction of 22.36% in LTO NO_x at the expense of an increase in block fuel (5.71%), GWP (6.63%) and DOC (6.28%). The cumulative noise margin goes up by 41.51% in comparison to the baseline. For the ATF the LTO NO_x reduces but remains above the reference value by 9.02% causing 11.98% increase in DOC in spite of a reduction in block fuel and GWP. On the other hand, the noise margin increases by 161.32%. The LTO-NO_x optimised CRTF improves all the figures of merits excluding the DOC which increases by 5.30%. Nevertheless, the GTF achieves improvements at different figures of merit when optimising for best LTO NO_x emissions.

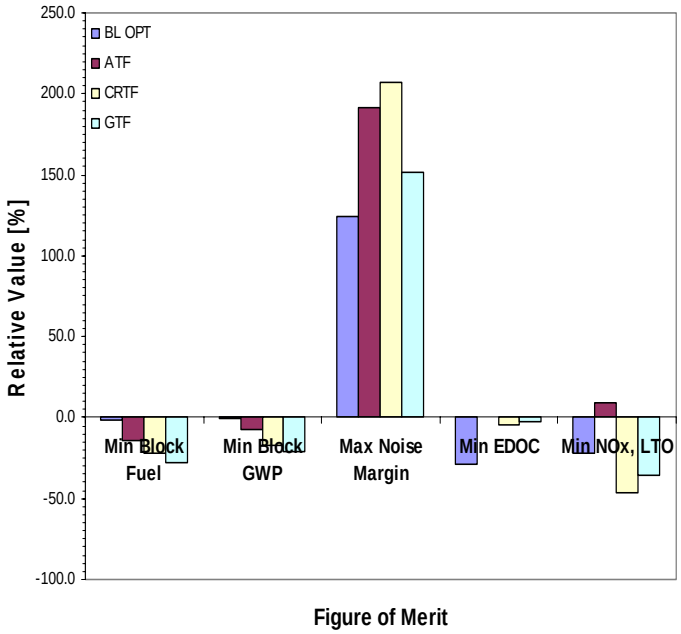

Figure 4.14: Comparison of single-objective optimisation results

Figure 4.14 compares all engine configurations for every optimised figure of merit. As can be observed from graph above, the cycle that gives the minimum block fuel is the GTF engine. Similar results are obtained when optimising for minimum GWP as CO_2 emissions, which is connected with fuel burn, is the main contributor to the global warming. In terms of noise margin, the turbofan with the best performance is the CRTF due to the low jet velocity (ultra BPR) and lower LP-system speed. The DOC-optimised baseline engine in terms of economical performance, seems to be very attractive but to the detriment of the environmental performance as discussed above. Lastly, the CRTF gives the best LTO NO_x reductions followed by the GTF configuration. The worst case scenario is given by the ATF leading to an introduction of new combustor technology which will increase the production cost of the engine and therefore the cost of ownership.

From the above discussions the following conclusion can be drawn: a reduction in one figure of merit may result in an increase of another, and also the introduction of new technology leads to increase engine operating cost, hence the tradeoffs in here are very challenging. Where there are conflicting objectives the Pareto front is highly recommended for design decision-making; the following section deals with situations where two figures of merit conflict with each other.

4.1.3.5 Multi-Objective Optimisation

A multi-objective optimisation run is done to find the optimum design compromise. A trade-off is made for fuel burn vs. LTO NO_x emissions and fuel burn vs. cumulative noise margin. Figure 4.15 and 4.16 presents the results of the optimum design compromise in the two case studies and their Pareto fronts.

A reduction in NO_x emissions can be obtained at the cost of a higher fuel burn. If NO_x emissions are reduced by 20% (from 1.0 to 0.80 for the BL), fuel burn increases by nearly 8%. For this reason, compliance with future emissions and economical requirements could imply a design compromise. The GTF gives the best compromise with regard to the two figures of merit analysed (see figure 4.15).

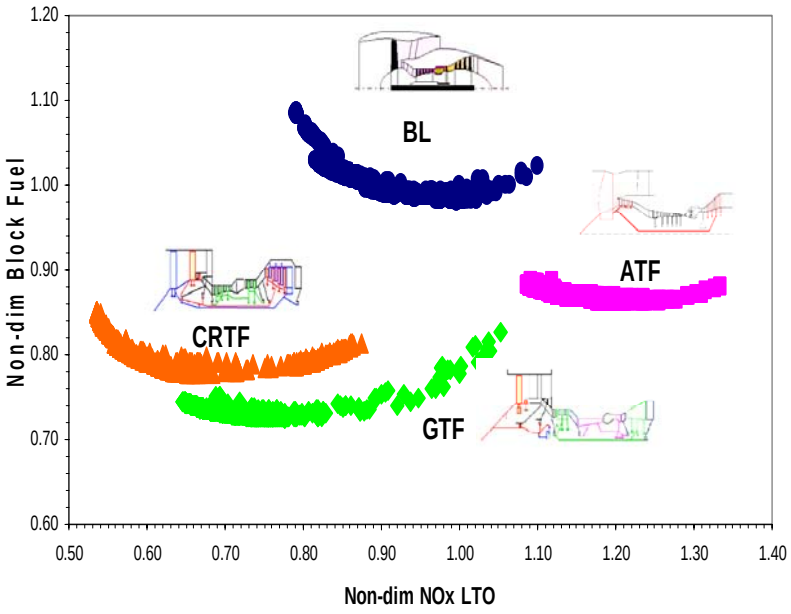

Figure 4.15: Pareto front non-dimensional block fuel vs. LTO NO_x

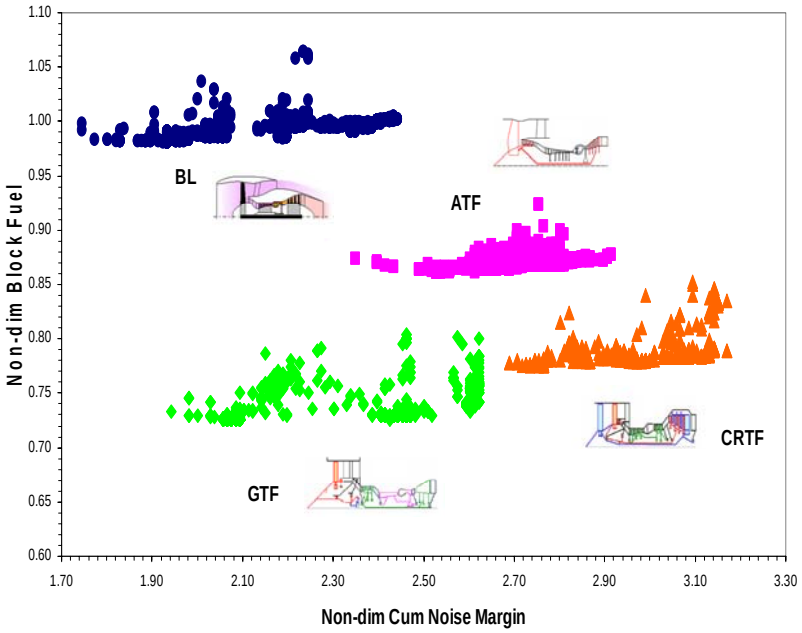

Figure 4.16: Pareto front non-dimensional block fuel vs. cumulative noise margin

The Pareto fronts for non-dimensionalised fuel burn and cumulative noise margin is shown in figure 4.16. In the case of all engine configurations, beyond the block-fuel-optimised BPR and FPR further reduction in noise leads to an increase in block fuel due to the weight and drag penalty involved. As expected, the CRTF has a great potential for noise margin growth while the GTF has a promising block fuel decrease at the expense of less noise margin achievement but is still attractive. The AFT performs better in comparison to the baseline turbofan but worse with regard to the afore-mentioned engine arrangements. A growth in 16% of noise margin generates a 1% fuel burn penalty for the baseline turbofan as shown above.

4.1.3.6 Risk Assessment

The risk analysis presented below is for one short-range configuration (i.e. geared turbofan - GTF) because of the similar tendencies obtained for the other configurations. This analysis is carried out for one optimal solution with regard to engine DOC (- 2% reduction) by changing two design parameters: FPR and BPR as shown in table 4.3.

Table 4.3: FPR and BPR for DOC (2% reduction) optimisation scenario

Objective	**Design Variables**	
	FPR	**BPR**
- 2% DOC	1.58	10.86

The following three risk scenarios were considered for this study:

- Risk Case 1:

Uncertain parameter: Fuel Price (FP).

Assumptions: Minimum FP value is 160 c$/US gallon while maximum FP is 400 c$/US gallon; noise threshold is 74.4 dB for the three different design scenarios (see table above) taking into account future regulation limits; carbon threshold is 0 implying a carbon tax for all fuel burned; carbon charge is 5 €/kg; and noise tax cost ranging from 50 to 5000 €/dB.

- Risk Case 2:

Uncertain parameter: Noise threshold for tax (NTT).
Assumptions: Several ranges for NTT are analysed (79.4/89.4; 74.4/84.4; 69.4/79.4; 64.4/74.4; and 59.4/69.4 dB) for improved DOC, fuel burn, and cumulative noise designs; carbon threshold is 0 kg; FP is 172 c$/US gallon; carbon charge is 5 €/kg; and noise tax cost between 50 and 5000 €/dB.

- Risk Case 3:

Uncertain parameter: Carbon threshold (CT).
Assumptions: Minimum CT value is 0 kg while maximum CT is 3000 kg; noise threshold is fixed at a value of 74.4 dB; FP is 172 c$/US gallon; carbon charges are set up between 4 and 64 €/kg; and noise tax cost between 50 and 5000 €/dB.

These case studies were run using the risk module, developed as part of this PhD project, which is integrated into the economic module of TERA (refer to section 3.9). The risk approach is based upon the Monte Carlo method with a Gaussian distribution to study the impact of the variations in some parameters (e.g. fuel price, downtime, emission and noise taxes) on the net present cost (NPC). A total of 10 000 scenarios was assumed and the NPC was calculated for an operational period of about 30 years.

The cumulative curve outcomes (see figure 4.17) show that there will be a 23-25% growth in net present cost (NPC) for the first case study. At a 50% of likelihood, the expected increase is roughly 25%.

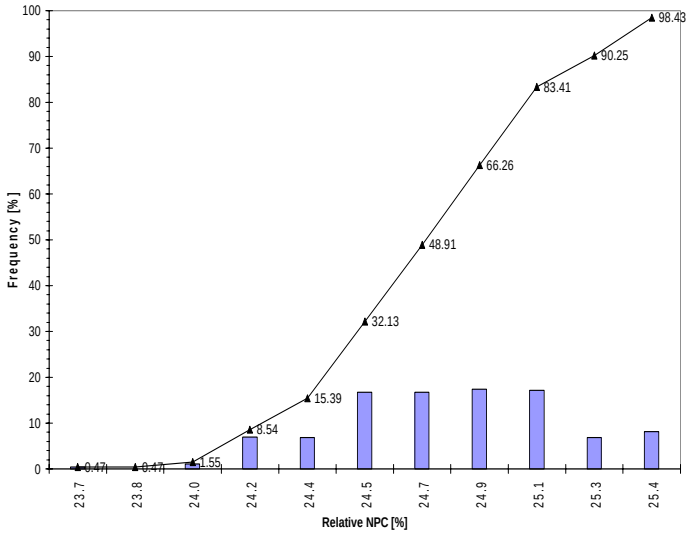

Figure 4.17: Cumulative curve: Risk case 1 (uncertain fuel price) for improved DOC GTF

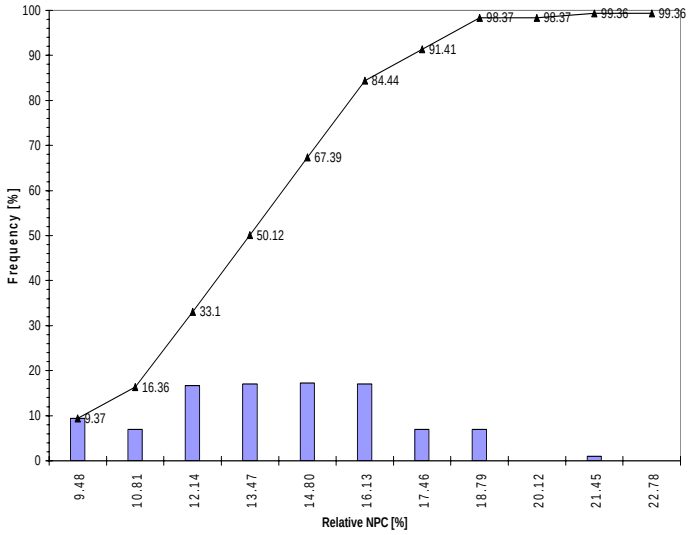

Figure 4.18: Cumulative curve: Risk Case 2 (uncertain noise threshold) for improved DOC

For the case of the uncertainty in future noise threshold, the NPC has a 50% probability of being lower than 13%, but as can be observed from figure 4.18 it can be as high as 22% higher than the reference value (i.e. -2% DOC). However, it is 100% probable to undergo a 23.5% increase in NPC, and there is a 50% probability that it will be as high as 18% for uncertain carbon threshold risk case study (see figure 4.19).

A general conclusion from the risk study can be deduced as follows: The increase in NPC is a concern, and is highly affected by fuel price, noise and carbon threshold, hence more radical configurations (i.e. CVC, ICR, IC, so on) need to be considered, optimised and assessed with respect to different uncertain parameters.

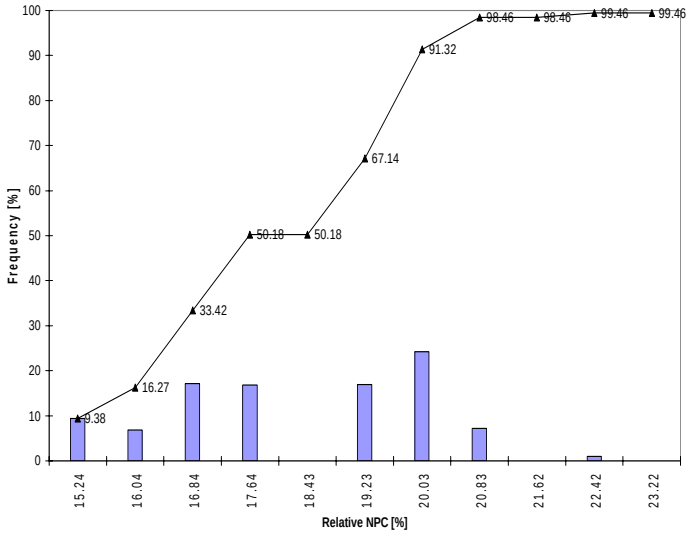

Figure 4.19: Cumulative curve: Risk Case 3 (uncertain carbon threshold) for improved DOC GTF

4.1.4 Conclusions and Recommendation for Future Work

This work shows a multidisciplinary optimisation approach for the analysis of environmental and economic performance at aircraft system level for the innovative propulsion systems based on propulsive efficiency improvements.

This research was limited to short-range transport applications and the installation aspects were included. Also, the current combustor technology was assumed. The design point of the selected cycles was set up at ToC operating conditions. On the other hand, the optimisation was performed minimising different figures of merit (i.e. NO_x emission, fuel burn, global warming potential, noise and direct operating cost) changing two design variables: FPR and BPR. These cycle parameters were used due to their great impact on the noise as well as the SFC reductions. However, some trade-off studies have to be carried out because BPR increases produce heavier engines leading to an increase in fuel burn as well as the operating cost. Moreover, the materials and manufacturing technologies should be considered to bring a reduction in total engine weight.

The CRTF gives the best noise improvement among the turbofans assessed because of relevant lower fan tip speed of the two fan rows. However, the GTF gives the lowest fuel burn leading to reduced direct operating cost and climate change impact. LTO NO_x emissions are benefited in this configuration.

In the case of single objective optimisation scenarios, the turbofan that gives the minimum block fuel and GWP is the GTF engine. Nevertheless, the CRTF is the best solution in terms of noise and NO_x production. The worst case scenario is given by the ATF leading to an introduction of new combustor technology which will increase the production cost of the engine therefore the cost of ownership.

For multi-objective optimisation, the GTF gives the best compromise with respect to LTO NO_x and fuel burn. However, for the fuel consumption and noise case the CRTF has a great potential for increased noise margin while the GTF has a promising block fuel decrease at the expense of less noise margin achievement but is still promising. The AFT performs better in comparison to the baseline turbofan but worse with regard to the CRTF and GTF.

The risk study shows that the increase in NPC is a concern, and is greatly affected by fuel price, noise and carbon threshold, hence more radical configurations (i.e. CVC, ICR, IC, so on) need to be considered, optimised and assessed with respect to different uncertain parameters.

4.2 Baseline, Intercooled, Recuperated, and Intercooled and Recuperated (ICR) Turbofans

4.2.1 A Preliminary Parametric Study for Intercooled, Recuperated and ICR Turbofans

4.2.1.1 Introduction

Aviation plays a key role in economic prosperity and quality of lifestyle. However there is an increasing concern that current trends of consumption of natural resources cannot continue. It is imperative that major targeted investments are made into economical and reliable environment friendly propulsion and power solutions. A significant amount of this investment will be in the aerospace sector. A well utilised civil aircraft may burn more than 2000 times its weight in fuel during its life, so the examination of the propulsion system is essential from an environmental point of view.

A preliminary parametric study for a geared, intercooled and/or recuperated turbofan for short range commercial transport applications has been performed with regard to fuel consumption and emissions. A high by-pass ratio turbofan engine with performance characteristics and technology from the year 2000 was set up as a baseline. The results offer interesting qualitative comparisons showing that, for instance, a recuperated engine will yield a lower fuel burn for lower OPR values. An engine with a mid-compressor intercooler may give significant reduction of NO_x emissions whilst increasing the amount of CO_2. The intercooled and recuperated cycle offers higher thermal efficiencies (i.e. higher fuel consumption benefit) in comparison to other cycles at medium OPR values; therefore NO_x formation may be reduced as well as the engine core weight.

Additionally, the inherent advantage of high BPR against low BPR turbofans in terms of SFC is evident (GTF). Clearly, therefore, an increase of BPR is an inevitable solution for the reduction of both fuel consumption and the level of noise produced, however this may involve NO_x and integration penalties, hence innovative cycles(e.g. ICR) and state of the art combustor technology (e.g. PERM and LDI combustors) must be considered.

4.2.1.2 Methodology

The engine cycles were evaluated using Gas Turb 10 which is a gas-turbine simulation program available commercially (Kurzke, 2004). This software offers a wide variety of predefined engine configurations, thus reducing set up time. Parametric studies, Monte Carlo simulations and cycle optimisation tasks can be carried out very quickly. Also, the effects of small changes can be found in order to estimate the influence of inlet flow distortion on compressor stability and the operating line excursions in the component maps that happen during transient operation.

A high by-pass ratio turbofan engine with performance characteristics and year 2000 technology was set up as a baseline and compared to the GTF, IC, REC and ICR configurations. The non-optimised design point was calculated at take-off conditions. Then the parametric study was carried out varying OPR values. These cycles were calculated using the baseline LP system and its core technology. The engine station numbering is given in appendix D.

4.2.1.3 Results Validation

The validation of the models is given below.

Table 4.4: Validation results for baseline engine

	Simulation	**Public Data**	**Deviation [%]**
SFC_{cr} [g/kN*s]	17.58	17.11	2.75
FN_{cr} [kN]	22.10	21.32	3.66
FN_{sls} [kN]	100.97	100.97	0.0
W2 [kg/s]	326	326	0.0
BPR [-]	2.55	2.51	1.59
OPR [-]	87.2	88	-0.91
EGT [K]	1193.28	1193	0.02

Table 4.5: Non-optimised design point data for selected cycles

	BL	GTF	IC	REC	ICR
FN_{sls} [kN]	100.97	100.97	100.97	100.97	100.97
SFC_{sls} [g/kN*s]	10.45	9.48	14.28	9.97	9.87
WF [kg/s]	1.06	0.96	1.44	1.01	1.00
SNO_x [-]	1.01	1.95	0.12	1.04	0.89
$EINO_x$ [g/kg]	23.23	44.85	2.76	23.92	20.47
η_{th} [-]	0.43	0.50	0.31	0.47	0.49
BPR [-]	5.3	12.8	5.3	5.3	5.3
OPR [-]	24.41	37.00	6.61	16.15	10.17
Gear Ratio [-]	N/A	3.0	N/A	N/A	N/A
εic [-]	N/A	N/A	0.6	N/A	0.72
εrec [-]	N/A	N/A	N/A	0.67	0.67
W2 [kg/s]	326.0	542.2	326.0	326.0	326.0
T4 [K]	1605	1605	1605	1605	1605
ΔSFC [%]	0.0	-9.28	36.65	-4.6	-5.55
$\Delta EINO_x$ [%]	0.0	93.07	-88.11	3.0	-11.88

ΔTSFC and Δ$EI\ NO_x$ values are relative with respect to those obtained in the baseline configuration.

4.2.1.4 Analysis

This section presents an overview of some of the parametric studies which were useful in identifying the most suitable cycle in terms of emission reduction and less fuel consumption. In addition to this, the design area was found to propose further cycle improvements by means of the optimisation process or to create the basis for further analyses.

Figure 4.20 shows the calculation of thermal efficiency for the cycles being proposed. As seen from this figure, ICR cycle offers higher thermal efficiencies in

comparison to other cycles at medium OPR values; thus the NO_x formation will be reduced as well as the engine core weight (on account of a reduction of HPC stages) regarding baseline configuration.

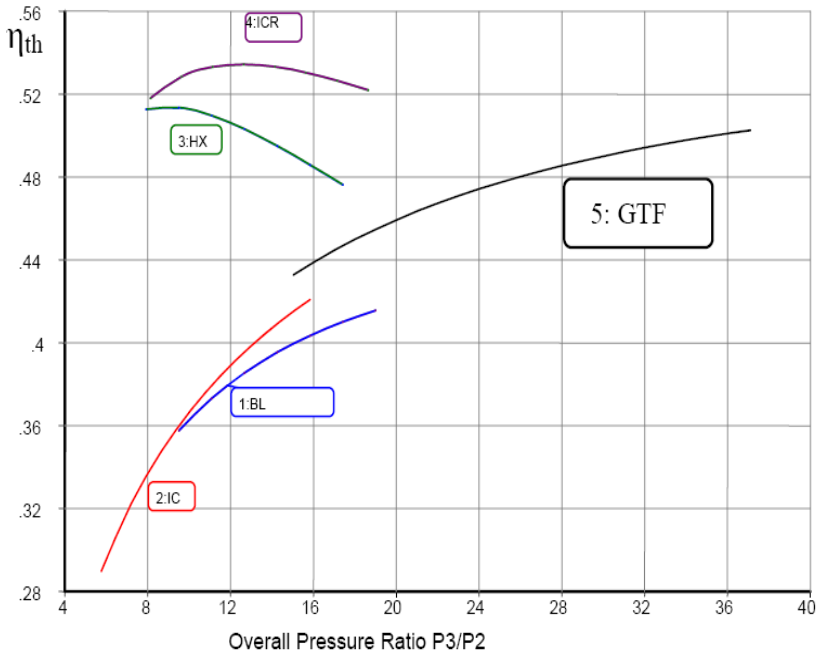

Figure 4.20: Variation of thermal efficiency with OPR at T-O SLS

From figure 4.21 we can observe the fuel consumption benefit for medium OPRs in the case of the ICR cycle, thus having a positive impact on environmental and economic performance (less fuel burn, less CO_2 emissions, less airport emission taxes, etc.). GTF configuration gives interesting results for high OPR values in terms of SFC while the NO_x emissions are set at high level. Therefore, an important conclusion about trade-offs can be obtained from this observation; that a reduction in one type of pollutant may result in an increase of another. In IC cycle, the trends of CO_2 and NO_x emissions are similar to this of GTF cycle but much higher at given OPR value.

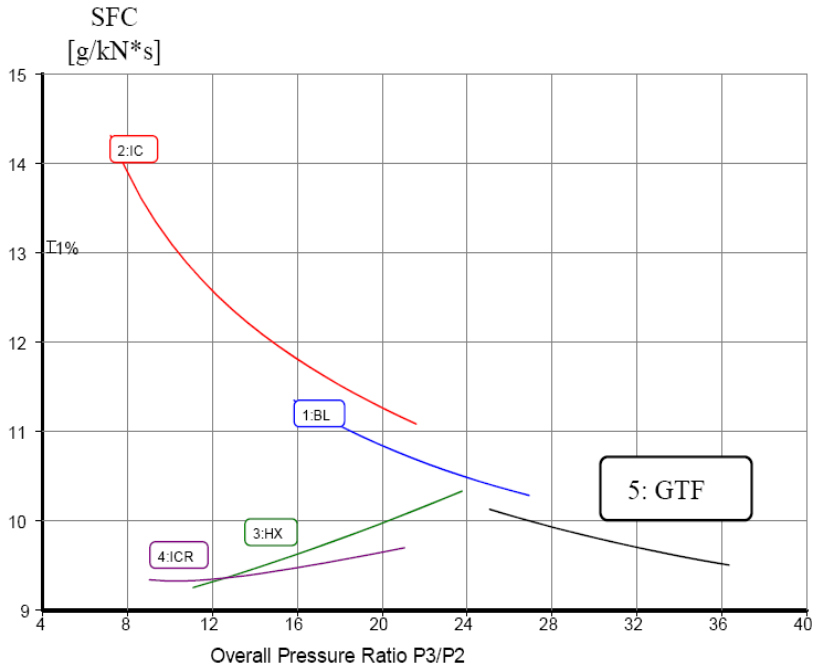

Figure 4.21: Variation of SFC with OPR at T-O SLS

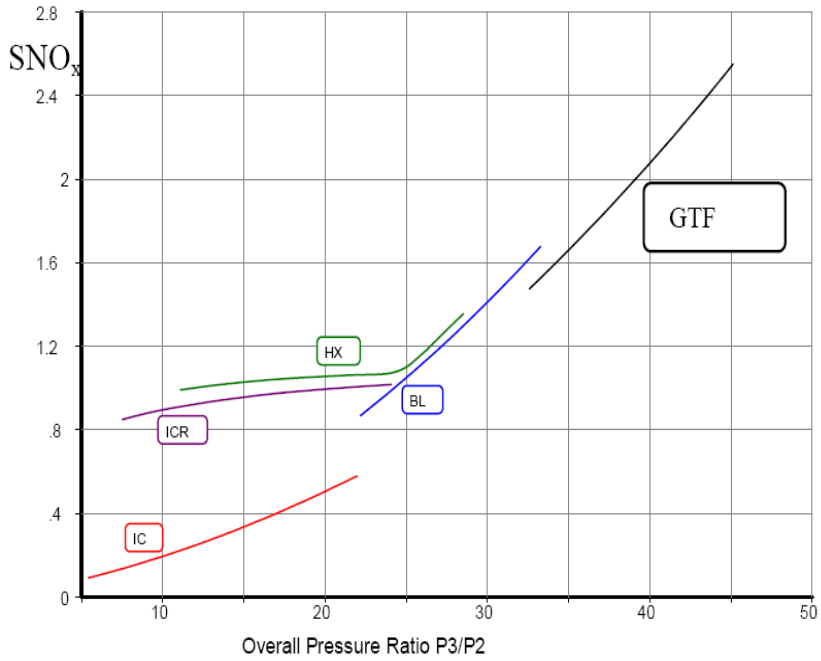

Figure 4.22: Variation of NO_x with OPR at T-O SLS

4.2.1.5 Discussions

The best results to mitigate NO_x emissions are given by the IC configuration but because of the negative impact on CO_2 emissions this cycle becomes unattractive. For the medium OPR engines, the ICR cycle shows moderate NO_x levels and combined with fuel burn advantages as presented previously leads to a very promising cycle at T-O SLS design point, as reported in figures D4-D8 given in appendix D, at least according to numerical simulations.

4.2.1.6 Conclusions and Recommendation for Future Work

Emissions of pollutants differ between the different phases of engine operation. Oxides of nitrogen emissions are higher when the engines are running at high power during take-off and climb-out. Particulate emissions per unit of fuel are high during taxiing and idling, but higher in absolute quantity during take-off and climb-out. Carbon monoxide emissions are higher during taxiing and idling. Whereas carbon dioxide and water vapour production are proportional to fuel use, production of oxides of nitrogen and particulates can be reduced by improved airframe and engine design and its integration.

The present study shows a simple but useful approach for preliminary parametric study of emissions in engine cycle feasibility. This study was limited to short range transport applications and integrations aspects were not included. The take-off static design point was not optimised. The results show the inherent advantage of high BPR against low BPR turbofans in terms of SFC is observed. Clearly, therefore, an increase of BPR is an inevitable solution for the reduction of both fuel consumption and the level of noise produced, however this may involve NO_x penalties. An important outcome is that a reduction in one type of pollutant

may result in an increase of another; hence innovative cycles and state of the art combustor technology must be incorporated.

The ICR cycle offers higher thermal efficiencies (i.e. higher fuel consumption benefit) in comparison to other cycles at medium OPR values; therefore NO_x formation will be reduced as well as the engine core weight.

For future work, the engine cycle must be optimised with the objective of minimising noise, emissions, Direct Operating Costs (DOCs) and fuel burn at different flight conditions and take into account the integration aspects (i.e. airframe and propulsion system). This assessment will be multidisciplinary, which involves aircraft and engine performance, weight, noise, emissions and economics. Additionally, these modules can be coupled with a commercially available optimiser and assess different cycles more precisely.

4.2.2 Optimisation of Intercooled, Recuperated and ICR Turbofans for Minimum NO_x

4.2.2.1 Introduction

Growth in air traffic and airport neighboring communities has resulted in increased pressure to severely penalise airlines that do not meet strict local noise and emissions legislation, and also to charge airlines and passengers with noise and emission fees. The objective of this research is to assess the trade-off between operating costs and environmental requirements of the new aero-engine concepts for short range commercial aircraft. This involves optimising the engines' design point to minimise emissions of nitrogen oxides (NO_x) and evaluating the economic impact with ideal jet velocity ratio $\frac{V_{id.18}}{V_{id.8}}$ as a constraint. A high by-pass ratio turbofan engine with performance characteristics and technology from the year

2000 was set up as a baseline and compared to heat exchanged turbofans. The results show that the ICR turbofan seems to be a very promising solution in terms of environmental performance, but the operating cost are high. This new technology can be competitive if the fuel price is several times higher than today.

4.2.2.2 Methodology

The multidisciplinary design framework used in this research is made up of several simulation models to calculate many aspects of engine design and performance as well as its economical concerns (refer to figure 4.23). Aircraft performance is assessed using in-house software called HERMES (Laskaridis, 2004) and economic and risk aspects are calculated using a module developed during this research project (Pascovici et al, 2007a-b and 2008). On the other hand, engine performance, NO_x emission and design optimisation have been carried out with Gas Turb 10.

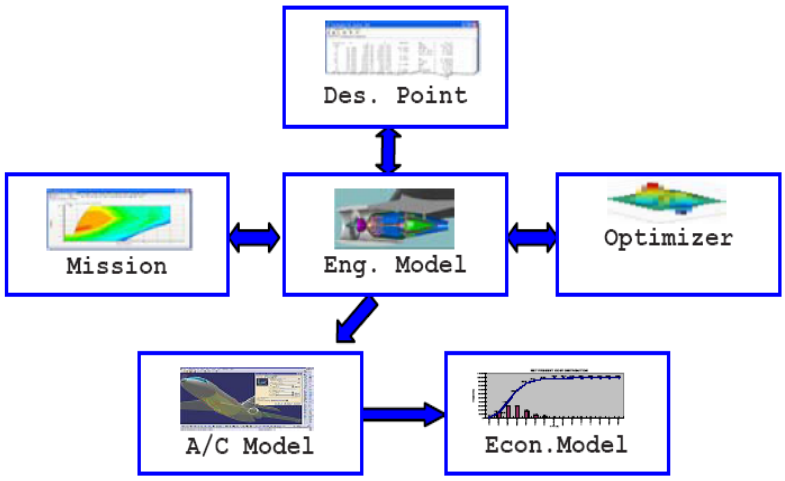

Figure 4.23: Structure of the multidisciplinary design method

First of all, the proposed engines' design point (take-off) has been optimised to minimise the NO_x emission while constraining ideal jet velocity ratio $\frac{V_{id.18}}{V_{id.8}}$. Then, four operating conditions have been evaluated throughout flight mission (off-design conditions): climb-out, cruise, approach and ground idle. All of this was performed using the engine model. The next step was to introduce the required output parameters in aircraft and economic and risk models. These models are coupled together allowing for their rapid execution and robustness. In this study, the risk was not considered.

4.2.2.3 Results

A preliminary parametric study for the investigated cycles were made in the previous section in order to identify the most promising solutions in terms of emission reduction and less fuel consumption. The results obtained from this can be used as a starting point to run different optimisation scenarios where the economic and environmental impact is considered.

In this work, the optimisation process was carried out to achieve the best optimal design reducing NO_x production (see table 4.6). The current technology was assumed.

4.2.2.4 Analysis

As can be observed from figure 4.24 and 4.25, the cycle that gives the lowest NO_x emission, in comparison to ICAO parameter limit and LTO cycle, is the intercooled turbofan; however this engine's operating costs are the highest as well as CO_2 emissions during cruise; this is due to the high burn and carried fuel involved in this concept.

Table 4.6: NO_x optimisation results

	BL	IC	REC	ICR
FN_{sls} [kN]	100.97	100.97	100.97	100.97
SFC_{sls} [g/kN*s]	10.45	14.54	9.93	10.24
WF [kg/s]	1.06	1.47	1.05	1.05
NO_x $(Dp/Foo)_{LTO}$ [g/kg]	45	10	42	31
$CO_{2,\ cruise}$ emissions [kg]	4615	5983	4500	4402
η_{th} [-]	0.43	0.30	0.49	0.49
BPR [-]	5.3	5.3	5.3	5.3
OPR [-]	24.41	7.01	14.14	12.41
Gear Ratio [-]	N/A	N/A	N/A	N/A
εic [-]	N/A	0.6	N/A	0.72
εrec [-]	N/A	N/A	0.67	0.67
W2 [kg/s]	326.0	326.0	326.0	326.0
T4 [K]	1605	1605	1605	1605
ΔSFC [%]	0.0	38.1	-5.7	-2.9
Δ NO_x $(Dp/Foo)_{LTO}$ [%]	0.0	-78.0	-7.0	-31.0
$\Delta CO_{2,\ cruise}$ [%]	0.0	30.0	-2.0	-5.0
ΔEDOC [%]	0.0	14.2	3.3	3.0

4.2.2.5 Discussions

The recuperated turbofan, in terms of environmental performance, seems to be very attractive, but its DOC is still high. However, the ICR turbofan shows improved environmental and economic performance with regard to the other cycles.

From the above observation the following conclusion can be made: a reduction in one type of pollutant may result in an increase of another, and also the introduction of new technology leads to increased engine operating cost, so the tradeoffs in here are very challenging.

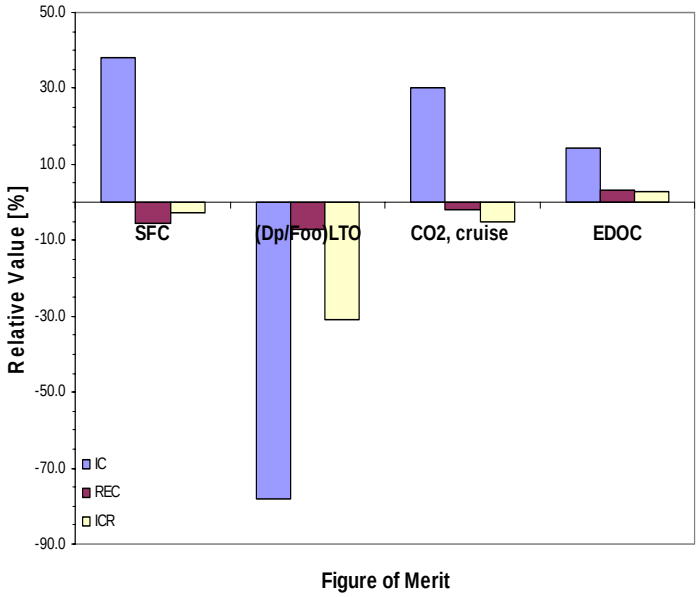

Figure 4.24: Relative values of SFC, $(Dp/Foo)_{LTO}$, $CO_{2,\ cruise}$ and EDOC for selected turbofans

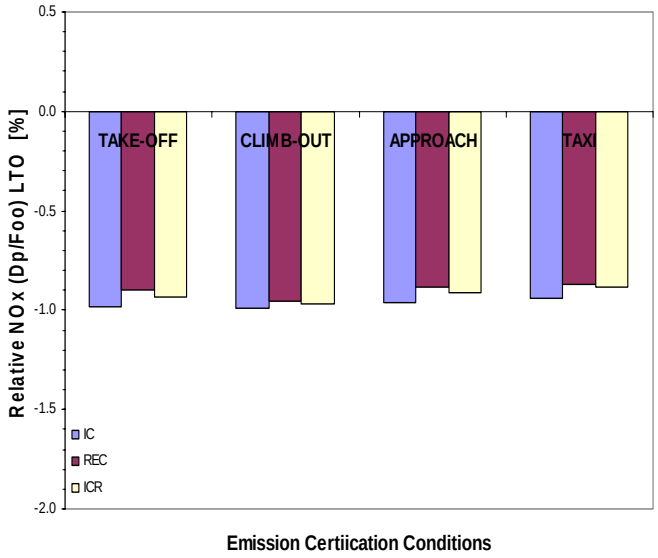

Figure 4.25: Relative NO_x (Dp/Foo) LTO for selected turbofans at ICAO certification operating conditions

4.2.2.6 Conclusions and Recommendation for Future Work

This work shows a simple but useful approach for the analysis of environmental and economic performance at aircraft system level for the new aero-engines' feasibility study.

This research was limited to short-range transport applications and the installation aspects were included. Also, the current core and combustor technology was assumed. The design point of the selected cycles was set up at take-off SLS operating conditions. The optimisation was performed minimising the NO_x emissions with ideal jet velocity ratio $\frac{V_{id.18}}{V_{id.8}}$ as a constraint.

The results show that the ICR turbofan seems to be, at least according to the simulations, a very promising solution in terms of environmental performance, but the operating costs are high (3% relative to baseline).

An important conclusion can be deduced from this study: the introduction of new technology leads to high operating costs, so they would become economically attractive at a sufficiently high fuel price.

Future work will be to make this approach more flexible and to be coupled with an optimiser available commercially to assess other scenarios as well as more radical power plants.

4.3 Baseline, Geared and Constant-Volume Combustion (CVC) Turbofans

4.3.1 Introduction

Aviation forms a vital part of the transportation system required for today's globalised economy. Furthermore, it generates revenue and provides jobs. The annual growth of air transport raises concerns about noise pollution and emissions. Soaring fuel prices affect airline operation and have an impact on the affordability of air transport.

Noise pollution is an issue for inhabitants of the airport's hinterland. The growth of air traffic and the probability of congestion near airports drive the call of local governments and residents for more stringent regulations. Furthermore, legislators consider the extension of emissions regulations to include cruise. Implementation of such legislation could have a considerable impact on airline operation and economics. Noise and emissions charges have been introduced on several, mainly European, airports. Besides, the European Union plans to add aviation to its Greenhouse Gas Emissions Trading Scheme. These measures are put in place to encourage airlines to operate clean and quiet aircraft.

The Advisory Council for Aviation Research in Europe (ACARE) has formulated a vision for the year 2020. Objectives set, for engines, are a 20% decrease of fuel burn and CO_2 emissions, 80% NO_x emissions reduction and 6dB less noise. The ACARE vision comprises a roadmap for the research-and-development effort required to achieve those aims. Novel and radical engine cycles are assessed and developed under several programs (e.g. VITAL, NEWAC and DREAM).

Colmenares et al. (2007a-c, 2008 a-c and 2009a-b), Pascovici et al. (2007 a-b and 2008) and Kyprianidis et al. (2008) have done techno-economic analyses and optimisations of multiple novel cycles including intercooled, intercooled-recuperated, contra-rotating turbofan and geared turbofan cycles (refer to previous sections). Several multidisciplinary design frameworks were utilised for the analyses.

A radical cycle under research is the constant volume combustion (CVC). Considerable effort has been invested to understand its unsteady flow behaviour (Akbari et al., 2006b-c and 2007). However, only one study is known to the author that assesses the operational feasibility of a conventional turbofan with CVC combustor (Won and Waters, 2003). In this study a geared turbofan mounted with a CVC (GTF-CVC) is considered. The main question is: Compared to a baseline geared turbofan, is the GTF-CVC cycle able to match noise and emissions regulations for an acceptable performance and cost of ownership?

Since the low pressure system of the geared turbofan can operate at its optimum speed, the stage count is reduced and the SFC is lower leading to a reduction in mission fuel burn. Besides, the pressure gain over the CVC – due to semi-constant volume combustion – potentially contributes to the reduced stage count and the diameter of the rotating components. The main disadvantage of the GTF-CVC cycle is its complexity. For a comprehensive description of the CVC cycle the reader is referred to research undertaken in the past (Smith et al., 2002).

The geared turbofan with constant volume combustor is simulated and benchmarked against a baseline geared turbofan engine. Results indicate that the former complies with CAEP/6 and FAR Part 36 regulations for noise and emissions. Furthermore, the acquisition cost of the engine is higher, but engine direct operating cost decreases by 25.2% which would be very attractive to the

airline operators. The technology requires further development to meet future noise and emissions requirements.

4.3.2 Methodology

First, a parametric study is performed to explore the design space. The objectives are minimum fuel burn, cruise SFC, NO_x emissions, noise and engine direct operating cost (DOC). Both the baseline GTF and GTF-CVC have a TET of 1650ºK, since the technology level of both engines is assumed to be similar. The optimum FPR is determined with the design parameters BPR and OPR. Main performance parameters of the baseline GTF and GTF-CVC are listed in the result section. A roadmap of the optimisation study is provided in figure 4.26.

Subsequently, five single-objective optimisations and one multi-objective optimisation are performed. The GTF-CVC cycle is optimised for every individual objective. Then a multi-objective trade case is run for fuel burn vs. cruise SFC vs. NO_x emissions vs. noise vs. engine DOC. The Kreisselmeier-Steinhauser method combined with the Davidon-Fletcher-Powell optimisation algorithm is used.

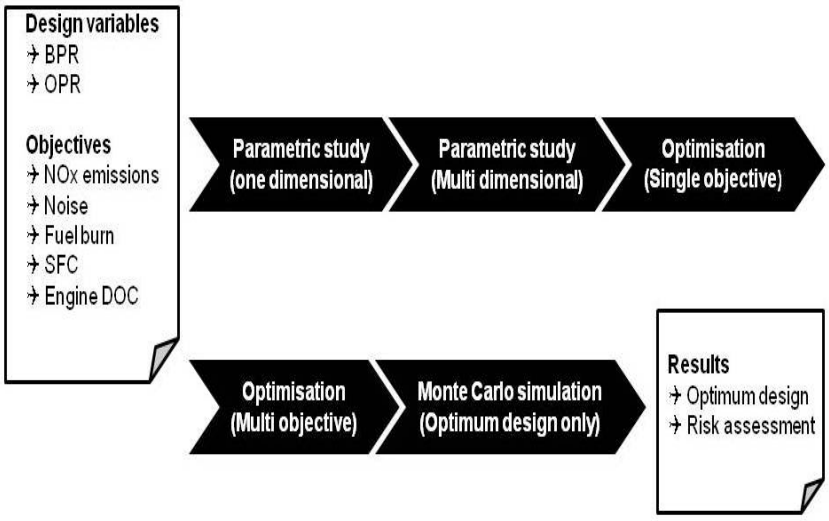

Figure 4.26: Roadmap optimisation study (Colmenares et al., 2009a)

A tool was developed for the assessment of novel and radical cycles. The Preliminary Multidisciplinary Design Framework (PMDF) consists of several interconnected modules which are linked to an optimisation and control unit. Figure 4.27 provides an overview of PMDF. The emissions, environmental and weight modules were developed as part of this PhD research. Additionally, an existing life cycle cost module was modified and remaining models were obtained from NASA. For further details of the framework as well as of its modules the reader is directed to chapter 3.

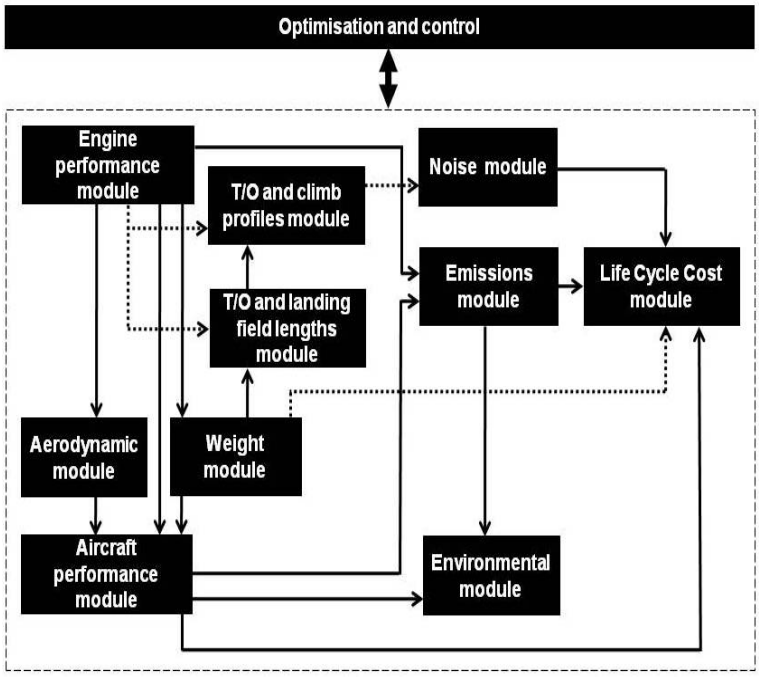

Figure 4.27: Overview of PMDF (Colmenares et al., 2009a)

4.3.2.1 Validation

PMDF is validated with data of an Airbus A320 mounted with CFM56 engines. A selection of validation results is listed in table 4.7. Data for the

validation is obtained from the public domain. The reliability of this data cannot be guaranteed.

However, the validation gives a good indication of the accuracy of PMDF results. The best engineering judgment is used where no validation data is available.

Table 4.7: Validation results for baseline engine

	Simulation	**Public Data**	**Deviation [%]**
SFC_{cr} [g/kN*s]	17.41	17.11	1.75
FN_{cr} [kN]	23.04	21.32	8.07
FN_{sls} [kN]	120.10	120.10	0.0
Engine weight [kg]	2206	2381	-7.47
Engine length [m]	2.50	2.51	-0.44
Fan diameter [m]	1.63	1.73	-6.09
Design range [kg]	4842.42	4815.2	0.57
MTOW [kg]	78401	74055	5.87
ZFW [kg]	61763	61136	1.02
Flyover noise	82.0	88.0	-6.82
Sideline noise	94.37	94.4	-0.03
Combined noise	176.36	96.3	-3.31
LTO $(D_p/F_{oo})_{NOx}$ [g/kN]	54.1	57.1	-5.25
Price CFM56 [USD million]	6.98	6.95	0.43
Price Airbus A320 [USD million]	77.17	76.9	0.35
Total maintenance [$ct/ASM]	2.02	2.01	0.50
Engine maintenance cost [$ct/ASM]	0.68	0.67	1.49

4.3.3 Results

The feasibility of the GTF-CVC cycle is assessed with a multidisciplinary design optimisation (MDO) study. Results presented in this section are relative to

the baseline GTF cycle. They represent the percentage increase or decrease compared to the baseline GTF.

4.3.3.1 Analysis

A comparison between the geared turbofan with the conventional combustor and with the CVC combustor was made in order to see the advantages and the drawbacks of the latter configuration.

As can be observed from the table below, the mass flow of the GTF-CVC is lower in comparison to GTF. At the same thrust level, this leads to an increase in specific thrust and as a result the engine becomes smaller for the given mission.

Table 4.8: Design point data for selected cycles

Configuration	GTF	GTF-CVC
FN_{TO} [kN]	120.10	120.10
BPR [-]	8.2	8.2
FPR [-]	1.45	1.45
OPR [-]	38.6	38.6
TET [K]	1650	1650
Mass Flow [kg/s]	446.4	421.3
Gear Ratio [-]	3.0	3.0
ΔBlock Fuel [%]	0.0	-17.0
ΔBlock RF [%]	0.0	-7.1
ΔCombined Noise [%]	0.0	-6.3
ΔEDOC [%]	0.0	-23.0
$\Delta NO_{x,LTO}$ [%]	0.0	-15.06
ΔSFC_{Cr} [%]	0.0	-9.6

The same outcome is noticed on the engine weight which becomes lighter than the GTF owing to the increase in the engine specific thrust, despite the CVC heavy combustor which deals with high pressures and the high pressure turbine weight due to the pressure growth at the exit of the combustor.

The SFC at cruise condition has roughly a 10% benefit. On the other hand, combined noise (i.e. flyover plus sideline) is reduced by approximately 6% while the NO_x for landing and take-off cycle by almost 15%.

All of these benefits lead to a reduction of 17% in fuel burn and 23% in engine DOC, which is a very attractive outcome to an airline. In summary, the GTF-CVC technology seems to be a promising solution to achieve the environmental and economical objectives imposed in the aviation field as in the case of ACARE.

4.3.3.2 Parametric Study

Variation of non-dimensional block fuel and LTO NO_x is presented in figure 4.28. LTO NO_x decreases if the BPR becomes larger. This is mainly due to the reduction of SFC caused by higher BPRs. On the other hand, the LTO NO_x of the GTF-CVC is lower than the value found for the baseline GTF despite high values of NO_x emission index which arise from constant volume combustion process.

Block fuel diminishes with rising BPR until an optimum value is reached where BPR equals 7.2. This reduction of fuel burn is because of a propulsive efficiency improvement. For BPRs greater than 7.2 the engine weight and the nacelle drag become dominant and the block fuel increases. The GTF-CVC burns almost 17% less fuel than a baseline GTF engine.

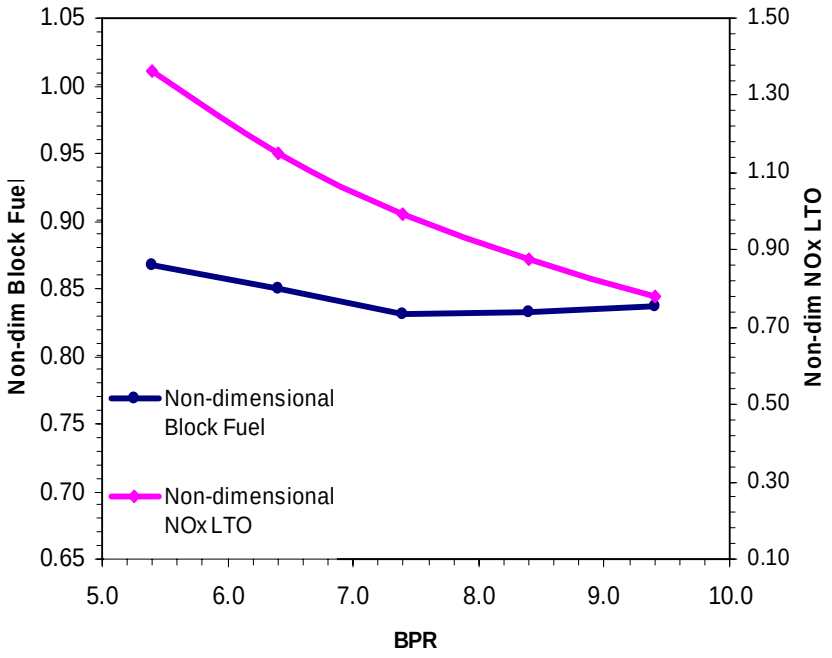

Figure 4.28: Parametric study of non-dimensional block fuel and LTO NO_x vs. BPR

Engine DOC (see figure 4.29) has a relatively constant value at 0.80 approximately. However, an optimum engine DOC can be identified, which coincides with the optimum block fuel for BPR equal to 7.2. The engine DOC curve levels off for BPR ranging from 8.3 to 9.4, since the combined noise levels are lower. Hence, the noise charges – that have a significant influence on the engine DOC – decrease and offset the rising fuel cost.

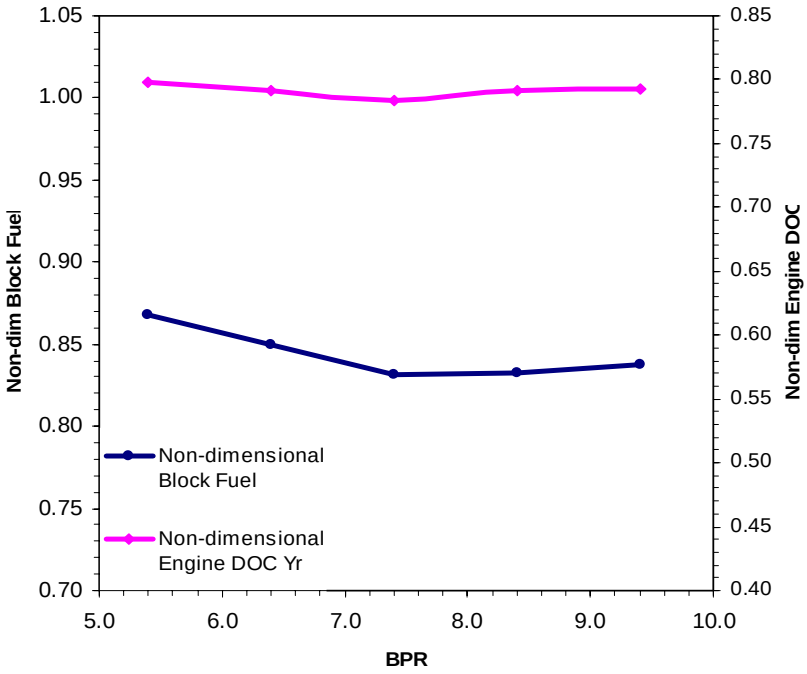

Figure 4.29: Parametric study of non-dimensional block fuel and engine DOC vs. BPR

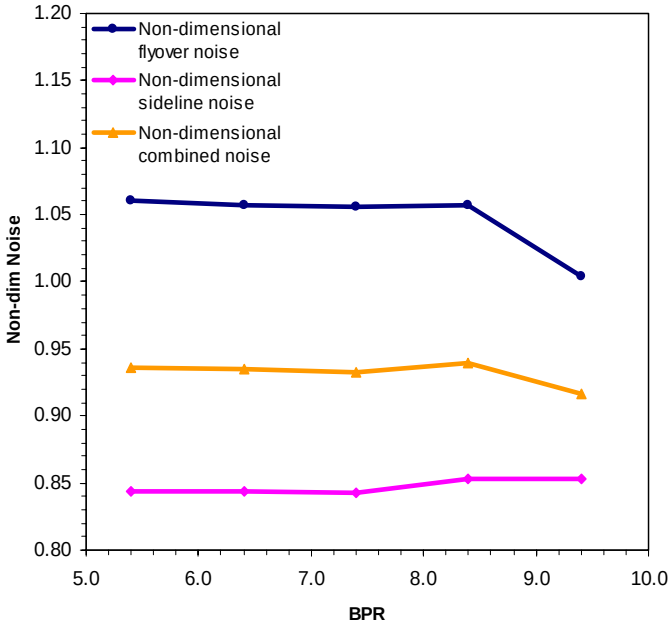

Figure 4.30: Parametric study of non-dimensional EPNL vs. BPR

Non-dimensional flyover (blue), sideline (pink) and combined (orange) noise are presented in figure 4.30. If BPR increases, the exhaust jet velocity drops and jet noise decreases. However, the fan diameter increases with BPR, which results in higher fan noise levels. Sideline noise is mainly controlled by fan broadband noise (i.e. the turbulence which develops in the wakes of the fan blades). Figure 4.30 shows that jet and fan noise balance over almost the complete BPR-domain. Flyover noise is dominated by the 8^{th} power of the jet velocity (the Lighthill's theory) which in turn reduces as the BPR does. In case of flyover the GTF-CVC produces more noise than the baseline GTF. Since the flyover noise is more dominant for higher values of BPR, the combined noise follows its trend leading to a drop in cumulative noise.

SFC in non-dimensional values as a function of BPR is provided in figure 4.31. If BPR rises, the SFC decreases because of an improvement of the propulsive efficiency. For BPR values above 7.2 the GTF-CVC has a lower SFC than the baseline GTF.

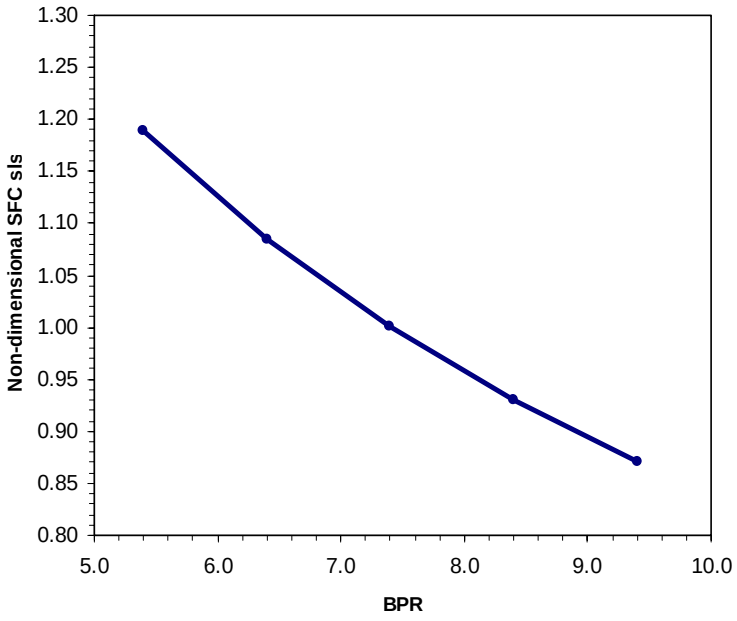

Figure 4.31: Parametric study of non-dimensional SFC vs. BPR

4.3.3.3 Single-Objective Optimisation

Single-objective optimisation is performed for minimum fuel burn, cruise SFC, LTO NO_x emissions, combined noise and engine DOC. Figures 4.32 to 4.35 display the results of the optimisation runs. Aero engine design requires a compromise between NO_x and CO/CO_2 emissions (fuel burn consequently engine DOC) to find the overall optimum. The single objective optimisations minimum for fuel burn, cruise SFC and NO_x emissions demonstrate this trade-off.

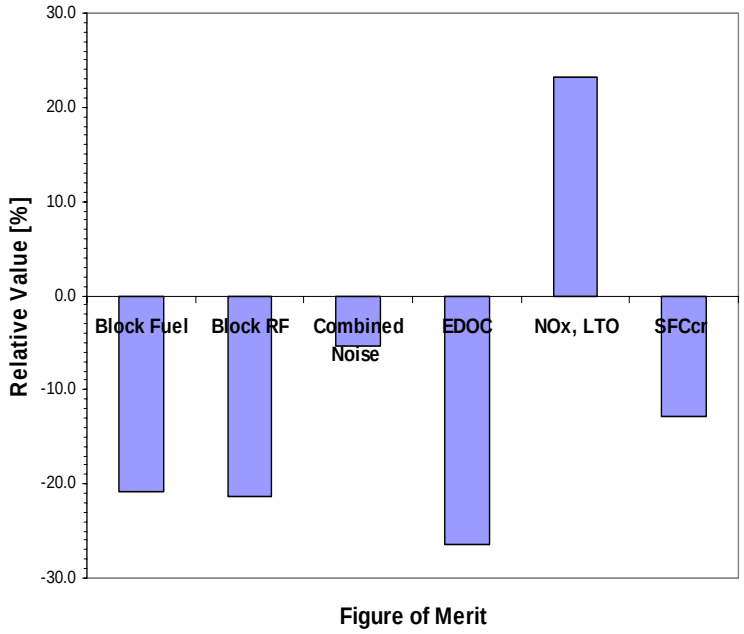

Figure 4.32: Single-objective optimisation for minimum fuel burn

Optimisation of the GTF-CVC cycle for fuel burn results in a 20.9% reduction compared to the baseline GTF (see figure 4.32 and appendix F). Besides, the cruise SFC improves by 12.8% due to the high OPR. This improvement of cruise SFC is offset by the lower BPR (GTF BPR=8.2 and GTF CVC BPR=7.5). The lower fuel burn is reflected in the engine DOC as a cost advantage. Combined noise is lower than the baseline, since the fan is smaller. Radiative Forcing (RF) contributions for

CO_2 and NO_x are calculated by PMDF. Block RF is over 21% lower because of the significant reduction in fuel burn, but is offset by higher NO_x emissions.

If the engine is optimised for minimum NO_x emissions, a 45.7% reduction is obtained (see figure 4.33). The OPR and combustion temperature are moderate, which results in low NO_x formation. Fuel burn decreases by 9.3% but the cruise SFC is higher than the baseline value. This trend may appear controversial on first sight. However, the cruise schedule selected for the mission (optimum altitude for given Mach number and range) allows the aircraft with a GTF-CVC engine to fly higher. Therefore, fuel burn in cruise is less than baseline, although the SFC is higher. Again, the reduction in fuel burn and noise results in a decrease of engine DOC. Block RF reduces under influence of lower fuel burn and NO_x emissions (refer to appendix F).

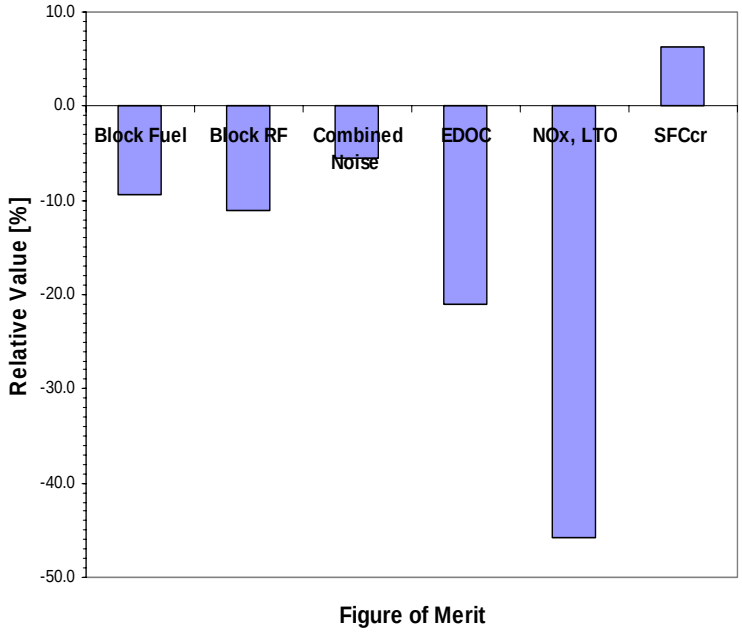

Figure 4.33: Single-objective optimisation for minimum NO_x emissions

The optimisation for minimum SFC (see figure 4.34) shows a trend similar to the optimisation for minimum fuel burn (see figure 4.32). A lower cruise SFC is obtained at the expense of a substantial increase of NO_x emissions.

Optimisations for minimum cruise SFC and minimum combined noise result in a similar engine (see figure 4.34 and appendix F). High BPR is favourable for both high propulsive efficiency and a low exhaust jet velocity. The high TET and OPR provide a favourable thermal efficiency. In this single-objective optimisation case an engine DOC reduction of 26.5% is obtained. A 20.5% block-RF reduction is obtained due to a significant reduction in fuel burn (read CO_2 emissions).

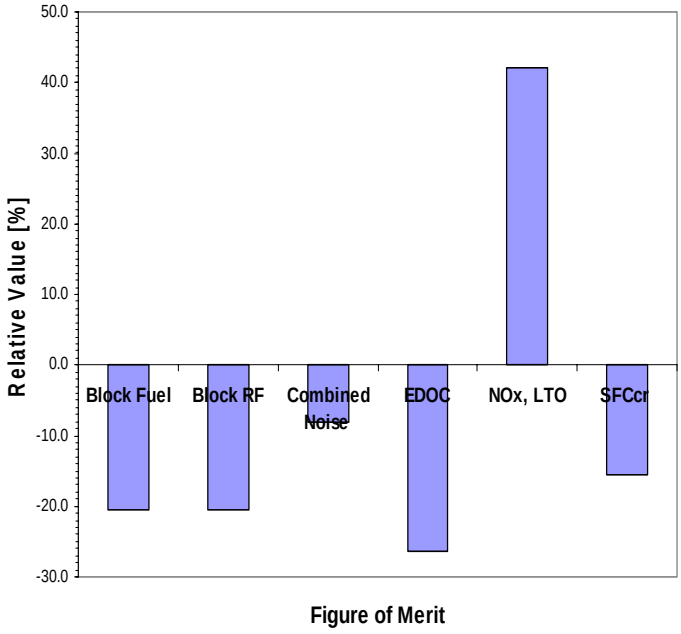

Figure 4.34: Single-objective optimisation for minimum cruise SFC and noise

Figure 4.35 demonstrates that the main contributors to engine DOC are fuel cost and noise charges. The 27% cost reduction is obtained with a 19.5% decrease of fuel burn, almost 21% less RF and 7.3% less noise. Interestingly, NO_x emissions remain virtually unchanged. The engine design for minimum operational cost gives

a 6.8% reduction of cruise SFC. This decrease is the product of a high OPR and modest BPR (refer to appendix F).

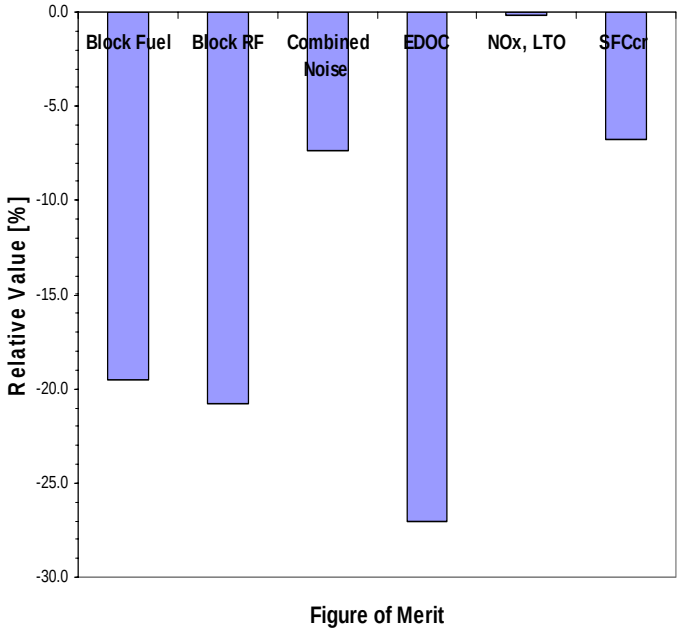

Figure 4.35: Single-objective optimisation for minimum engine DOC

4.3.3.4 Multi-Objective Optimisation

A multi-objective optimisation run is done to find the optimum design compromise. A trade-off is made for fuel burn vs. cruise SFC vs. NO_x emissions vs. combined noise vs. engine DOC. Figure 4.36 presents the results of the optimum design compromise (also refer to appendix G).

The optimised design induces a 17.2% decrease of fuel burn, 18.2% decline of radiative forcing, 6.4% lower cruise SFC, 12.4% reduction of NO_x emissions, 6.5% less noise and 25.2% lower engine DOC. Potential advantages over the baseline for individual figures of merit are higher in case of the single-objective optimisation

cases. Obviously, the design optimised for several figures of merit is a compromise to achieve the best overall result.

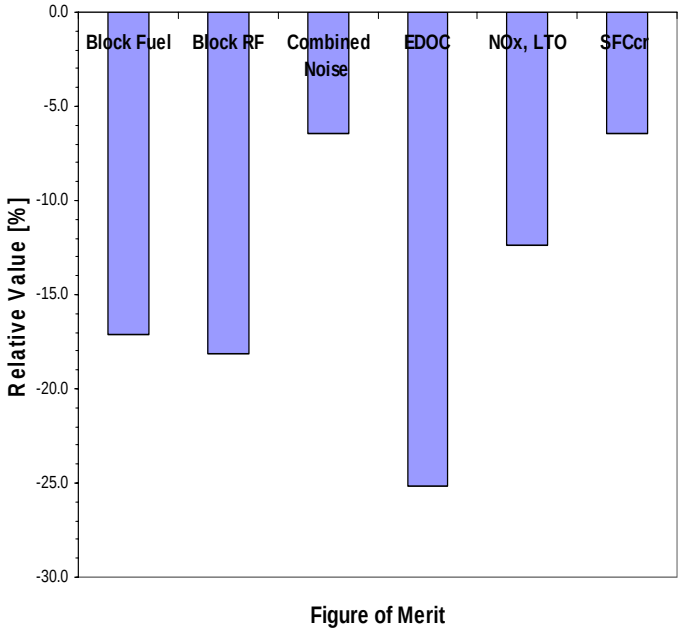

Figure 4.36: Multi-objective optimisation for FB vs. NO_x vs. cruise SFC vs. noise vs. engine DOC

NO_x emissions are mainly driven by flame temperature, residence time and the homogeneity of the fuel-air mixture. The unsteady flow behavior of the combustion wave rotor potentially allows for short residence times. However, the CVC adiabatic flame temperature is higher due to the constant volume combustion process. No work is done on the flow during combustion. Therefore, the internal energy of the flow is higher than in the case of the baseline GTF. Consequently, the SFC of the GTF-CVC cycle is lower but NO_x emissions are potentially higher. Ultimately, the balance of SFC reduction and emission index rise determines the NO_x emissions per unit net thrust. Therefore, compromise is required to achieve the optimum design.

4.3.3.5 Risk Assessment

An uncertainty assessment is performed for the engine DOC. Monte Carlo simulation is applied to the optimised GTF-CVC cycle (i.e. BPR=6.9, FPR=1.45, OPR=41.6 and TET=1650K) for this purpose. K-factors are used to access the uncertainty of noise and emissions charges, maintenance labour rate and cost technology factors for engine research and development (R&D), production and maintenance (see table 4.9). The range for the fuel price is set from $3.57 to $6.00 per gallon, based on the kerosene price of June 2008 (IATA, 2008).

Table 4.9: Ranges K-factors

K-factor	Range
Maintenance labour rate	1.0 - 1.03
Noise charges	1.0 - 1.2
Emissions charges	1.0 - 1.2
Cost technology factors	0.9 - 1.1

The cumulative curve for the relative engine DOC is presented in figure 4.37. Furthermore, table 4.10 shows the median, quartiles and inter quartile range. There is a 50% probability that the engine DOC has a value between -3.2% and 3.9%. There is also a 25% chance that the relative engine DOC is higher than 3.9%.

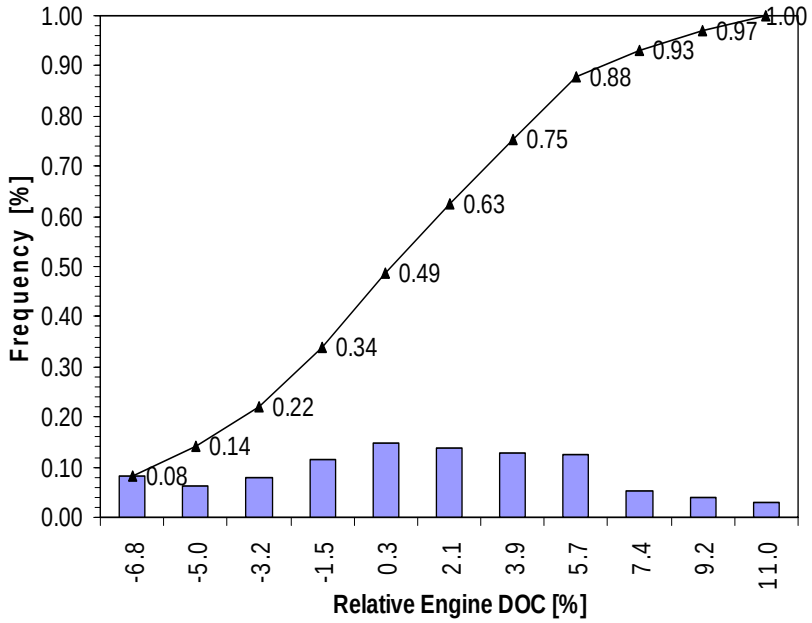

Figure 4.37: Cumulative curve EDOC

Table 4.10: Quartiles and median of the cumulative curve

Parameter	EDOC [%]
Median	0.95
Lower quartile	-2.01
Upper quartile	3.90
Inter quartile range	5.91

4.3.3.6 Breakdown of Engine DOC

Engine DOC is broken down into categories for the baseline GTF and multi-objective optimised GTF-CVC in figures 4.38 and 4.39. The category "other" comprises depreciation and insurance cost. Three major items in the engine DOC of the baseline GTF are maintenance and fuel costs as well as noise charges. The

optimised GTF-CVC produces slightly less noise, which is reflected in the engine DOC. Main contributors to the engine DOC of the GTF-CVC are fuel (81.7%) and maintenance (10.7%) costs. Emissions charges have a similar contribution for both engines. Depreciation and insurance cost shares differ 0.85% between the GTF and GTF-CVC engines.

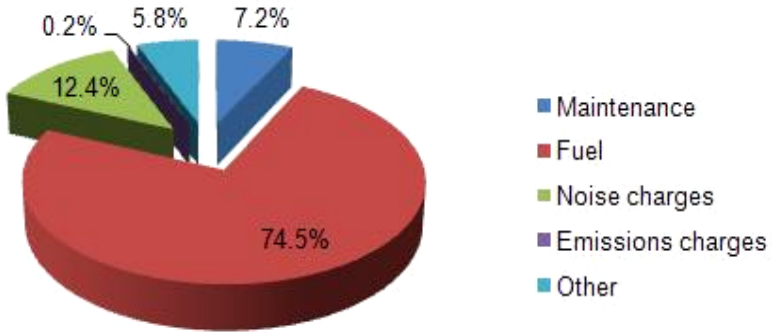

Figure 4.38: Breakdown of the engine DOC for the baseline GTF

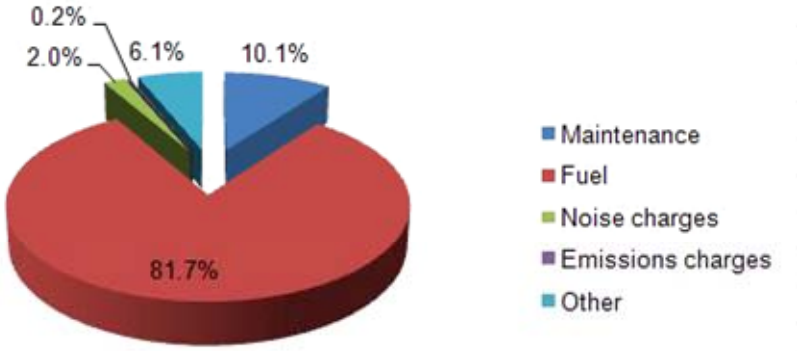

Figure 4.39: Breakdown of the engine DOC for the GTF-CVC

The lower contribution of fuel cost for the baseline GTF (74.5% compared to 81.7% for the GTF-CVC) may seem controversial at first sight. However, the baseline GTF has a lower contribution of fuel cost due to the high (12.4%) noise charge. The lower contribution of noise charges for the GTF-CVC drives the fuel contribution up to 81.7%. Also, a small shift can be identified in maintenance cost.

In absolute figures, the GTF-CVC burns less fuel and therefore its fuel cost is lower.

4.3.3.7 Pareto Front

The Pareto front is an effective methodology to validate feasible aero engine designs. An n-parameter design space is defined and k criteria are applied to assess all design points. Each design space point x is assigned a criteria space point f(x). The dimensions of criterium vector X have to be minimised to find feasible criterium points for the Pareto front. Therefore, image vector Y must be strictly dominated by criterium vector X. Mathematically the process is expressed as follows:

$$f : R^n \rightarrow R^k \quad \textbf{(4.8)}$$

Where: X is a set of feasible designs in R^n.

$$Y = f(X) \quad \textbf{(4.9)}$$

$$X \succ Y \quad \textbf{(4.10)}$$

Figure 4.40 shows the Pareto front of the non-dimensionalised fuel burn vs. NO_x emissions. A reduction in NO_x emission can be obtained at the cost of a higher fuel burn. If NO_x emissions are reduced by 20% (from 1.0 to 0.8 for the GTF-CVC), fuel burn increases 4%. Hence, compliance with future emissions and economical requirements could imply a design compromise.

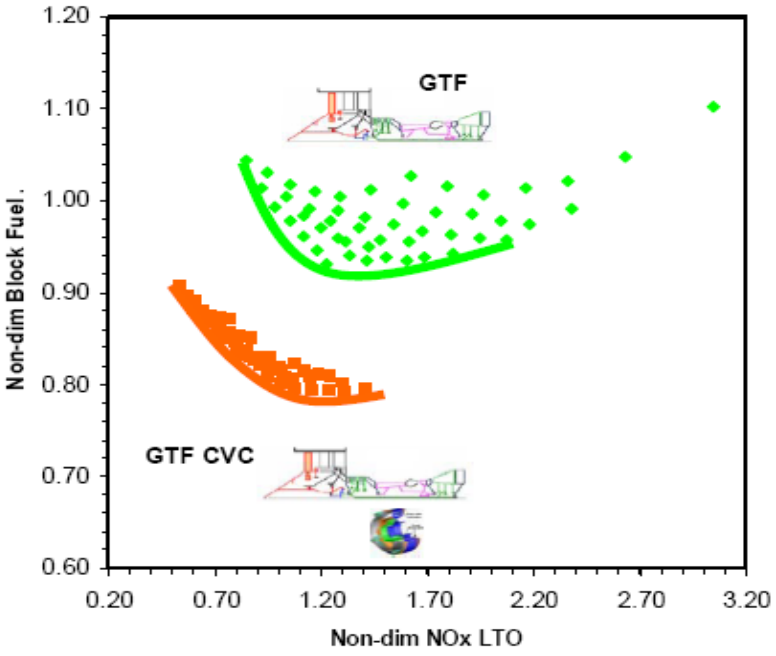

Figure 4.40: Pareto front non-dimensional FB vs. NO_x

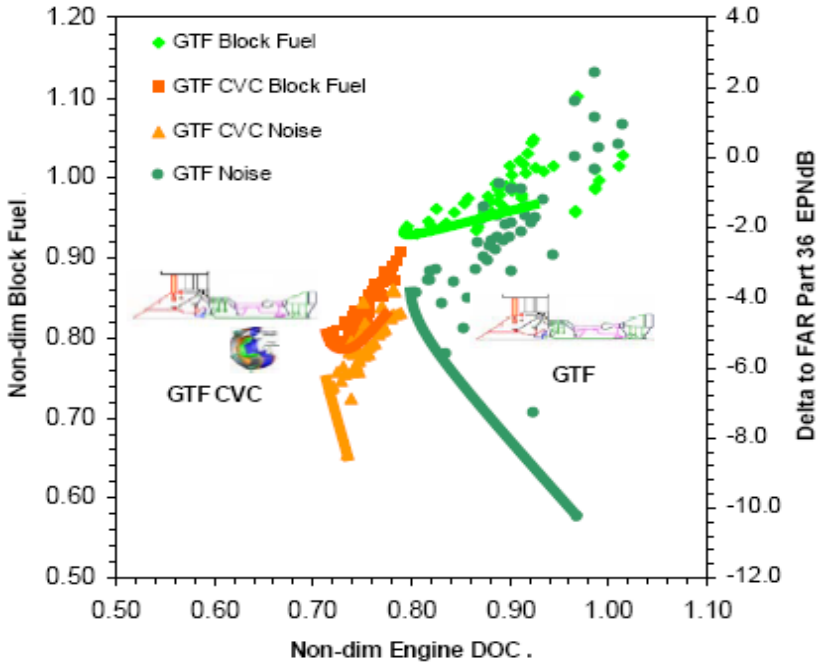

Figure 4.41: Pareto front non-dimensional NO_x / Noise vs. EDOC

The Pareto fronts for non-dimensionalised fuel burn and noise vs. engine DOC are shown in figure 4.41. Note that the Pareto front for EDOC vs. FB of the GTF-CVC is small. Hence, variations in fuel burn have a small impact on engine DOC for the design points on the Pareto front. In the case of the GTF-CVC, a modest reduction of noise (e.g. 2 EPNdB) results in 2.7% higher engine DOC due to increased maintenance cost. The BPR rises from 5.5 to 8.5.

Figure 4.41 shows that compared to a baseline geared turbofan (EDOC=1.0, FB=1.0 and delta noise=0.0 EPNdB), the GTF-CVC cycle consumes less fuel and produces less noise for lower engine DOC.

4.3.3.8 Comparison Baseline GTF and Optimised GTF-CVC Turbofan

The main cycle and performance parameters of the baseline GTF and optimised GTF-CVC engines are listed in table 4.11. FPR, TET and net thrust at SLS (FN) of the engines are similar. BPR and mass flow of the GTF-CVC are lower. Conversely, the engine with a combustion wave rotor has a higher overall pressure ratio.

Table 4.11: Main cycle and performance parameters of the baseline GTF and optimised GTF-CVC

Parameter	Units	GTF	GTF-CVC
TET	K	1650	1650
BPR	-	8.2	6.9
FPR	-	1.45	1.45
OPR	-	38.6	41.6
Mass Flow	kg/s	446.5	401.6
FN	kN	121.56	121.56

Table 4.12: Dimensions and weight delta to baseline of the GTF-CVC

Parameter	Δ to GTF [%]
Bare engine weight	-18.0
Bare engine length	15.7
Bare engine max. radius	-1.7
Nacelle length	5.6
Nacelle weight	4.5
Power plant weight	-13.2

Deviations in dimensions and weight of the GTF-CVC from the baseline GTF are listed in table 4.12. Bare engine, as well as powerplant, weight is lower. However the nacelle weight has increased by 4.5%. Supplementary ducting and a longer burner (CVC) contribute to additional length and weight. Conversely, the fan of the GTF-CVC, and gear system are 23.9% lighter. Therefore, the overall powerplant weight diminishes by 13.2%.

4.3.3.9 Compliance to Noise and Emissions Requirements

Apart from cost of ownership, compliance to noise and emissions requirements is an important consideration in aero engine design. Noise pollution is a local problem confined to the vicinity of airports. However, pollutant emissions have both a local and global impact. Noise and emissions regulations become more stringent as air traffic increases. Emissions have an environmental as well as an economical impact. The European Union decided to add aviation to the EU Greenhouse Gas Emissions Trading Scheme. Besides, ICAO considers emissions legislation for cruising operating condition. These measures could have a considerable economical impact on airline operations. Table 4.13 shows that the

GTF-CVC cycle complies with FAR36 and CAEP/6 regulations. Furthermore, the cycle has development potential to meet future noise and emissions requirements.

Table 4.13: Compliance of the optimised GTF-CVC to noise and emissions requirements

Combined Noise Δ to FAR36 [EPNdB]	NO_x Emissions LTO Fraction of CAEP/6 [%]
-5.25	56.6

4.3.4 Conclusions and Recommendation for Future Work

The GTF-CVC has a significant cost of ownership advantage over geared turbofans. Acquisition and maintenance costs of GTF-CVC engines are higher, although a substantially lower fuel burn offsets these costs. Hence, life cycle cost of GTF-CVC engines is lower.

Replacement of the annular combustor by a CVC allows for a reduction of HPC size for a given net thrust. Furthermore, lower stage count for the HPT and LPT can be achieved. However, the relative weight of individual stages could be higher due to elevated pressures and temperatures. Careful design of ducting between the turbomachinery and CVC is required to curb its weight.

NO_x emissions of the GTF CVC are lower than the baseline. A higher emission index is offset by a lower SFC. The net result is lower NO_x production.

Results of the multi-objective trade case study show that the GTF CVC complies with FAR36 and CAEP/6 noise and emissions requirements. Also, a

substantial cost of ownership reduction has been identified. However, a considerable R&D effort is required before GTF-CVC engines can enter service.

Design, production and development of a CVC cycle test set-up could contribute to the effort undertaken to understand its behaviour. Furthermore, this test set-up could provide detailed data and component maps, which can be used for further MDO studies.

CHAPTER 5

CONCLUSION:

COMMENTS AND RECOMMENDATIONS

5.1 Comments

The main objective of this research is to assess the potential of different novel propulsion systems with respect to propulsive and thermal efficiency improvements to meet environmental and economical goals as well as the trade-offs to be made between noise, emissions, operating cost, fuel burn and performance using single- and multi-objective optimisation case study. This research was limited to short-range transport applications (i.e. A320) and the installation aspects were included.

In order to achieve this objective, a multidisciplinary design framework was developed which is made up of: aircraft and engine performance, weight, cost, noise, emissions, environment and economics and risk models. These modules are linked to an available optimiser to make this framework a powerful aero-engine preliminary design tool.

The innovative propulsion systems based upon propulsive efficiency improvement are: advanced, contra-rotating and geared turbofans. In the feasibility study of the engines, the current combustor technology was assumed. The design point was set up at ToC operating conditions. The optimisation was performed by minimising different figures of merit (i.e. NO_x emission, fuel burn, global warming potential, noise and direct operating cost) and changing two design variables: FPR and BPR. These cycle parameters were used due to their great impact on noise as

well as the SFC reductions. However, some trade-off studies have to be carried out because increases in BPR produce heavier engines leading to an increase in fuel burn as well as the operating cost. Moreover, the materials and manufacturing technologies should be considered to bring a reduction in total engine weight.

The CRTF gives the best noise improvement among the turbofans which were assessed because of relevant lower fan tip speed of the two fan rows. Furthermore, this configuration gives reductions in fuel burn and CO_2 emissions' reductions (21.8%) due to a moderate increase in BPR which leads to weight and drag advantages. Furthermore, the global warming impact is even less than in the ATF (6%) alternative which represents a reduction of 16.53% relative to the baseline engine. The DOC is still higher (3.54%) but less than the ATF (nearly 10%) becoming a very attractive option to the airline customers. Also, there would be a relative reduction of NO_x at LTO cycle by 31% which is very relevant from the point of view of airport emissions impact.

In the CRTF, a very compact booster is required to control dynamic instability in order to make this turbofan concept possible. In addition, this advanced booster needs higher pressure ratio values to balance the inner fan pressure ratio.

The cruising SFC of the GTF engine is the lowest. This potential, along with the advantages of having a gearbox in terms of LP-system dimension and weight, despite the additional weight of gearbox, brings the lowest fuel burn (27%) and one of the lowest operating costs (3.58%) between the novel propulsion systems considered in this study. Furthermore, the global warming potential is decreased by 19.21% (the lowest value in the pool of engines considered in this research). Finally, the cumulative noise margin is increased by approximately 129.25% (the second highest value in the assessed innovative engines) while the NO_x, for the landing and take-off cycle, goes down by almost 18.75% (the second lowest values).

Based upon the single-objective optimisation studies, the cycle that gives the minimum block fuel is the GTF engine. Similar results are obtained when optimising for minimum GWP as CO_2 emissions, which are connected with fuel burn, are the main contributors to global warming. In terms of noise margin, the turbofan with the best performance is the CRTF due to the low jet velocity (ultra BPR) and lower LP-system speed. The DOC-optmised baseline engine, in terms of economical performance, seems to be very attractive but to the detriment of the environmental performance as discussed above. Lastly, the CRTF gives the best LTO NO_x reductions followed by the GTF configuration. The worst case scenario is given by the ATF leading to an introduction of new combustor technology which will increase the production cost of the engine and therefore the cost of ownership.

For multi-objective optimisation a trade-off was done for fuel burn vs. LTO NO_x emissions and fuel burn vs. cumulative noise margin. A reduction in NO_x emission can be obtained at the cost of a higher fuel burn (i.e. LTO NO_x reductions of 20% lead to fuel burn increases of 8%). The GTF gives the best compromise with regard to these two figures of merit. In the case of fuel consumption and noise, the CRTF has a great potential for increased noise margin while the GTF has a promising block fuel decrease at the expense of less noise margin achievement but is still attractive. The AFT performs better in comparison to the baseline turbofan but worse with regard to the afore-mentioned engine arrangements. An increase in 16% of noise margin generates a 1% fuel burn penalty for the baseline turbofan.

The risk study shows that the increase in NPC is a concern and is greatly affected by fuel price, noise and carbon threshold, hence more radical configurations (i.e. CVC, ICR, IC, so on) need to be considered, optimised and assessed with respect to different uncertain parameters.

From the point of view of thermal efficiency the following configurations were studied: intercooled, recuperated and intercooled recuperative (ICR) and geared with-constant-volume-combustion (GTF-CVC) turbofans. The engine design point was calculated at sea level static take-off operating conditions.

The NO_x-optimised ICR turbofan seems to be, at least according to the simulations, a very promising solution in terms of environmental performance, but the operating costs are high (3% relative to baseline). This configuration should be optimised for other objectives to assess the impact on the direct operating costs.

However, the GTF-CVC has a significant cost of ownership benefit over geared turbofans despite the higher values of engine acquisition and maintenance costs. This is due to the considerable lower fuel consumption which compensates these costs leading to the lower engine life cycle costs.

The engine weight becomes lighter than the conventional GTF due to the reduction of the engine specific thrust, despite the CVC heavy combustor which deals with high pressures and the high pressure turbine weight due to the pressure growth at the exit of the combustor.

The cruise condition SFC is reduced as well as noise and LTO NO_x emissions in the vicinity of the airports. All of these benefits lead to an overall reduction in fuel burn and consequently in engine DOC, which is a very attractive outcome to an airline. In summary, the GTF-CVC technology appears to be an attractive solution to achieve the environmental and economical objectives imposed in the aviation field as in the case of ACARE in Europe.

The risk simulations with the four uncertain parameters (i.e. maintenance labour rate, noise and emissions charges, and cost technology factors) show that there is a 50% probability that the engine DOC has a value between -3.2% and 3.9%. There is also a 25% chance that the relative engine DOC is higher than 3.9%.

A general conclusion can be drawn from this study: the introduction of new technology leads to a penalty in operating costs, so they would become economically attractive at a sufficiently high fuel price.

5.2 Recommendations for Future Work

One of the difficulties of this study was to obtain proper data for the more radical turbofan as was the case of the CVC engine. This study can be used as a starting point for more detailed assessments and optimisation using a high fidelity package of finite elements and computational fluid dynamics. Afterwards, the innovative turbofan demonstrator can be manufactured and used to recalibrate this multidisciplinary optimisation tool which can be used for other studies and other innovative aircraft which could be compared to the conventional configuration (e.g. A320) used in this research.

More cycle variables, constraints and objectives should be considered for further design exploration. Also, the study of the technological impact on an innovative design using a sensitivity analysis with a response surface would be interesting to study.

REFERENCES

Airport Charges (2008). Fraport AG, Frankfurt Main.

Akbari, P. and Mueller, N. (2003). Performance Investigation of Small Gas Turbine Engines Topped with Wave Rotors. In: *39th AIAA/ASME/SAE/ASEE Joint Propulsion Conference and Exhibit,* Huntsville, Alabama, July 20-23 1998, AIAA, Reston, VA, AIAA 2003-4414.

Akbari, P., Nalim, R. and Muller, N. (2006a). A Review of Wave Rotor Technology and its Applications.In: *Journal of Engineering for Gas Turbine and Power*, 128(4), 717-735.

Akbari, P., Nalim, M. R. and Li, H. (2006b). Analytic Aerothermodynamic Cycle Model of the Combustion Wave Rotor in a Gas Turbine Engine. In: *4th International Energy Conversion Engineering Conference and Exhibit,* June 26-29 2006, San Diego, CA, AIAA, Reston, VA, AIAA 2006-4176.

Akbari, P., Nalim, M. R. and Snyder, P. H. (2006c). Numerical Simulation and Design of a Combustion Wave Rotor for Deflagrative and Detonative Propagation. In: *42nd AIAA/ASME/SAE/ASEE Joint Propulsion Conference & Exhibit,* July 9-1 2006, AIAA, Reston, VA, AIAA 2006-5134.

Akbari, P., Szpynda, E. and Nalim, M. R. (2007). Recent Developments in Wave Rotor Combustion Technology and Future Perspectives: A Progress View. In: *43rd AIAA/ASME/SAE/ASEE Joint Propulsion Conference & Exhibit,* July 8-11 2007, Cincinnati, OH, AIAA, Reston, VA, AIAA 2007-5055 .

Allaire, D. (2006). A Physics-based Emissions Model for Aircraft Gas Turbine Combustors, MSc Thesis MIT, MIT 74491770.

American Airlines (1978). A New Method for Estimating Current and Future Transport Aircraft Operating Economics, NASA CR-145190, NASA, Langley, VA.

Andriani, R. and Ghezzi, U. (1996). Regeneration in Propulsion. In: *32nd AIAA/ASME/SAE/ASEE Joint Propulsion Conference and Exhibit*, Lake Buena Vista, FL, May 1-3 1996, AIAA 96-2792.

Andriani, R. and Ghezzi, U. (2000). Off-design Analysis of a Jet Engine with Heat Recovery. In: *38th AIAA Aerospace Sciences Meeting and Exhibit*, Reno, NV, January 10 – 13 2000, AIAA-2000-0743.

Andriani, R., Ghezzi, U. and Infante, E. (2005). Thermal Analysis of Constant Volume Combustion Gas Turbine. In: *43rd AIAA Aerospace Sciences Meeting and Exhibit*, Reno, Nevada, January 10 - 13 2005, AIAA 2005-1010.

Andriani, R. and Ghezzi, U. (2005). Numerical Analysis of Main Performances of Gas Turbine Engines with Heat Recovery. In: *41st AIAA/ASME/SAE/ASEE Joint Propulsion Conference and Exhibit*, Tucson, Arizona, July 10 - 13 2005, AIAA-2005-4199.

Anon. (1993). ICAO Annex 16 Volume II: Aircraft Engine Emissions, 2nd edition, International Civil Aviation Organization.

Anon. (1993). ICAO Annex 16 Volume I : Aircraft Noise, 3rd Edition, International Civil Aviation Organization, 1993.

Anon. (1999). Night Noise Quotas at Heathrow, Gatwick and Stansted Airports, Department for Transport.

Anon. (2006). Basic Principles of the Continuous Descent Approach (CDA) for the Non-aviation Community, Environmental Research and Consultancy Department, Civil Aviation Authority.

ANOTEC Consulting S.L. (2007). http://www.anotecc.com/ (accessed on 15th March, 2007)

Antoine, N.E. and Kroo, I.M. (2002). Aircraft Optimization for Minimal Environmental Impact. In: *9th AIAA/ISSMO Symposium on Multidisciplinary Analysis and Optimization*, Atlanta, Georgia, September 4 - 6 2002, AIAA 2002-5667.

Antoine, N. E. (2004). Aircraft Optimization for Minimal Environmental Impact, PhD Thesis, Stanford University, USA.

Baudier, D. and Piquet, F. (2004). Snecma, a VITAL Player. Snecma Magazine, No. 7, November 2004.

Beltramo, M. N. Trapp, D. L. Kimoto, B. W. and Marsh, D. P. (1977). Parametric Study of Transport Aircraft Systems Cost and Weight, NASA CR-151970, NASA, Langley, VA.

Blank, L. and Tarquin, A. (1999). *Ingeniería económica*. 4th Edition, McGraw- Hill Interamericana, S.A., Bogotá, Colombia.

Boggia, S. and Rüd, K. (2004). Intercooled Recuperated Aero Engine. In: *Programme Deutscher Luft- und Raumfahrtkongress*, Dresden, Germany, September 20-23 2004, DGLR-Paper 2004-179.

Boggia, S. and Rüd, K. (2005). Intercooled Recuperated Gas Turbine Engine Concept. In: *41st AIAA/ASME/SAE/ASEE Joint Propulsion Conference and Exhibit*, Tucson, Arizona, July 10-13 2005, AIAA 2005-4192.

Bretschneider, S., Staudacher, S. and Arago, O. (2007). Architecture of a Techno-economic and Environmental Risk Assessment Tool using a Multi-modular Build Approach. In: *18th ISABE Conference,* September 2-7 2007, Beijing, China, ISABE, Blacksburg, VA, ISABE 2007-1103.

Brink, R. (2008). Feasibility Study of Novel Aero Engine Cycles for Short-Range Missions, MSc Thesis, Cranfield University, UK.

Byrne, D. M.; Taguchi, S. 1987: The Taguchi Approach to Parameter Design. In: *40th Annual Quality Congress Transactions*, Milwaukee, Wisconsin, American Society for Quality Control, 19-26.

Carlson, H.W. (1978). Simplified Sonic-Boom Prediction. NASA TP1122, March 1978

Chen, W., Allen, J. K., Tsui, K.-L. and Mistree, F. (1996). A Procedure for Robust Design: Minimizing Variations Caused by Noise Factors and Control Factors. In: *ASME Journal of Mechanical Design,* 118(4), 478-485.

Chen, X., Hasselman, T.K. and Neill, D.J. (1997). Reliability Based Structural Design Optimization for Practical Applications.In: *38th AIAA/ASME/ASCE/AHS/ASC, Structures, Structural Dynamics and Materials Conference*, Kissimmee, FL. Paper No. AIAA-97-1403.

Chien and Soroka (1982). Aircraft Noise Prediction Program Theoretical Manual: 3.2 Ground Reflection and Attenuation Module, NASA Tech Memo 83199, Feb. 1982.

Chiu, Y. (2004). A Performance Study of a Super-Cruise Engine with Isothermal Combustion inside the Turbine, PhD Thesis, Virginia Polytechnic Institute and State University, Blacksburg, USA.

Ciokajlo, J.J. (1992). Blade Tip Clearance Control Apparatus using Shroud Segment Annular Support Ring Thermal Expansion. U.S. Patent 5,116,199, 1992.

Clark, B. J. (1981). Computer Program to Predict Aircraft Noise Levels, NASA Technical Paper 1913, Sep. 1981.

Colmenares, R.F., Ogaji, S. and Pilidis, P. (2007a). An Overview on Innovative Aero Engines Concept, Colombian Scientific Journal INGENIUM No. 15.

Colmenares, R.F., Pascovici, D., Ogaji, S., and Pilidis, P. (2007b). A Preliminary Parametric Study for Geared, Intercooled and/or Recuperated Turbofan for Short Range Civil Aircrafts. In: *ASME Turbo Expo 2007 Power for Land, Sea and Air Conference*, Montreal, Canada, May 14-17 2007, GT2007-27234..

Colmenares, R.F, Gómez, J., Pascovici, D., and Ogaji, S (2007c). A Preliminary Feasibility Study for Future Aero Engines. In: *18th International Symposium on Air-Breathing Engines*, Beijing, China, September 3 - 7 2007, ISABE-2007-1194.

Colmenares, R.F, Kyprianidis**,** K., Ogaji, S., Pilidis, P., Latorre, S. (2008a). Future Aero-Engines' Optimization for Minimal Block Fuel Burn. In: *ASME Turbo Expo 2008 Power for Land, Sea and Air Conference*, Berlin, Germany, June 9-13 2008, GT2008-50216.

Colmenares, R.F, Pascovici, D., Ogaji, S., Pilidis, P., García, A., and Latorre, L. (2008b). Future Aero-Engines' Optimization for Minimal Operating Costs. In: *ASME Turbo Expo 2008 Power for Land, Sea and Air Conference*, Berlin, Germany, June 9-13 2008, GT2008-50217.

Colmenares, R.F, Ogaji, S., Pilidis, P., García, A. and Latorre, S. (2008c). Future Aero-Engines' Optimization for Minimal Global Warming Potential, Colombian Scientific Journal INGENIUM No.17.

Colmenares, R.F, Brink, R., Ogaji, S., Pilidis, P., Singh, R., Colmenares, J.C. and García, A. (2009a). Application of the Geared Turbofan with Constant Volume Combustor on Short-Range Aircraft: A Feasibility Study. In: *ASME Turbo Expo 2009 Power for Land, Sea and Air Conference*, Orlando, USA, June 8-12 2009, GT2009-59096.

Colmenares, R.F, Coutinho, A., Ogaji, S., Pilidis, P., Singh, R., Pincay, N. A. and Hernandez, J. C. (2009b). Feasibility Study of a Conventional Turbofan with a Constant Volume Combustor. In: *ASME Turbo Expo 2009 Power for Land, Sea and Air Conference*, Orlando, USA, June 8-12 2009, GT2009-59097.

Cornell, C. A. (1969). A Probability-based Structural Code. In: *Journal of American Concrete Institute,* 66(12), 974-985.

Coutinho, A. (2008). Performance and Emission Optimisation of Novel Aero-

Engine Concepts, MSc Thesis, Cranfield University, Cranfield.
da Cunha Alves, M. A., de Franca Mendes Carneiro, H. F., Barbosa, J. R., Travieso, L E, Pilidis, P. and Ramsden, K. W. (2001). An Insight on Intercooling and Reheat Gas Turbine Cycles.In: *Proceedings of Institute of Mechanical Engineers*, 215(A), 163-171.

Deb, K. (2001). Multi-objective Optimization Using Evolutionary Algorithms, Wiley, 2001, 28-41.

Depcik, C. (2008). Adiabatic Flame Temperature Program v1.2.1. http://www.depcik.com/eduprograms/aftp.htm (accessed on 1st August, 2008).

Dorsch, R. G., Clark, B. J. and Reshotko, M. (1975). Interim Prediction Method for Externally Blown Flap Noise, NASA TM X-71768, 1975.

Dovi, A. R. and Wrenn, G. A. (1990). Aircraft Design for Mission Performance Using Nonlinear Multi-objective Optimization Methods, NASA CR-4328, NASA, Langley, VA.

Eide, D.G. (1980). Cost Estimating Relationships for Airframes in the Development and Production Phases, NASA TM-80229, NASA, Langley, VA.

Engineous Software. http://www.engineous.com/ (accessed 13th September 2007).
Engineous Software (2004). i-SIGHT Version 9.0: User's Guide. Printed in USA, 2004.

Engineous Software (2004). i-SIGHT Version 9.0:Reference Guide. Printed in USA, 2004.

Feagin, R. C. and Morrison Jr., W. D. (1979). Delta Method, an Empirical Drag Buildup Technique, NASA CR-151971, NASA, Ames, CA.

Fiacco, A. and McCormick, G. P.: The Sequential Unconstrained Minimization Technique for Nonlinear Programming, a Primal-Dual Method. In: *Management Science*, Vol. 10, 1964.

Fink, M.R. (1977). Airframe Noise Prediction, FAA-RD-77–29, 1977.

FLight OPtimization System (FLOPS) Manual (1995), NASA Langley Research Centre.

Geiselhart, K. A., Caddy, M. J. and Morris, S. J., Jr. (1991). Computer Program for Estimating Performance of Airbreathing Aircraft Engines, NASA TM 4254.

Geiselhart, K. A. (1994). A Technique for Integrating Engine Cycle and Aircraft Configuration Optimization, NASA CR-191602, NASA, Langley, VA.

Gerend R P and Roundhill J P. (1970). Correlation of Gas Turbine Weights and Dimensions, AIAA Paper 70-669, June 1970.

Giesing, J. P. and Wakayama, S. (1997). A Simple Cost Related Objective Function for MDO of Transport Aircraft. In: *35th Aerospace Sciences Meeting & Exhibit,* January 6-10 1997, Reno, NV, AIAA, Reston, VA, AIAA 1997-0356.

Giunta, A. A., Balbanov, V., Kaufmann, M., Burgee, S., Grossman, B., Haftka, R. T., Mason,W. H. and Watson, L. T. (1995). Variable Complexity Response Surface design of an HSCT Configuration. In: *Multidisciplinary Design Optimization State of the Art-Proceedings of the ICASE/NASA Langley Workshop on Multidisciplinary Design Optimization,* Hampton, VA, 348-367.

Goodger, E.M. (1977). Combustion Calculations: Theory, Worked Examples and Problems, MacMillan Press, London.

Guénon, V. (2003). Framework Programme 6: Engine Research Orientations. In: *Engine Industry Management Group (EIMG) Presentation*, Moscow, Russia, October 20-21 2003.

Halila, E.E., Lenahan, D.T. and Thomas, T.T. (2002). Energy Efficient Engine, High Pressure Turbine Test Hardware Detailed Design Report, NASA CR-167955, 1982.

Han, S.P. (1976). Superlinearly Convergent Variable Metric Algorithms for General Nonlinear Programming Problems.In: *Mathematical Programming*, 11, 263-282.

Han, S.P. (1977). A Globally Convergent Method for Nonlinear Programming. In: *Journal of Optimization Theory and Applications*, 22, 297-305.

Hasofer, A.M. and Lind, N.C. 1974: Exact and Invariant Second Moment Code Format.In: *Journal of Engineering Mechanics*, 100, 111-121.

Hays, W. L. (1981). Statistics. CBS College Publishing, Japan.

Heidmann, M.F. (1979). Interim Prediction Method for Fan Compressor Source Noise, NASA TM X-71763, 1979.

Hertel, J. and Albers, M. (1993). The Impact of Engine and Aircraft Interrelations on DOC and its Application to Engine Design. In: *AIAA Aircraft Design, Systems and Operations Meeting,* August 11-13 1993, Monterey, CA, AIAA, Reston, VA, AIAA 1993-3930.

Huff, R.G. Clark, B.J. and Dorsch, R.G. (1974). Interim Prediction Method for Low Frequency Core Engine Noise, NASA TM X-71627, 1974

Hurtodao, J.E. and Barbat, A.H. (1997). Simulation Methods in Stochastic Mechanics.In: *Computational Stochastic Mechanics in a Meta-Computing Perspective*, J. Marczyk, Edition, Barcelona.

IATA (2008). http://www.iata.org/index.htm (accessed on 1st June, 2008). International Civil Aviation Organization (2007). Environmental Report.

ICAO(2008). Aircraft Engine Emissions.
http://www.caa.co.uk/default.aspx?catid=702 (accessed on 1st August, 2008).

IPCC (1999). Aviation and the Global Atmosphere. http://www.ipcc.ch/ipccreports/sres/aviation/index.htm (accessed on 1st August, 2008).

IPCC (2001). The Scientific Basis, Cambridge University Press, Cambridge, UK and New York, USA.

Jacob, H.G. (1982). Rechnergestützte Optimierung Statischer und Dynamischer Systeme, Fachberichte Messen - Steuern - Regeln, Springer Verlag 1982.

J&L Software (2006). Retirement and Financial Planning Software.
http://www.jlplanner.com/index.html (accessed 5th June, 2006).

Jenkinson, L. R. Simpkin, P. and Rhodes, D. (1999). Civil Jet Aircraft Design, Butterworth-Heinemann Ltd, Oxford.

Johnson, V. S. (1988). Life Cycle Cost in the Conceptual Design of Subsonic Commercial Aircraft, PhD Thesis, University of Kansas, Lawrence, USA.

Kazin, S.B. and Matta, R.K. (1976). Turbine Noise Generation, Reduction, and Prediction. In: *Aeroacoustics: Fan Noise and Control; Duct Acoustics; Rotor Noise,* Progress in Astronautics and Aeronautics, , I. R.Schwartz Edition, American Institute of Aeronautics and Astronautics, 44, 109–138.

Klug H. G., Bakan S. and Gayler V. (1996). CRYOPLANE - Quantitative Comparison of Contribution to Anthropogenic Greenhouse Effect of Liquid Hydrogen Aircraft versus Conventional Kerosene Aircraft, EGS XXI General Assembly, Den Haag, 6-10 May 1996.

Koch, P.N., Evans, J.P. and Powell, D. (2002). Interdigitation for Effective Design Space Exploration using i-SIGHT. In: *Journal of Structural and Multidisciplinary Optimization*, 23 (2).

Kodiyalam, S., Su Lin, J. and Wujek, B.A. (1998). Design of Experiments Based Response Surface Models for Design Optimization.In: *39th AIAA/ASME/ASCE/AHS/ASC Structures, Structural Dynamics and Materials Conference,* Long Beach, CA, 2718-2727.

Koehler, M. O. et al (2008). Impact of Perturbations to Nitrogen Oxide Emissions from Global Aviation.In: *Journal of Geographical Research*, 113, 1-15.

Kolthoff, P. (1962). Device for Controlling Clearance between Rotor and Shroud of a Turbine. U.S. Patent 3,039,737, 1962.

Krammer, P., Rued, K. and Truebenbach, J. (2003). Technology Preparation for Green Aero Engines. In: *AIAA/ICAS International Air and Space Symposium and Exposition: The Next 100 Y*, July 14-17 2003, Dayton, Ohio, AIAA 2003-2790.

Kreisselmeier,G., Steinhauser, G. (1975). Multilevel Approach to Optimum Structural Design. In: *Journal of the Structural Division*, ASCE,ST4, April, 1975, 957-974.

Krejsa, E. A. and Valerin, O.M. F. (1976). Interim Prediction Method for Turbine Noise, NASA TM X-73566, 1976.

Kyprianidis**,** K., Colmenares, F., Pascovici, D., Ogaji, S., Pilidis, P., and Kalfas, A.I. (2008). EVA – A Tool for Environmental Assessment of Novel Propulsion Cycles. In: *ASME Turbo Expo 2008 Power for Land, Sea and Air Conference*, Berlin, Germany, June 9-13 2008, GT2008-50602..

Kurzke, J. (2004). Gas Turb 10: User's Manual. Printed in Germany, 2004.

Laganelli, A.L., Rodgers, C., Lear, W.E. and Meitner, P.L. Semi-closed Gas Turbine Cycles: an Ecological Solution, to be published.

Lapin, L.L. (1990). Probability and Statistics for Modern Engineering, 2nd Edition, PWS-KENT Publishing Company, Boston, USA.

Laskaridis, P. (2004). Performance Investigations and Systems Architectures for the More-electric Aircraft, PhD Thesis, Cranfield University.

Lattime, S. and Steinetz, B. (2002). Turbine Engine Clearance Control Systems: Current Practices and Future Directions. In: *38th AIAA/ASME/SAE/ASEE Joint*

Propulsion Conference and Exhibit, Indianapolis, Indiana, July 7-10 2002, AIAA-2002-3790.

Lapin, L.L. (1990). Probability and Statistics for Modern Engineering. 2nd Edition, PWS-KENT Publishing Company, Boston, USA.

Lear, W.E. and Laganelli, A.L. (2001). High Pressure Regenerative Turbine Engine: 21st Century Propulsion. Final report for NASA contract NAS3-27396, March 2001, NASA / CRm2001-210675.

Le Dilosquer M. (1998). Influence of Subsonic Aero Engine Design and Flight Routes on Atmospheric Pollution, PhD Thesis, Cranfield University, UK.

Lefebvre, A. H. (1995). The Role of Fuel Preparation in Low-Emission Combustion. In: *Journal of Engineering for Gas Turbines and Power*, 117 (4), 617 – 654.

Lefebvre A.H. (1998). Gas Turbine Combustion, 2th Edition, Edwards Brothers, Ann Arbor, MI, Philadelphia, USA.

Lefebvre, A. H. (1999). Gas Turbine Combustion, 2th Edition, McGraw-Hill.

Liew, K.H., Urip, E., Yang, S.L. and Siow, Y.K. (2003). A Complete Parametric Cycle Analysis of a Turbofan with Interstage Turbine Burner. In: *41st AIAA Aerospace Sciences Meeting and Exhibit*, Reno, Nevada, January 6-9 2003, AIAA 2003-685.

Liew, K.H., Urip, E., Yang, S.L., Mattingly, J. and Marek, C. (2004). Performance Cycle Analysis of a Two-spool, Separate-exhaust Turbofan with Interstage Turbine Burner. In: *40th AIAA/ASME/SAE/ASEE Joint Propulsion Conference and Exhibit*, Fort Lauderdale, Florida, July 11-14 2004, AIAA-2004-3311.

Liu, F. and Sirignano, W.A. (1999). Performance Increases for Gas-turbine Engines through Combustion inside the Turbine. In: *Journal of Propulsion and Power*, 15(1), 111- 118.

Liu, F. and Sirignano, W.A. (2001). Turbojet and Turbofan Engine Performance Increases through Turbine Burners. In: *Journal of Propulsion and Power*, 17(3), 695- 705.

Lundbladh, A. and Sjunnesson, A. (2003). Heat Exchanger Weight and Efficiency Impact on Jet Engine Transport Applications. In: *16th International Symposium on Air-Breathing Engines*, Cleveland, Ohio, August 31 - September 5 2003, ISABE-2003-1122.

Madsen, H.O., Krenk, S. and Lind, N.C. (1986). Methods of Structural Safety. Englewood Cliffs, New Jersey, Prentice-Hall.

Marais, K., Lukachko, S.P., Mina, J., Mahashabde, A. and Waitz, I.A. (2008). Assessing the Impact of Aviation on Climate, Meteorologische Zeitschrift, 17 (2), 157-172.

McGregor, D.L. and Wat, J.K. (2004). Efficient Low-Noise Airplane Operations. In: *Jet Set Go — Environmental Aviation Takes Off*, Palm Springs, CA, February 29 - March 4, 2004.

Meitner, P.L., Laganelli, A. L., Senick, P.F. and Lear, W.E. (2000). Demonstration of a Semi-closed Cycle, Turboshaft Gas Turbine Engine. In: *ASME Turbo Expo 2000 Power for Land, Sea and Air Conference*, Munich, Germany, May 8-11 2000, 2000-GT-0535.

Melchers, R.E. (1987). Structural Reliability: Analysis and Prediction, Ellis Horwood Series in Civil Engineering, New York, John Wiley & Sons.

Montgomery, D.C. (1996). Design and Analysis of Experiments, New York, John Wiley & Sons.

Moss, J.B. (2007). Combustion Thermodynamics and Thermochemistry, Fuels and Combustion, Course Notes for MSc in Thermal Power, Cranfield University, UK.
Mühling O. and Vollmuth, M. (2002). High-pressure Compressor, Geared Fan and Recuperative Engine: MTU Features Technological Highlights. Press Release, Berlin, Germany, May 6 2002.

Muley, N. and Lear, W. (2003). Effect of Exhaust Gas Recirculation (EGR) on Thermal NO_x Formation Rate. In: *41st Aerospace Sciences Meeting and Exhibit*, Reno, Nevada, January 6-9 2003, AIAA-2003-503.

Münzberg, H. G. (1972). Flugantriebe Springer Verlag, 1972.

Myers, R.H. and Montgomery, D.C. (1995). Response Surface Methodology: Process and Product Optimization Using Designed Experiments, New York, John Wiley & Sons.

Nair, S., Muruganandam, T. M., Olsen, R., Meyers, A., Seitzman, J., Zinn, B., Lieuwen, T. (2004). Lean Blowout Detection in a Single Nozzle Swirl Cup Combustor. In: *42nd AIAA Aerospace Sciences Meeting and Exhibit*, Reno, Nevada, AIAA 2004-138.

Nelson, J. R. and Timson, F. S. (1974). Relating Technology to Acquisition Costs: Aircraft Turbine Engines. R-1288-PR. Rand Corporation, Santa Monica, CA.

NEWAC (2006): New Aero Engine Concepts. http://www.eurtd.com/newac/home.htm (accessed 20th June 2006).

Nichols, H. E. (1988). UDF Engine/MD-80 Flight Test Program. *24th AIAA/ASME/SAE/AASEE Joint Propulsion Conference,* 11-13 July 1988, Boston, MA, AIAA, Reston, VA, AIAA 1988-2805.

Noppel, F. and Singh, R. (2007) Overview on Contrail and Cirrus Cloud Avoidance Technology. In: *Journal of Aircraft*, Vol. 44, No. 5, September–October 2007.

Noppel, F. and Singh, R. (2008). Contrail Avoidance in the Aircraft Design Process. In: *The Aeronautical Journal*, December 2008, Volume 112, No 1138.

Noppel, F., Lucisano, D. and Singh, R. (2009). Performance of the Clean Exhaust Engine Concept. In: *Journal of Engineering for Gas Turbines and Power*, May 2009, Vol. 131

Onat, E. and Klees, G.W. (1979). A Method to Estimate Weight and Dimensions of Large and Small Gas Turbine Engines, NASA CR-159481.

Ostwald, F. O. and McLaren, T. S. (2004). Cost Analysis and Estimating for Engineering and Management, Pearson Education Ltd, London.

Pacull, M. (2002). Transport Aircraft Technologies. In: *International Symposium: Which Technologies for Future Aircraft Noise Reduction?* Arcachon, France, October, 2002.

Palmer, J.R. (1999). The TURBOMATCH Scheme for Gas-Turbine Performance Calculations: User's Guide, Cranfield University, Cranfield, UK.

Pascovici, D., Colmenares, F., Ogaji, S. and Pilidis, P. (2007a). An economic and risk analysis model for aircrafts and engines. In: *ASME Turbo Expo 2007 Power for Land, Sea and Air Conference*, Montreal, Canada, May 14-17 2007, GT2007-27236.

Pascovici, D., Colmenares, F., Ogaji, S., and Pilidis, P. (2007b). Analysis of Direct Operating Costs of Future Engines. In: *18th International Symposium on Air-Breathing Engines*, Beijing, China, September 3 - 7 2007, ISABE-2007-1106.

Pascovici, D., Colmenares, F., Kyprianidis, K., Ogaji, S., and Pilidis, P. (2008). Weibull Distributions Applied to Cost and Risk Analysis for Aero Engines. In: *ASME Turbo Expo 2008 Power for Land, Sea and Air Conference*, Berlin, Germany, June 9-13 2008, GT2008-51060.

Pasini, S., Ghezzi, U., Andriani, R. and Ferri, L. D. A. (2000). Heat Recovery from Aircraft Engines. In: *35th Intersociety Energy Conversion Engineering Conference and Exhibit (IECEC),* Las Vegas, NV, July 24-28 2000, AIAA-2000-2901.
Pera, R. J, Onat E., Klees G.W. and Tjonneland, E. (1977). A Method to Estimate Weight and Dimensions of Aircraft Gas Turbine Engines: Final Report, NASA Report CR135170, 1977.

Pilidis, P. and Palmer, J.R. (2005). Gas Turbine Performance Lecture Notes, Cranfield University, Cranfield, UK.

Ponater, M., Marquart, S. and Sausen, R. (2001). Contrails in a Comprehensive Global Climate Model: Parameterisation and Radiative Forcing Results, Report No.147, Institut für Physik der Atmosphäre, DLR, January, 2001.

Powell, M.J.D. (1978a). A Fast Algorithm for Nonlinearly Constrained Optimization Calculations. Numerical Analysis, G. A. Watson Edition, Lecture Notes in Mathematics, 630, Springer.

Powell, M.J.D. (1978b). The Convergence of Variable Metric Methods for Nonlinearly Constrained Optimization Calculations. Nonlinear Programming 3, O. L. Mangasarian, R. R. Meyer, S. M. Robinson Editions, Academic Press.

Powell, D.J. (1990). Inter-GEN: A Hybrid Approach to Engineering Design Automation, PhD Thesis, Rensselaer Polytechnic Institute, USA.

Rackwitz, R. and Fiessler, B. (1978). Structural Stability under Combined Random Load Sequences. Computers and Structures, 9, 489-494.

Raymer, D.P. (1999). Aircraft Design: A Conceptual Approach, 3rd Edition, AIAA, Reston, VA.

Rizk, N.K., and Mongia, H.C. (1992). Semianalytical Correlations for NO_x, CO and UHC Emissions. In: *International Gas Turbine and Aeroengine Congress and Exposition*, ASME 92-GT-130.

Roffe, G. and K.S. Venkataramani (1978). Emissions Measurements for a Lean Premixed Propane/Air System at Pressures up to 30 Atmospheres, NASA CR-159421.

Rogers H.L., Lee D.S., Raper D.W., Foster P.M. de F., Wilson C.W. and Newton P.J. (2002). The Impacts of Aviation on the Atmosphere. In: *The Aeronautical Journal*, 106 (1064), 521-546.

Rolls-Royce plc (1986). The Jet Engine, 5th edition, The Technical Publications Department, Derby, UK.

Rolls-Royce plc (2007). DREAM – valiDation of Radical Engine Architecture systeMs, Derby, UK.

Roskam, J. (1990). Airplane Design Part VIII: Airplane Cost Estimation: Design, Development, Manufacturing and Operating.

SAE (1975). Standard Values of Atmospheric Absorption as a Function of Temperature Humidity, ARP 866A, 1975.

SAE (1981). Prediction Method for Lateral Attenuation of Airplane Noise during Takeoff and Landing, AIR 1751, 1981.

SAE (1994). Gas Turbine Jet Exhaust Noise Prediction, Report ARP 876-D, 1994.

Shi, G. Y. (1992). Radiative Forcing and Greenhouse Effect due to the Atmospheric Trace Gases, Science in China, Series B, 35(2), 217-229.

Saliby, E. (1990). Descriptive Sampling: A Better Approach to Monte Carlo Simulation. In: *J. Opl. Res. Soc.*, 41(12), 1133-1142.

Sausen R. (2005). Global Atmospheric Effects of Aviation and Surface Transport, 3rd Japan-EU Workshop on Climate Change Research, January 2005.

Schönenborn, H., Ebert, E., Simon, B. and Storm, P. (2004). Thermomechanical Design of a Heat Exchanger for a Recuperative Aero Engine. In: *ASME Turbo Expo 2004 Power for Land, Sea and Air Conference*, Vienna, Austria, June 14-17 2004, GT2004-53696.

Schulte, P., Schlager, H., Ziereis, H., Schumann, U., Baughcum, S. L. and Deidewig, F. (1997). NO_x Emission Indices of Subsonic Long-range Jet Aircraft at Cruise Altitude: In Situ Measurements and Predictions, J. Geophys. Res., 102(D17), 21431-21442.

Schumann, U. (2000). Influence of Propulsion Efficiency on Contrail Formation, Aerosp. Sci. Technol., 4(6), 391-401.

Simpson, T. W., Peplinski, J., Koch, P. N. and Allen, J. K. (1997). On the Use of Statistics in Design and the Implications for Deterministic Computer Experiments.

Design Theory and Methodology – DTM'97, Sacramento, CA. ASME Paper No. DETC97/DTM-3881.

Singh, R. (2007). An Overview: Gas Turbine Generated Pollutants and the Emerging Technology Solutions. Gas Turbine Combustors, Lecture Notes for MSc Thermal Power, Cranfield University, UK.

Sixth Framework Programme. (2005). FP6-2003-AERO-1, *Annex I: Description of Work*, December 5-12 2005.

Smith, M.J.T. (1989). Aircraft Noise, Cambridge University Press.

Smith, C.F., Snyder, P.H., Emmerson, C.W. and Nalim, M.R. (2002). Impact of the Constant Volume Combustor on a Supersonic Turbofan Engine. In: *38th AIAA/ASME/SAE/ASEE Joint Propulsion Conference & Exhibit,* July 7-10 2002, Indianapolis, Indiana, AIAA, Reston, VA, AIAA 2002-3916.

Sobieski-Sobieszczanski, J., Dovi, A.R. and Wrenn,G. A. (1988). A New Algorithm for General Multiobjective Optimization, NASA TM- 100536, March 1988.

Sobieszczanski-Sobieski, J. and Haftka, R.T. (1996). Multidisciplinary Aerospace Design Optimization: Survey of Recent Developments, AIAA Paper 96-0711, Jan. 1996.

Sommer, S. C. and Short, B. J. (1955). Free-Flight Measurements of Turbulent-Boundary-Layer Skin Friction in the Presence of Severe Aerodynamic Heating at Mach Numbers 2.8 to 7.0, NACA TN-3391, 1955.

Spakovszky, Z.S., Greitzer, E.M., Waitz, I.A. and Quattrochi, D. (2006). Thermodynamics and Propulsion: Generating Heat (Thermochemistry), MIT web course notes for Propulsion, Massachusetts Institute of Technology. http://web.mit.edu/16.unified/www/SPRING/propulsion/notes/notes.html (accessed on 1st August, 2008).

Steinetz, B., Lattime, S., Taylor, S., DeCastro J., Oswald, J. and Melcher, K. (2005). Preliminary Evaluation of an Active Clearance Control System Concept. In: *41st AIAA/ASME/SAE/ASEE Joint Propulsion Conference and Exhibit*, Tucson, Arizona, July 10-13 2005, AIAA-2005-3989.

Stoessel, R. F. (1970). A Proposed Standard Method for Estimating Airline Indirect Operating Expenses. LW70-500R. Lockheed-Georgia Company, Marietta, GA.

Stone, J.R. (1974). Interim Prediction Method for Jet Noise, NASA TM X-71618, 1974.

Strategic Research Agenda – ACARE (2005), Volume 2.
http://www.acare4europe.org/ (accessed 15th October, 2005).

Svensson F. (2004). Potential of Reducing the Environmental Impact of Civil Subsonic Aviation by Using Liquid Hydrogen, Ph.D. Thesis, Cranfield University, UK.

Svoboda, C. (2000). Turbofan Engine Database as a Preliminary Design Tool, Aircraft Design, Vol.3, pp 17-31, 2000.

Sweeney, F.D. (2003). New Sampling Distributions for Evolution Algorithms, Ph.D. Thesis, Stanford University, USA.

Taguchi, G. and Konishi, S. (1987). Orthogonal Arrays and Linear Graphs. American Supplier Institute, Dearborn, USA.

Tintani, P. (2008). Aero Engines Atmospheric Impact and Evaluation, MSc Thesis, Cranfield University, UK.

Trouvé, A., Im, H. G., Rutland, C. J., Chen, J. H., Reddy, R. and Sanielevici, S. (2003). Terascale High-fidelity Simulations of Turbulent Combustion with Detailed Chemistry,http://www.scidac.gov/BES/BES_TSTC/reports/TSTCYear2_Report1.pdf (accessed on 1st August, 2008)

Tseng, W. and Hauser, A.A. (1991). Blade Tip Clearance Control Apparatus with Shroud Segment Position Adjustment by Unison Ring Movement. U.S. Patent 5,035,573, 1991.

University of Cambridge.http://www.eng.cam.ac.uk/news/stories/2007/Whittle/ (accessed 9th May 2007).

US Department of Labor (2008). Bureau of Labor Statistics. http://www.bls.gov (accessed 5 May 2008).

van Bodegraven, G. (1990). Commercial Aircraft DOC. In: *AIAA/AHS/ASEE Aircraft Design, Systems and Operations Conference,* September 17-19 1990, Dayton, OH, AIAA, Reston, VA, AIAA 1990-3224.

Walsh, P.P. and Fletcher, P. (2004). Gas Turbine Performance**,** 2nd edition**,** Blackwell Science, Oxford, UK.

Whellens, W. M. (2002). Multidiscplinary Optimisation of Aero Engines Using Genetic Algorithms and Preliminary Design Tools, Ph.D. Thesis, Cranfield University, UK.

Wikipedia. http://en.wikipedia.org/wiki/Contrail and http://en.wikipedia.org/wiki/Cirrus_cloud (accessed 15th January 2007).

Wilfert, G. and Masse, B. (2001). Technology Integration in a Low Emission Heat Exchanger Engine. In: *8th CEAS European Propulsion Forum, Affordability and the Environment, Key Challenges for Propulsion in the 21st Century*, Nottingham, UK, March 26-28 2001.

Wilfert, G., Kriegl, B., Wald, L and Johanssen, O. (2005). CLEAN - Validation of a GTF High Speed Turbine and Integration of Heat Exchanger Technology in an Environmental Friendly Engine Concept. In: *17th International Symposium on Air-Breathing Engines*, Munich, Germany, September 4-9 2005, ISABE – 2005 – 1156.

Wilfert, G., Kriegl, B., Scheugenpflug, H., Bernard, J., Ruiz, X. and Eury, S. (2005). CLEAN - Validation of a High Efficient Low NO_x Core, a GTF High Speed Turbine and an Integration of a Recuperator in an Environmental Friendly Engine Concept. In: *41st AIAA/ASME/SAE/ASEE Joint Propulsion Conference and Exhibit*, Tucson, Arizona, July 10 – 13 2005, AIAA 2005-4195.

Won, H.T. and Waters, M. (2003). Constant Volume Combustor Implementation on a 50 Passenger Commercial Regional Transport Mission Simulation. In: *39th AIAA/ASME/SAE/ASEE Joint Propulsion Conference and Exhibit,* 20-23 July 2003, Huntsville, Alabama, AIAA, Reston, VA, AIAA 2003-4413.

Wrenn, G. A. (1989). An Indirect Method for Numerical Optimization Using the Kreisselmeier-Steinhauser Function, NASA CR 4220, March 1989.

Ziha, K. (1995). Descriptive sampling in structural safety. Structural Safety, 17, 33-41.

BIBLIOGRAPHY

Andriani, R., Ferri, L. and Ghezzi, U. (2000). Thermodynamic Study of an Adiabatic Piston Engine with Heat Recovery for Aeronautical Application. In: *36th AIAA/ASME/SAE Joint Propulsion Conference and Exhibit*, Huntsville, Alabama, July 16-19 2000, Paper 00-3482.

Antas, S. and Wolanski, P. (1989). Obliczenia Termogazodynamiczne Lotniczych Silników Turbinowych. WPW, Warsaw, Poland.

Aircraft Noise Rating Index (2005). Airports Council International, Geneva. Long Range Aircraft AEA Requirements (1989). Association of European Airlines, Brussels.

Aircraft Owners & Operators Guide (2006). A320 Family. Aircraft Commerce, March 2006, 44, 5-33.

Baca, G. (2002). Ingeniería Económica. Fondo Educativo Panamericano, Bogotá, Colombia.

Baker, N. J. and Bewick, C. L. (2001). Noise test of a Negatively Scarfed Inlet Flare. In: *AIAA/CEAS Aeroacoustics Conference and Exhibit*, Maastricht, Netherlands, May 28-30 2001, AIAA-2001-2139.

Blythe, A. (1988). Potential Application of Advanced Propulsion Systems to Civil Aircraft. In: *Journal of Aircraft*, 25(2), 141-146.

Bussing, T.R.A. (1995). A Rotary Valve Multiple Pulse Detonation Engine, AIAA-95-2577.

Chivers, I. and Sleightholme, J. (2000). Introducing Fortran 95, Springer, London, UK.

Cohen, J. Cohen, P. West, S. G. and Aiken, L. S. (2003). Applied Multiple Regression/Correlation Analysis for the Behavioural Sciences, 3rd Edition, Lawrence Erlbaum Associates, Mahwah, New Jersey.

De Laurentis, D.A. and Mavris, D.N. (2000). Uncertainty Modeling and Management in Multidisciplinary Analysis and Synthesis. In: *38th Aerospace Sciences Meeting & Exhibit,* 10 - 13 January 2000, Reno, NV, AIAA, Reston, VA, AIAA 2000-0422.

Eyers, C. J., Norman, P., Middel, J., Plohr, M, Michot, S, Atkinson, K and Christou, R.A. (2004). AERO2k Global Aviation Emissions Inventories for 2002 and 2025. A report by QinetiQ prepared for European Commission.

Gunston, B. (2007). Janes Aero Engines, 21th Edition, Jane's Information Group, Coulsdon.

Gülder, Ö. L. (1986). Flame Temperature Estimation of Conventional and Future Jet Fuels. In: *ASME Journal of Engineering for Gas Turbines and Power*, 108, 376-380.

Harvey, D. et al. (1997). An Introduction to Simple Climate Models Used in the IPCC Second Assessment Report. IPCC, Geneva.

Heiser, W. H. and Pratt, D. T. (2002). Thermodynamic Cycle Analysis of Pulse Detonation Engines. In: *Journal of Power and Propulsion,* 18 (1), 68-76.

Howse, M. (2004). Aero Gas Turbines: An Ever-changing Engineering Challenge, Rolls-Royce PLC, Sir Frank Whittle Lecture to the Royal Aeronautical Society on 3rd February, 2004.

http://www.rolls-royce.com/history/overview/whittle.pdf (accessed on 1st August, 2008)

Jane, F.T. (2007). Jane's All the World's Aircraft , Edition: 2006-2007), Jane's Information Group, Coulsdon.

Johnson, V. S. (1990). Minimizing Life Cycle Cost for Subsonic Commercial Aircraft. In: *Journal of Aircraft,* 27 (2), 139-145.

Kailasanath, K. (2000). Review of Propulsion Applications of Detonation Waves. In: *AIAA Journal,* 38 (9), 1698-1708.

Kirby, M. R. and Mavris, D. N. (2002). An Approach for the Intelligent Assessment of Future Technology Portfolios. In: *40th AIAA Aerospace Sciences Meeting & Exhibit,* 14-17 January 2002, Reno, NV, American AIAA, Reston, VA, AIAA 2002-0514.

Kirby, M. R. and Mavris, D. N. (2001). A Technique for Selecting Emerging Technologies for a Fleet of Commercial Aircraft to Maximize R&D Investment. *SAE World Congress,* March 5-8 2001, Detroit, MI, SAE, Warrendale, PA, SAE 2001-01-3018.

Klaus, S. (2001). Advanced Compressor Technology: Key Success Factor for Competitiveness in Modern Aero-engines. In: *15th International Symposium on Air-Breathing Engines*, Bangalore, India, September 3-7 2001, ISABE-2001-1009.

Korsi, J. J. (2007). VITAL – European R&D Programme for Greener Aero Engines. In: *18th ISABE Conference,* September 2-7 2007, Beijing, China,ISABE, Blacksburg, VA, ISABE 2007-1118.

Lemon, D. R. and Schafer, J.L. (2005). Developing Statistical Software in Fortran 95, Springer, New York, NY, USA.

Li, H. Akbari, P. and Nalim, M. R. (2007). Air-Standard Thermodynamic Analysis of Gas Turbine Engines Using Wave Rotor Combustion. In: *43rd AIAA/ASME/SAE/ASEE Joint Propulsion Conference & Exhibit,* July 8-11 2007, Cincinnati, OH, AIAA, Reston, VA, AIAA 2007-5050.

Lu, F.K. and Wilson, D.R. (2004). Some Perspectives on Pulse Detonation Propulsion Systems. In: *24th International Symposium on Shock Waves*, Beijing, China, Paper No. 1051.

Lucisano, D. (2007). Analysis and Optimization of a Novel Aero Engine Concept, MSc Thesis, Cranfield University, UK.

Lord, W.K., Mac Martin, D. G. and Tillman, G. (2000). Flow Control Opportunities in Gas Turbine Engines. In: *Fluids 2000 Conference and Exhibit, Denver*, CO, June 19-22 2000, AIAA-2000-2234.

Mattingly, J.D. (1996). Elements of Gas Turbine Propulsion, McGraw-Hill, Inc, Singapore.

Nalim, M. R. (1998). Thermodynamic Limits of Pressure Gain and Work Production in Combustion and Evaporation Processes. In: *34th AIAA/ASME/SAE/ASEE Joint Propulsion Conference & Exhibit,* 13-15 July 1998, Cleveland, OH, AIAA, Reston, VA, AIAA 1998-3398.

Nalim, M. R. and Resler, E. L. (1996). Wave Cycle Design for Wave Rotor Gas Turbine Engines with Low NO_x Emissions. Transactions of the ASME, 118, 474-480.

Nalim, M. R. and Pekkan, K. (2003). Internal Combustion Wave Rotors for Gas Turbine Engine Enhancement. In: *Proceedings of the International Gas Turbine Congress 2003*, Tokyo, IGTC2003 Tokyo FR-303.

Nichols, H. E. (1988). UDF Engine/MD-80 Flight Test Program. In: *24th AIAA/ASME/SAE/AASEE Joint Propulsion Conference,* 11-13 July 1988, Boston, MA, AIAA, Reston, VA, AIAA 1988-2805.

Owner's & Operator's Guide: CFM56-5A/-5B. Aircraft Commerce, February/March 2007, no. 50, p. 5-28.

Pachidis, V.A. (2005). Gas Turbine Performance Simulation Lecture Notes, Cranfield University, Cranfield, UK.

Patnaik, S. N., Lavelle, T. M. and Hopkins, D. A. (1997). Optimization of Air-Breathing Propulsion Engine Concept. In: *Communications in Numerical Methods in Engineering*, 13, 635-641.

Paxson, D.E. and Perkins, H.D. (2004). Thermal Load Considerations for Detonative Combustion-Based Gas Turbine Engines, NASA TM-2004-213190, NASA, Cleveland, OH.

Pekkan, K. and Nalim, M. R. (2002). Control of Fuel and Hot-Gas Leakage in a Stratified Internal Combustion Wave Rotor. In: *38th AIAA/ASME/SAE/ASEE Joint Propulsion Conference & Exhibit,* 7-10 July 2002, Indianapolis, Indiana, AIAA, Reston, VA, AIAA 2002-4067.

Pekkan, P. and Nalim, M. R. (2003). Two-Dimensional Flow and NO_x Emissions in Deflagrative Internal Combustion Wave Rotor Configurations. Transactions of the ASME, 125, 720-733.

Pilidis, P., Moss, J.B. and Eshelby, M (2006). Propulsion System Performance and Integration Lecture Notes: Volume 2, Cranfield University, Cranfield, UK.

Rasheed, A. Tangirala, V. E. Vandervort, C. L. Dean, A. J. and Haubert, C. (2004). Interactions of a Pulse Detonation Engine with a 2D Turbine Blade Cascade. In: *42nd Aerospace Sciences Meeting and Exhibit,* January 5-9 2004, Reno, Nevada, AIAA, Reston, VA, AIAA 2004-1207.

Reid, C. (1988). Overview of Flight Testing of GE Aircraft Engines UDF Engine. In: *24th AIAA/ASME/SAE/ASEE Joint Propulsion Conference,* 11-13 July 1988, Boston, MA, AIAA, Reston, VA, AIAA 1988-3082.

Rizk, N.K. and Mongia, H.C. (1994). Emissions Predictions of Different Gas Turbine Combustors, AIAA-1994-0118 (REPORT-C).

Rued K and Lichtfuss, H.J. (1996). Trends in Aero-engines Development. In: *Proceedings of the DLR Workshop on Aspects of Airframe Engine Integration of Transport Aircraft*, Braunschweig, Germany, March 6-7 1996, 4-1 to 4-23.

Sallee, G. P. (1978). Economic Effects of Propulsion System Technology, NASA CR-134645, NASA, Langley, VA.

Saravanamutto, H.I.H., Rogers, G.F.C. and Cohen H. (2001). Gas Turbine Theory, 5th Edition, Pearson Education, Essex, UK.

Sharma, P. B. Pundhir, D. S. and Chaudhry, K. K. (1987). A Study of Some Factors Affecting the Aeroacoustic Performance of a Ducted Contra-Rotating Axial Flow Fan Stage. In: *11th AIAA Aeroacoustics Conference,* 19-21 October 1987, Palo Alto, California, AIAA, Reston, VA, AIAA 1987-2730.

Sirignano, W.A. and Liu, F. (1999). Performance Increases for Gas-Turbine Engines through Combustion inside the Turbine. In: *Journal of Propulsion and Power,* 15(1), 111-118.

Sirignano, W. A. and Liu, F. (2001). Turbojet and Turbofan Engine Performance Increases through Turbine Burners. In: *Journal of Power and Propulsion,* 17 (3), 695-705.

Snyder, P. H. Alparslan, B. and Nalim, M. R. (2002). Gas Dynamic Analysis of the CVC, a Novel Detonation Cycle. In: *38th AIAA/ASME/SAE/ASEE Joint Propulsion Conference & Exhibit,* July 7-10 2002, Indianapolis, Indiana, AIAA, Reston, VA, AIAA 2002-4069.

Standard Method of Estimating Comparative Direct Operating Costs of Turbine Powered Transport Airplanes (1967). ATA, Washington, 1967.

Walther, R., Frischbier, J. and Selmeier, R. (2001). Aeromechanical Design of Advanced Engine Compressors. In: *15th International Symposium on Air-Breathing Engines*, Bangalore, India, September 3-7 2001, ISABE-2001-1141.

Wilfert, G. Sieber, J. Rolt, W. Baker, N. Touyeras, A. and Colantuoni, S. (2007). New Environmental Friendly Aero Engine Core Concepts. In: *18th ISABE Conference,* September 2-7 2007, Beijing, ISABE, Blackburg, VA, ISABE 2007-1120.

Williams, D. (2006). Propulsion System Performance and Integration Lecture Notes : Volume 3, Cranfield University, Cranfield, UK.

Wilson, J., and Paxson, D.E. (1993). Jet Engine Performance Enhancement Through the use of a Wave-Rotor Topping Cycle, NASA TM 4486.

Wu, Y., Ma, F. and Yang, V. (2003). System Performance and Thermodynamic Cycle Analysis of Airbreathing Pulse Detonation Engines, *Journal of Propulsion and Power*, 19 (4), 556-567.

Zimbrick, R. A. and Colehour, J. L. (1988). An Investigation of Very High Bypass Ratio Engines for Subsonic Transports.In: *Propulsion Specialist Conference,* 1988, Boston, AIAA, Reston, VA, AIAA 1988-2953.

APPENDICES

APPENDIX A: TERA VALIDATION RESULTS

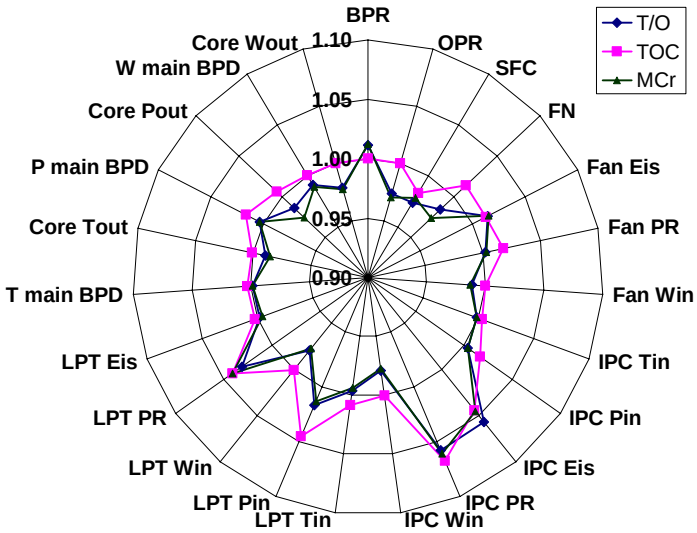

Figure A.1: Performance validation results for baseline turbofan

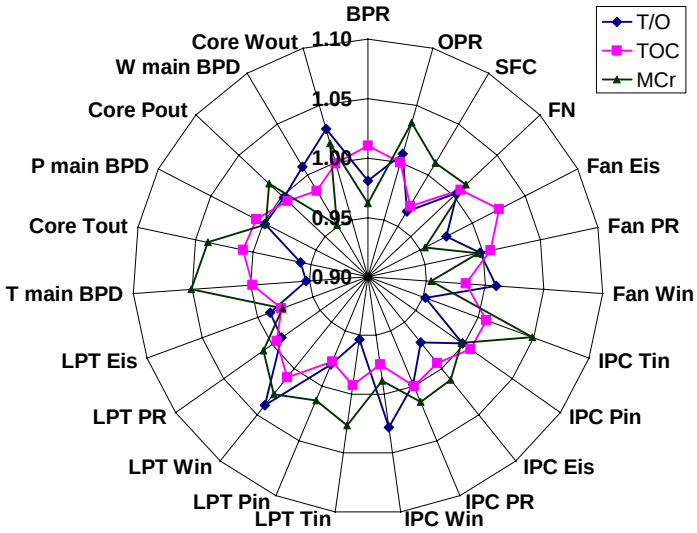

Figure A.2: Performance validation results for advanced turbofan

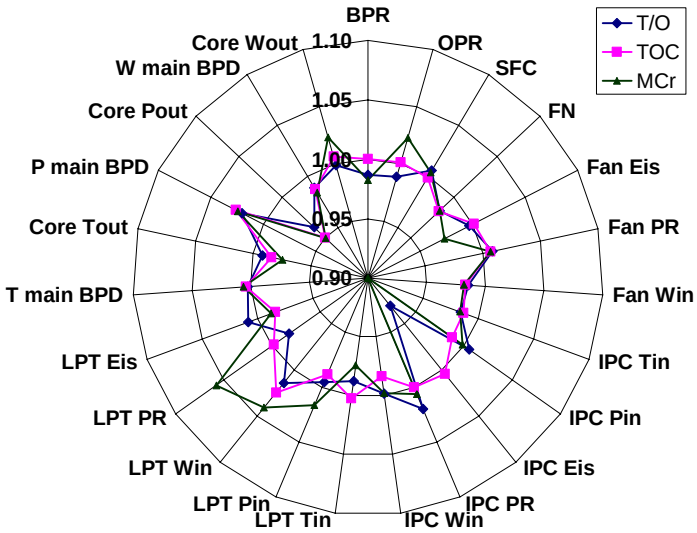

Figure A.3: Performance validation results for contra-rotating turbofan

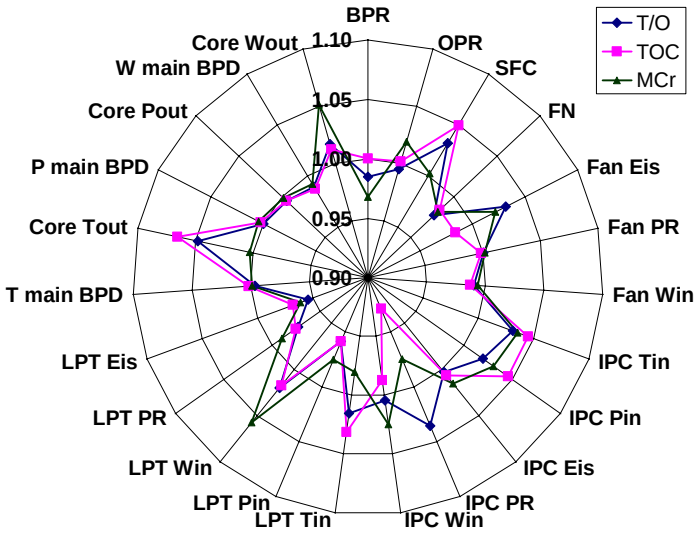

Figure A.4: Performance validation results for geared turbofan

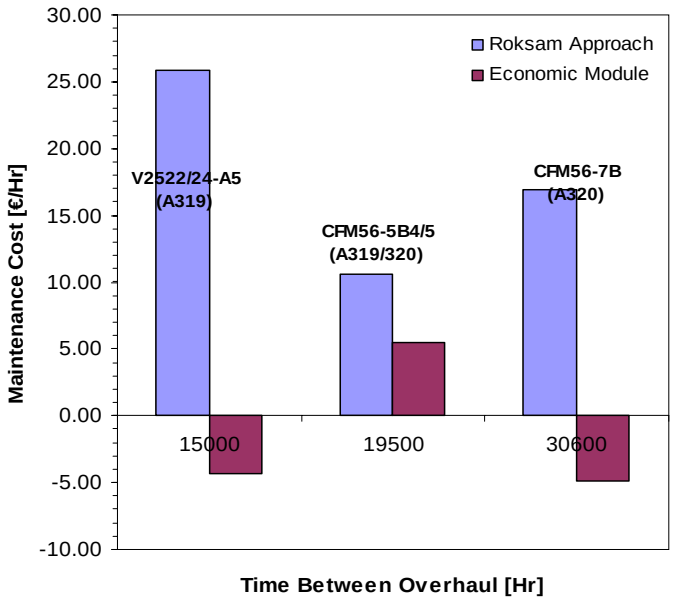

Figure A.5: Economics validation results for baseline turbofan

APPENDIX B: TERA PARAMETRIC STUDY RESULTS

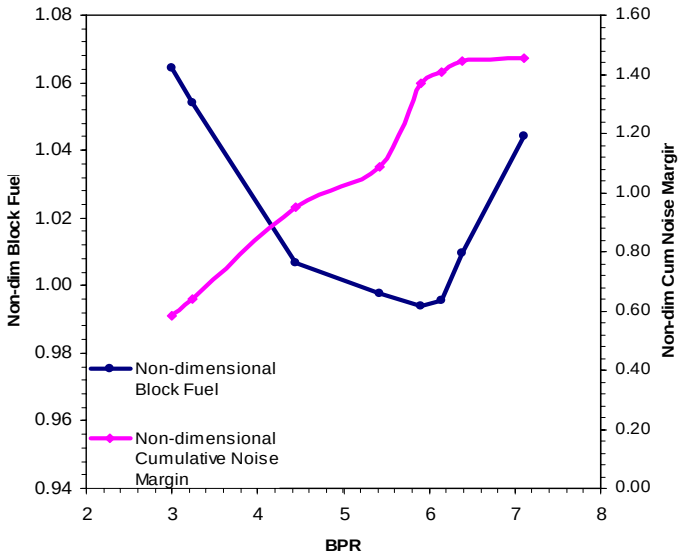

Figure B.1: Parametric study of non-dimensional block fuel and non-dimensional cumulative noise vs. BPR: Baseline turbofan

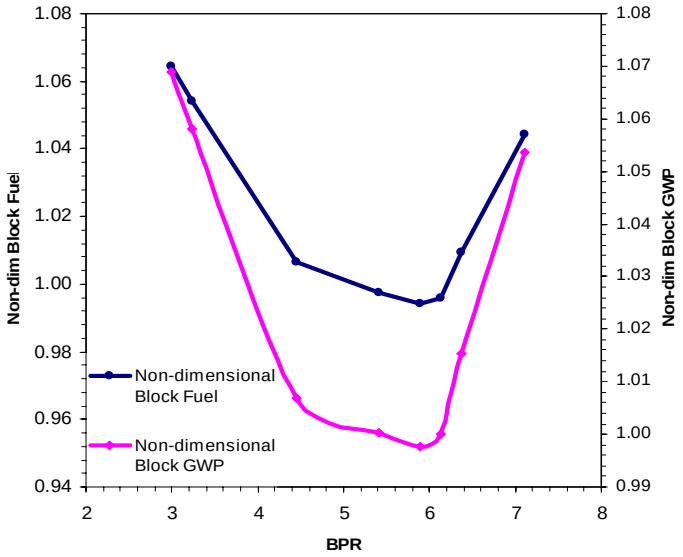

Figure B.2: Parametric study of non-dimensional block fuel and non-dimensional block GWP vs. BPR: Baseline turbofan

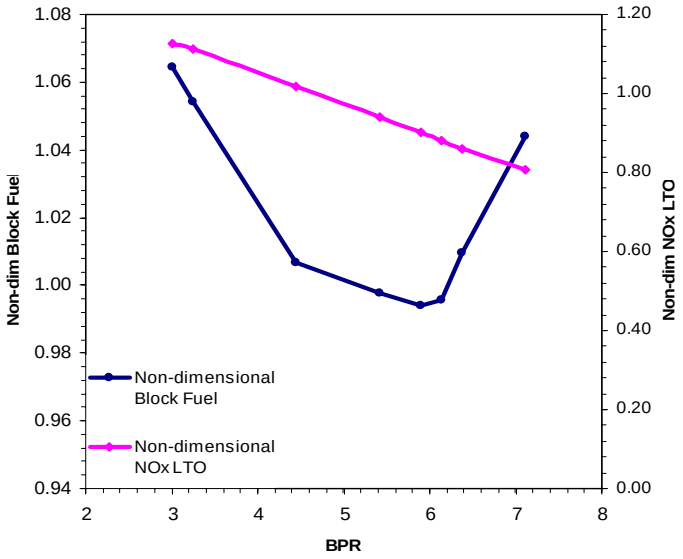

Figure B.3: Parametric study of non-dimensional block fuel and non-dimensional LTO NO_x vs. BPR: Baseline turbofan

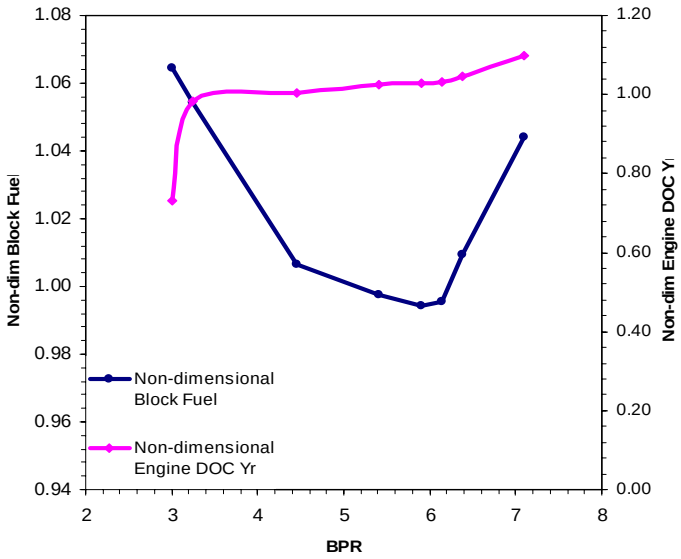

Figure B.4: Parametric study of non-dimensional block fuel and non-dimensional engine DOC yearly vs. BPR: Baseline turbofan

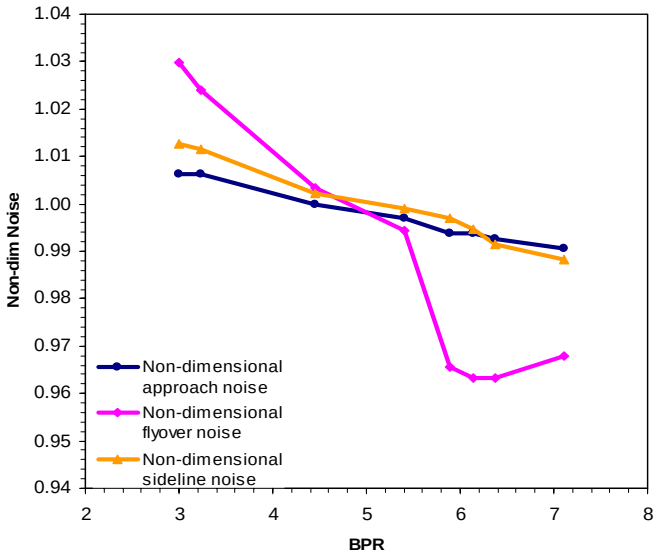

Figure B.5: Parametric study of non-dimensional noise at certification points vs. BPR: Baseline turbofan

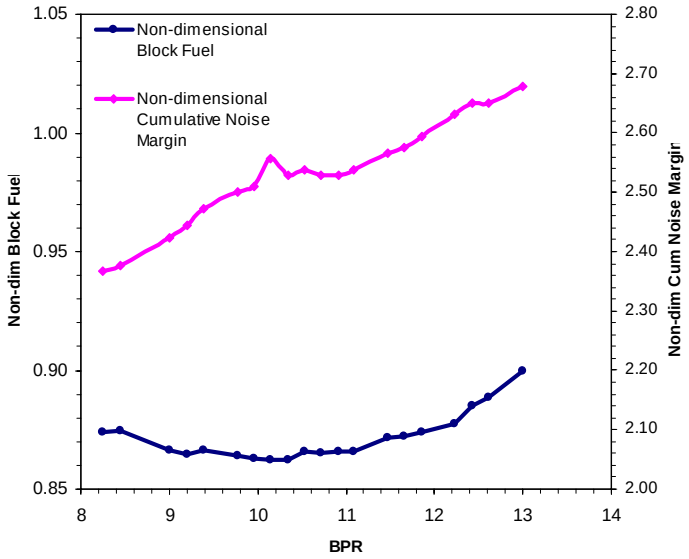

Figure B.6: Parametric study of non-dimensional block fuel and non-dimensional cumulative noise vs. BPR : Advanced turbofan

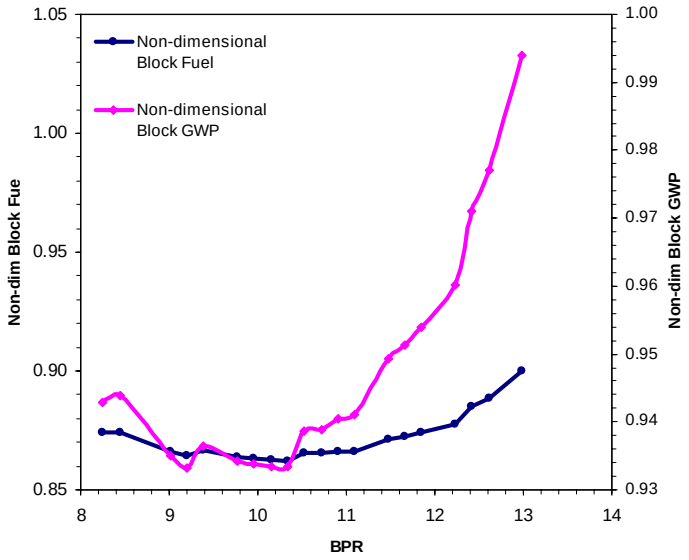

Figure B.7: Parametric study of non-dimensional block fuel and non-dimensional block GWP vs. BPR: Advanced turbofan

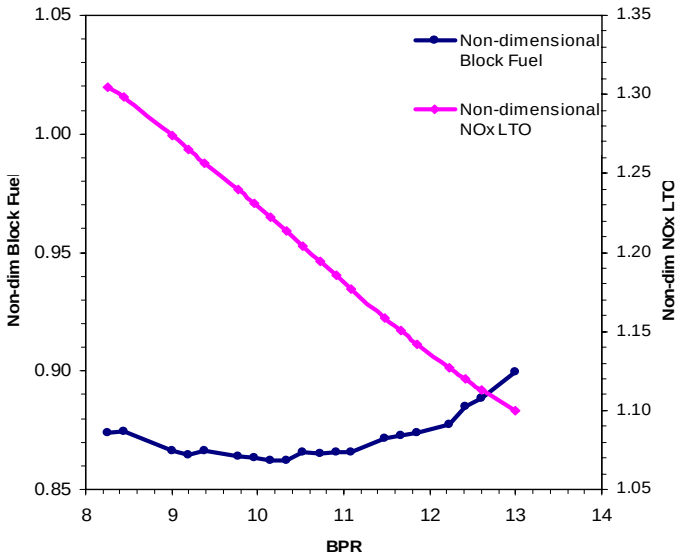

Figure B.8: Parametric study of non-dimensional block fuel and non-dimensional LTO NO_x vs. BPR: Advanced turbofan

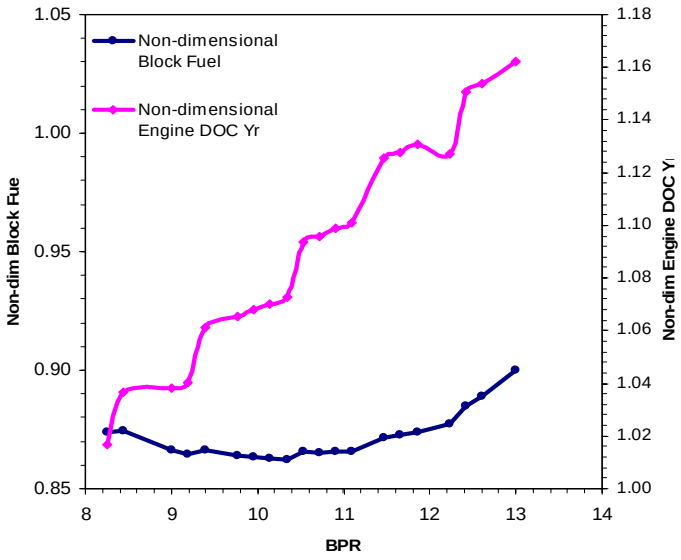

Figure B.9: Parametric study of non-dimensional block fuel and non-dimensional engine DOC yearly vs. BPR: Advanced turbofan

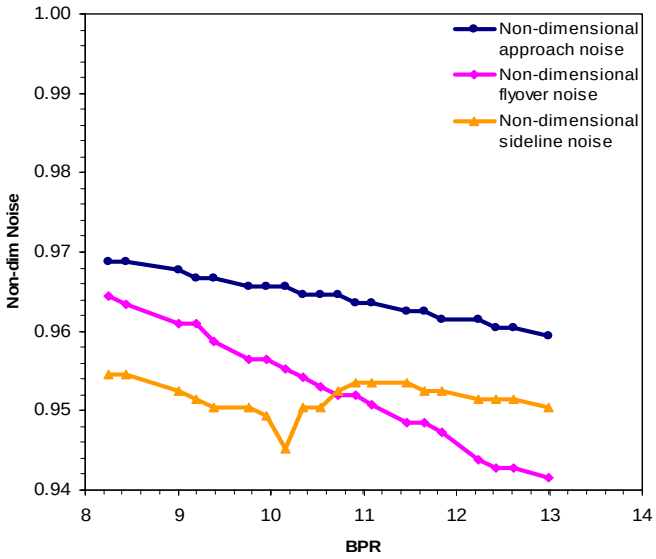

Figure B.10: Parametric study of non-dimensional noise at certification points vs. BPR: Advanced turbofan

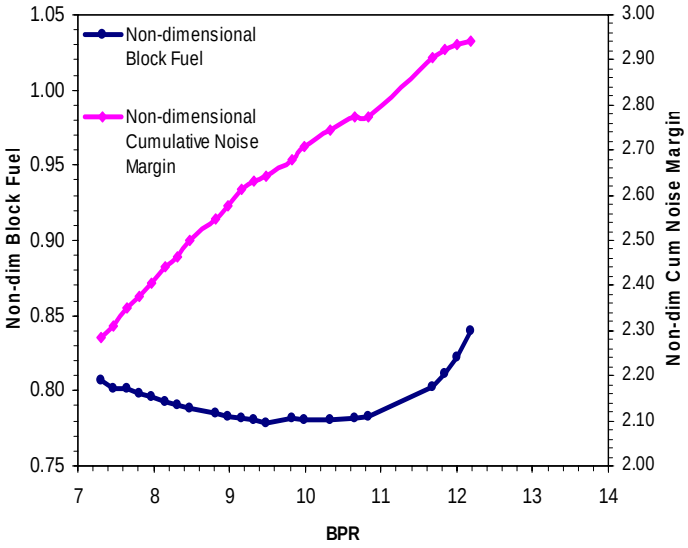

Figure B.11: Parametric study of non-dimensional block fuel and non-dimensional cumulative noise vs. BPR : Contra-rotating turbofan

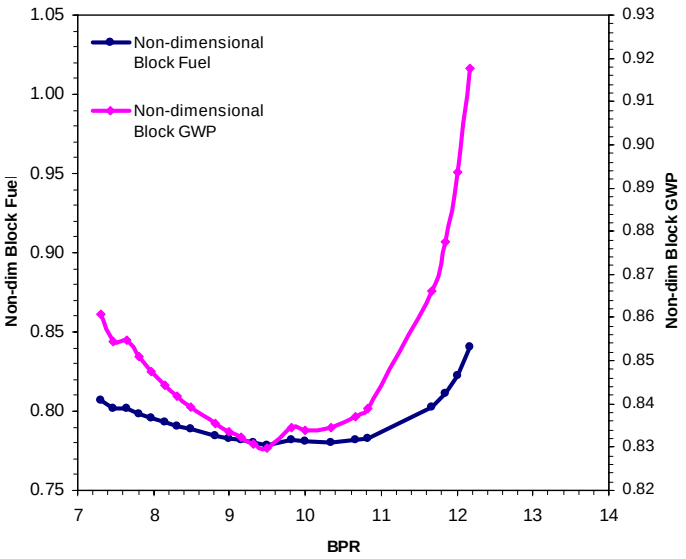

Figure B.12: Parametric study of non-dimensional block fuel and non-dimensional block GWP vs. BPR: Contra-rotating turbofan

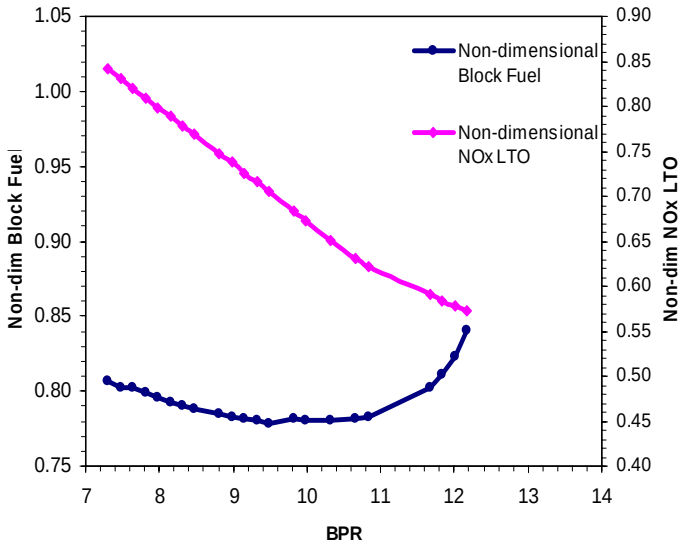

Figure B.13: Parametric study of non-dimensional block fuel and non-dimensional LTO NO_x vs. BPR: Contra-rotating turbofan

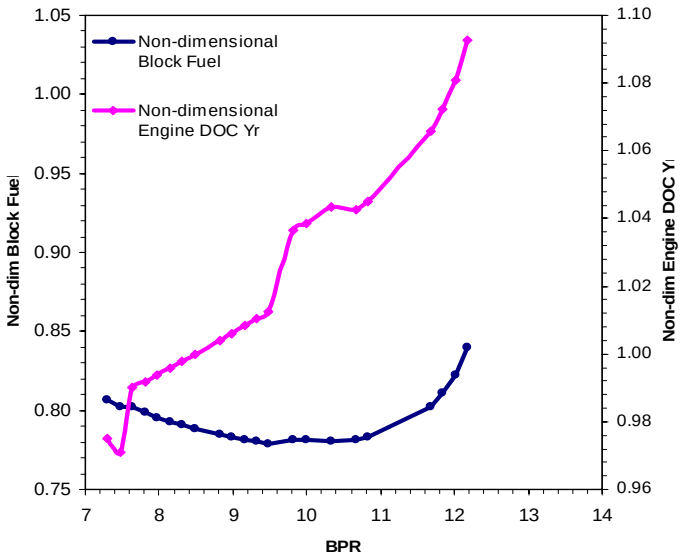

Figure B.14: Parametric study of non-dimensional block fuel and non-dimensional engine DOC yearly vs. BPR: Contra-rotating turbofan

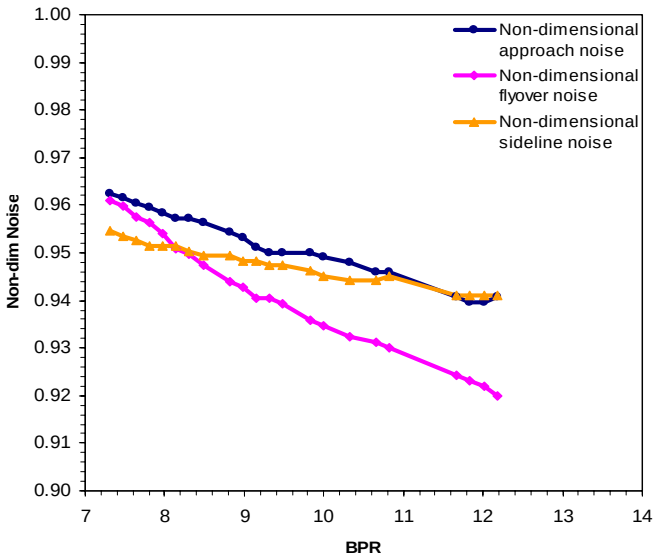

Figure B.15: Parametric study of non-dimensional noise at certification points vs. BPR: Contra-rotating turbofan

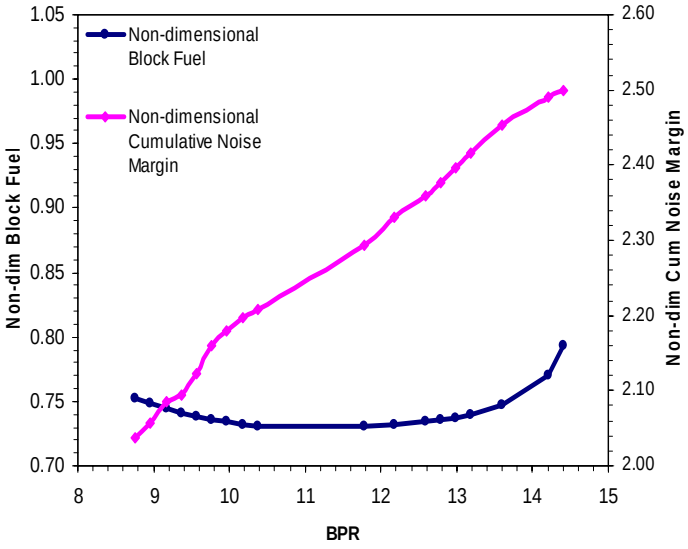

Figure B.16: Parametric study of non-dimensional block fuel and non-dimensional cumulative noise vs. BPR : Geared turbofan

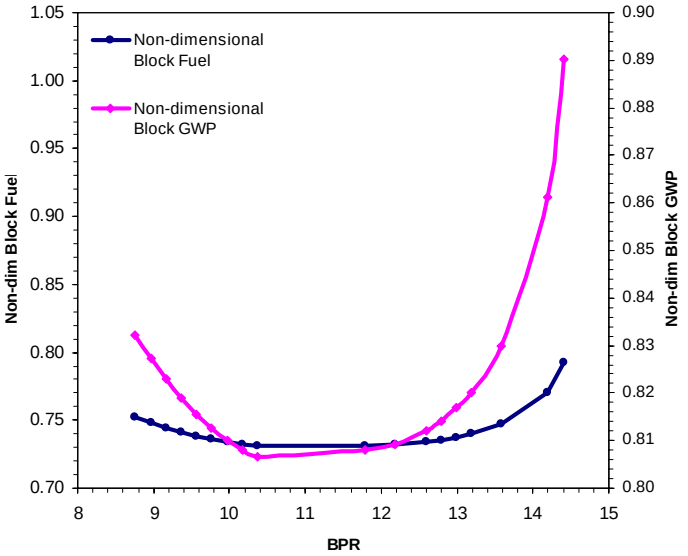

Figure B.17: Parametric study of non-dimensional block fuel and non-dimensional block GWP vs. BPR: Geared turbofan

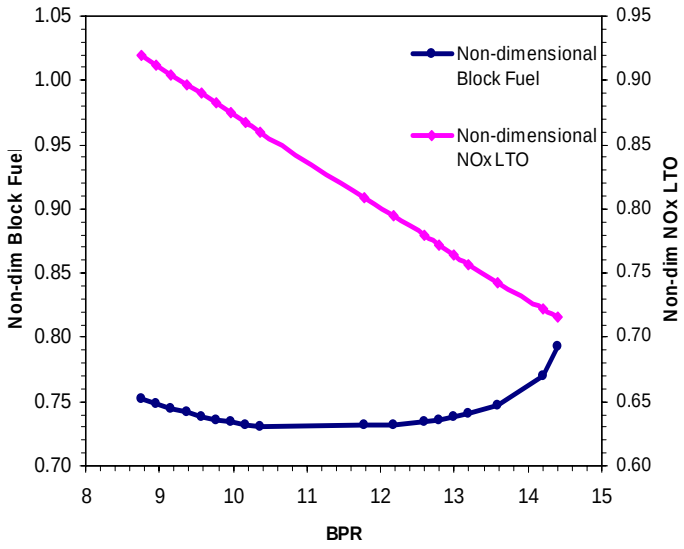

Figure B.18: Parametric study of non-dimensional block fuel and non-dimensional LTO NO_x vs. BPR: Geared turbofan

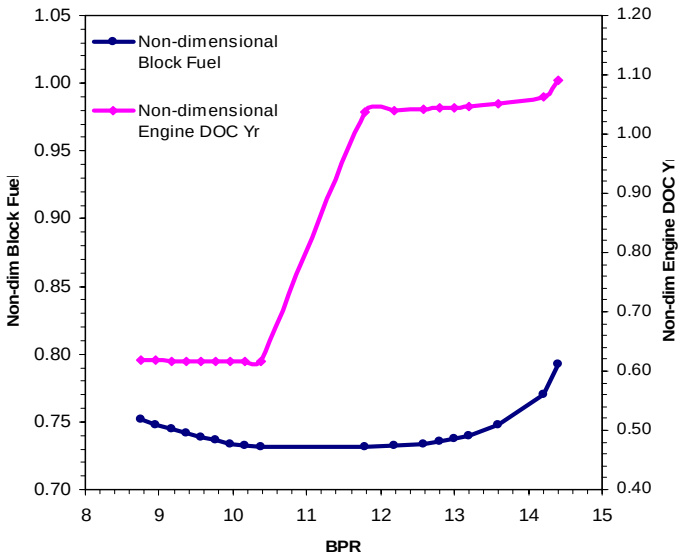

Figure B.19: Parametric study of non-dimensional block fuel and non-dimensional engine DOC yearly vs. BPR: Geared turbofan

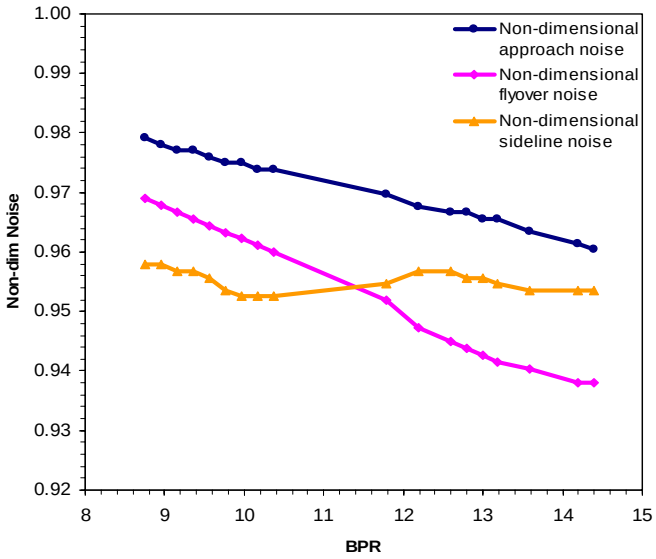

Figure B.20: Parametric study of non-dimensional noise at certification points vs. BPR: Geared turbofan

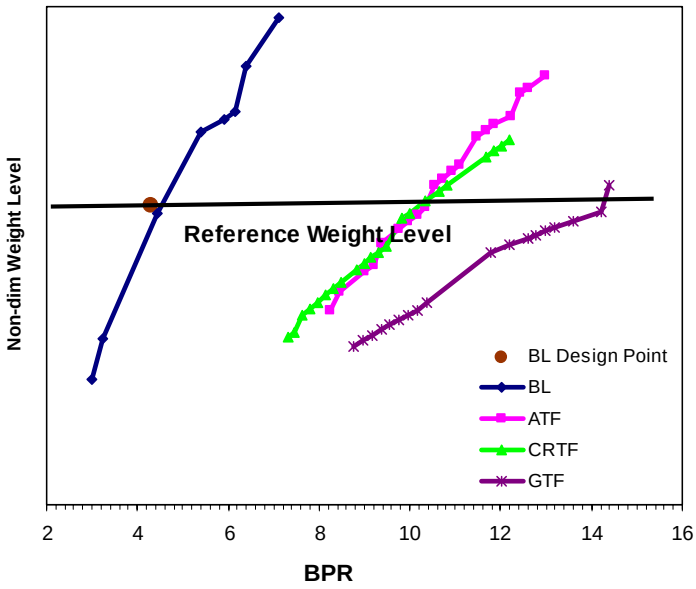

Figure B.21: Parametric study of non-dimensional engine weight vs. BPR for all configurations

APPENDIX C: TERA SINGLE-OBJECTIVE OPTIMISATION RESULTS

Table C.1: Single-objective optimisation for minimum fuel burn

Configuration	BL	BL OPT	ATF	CRTF	GTF
FN_{TOC} [kN]	30	30	30	30	30
BPR [-]	4.63	6.89	10.48	11.08	9.50
FPR [-]	1.55	1.59	1.50	1.56	1.66
OPR [-]	35.5	35.5	40.0	37.9	47.6
TET [K]	1660	1660	1850	1920	1955
Mass Flow [kg/s]	149.7	149.7	239.1	213.0	224.5
Gear Ratio [-]	N/A	N/A	N/A	N/A	3.0
ΔBlock Fuel [%]	0.00	-1.89	-13.83	-22.17	-27.47
ΔBlock GWP [%]	0.00	-0.55	-6.60	-16.60	-20.57
ΔNoise Margin [%]	0.00	90.57	152.83	180.19	108.49
ΔEDOC [%]	0.00	7.75	7.48	2.87	-1.11
$\Delta NO_{x,\,LTO}$ [%]	0.00	0.03	23.09	-37.64	-21.77

Table C.2: Single-objective optimisation for minimum GWP

Configuration	BL	BL OPT	ATF	CRTF	GTF
FN_{TOC} [kN]	30	30	30	30	30
BPR [-]	4.63	6.23	9.08	9.63	9.40
FPR [-]	1.55	1.78	1.57	1.57	1.69
OPR [-]	35.5	35.5	40.0	37.9	47.6
TET [K]	1660	1660	1850	1920	1955
Mass Flow [kg/s]	149.7	149.7	239.1	213.0	224.5
Gear Ratio [-]	N/A	N/A	N/A	N/A	3.0
ΔBlock Fuel [%]	0.00	-1.45	-13.69	-22.24	-27.39
ΔBlock GWP [%]	0.00	-0.89	-7.00	-17.15	-20.59
ΔNoise Margin [%]	0.00	49.06	139.62	167.92	106.60
ΔEDOC [%]	0.00	2.68	3.77	1.39	-1.37
$\Delta NO_{x,\,LTO}$ [%]	0.00	-6.52	22.07	-30.72	-24.10

Table C.3: Single-objective optimisation for maximum cumulative noise

Configuration	BL	BL OPT	ATF	CRTF	GTF
FN_{TOC} [kN]	30	30	30	30	30
BPR [-]	4.63	9.21	13.40	12.80	14.60
FPR [-]	1.55	1.58	1.31	1.51	1.50
OPR [-]	35.5	35.5	40.0	37.9	47.6
TET [K]	1660	1660	1850	1920	1955
Mass Flow [kg/s]	149.7	149.7	239.1	213.0	224.5
Gear Ratio [-]	N/A	N/A	N/A	N/A	3.0
ΔBlock Fuel [%]	0.00	0.76	-11.42	-19.78	-25.36
ΔBlock GWP [%]	0.00	2.70	-1.88	-13.05	-16.81
ΔNoise Margin [%]	0.00	124.53	191.51	207.55	151.89
ΔEDOC [%]	0.00	15.02	13.60	10.73	5.64
$\Delta NO_{x,LTO}$ [%]	0.00	-9.51	33.18	-39.57	-23.94

Table C.4: Single-objective optimisation for minimum engine DOC

Configuration	BL	BL OPT	ATF	CRTF	GTF
FN_{TOC} [kN]	30	30	30	30	30
BPR [-]	4.63	3.08	7.43	6.57	8.83
FPR [-]	1.55	1.85	1.63	1.65	1.85
OPR [-]	35.5	35.5	40.0	37.9	47.6
TET [K]	1660	1660	1850	1920	1955
Mass Flow [kg/s]	149.7	149.7	239.1	213.0	224.5
Gear Ratio [-]	N/A	N/A	N/A	N/A	3.0
ΔBlock Fuel [%]	0.00	6.00	-12.69	-19.11	-25.79
ΔBlock GWP [%]	0.00	6.49	-6.39	-14.14	-19.31
ΔNoise Margin [%]	0.00	-34.91	116.98	104.72	105.66
ΔEDOC [%]	0.00	-28.57	0.40	-4.03	-2.93
$\Delta NO_{x,LTO}$ [%]	0.00	12.62	25.84	-17.51	-35.03

Table C.5: Single-objective optimisation for minimum LTO NO_x emissions

Configuration	BL	BL OPT	ATF	CRTF	GTF
FN_{TOC} [kN]	30	30	30	30	30
BPR [-]	4.63	6.75	11.69	8.63	8.67
FPR [-]	1.55	1.95	1.57	1.83	1.86
OPR [-]	35.5	35.5	40.0	37.9	47.6
TET [K]	1660	1660	1850	1920	1955
Mass Flow [kg/s]	149.7	149.7	239.1	213.0	224.5
Gear Ratio [-]	N/A	N/A	N/A	N/A	3.0
ΔBlock Fuel [%]	0.00	5.71	-11.02	-14.81	-25.60
ΔBlock GWP [%]	0.00	6.63	-2.44	-8.21	-19.15
ΔNoise Margin [%]	0.00	41.51	161.32	156.60	102.83
ΔEDOC [%]	0.00	6.28	11.98	5.30	-2.68
$\Delta NO_{x,LTO}$ [%]	0.00	-22.36	9.02	-46.56	-35.36

APPENDIX D: ICHXMDO PARAMETRIC STUDY RESULTS

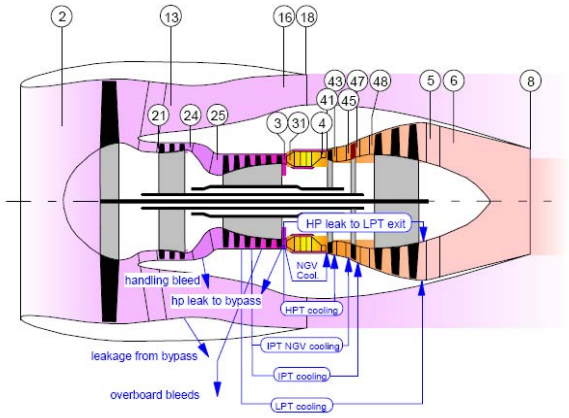

Figure D.1: Station numbering for baseline turbofan

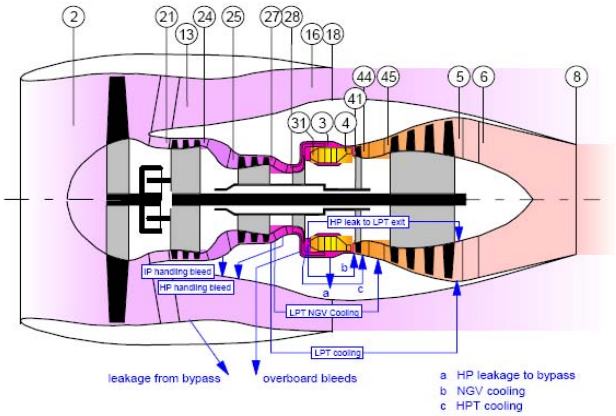

Figure D.2: Station numbering for geared turbofan

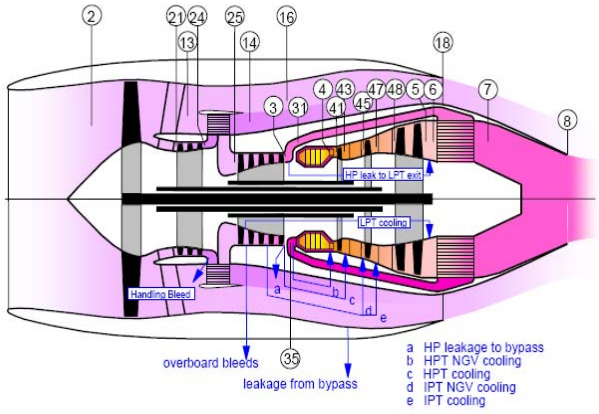

Figure D.3: Station numbering for ICR turbofan

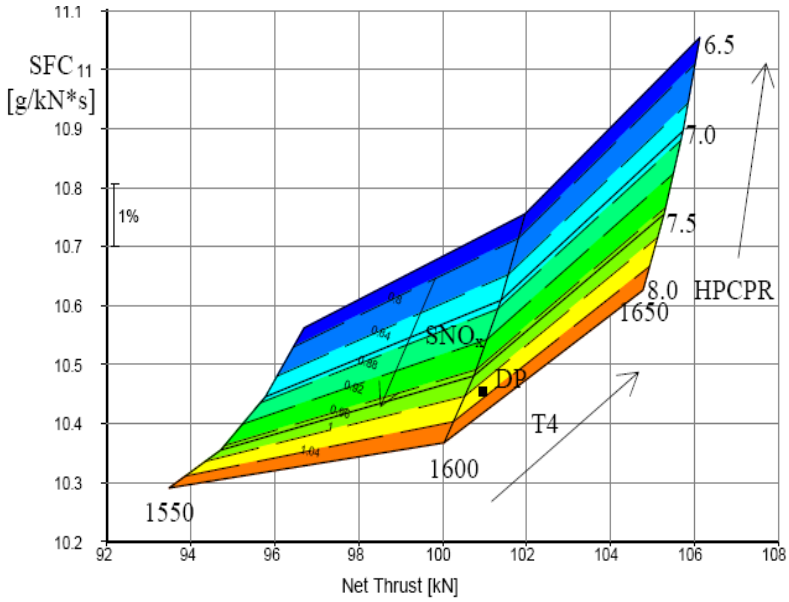

Figure D.4: Carpet plot for SFC/F_N/TET/OPR/NO_x for baseline turbofan

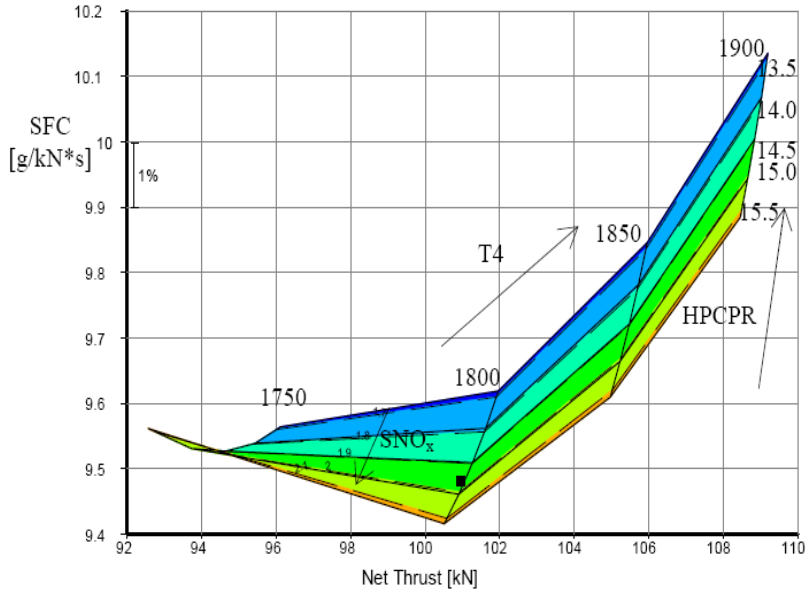

Figure D.5: Carpet plot for SFC/F_N/TET/OPR/NO_x for geared turbofan

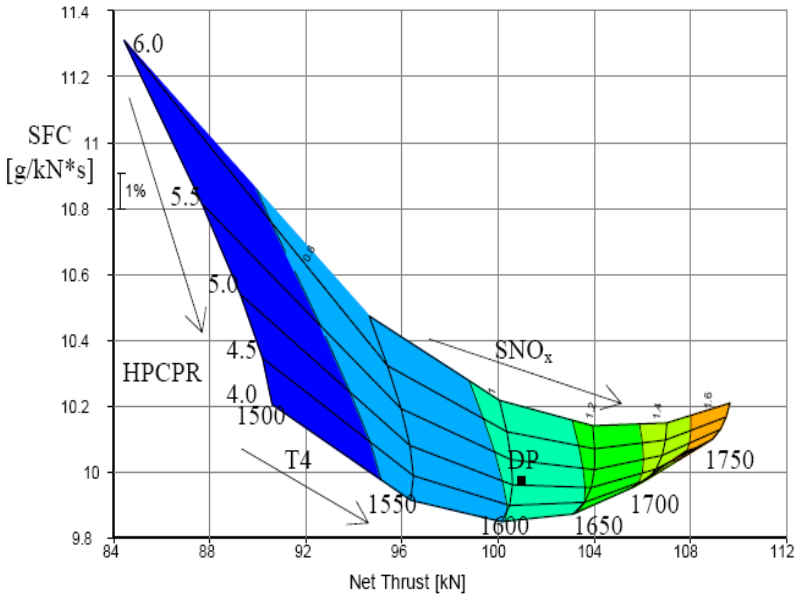

Figure D.6: Carpet plot for SFC/F_N/TET/OPR/NO_x for recuperated turbofan

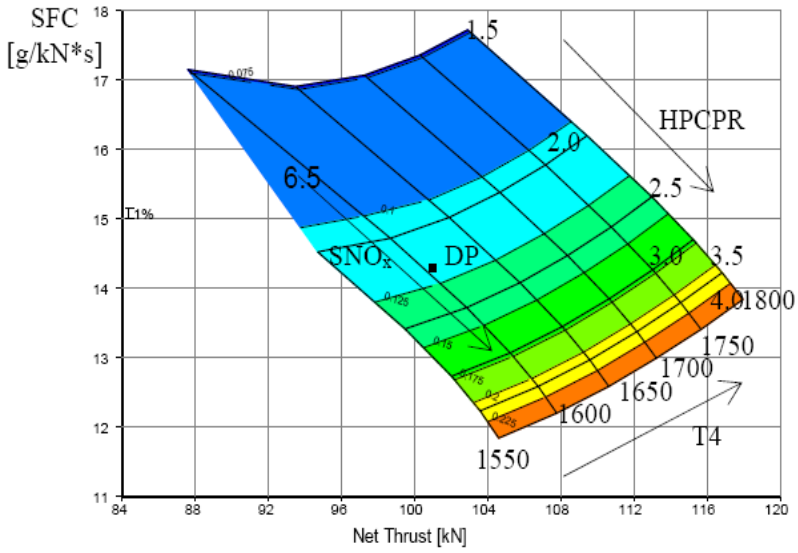

Figure D.7: Carpet plot for SFC/F_N/TET/OPR/NO_x for intercooled turbofan

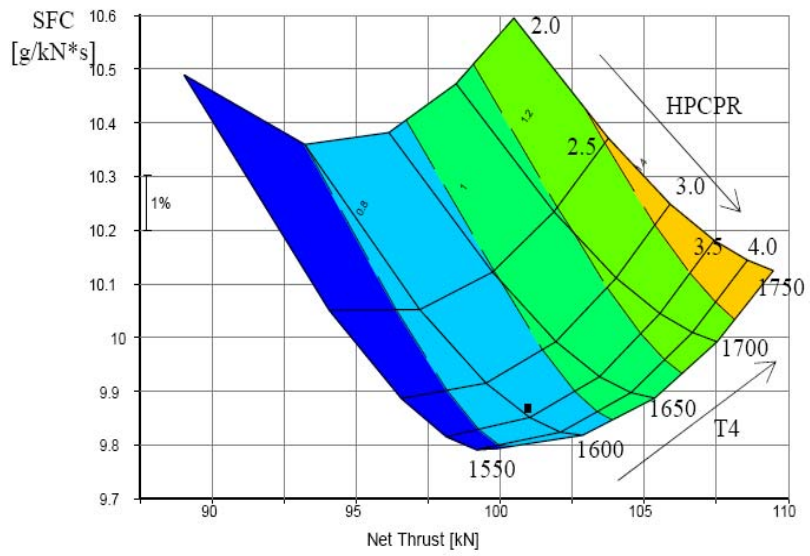

Figure D.8: Carpet plot for SFC/F_N/TET/OPR/NO_x for ICR turbofan

APPENDIX E: PMDF PARAMETRIC STUDY RESULTS

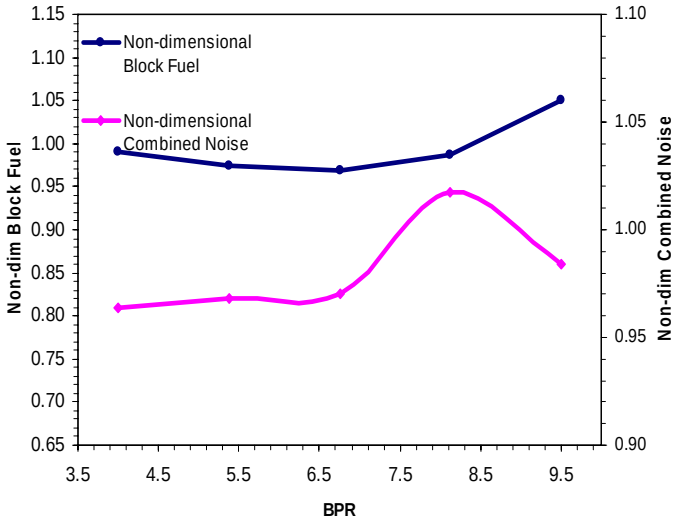

Figure E.1: Parametric study of non-dimensional block fuel and non-dimensional combined noise vs. BPR : Geared turbofan

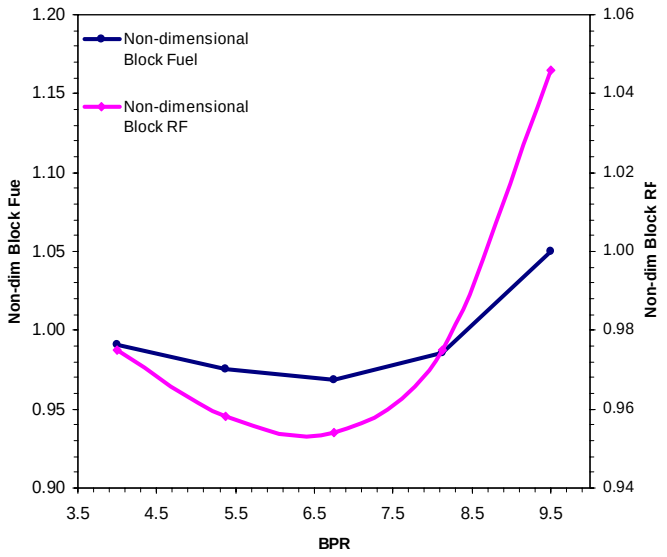

Figure E.2: Parametric study of non-dimensional block fuel and non-dimensional block RF vs. BPR : Geared turbofan

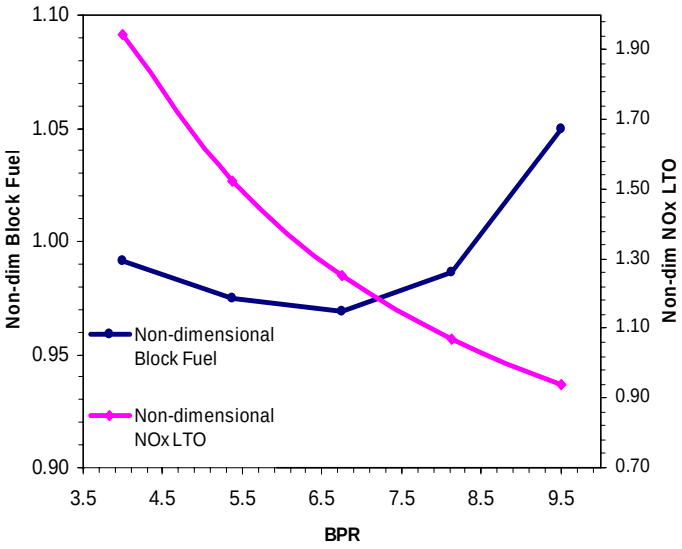

Figure E.3: Parametric study of non-dimensional block fuel and non-dimensional LTO vs. BPR : Geared turbofan

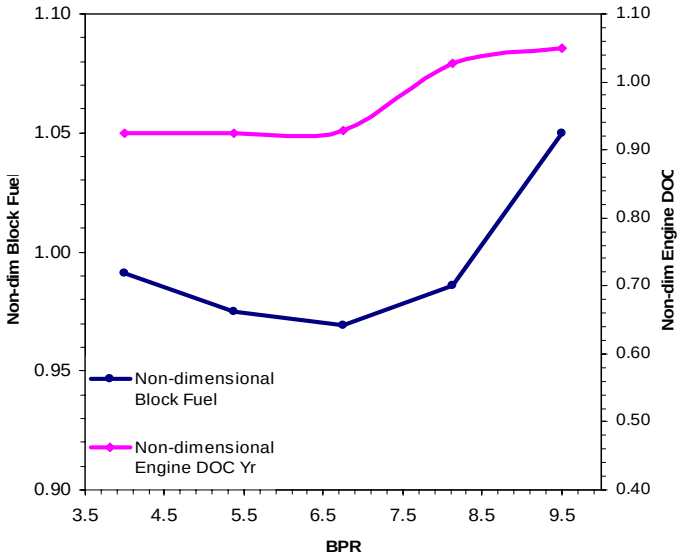

Figure E.4: Parametric study of non-dimensional block fuel and non-dimensional engine DOC vs. BPR : Geared turbofan

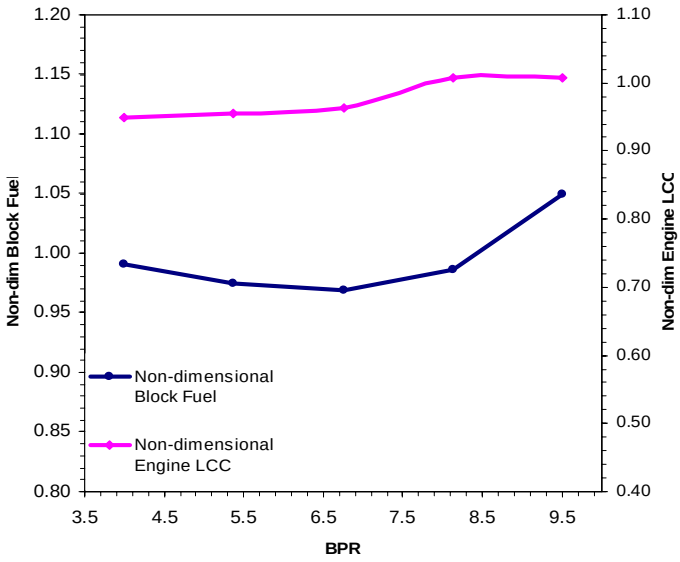

Figure E.5: Parametric study of non-dimensional block fuel and non-dimensional LCC vs. BPR : Geared turbofan

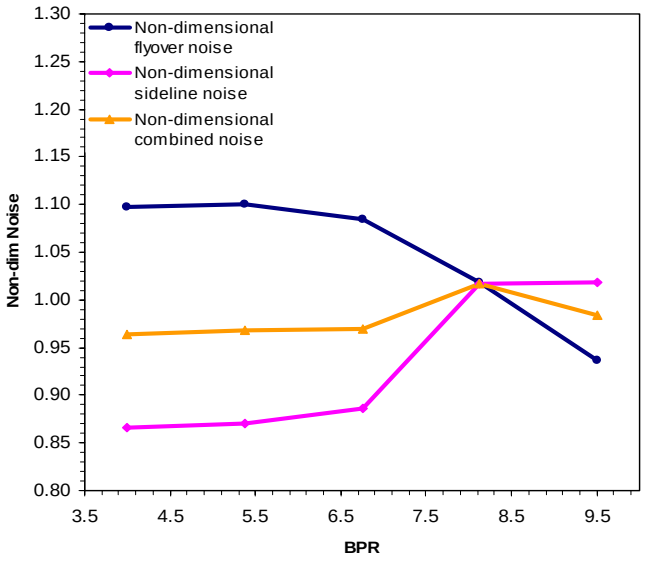

Figure E.6: Parametric study of non-dimensional noise at certification points vs. BPR : Geared turbofan

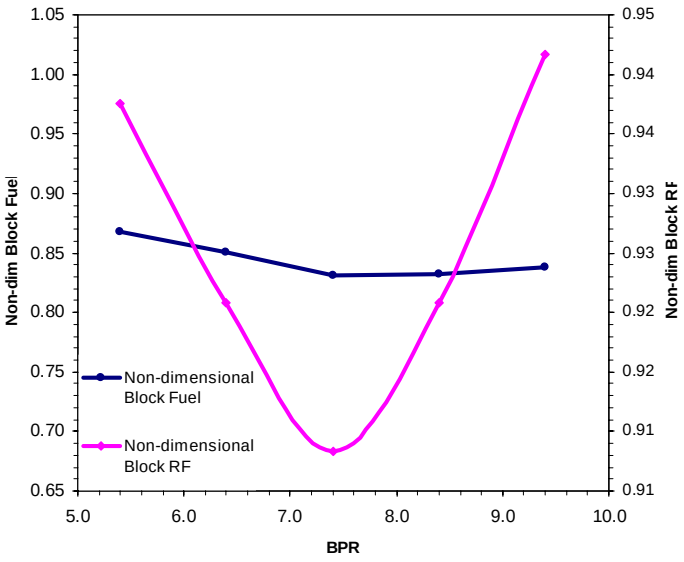

Figure E.7: Parametric study of non-dimensional block fuel and non-dimensional block RF vs. BPR : Geared constant-volume-combustion turbofan

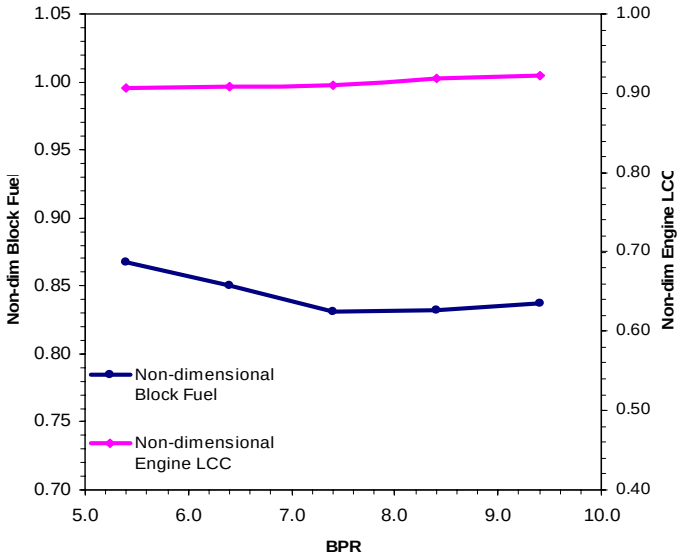

Figure E.8: Parametric study of non-dimensional block fuel and non-dimensional LCC vs. BPR : Geared constant-volume-combustion turbofan

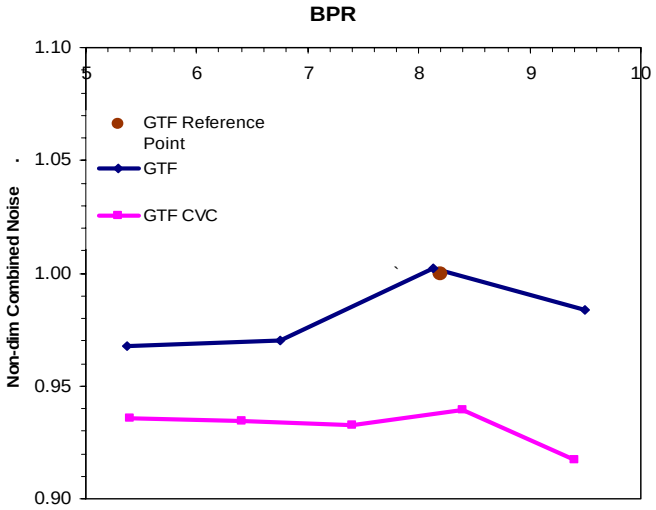

Figure E.9: Non-dimensional combined noise vs. BPR

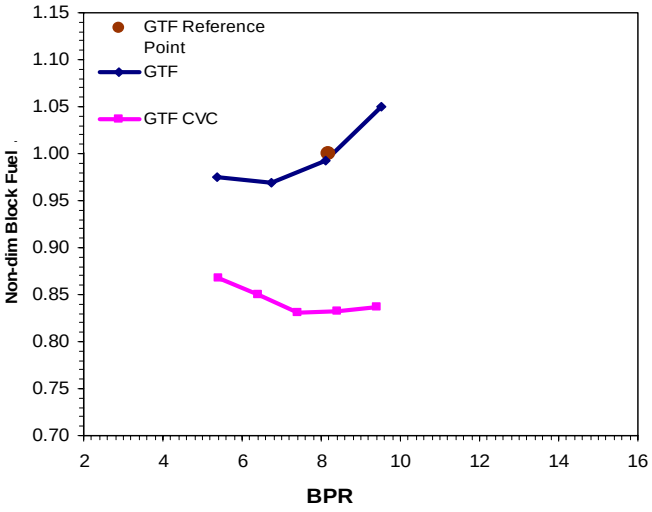

Figure E.10: Non-dimensional block fuel vs. BPR

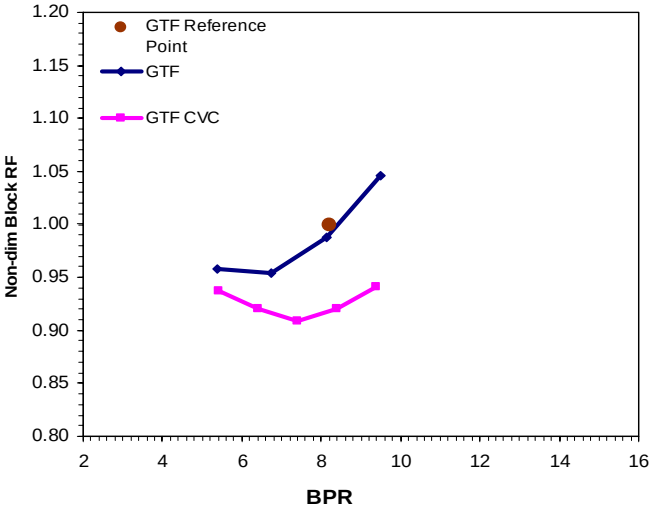

Figure E.11: Non-dimensional block RF vs. BPR

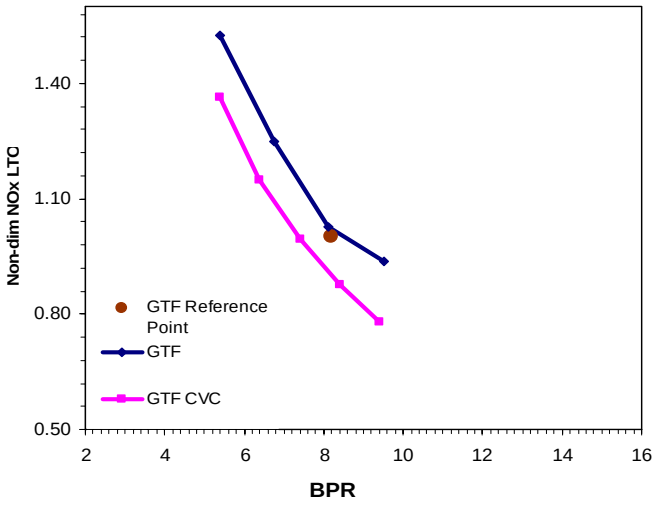

Figure E.12: Non-dimensional LTO NO_x vs. BPR

APPENDIX F: PMDF SINGLE-OBJECTIVE OPTIMISATION RESULTS

Table F.1: Single-objective optimisation for minimum fuel burn

Configuration	GTF	GTF-CVC	GTF-CVC OPT
FN_{TO} [kN]	120.10	120.10	120.10
BPR [-]	8.2	8.2	7.5
FPR [-]	1.45	1.45	1.45
OPR [-]	38.6	38.6	53.9
TET [K]	1650	1650	1650
Gear Ratio [-]	3.0	3.0	3.0
ΔBlock Fuel [%]	0.0	-17.0	-20.9
ΔBlock RF [%]	0.0	-17.5	-21.4
ΔNoise [%]	0.0	-5.2	-5.4
ΔEDOC [%]	0.0	15.7	-26.5
$\Delta NO_{x,LTO}$ [%]	0.0	-2.1	23.1
ΔSFC_{Cr} [%]	0.0	-10.2	-12.8

Table F.2: Single-objective optimisation for minimum LTO NO_x

Configuration	GTF	GTF-CVC	GTF-CVC OPT
FN_{TO} [kN]	120.10	120.10	120.10
BPR [-]	8.2	8.2	5.5
FPR [-]	1.45	1.45	1.45
OPR [-]	38.6	38.6	30.0
TET [K]	1650	1650	1650
Gear Ratio [-]	3.0	3.0	3.0
ΔBlock Fuel [%]	0.0	-17.0	-9.3
ΔBlock RF [%]	0.0	-17.5	-11.1
ΔNoise [%]	0.0	-5.2	-5.6
ΔEDOC [%]	0.0	15.7	-21.0
$\Delta NO_{x,LTO}$ [%]	0.0	-2.1	-45.7
ΔSFC_{Cr} [%]	0.0	-10.2	6.2

Table F.3: Single-objective optimisation for minimum combined noise and cruise SFC

Configuration	GTF	GTF-CVC	GTF-CVC OPT
FN_{TO} [kN]	120.10	120.10	120.10
BPR [-]	8.2	8.2	8.5
FPR [-]	1.45	1.45	1.45
OPR [-]	38.6	38.6	54.0
TET [K]	1650	1650	1650
Gear Ratio [-]	3.0	3.0	3.0
ΔBlock Fuel [%]	0.0	-17.0	-20.4
ΔBlock RF [%]	0.0	-17.5	-20.5
ΔNoise [%]	0.0	-5.2	-8.1
ΔEDOC [%]	0.0	15.7	-26.5
$\Delta NO_{x,LTO}$ [%]	0.0	-2.1	42.0
ΔSFC_{Cr} [%]	0.0	-10.2	-15.4

Table F.4: Single-objective optimisation for minimum engine DOC

Configuration	GTF	GTF-CVC	GTF-CVC OPT
FN_{TO} [kN]	120.10	120.10	120.10
BPR [-]	8.2	8.2	5.8
FPR [-]	1.45	1.45	1.45
OPR [-]	38.6	38.6	54.0
TET [K]	1650	1650	1650
Gear Ratio [-]	3.0	3.0	3.0
ΔBlock Fuel [%]	0.0	-17.0	-19.5
ΔBlock RF [%]	0.0	-17.5	-20.8
ΔNoise [%]	0.0	-5.2	-7.3
ΔEDOC [%]	0.0	15.7	-27.0
$\Delta NO_{x,LTO}$ [%]	0.0	-2.1	-0.1
ΔSFC_{Cr} [%]	0.0	-10.2	-6.8

APPENDIX G: PMDF MULTI-OBJECTIVE OPTIMISATION RESULTS

Table G.1: Multi-objective optimisation: FB vs. NO_x vs. cruise SFC vs. noise vs. engine DOC

Configuration	GTF	GTF-CVC	GTF-CVC OPT
FN_{TO} [kN]	120.10	120.10	120.10
BPR [-]	8.2	8.2	6.9
FPR [-]	1.45	1.45	1.45
OPR [-]	38.6	38.6	41.6
TET [K]	1650	1650	1650
Gear Ratio [-]	3.0	3.0	3.0
ΔBlock Fuel [%]	0.0	-17.0	-17.2
ΔBlock RF [%]	0.0	-17.5	-18.2
ΔNoise [%]	0.0	-5.2	-6.5
ΔEDOC [%]	0.0	15.7	-25.2
$\Delta NO_{x,LTO}$ [%]	0.0	-2.1	-12.4
ΔSFC_{Cr} [%]	0.0	-10.2	-6.4